

Max-Planck-Institut für Kolloid- und Grenzflächenforschung

**Self-Assembly of Double Hydrophilic Block  
Copolymers:  
Organized Particles and Vesicles Beyond  
Amphiphiles**

**Dissertation**

zur Erlangung des akademischen Grades  
Doktor der Naturwissenschaften (Dr. rer. nat.)  
in der Wissenschaftsdisziplin „Kolloid- und Polymerchemie“

eingereicht an der  
Mathematisch-Naturwissenschaftlichen Fakultät  
der Universität Potsdam

von

**Jochen Willersinn**

Geboren am 19.09.1988 in Mainz

Potsdam-Golm, im April 2017

This work is licensed under a Creative Commons License:  
Attribution 4.0 International  
To view a copy of this license visit  
<http://creativecommons.org/licenses/by/4.0/>

Published online at the  
Institutional Repository of the University of Potsdam:  
URN [urn:nbn:de:kobv:517-opus4-408578](http://nbn-resolving.de/urn:nbn:de:kobv:517-opus4-408578)  
<http://nbn-resolving.de/urn:nbn:de:kobv:517-opus4-408578>



## Acknowledgements

To begin with, I would like to thank **Prof. Dr. Markus Antonietti**, for giving me the opportunity to do my PhD in his department and providing this interesting topic I was working on. Moreover, I would like to thank him for the creative and multi-faceted scientific environment he created in the department.

My deepest gratitude goes to my direct supervisor **Dr. Bernhard V. K. J. Schmidt** for his wonderful support during my PhD time. Without the billion ideas, fruitful discussions, advices, and his constant motivation and amazing supervision, this work and moreover my scientific education would not have reached this level.

Furthermore, I would like to thank **Marlies Gräwert** for the countless number of SEC measurements and further for keeping things running so nicely in our group.

Moreover, I thank **Noah Al Nakeeb and Dr. Tingting Li** for the fruitful discussions and collaborations on our beloved DHBC topic.

In addition, **Dr. Markus Drechsler** (Universität Bayreuth) and **Dr. Anna Bogomolova** are thanked for successful collaborations with cryo TEM and DLS/SLS measurements.

Heike Runge, Rona Pitschke, Carmen Remde, Dr. Tom Robinson, Antje Völkel, and Olaf Niemeyer are acknowledged for cryo SEM, TEM, LSCM, turbidimetry, and NMR measurements as well as for their constant technical support.

Furthermore, I would like to thank Marc Brunet Cabré for his contribution during his Erasmus time. I wish you all the best for your future.

Additionally, I would like to thank Christian, Berti, Afroditi, Noah, Baris, Valerio, Hui, Steffen, Karoline, Konrad, Eddie, Claudio, Rémi, Martin, the novel self-assembly polymers group, and all of those that possibly forgot to mention for the amazing working environment that you all created making my time at the MPI unforgettable.

Caro, Lukas, Marianne, and Grischa are thanked for control reading this thesis and trying to find all spelling and grammar mistakes, and revising the things that only I was able to understand.

Finally, I would like to express my gratitude to my family and my friends for the never ending support and their understanding.

## Table of Contents

<b>I. Motivation and Background .....</b>	<b>1</b>
I.1. The Challenge of Precise Drug Delivery for Future Pharmaceuticals.....	1
I.2. Controlled Polymerizations and Their Impact on Biomedical Science.....	2
I.3. Self-Assembly of Block Copolymers .....	11
I.4. Purely Hydrophilic Block Copolymers.....	21
<b>II. Outline .....</b>	<b>27</b>
<b>III. Organized Polymeric Submicron Particles <i>via</i> Self-Assembly and Crosslinking of Double Hydrophilic Poly(ethylene oxide)-<i>b</i>-Poly(<i>N</i>-vinylpyrrolidone) in Aqueous Solution .....</b>	<b>29</b>
III.1. Preface.....	29
III.2. Synthesis of PEO- <i>b</i> -PVP Block Copolymer.....	32
III.3. Self-Assembly of PEO- <i>b</i> -PVP Block Copolymers in Aqueous Solution.....	35
III.4. Synthesis of PEO- <i>b</i> -P(VP- <i>co</i> -VIm) Block Copolymers .....	39
III.5. Self-Assembly of PEO- <i>b</i> -P(VP- <i>co</i> -VIm) .....	42
III.6. Crosslinking of Self-Assembled PEO- <i>b</i> -P(VP- <i>co</i> -VIm) Submicron Particles .....	45
III.7. Self-Assembly and Crosslinking of PEO- <i>b</i> -P(VP- <i>co</i> -VIm) in DMF .....	52
III.8. Labelling of PEO- <i>b</i> -P(VP- <i>co</i> -VIm) Submicron Particles with Rhodamine B .....	58
III.9. Conclusion.....	59
<b>IV. Vesicles of Double Hydrophilic Pullulan and Poly(acrylamide) Block Copolymers: A Combination of Synthetic- and Bio-derived Blocks.....</b>	<b>61</b>
IV.1. Preface.....	61
IV.2. Synthesis of Alkyne Functionalized Pullulan .....	64
IV.3. Synthesis of Azide Terminated Acrylamide Homopolymers .....	67
IV.4. Conjugation of Block Copolymers via Copper Catalyzed Azide Alkyne Cycloaddition.....	69

IV.5.	Aqueous Self-Assembly of Pull- <i>b</i> -PDMA and Pull- <i>b</i> -PEA.....	73
IV.6.	Conclusion.....	87
<b>V.</b>	<b>pH and Redox Responsive Vesicles from Double Hydrophilic Pullulan-<i>b</i>-Poly(vinylpyrrolidone) Block Copolymers .....</b>	<b>88</b>
V.1.	Preface.....	88
V.2.	Synthesis of $\omega$ -functionalized Pullulan-xanthate.....	89
V.3.	Block Copolymerization of Pull- <i>b</i> -PVP .....	95
V.4.	Self-Assembly of Pull- <i>b</i> -PVP Block Copolymers in Aqueous Solution .....	97
V.5.	Oxidation and Crosslinking of Pull- <i>b</i> -PVP Vesicles.....	102
V.6.	Conclusion.....	115
<b>VI.</b>	<b>Conclusion and Perspectives .....</b>	<b>116</b>
<b>VII.</b>	<b>Appendix .....</b>	<b>CXX</b>
VII.1.	Abbreviations.....	CXX
VII.2.	Applied Methods.....	CXXII
VII.3.	Chemicals .....	CXXXIV
VII.4.	Experimental Part .....	CXXXVI
VII.4.1.	General procedure for the preparation of solutions for DLS investigation.....	CXXXVI
VII.4.2.	Organized polymeric submicron particles via self-assembly and crosslinking of double hydrophilic poly(ethylene oxide)- <i>b</i> -poly( <i>N</i> -vinylpyrrolidone) in aqueous solution .....	CXXXVI
VII.4.3.	Vesicles of double hydrophilic pullulan and poly(acrylamide) block copolymers: A combination of synthetic- and bio-derived blocks .....	CXLIV
VII.4.4.	pH and redox responsive vesicles from double hydrophilic pullulan- <i>b</i> -poly( <i>N</i> -vinylpyrrolidone) block copolymers.....	CLVII
<b>VIII.</b>	<b>References .....</b>	<b>CLXIV</b>
<b>IX.</b>	<b>List of Publications .....</b>	<b>CLXXIII</b>
<b>X.</b>	<b>Declaration .....</b>	<b>CLXXIV</b>

# I. Motivation and Background

## 1.1. *The Challenge of Precise Drug Delivery for Future Pharmaceuticals*

In the early 20<sup>th</sup> century Alexander Fleming discovered that a stem of mold, *penicillium chrysogenum*, produced a specific type of molecules in order to protect itself from bacteria.<sup>1</sup> The so discovered *antibiotic* compounds proved to be applicable against various bacterial infections. Simultaneously, Paul Ehrlich and Sahachiro Hata developed the synthetic antibacterium *Salvarsan*, a drug containing arsine,<sup>2</sup> which proved to be effective in the treatment of syphilis.<sup>3,4</sup> Moreover, the sulfonamide derived antibacterial compound *Prontosil* (sulfamidochrysoidin) was synthesized by Mietzsch and Klarer in 1934. Its antibacterial potential was discovered by Gerhard Domagk, who was awarded the Nobel prize for medicine in 1939 for his discovery.<sup>5</sup> These groundbreaking discoveries opened up a new field in medicine and allowed the development and improvement of synthetic and bio-derived antibiotics. Combined with the discovery of vaccinations,<sup>6</sup> an increase in general health could be obtained.<sup>1,7</sup> However, with time the number of bacterial tribes that developed certain resistances against common antibiotics was steadily increasing.<sup>8</sup> Therefore, the development of new and more advanced drugs and medical treatments in order to prevent epidemics is a crucial aim of biomedical research.<sup>8,9</sup> Thus, the deliberated design of powerful drug delivery systems for specific drugs and treatments could be an elaborate approach to overcome present and future challenges.<sup>10-13</sup> Furthermore, the development of new drugs for diseases caused by genetic predisposition, cancer or immune system deficiencies such as AIDS<sup>14</sup> requires sometimes a new approach for the transportation of the corresponding drug to target areas inside the body.<sup>15,16</sup> Chemotherapy for instance affects the whole body and relies on the high metabolic activity of cancer cells in order to be successful. A target-oriented therapy that is locally applied would be of higher benefit since the anticancer drug dose can be significantly reduced with a simultaneous increase in efficiency.<sup>17</sup> Therefore, it is not surprising that in the past 20 years researchers have set their focus on improving targeted drug delivery. Noteworthy discoveries have been made in the field of polymer based drug components,<sup>18-20</sup> such as PEGylated drugs,<sup>21,22</sup> polymersomes as drug delivery vehicles,<sup>23-26</sup> and bioconjugates with polymeric attachments.<sup>27-30</sup>

In order to tackle the demanded requirements for novel approaches towards drugs and medical treatments, a new type of delivery system has to be developed. By optimizing the block copolymer based systems that are already known and sometimes already applied,<sup>31, 32</sup> delivery systems and reaction compartments designed from block copolymer self-assemblies can contribute to a large degree to modern medicine.

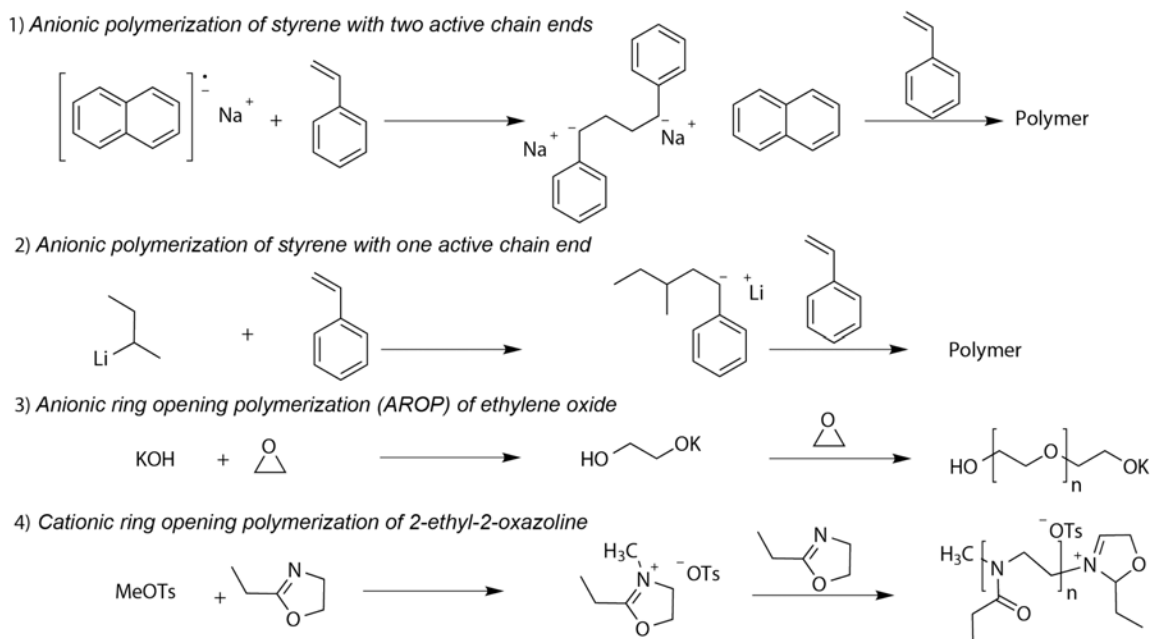
Block copolymer based drug delivery vehicles such as micelles and vesicles composed of biocompatible or even biodegradable highly functionalized polymer blocks bear the potential to revolutionize the biomedical field due to their high diversity and flexibility regarding their applications.<sup>16, 33, 34</sup> Novel systems which are based on double hydrophilic block copolymers have the potential to fulfill the challenging tasks for future applications. However, a long process of investigations and groundbreaking discoveries in the field of polymer and block copolymer synthesis was necessary to reach the current state of the art. The pathway starting from the first block copolymers to the present state will therefore be highlighted in the following chapter.

## *1.2. Controlled Polymerizations and Their Impact on Biomedical Science*

The synthesis of defined block copolymers *via* free radical polymerization was a major challenge in the early stages of polymer science. The main problem in free radical copolymerization is that both monomers (A and B) have to be present from the beginning on in the reaction mixture. Therefore, a number of non-AB-type block copolymers can be formed, such as alternating or gradient copolymers.<sup>35-39</sup> Both mentioned examples of copolymers have found various applications in material science, ranging from rubbers and injection molds to acryl fibers as examples of radical copolymerizations.<sup>35, 40-43</sup> However, when addressing biomedical applications more defined polymer architecture is of higher benefit. Furthermore, the lack of control in free radical polymerization reactions affords high polydispersities and the synthesis of rather defined polymers is quite complicated. Nowadays, most industrial polymers are synthesized employing highly efficient Ziegler-Natta-polymerization techniques due to their improved feasibility.<sup>44, 45</sup> For that reason, the utilization of synthetic polymers was rather uncommon in the medical field at early stages, leaving poly(*N*-vinylpyrrolidone) (PVP), which is used as a blood plasma substitute, as a sole exception.<sup>46, 47</sup>



The discovery of living polymerization techniques, namely anionic and carbocationic polymerization in the early 1950s not only enhanced the accessibility of new polymers and block copolymers,<sup>45, 48</sup> but also generated a huge impact on the pharmaceutical field.<sup>49</sup> The term of living polymerization was first proposed by Szwarc et al., who reported on the polymerization of styrene initiated by an electron transfer from a suitable electron donor.<sup>50, 51</sup> Initiated by a sodium naphthalene complex, the generated carbanions of the polystyrene chains were stable for several days under the reported conditions. The more outstanding fact of this polymerization technique was that two active chain ends were produced and the nearly quantitative conversion of monomer B. The addition of a second monomer A led to precise ABA type block copolymers (Scheme I.1-1).<sup>51</sup> Moreover, AB type block copolymers could be synthesized using *sec*-BuLi as initiator (Scheme I.1-2). The application of anionic polymerization of vinylic monomers in material science improved the properties of polymeric materials significantly. Drawbacks of anionic polymerization are the requirement of monomers which are stable under strongly basic conditions as well as the non-convenient polymerization procedures. Acrylates, for instance, cannot be polymerized due to the abstraction of the  $\alpha$ -proton under basic conditions leading to termination of active chain ends, such as transesterification or back-biting.<sup>52-54</sup> Therefore, special conditions had to be developed.<sup>55, 56</sup>



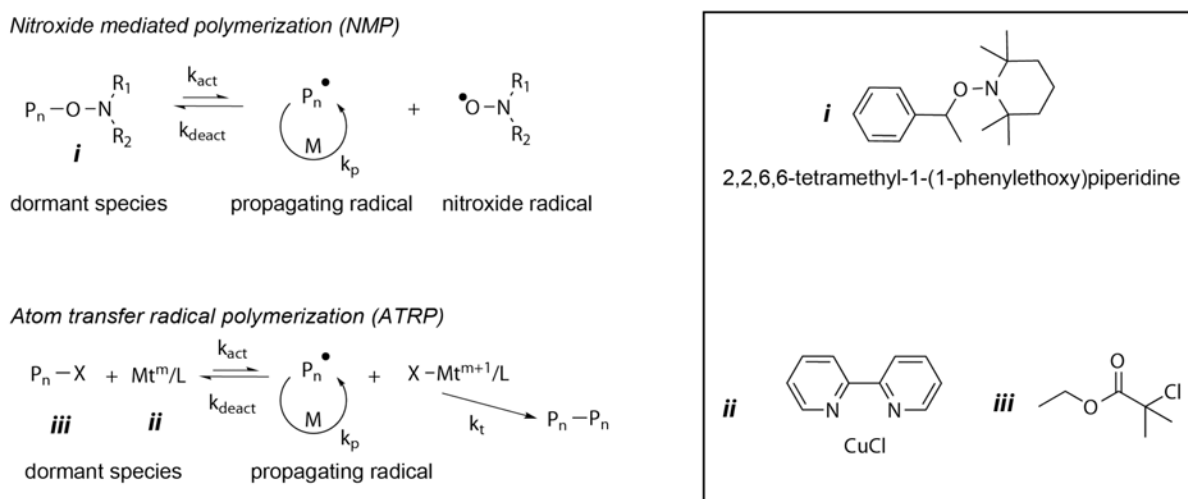
**Scheme I.1** Examples of living polymerizations: 1) Sodium naphthalenide initiated polymerization of styrene, leading to two active chain ends; 2) Initiation of styrene with *sec*-BuLi leading to a single active chain end; 3) exemplary anionic ring opening polymerization of ethylene oxide; 4) Exemplary cationic ring opening polymerization of 2-ethyl-2-oxazoline.

Another important type of anionic polymerizations is the anionic ring opening polymerization (AROP) of epoxides.<sup>57</sup> The most prominent polymer synthesized *via* AROP is poly(ethylene oxide) (PEO). PEO was already synthesized in the 1930s by Staudinger and Flory, who recognized the controlled character of the reaction.<sup>58, 59</sup> The polymerization of ethylene oxide (EO) is initiated with strong bases such as KOH or trimethylamine and it is up to this date the most important polymerization of epoxides on industrial scale (Scheme I.1-3).<sup>60</sup> Furthermore, AROP of epoxides tolerates a broad spectrum of functional groups that can be incorporated to afford highly functional polymers.<sup>60</sup> The high functionality, water solubility and the good biocompatibility of PEO and derivatives still create a high impact of this polymer on the scientific and industrial community, for example in biomedical and drug delivery fields,<sup>23, 25, 29, 61, 62</sup> but also in the preservation of archeological artifacts like in the case of the sunk Swedish battleship Vasa.<sup>63</sup>

Another noteworthy living polymerization to be mentioned here is the carbocationic polymerization.<sup>64, 65</sup> Polymerizations of vinyl monomers with simple protic acids are a lot more complex than their anionic counterpart due to the transfer of  $\beta$ -protons of the active chain in acidic environment,<sup>66</sup> causing a large number of dead chain ends and therefore broad molecular mass distributions. The application of Lewis acids such as  $\text{BCl}_3$  as initiators displayed a more efficient system for cationic polymerizations of vinyl monomers.<sup>67-70</sup> However, the even more pronounced sensitivity towards moisture, air, and functional groups in contrast to anionic polymerizations decreases its applicability. In contrast to vinyl monomers, the cationic polymerization of heterocyclic rings such as THF and oxazolines is frequently applied. The utilization of alkyl tosylate as initiator affords a cationic ring opening polymerization of the five membered 2-oxazoline ring (Scheme I.1-4).<sup>49, 71</sup> Due to the large amount of functional groups that can be attached to 2-oxazolines and their good biocompatibility, poly(2-oxazolines) are promising candidates for applications in biomedical fields as well as in material science.<sup>72-74</sup>

Despite granting significant control over the resulting polymer in terms of polydispersity and molecular weight, the limitation in the choice of monomers bearing functional groups and the synthetic requirements for polymerization decreases the applicability of living polymerizations.<sup>75, 76</sup> Several important polymers cannot be synthesized *via* living polymerizations without high effort and low cost efficiency. Free radical polymerization techniques are capable of polymerizing those monomers, but result in rather broad distributed

and undefined products. A solution to overcome these drawbacks concerning radical polymerizations was presented by Moad et al. applying an alkoxyamine derived compound which undergoes a homolytical cleavage of the weak C—O bond to afford two radicals, a stable nitroxide radical, and a polymeric radical that can undergo chain addition.<sup>77</sup> The nitroxide radical is unable to create new radical species, but recombines reversibly with active polymeric chains to an unreactive dormant species. The reversible radical generation and recombination is defined by a temperature dependent equilibrium allowing to conduct the polymerization under a certain control.<sup>78</sup> With this discovery, the “living” free radical polymerization or reversible deactivation radical polymerization (RDRP) was born.<sup>79</sup>



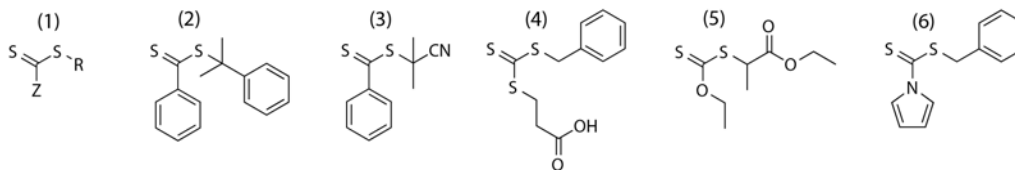
**Scheme I.2** Polymerization schemes of NMP with the common initiator depicted in the box and ATRP with the exemplary initiation complex 2,2'-bipyridine/CuCl and ethyl 2-chloro-2-methylpropanoate.

A standard example of nitroxide mediated radical polymerizations is the polymerization of styrene with 2,2,6,6-tetramethyl-1-(1-phenylethoxy)piperidine (**i**), a TEMPO based alkoxyamine, at 125 °C, resulting in defined polymers with narrow polydispersities.<sup>77</sup>

In 1995, Matyjaszewski and coworkers and Swamoto and coworkers independently developed a transition metal based polymerization technique with the conceptual similarity of reversibly generated radical pairs.<sup>80, 81</sup> In contrast to NMP, where a weak C—O bond cleaves homolytically to generate the propagating radical, the abstraction of a halide from an initiator to a transition metal complex generates the radical in the so called atom transfer radical polymerization (ATRP). The catalyst, which is prepared from a transition metal halide, such as Cu(I)Cl, and a suitable ligand like 2,2'-bipyridine (**ii**), is able to undergo a reversible single electron oxidation *via* abstraction of a chlorine radical from the initiator molecule ethyl 2-chloro-2-

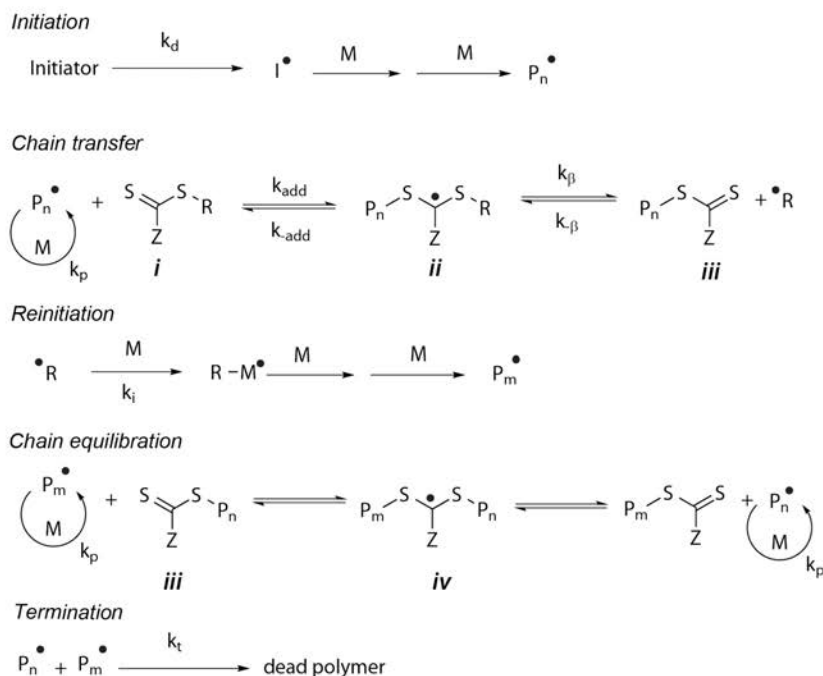
methylpropanoate (*iii*). Thus, an active initiator radical at the compound is formed. Subsequently, the active chain end can grow to a certain degree until it undergoes a recombination with a chlorine from the oxidized Cu(II) complex to form the inactive species and the reduced Cu(I) complex.<sup>82</sup> The equilibrium at the radical generating step is shifted predominantly to the side of the dormant species, giving the polymerization a very controlled character because only a very little amount of active propagating chains is present. Initial problems and limitations due to the sensitivity of the Cu(I) species towards moisture and oxygen could be overcome with optimized reaction conditions making ATRP one of the most versatile polymerization techniques known.<sup>83</sup> The introduction of a regenerating system for the catalyst decreased the necessary amount of copper in an ATRP significantly, which was afforded *via* activator regenerated by electron transfer (ARGET), i.e. a regenerating system which constantly reoxidizes inactivated copper complexes.<sup>83, 84</sup> By a careful choice of ligand and initiator, a wide range of highly functional polymers can be synthesized. Furthermore, ATRP delivers an excellent starting point for the synthesis of block copolymers since each chain is theoretically terminated with an alkyl halide and is therefore able to act as macro initiator for a second polymerization. Thus, block copolymers and more complex macromolecular architectures with completely different functionalities can be synthesized.<sup>83</sup> Furthermore, the halide can be easily exchanged by different functional groups to enable further applications for polymers synthesized *via* ATRP. A slight drawback of ATRP is the presence of copper contaminations in the polymers which cannot be removed easily. Because copper is a toxic metal,<sup>85, 86</sup> possible biomedical applications have to be taken with care.

Further approaches towards controlled radical polymerization are the reversible addition-fragmentation chain transfer (RAFT) process or the macromolecular design *via* the interchange of xanthates (MADIX) process. Those polymerization techniques utilize the same conditions as conventional free radical polymerizations such as initiator, monomers, and solvent, but a chain transfer agent (CTA) is added. Usually, the CTA is a dithiocarbonyl derived compound that gives control over the reaction.<sup>87</sup> The key feature of the RAFT CTAs is the ability to capture a radical species for a certain amount of time *via* an addition to the thiocarbonyl sulfur atom. The so formed intermediate radical species is rather unstable and undergoes fragmentation to release a propagating chain radical. This addition-fragmentation process is crucial to allow control over the polymerization reactions.



**Scheme I.3** Examples of RAFT/MADIX CTAs: 1) general scheme; 2) cumyl dithiobenzoate; 3) cyanoisopropyl dithiobenzoate; 4) 3-benzylsulfanylthiocarbonylsulfanyl-propionic acid 5) *S*-(1-ethoxycarbonyl) *O*-ethyl xanthate and 6) benzyl 1-pyrrolcabodithioate.

The CTAs in Scheme I.3 display five different types of RAFT/MADIX agents. In order to provide a good control over the chain transfer reaction, the functional group Z has to have the right activity to ensure a high transfer constant. The Z-group possesses the main influence on the rate of the chain transfer, as it activates the thiocarbonyl function to approach a compatible rate as the one of the propagation reaction. The intermediate radical (Scheme I.4) should therefore possess a lifetime as short as possible. Slightly activating Z-groups such as dithiobenzoates (Scheme I.3 (2) and (3)) are therefore commonly used for monomers which create a reactive propagating radical, e.g. methacrylates. Xanthates, on the other hand, are capable of stabilizing poorly stabilized and therefore highly reactive monomers like vinyl acetate (VAc) or *N*-vinylpyrrolidone (VP). The activity of the CTAs has to be adjusted to match the polymerization conditions, such as solvent and the corresponding monomer. Furthermore, the radical of the leaving group R has to possess similar reactivity towards radical addition as the propagating chain to maintain the propagation rate. The examples (2) and (3) display common RAFT CTAs possessing a benzyl Z group and R groups that form tertiary radical upon fragmentation. The CTAs (2) and (3) are commonly used for polymerizations of styrene and methyl methacrylate (MMA). The trithiocarbonate (4) is a CTA which is often used for acrylamides,<sup>88-90</sup> such as *N,N*-dimethylacrylamide (DMA), *N,N*-diethylacrylamide (DEA), and *N*-isopropylacrylamide (NIPAm),<sup>91-93</sup> furthermore *n*-butylacrylate (*n*-BuA),<sup>94</sup> but also polymerizations with styrene and MMA are reported.<sup>95, 96</sup> The xanthate CTA (5) is frequently used in MADIX polymerizations to stabilize more reactive propagating radicals, such as acrylic acid (AA), VAc, VP, and 2-(acetoxyl)ethyl methacrylate (AEMA).<sup>97-99</sup> The last example of CTAs bearing a pyrrole in CTA (6) is a more rare type of Z groups. It is used for the polymerization of acrylamides and methacrylates, such as NIPAm and MMA, for example.<sup>100, 101</sup> The mechanism of RAFT/MADIX polymerizations is similar in all cases and illustrated in Scheme I.4.



**Scheme I.4** General RAFT/MADIX mechanism.

The RAFT process is a polymerization technique applying the same fundamental steps as a free radical polymerization, but incorporates a thiocarbonylthio component *i* as chain transfer agent.<sup>102, 103</sup> Therefore, initiation occurs in similar fashion to conventional free radical polymerizations with the radical generation starting from a suitable initiator, such as AIBN. Thus initialized, the propagating radical can either add to monomer units or to the RAFT agent *i*. The latter is more favorable due to its high chain transfer constant furnishing the intermediate radical *ii*. Two pathways are possible to occur after the formation of the intermediate radical. The propagated chain can fragment back to the radical species or the R-group is abstracted as a new radical from the intermediate radical species *iii*. By the right choice of the R-group, the solvent and the monomer, the last pathway should be the preferred one due to R being the favored leaving group. The R-radical therefore can act as new propagating chain end adding to monomer units and eventually add to another RAFT agent to release a new chain *via* the same mechanism. The reversible mechanism of addition and fragmentation allows one single radical to activate a high amount of RAFT agent molecules. The number of active chains is therefore determined by the initiator concentration and the number of polymer chains is related to the amount of RAFT agent. The controlled character of the RAFT process hence originates from only a small amount of active radicals being present and the majority of chains is deactivated as thiocarbonylthio end capped

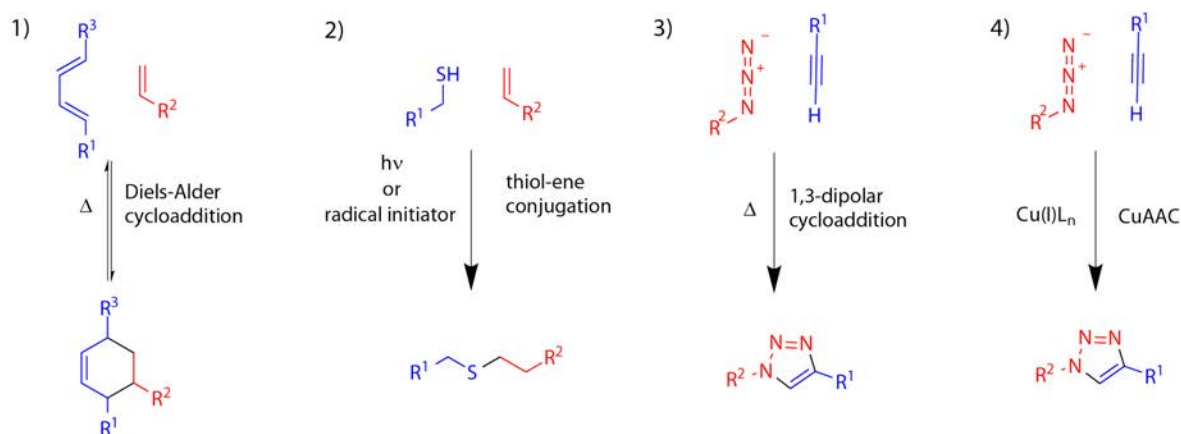
“dormant” species. As soon as all RAFT agents are activated and the pre-equilibrium is reached, the polymerization enters the main equilibrium of the RAFT process. This phase involves the degenerative transfer of the thiocarbonylthio species between the polymer chains *via* the radical intermediate *iv*. Therefore, propagating chain growth of all polymer chains occurs with the same probability. Since the RAFT process is still a radical polymerization, irreversible terminations such as recombinations, H-atom abstractions, and disproportionation reactions do still occur, however, with a lower probability due to the low concentration of active radicals during the polymerization.

The benefit of RAFT/MADIX polymerizations in contrast to ATRP is on the one hand the lack of toxic transition-metal complexes and on the other hand the higher diversity of the polymerization reaction. Thus, almost all polymers produced *via* free radical polymerization can be polymerized with RAFT/MADIX techniques as long as a suitable CTA is provided to afford the necessary control. Moreover, the RAFT/MADIX process can be carried out in aqueous media similar to free radical polymerizations decreasing the utilization of toxic chemicals.<sup>104</sup> Only slight limitations are given by the design of the CTA allowing different architectures and functionalities at the end groups of the polymers, such as azide, alkyne, or carboxylic acids.<sup>105</sup> This enlarges the scope of possible block copolymers *via* different conjugation reactions. Furthermore, the polymer chains are still connected to the CTA when the reaction is terminated allowing a block copolymer formations with a different monomer. The chain transfer group can be easily functionalized or even removed if necessary, which facilitates possible biomedical applications.

Controlled polymerizations are versatile and functional tools for the synthesis of defined block and highly specialized block copolymers. The use of biomacromolecules or biopolymers as blocks is rather challenging. Some reports describe the transformation of a biopolymer to act as a macro initiator for RDRP,<sup>99</sup> but due to the high density of functional groups or solubility issues the attachment of a single initiating group is very challenging. Therefore, most block copolymers containing a natural derived block have to be synthesized in an additional step, namely a conjugation reaction.

As described previously, polymers synthesized *via* controlled polymerization techniques can be easily functionalized with various end groups, such as alkynes, azides, alcohols, or thiols.

Furthermore, end groups of biomacromolecules can be functionalized in a similar fashion, however, with a higher expenditure. The benefit of these functionalizations arises with the application of conjugation reactions, i.e. reactions that are able to conjugate two different polymers to a block copolymer which cannot be synthesized directly. As shown in Scheme I.5, several techniques for a conjugation between two polymer blocks are known. Among these techniques thermal Diels-Alder cycloadditions of conjugated dienes are less common since they usually require high temperatures.<sup>106, 107</sup> Nonetheless, the reversibility of a Diels-Alder reaction can be beneficial for material sciences in terms of self-healing applications and crosslinking.



**Scheme I.5** Schematic reaction pathways for conjugation reactions: 1) Diels-Alder cycloaddition of a conjugated diene and an alkene; 2) thiol-ene conjugation of a primary thiol and a terminal alkene; 3) thermal 1,3-dipolar cycloaddition of an azide and a terminal alkyne and 4) copper(I) catalyzed azide-alkyne cycloaddition.

A more versatile and straightforward conjugation reaction is the light or radical initiated thiol-ene conjugation reaction. Here, a thiol reacts *via* a radical addition to an alkene in an anti-Markovnikov fashion.<sup>108</sup> The initiation occurs either by a photon or a radical making the conjugation more facile to conduct in comparison to thermal Diels-Alder cycloadditions.<sup>109, 110</sup> Furthermore, thiols can be frequently found in biomacromolecules such as enzymes or peptides or attached as functional groups similar to alkene functionalities.<sup>111</sup> Thiol-ene conjugations are therefore a very versatile approach for the formation of bio-derived block copolymers and complex polymer architectures.<sup>108</sup>

The most frequently used conjugation technique in polymer science is the 1,3 dipolar cycloaddition of azides and alkynes discovered by Huisgen et al. (Scheme I.5-3).<sup>112</sup> Since the reaction requires high thermal energy, it was rather disregarded in polymer science until Sharpless and coworkers discovered a transition metal catalyzed pathway for this cycloaddition



reaction.<sup>113</sup> The cycloaddition is mediated by a Cu(I) catalyst and can be carried out at room temperature in various solvents with almost quantitative conversion. The improvement of the Huisgen 1,3-dipolar cycloaddition to a copper(I) catalyzed azide alkyne cycloaddition (CuAAC) created a high impact due to its high conversions and the uncomplicated conjugation conditions.<sup>114, 115</sup> The application of CuAAC reactions opened a new pathway for the synthesis of highly functionalized polymer architectures such as dendrimers and the introduction of functional groups to polymers.<sup>116-118</sup> Moreover, 1,3-dipolar cycloadditions proved to be applicable in bio-orthogonal chemistry, too.<sup>119, 120</sup>

The development of novel controlled block copolymer conjugation techniques facilitated the synthesis of block copolymers addressed for biomedical applications. Polymers with special functionalities can be easily synthesized and conjugated with other polymers to match with the targeted properties for the desired applications.

### 1.3. Self-Assembly of Block Copolymers

In similarity to mixtures of homopolymers, linear block copolymers rarely form homogeneous mixtures. Due to thermodynamic reasons, the separate polymer blocks are not miscible with each other. Therefore, demixing of the polymer blocks occurs in the bulk state or in the polymer melt. The phenomenon can be described by the Gibbs free energy of mixing.

$$\Delta G_{\text{mix}} = \Delta H_{\text{mix}} - T\Delta S_{\text{mix}}$$

**Equation 1**

The mixing of a block copolymers polymer blocks is only favorable for a positive  $\Delta G_{\text{mix}}$ . The crucial parameters for the determination of whether mixing or demixing takes place can be found in the free enthalpy term of mixing  $\Delta H_{\text{mix}}$ . The term describes the interaction between the different polymer blocks depending on the block copolymer composition.

$$\Delta H_{\text{mix}} \approx k_{\text{B}}T\chi\phi(1 - \phi)$$

**Equation 2**

$k_{\text{B}}$  is the Boltzmann constant,  $T$  the temperature,  $\phi$  the monomer fraction of the polymer, and  $\chi$  the Flory-Huggins parameter. The equation relates from the model described by Flory and Huggins in the 1940s and gives a mathematical approach towards the determination of the segregated block copolymer phases.<sup>121, 122</sup> Originally developed to describe the interaction of polymers with solvent molecules, the Flory-Huggins theory can be applied to describe the

formation of microdomains of a block copolymer.<sup>123</sup> In order to assess the structure of the phase equilibrium of the microdomains, two parameters must be known: The fraction  $f$  of monomers A in a polymer chain and the product of the Flory-Huggins parameter of the segment-segment interaction with the polymerization index  $\chi_N$ . The monomer fraction  $f$  can be determined *via* the fraction of the number of monomers A,  $N_A$  by the index of polymerization.<sup>124, 125</sup>

$$f = \frac{N_A}{N}; \text{ with } N = N_A + N_B; N_A \gg 1; N_B \gg 1$$

**Equation 3**

The Flory-Huggins parameter  $\chi$  determines the interaction of a chain segment of polymer A with another segment of polymer B.<sup>121, 122</sup> In order to understand the driving forces of a block copolymer microphase separation, a closer look on the fundamentals of a block copolymer melt is necessary.<sup>123</sup> The compressibility of a molten polymer is close to zero and the reduced density of the monomers A and B,  $\rho_A$  and  $\rho_B$  of the overall melt is constant. However, local fluctuations in the reduced density occur leading to the microphase separation for positive  $\chi$ . The reason for this is the attempt of the system to minimize the Gibbs energy  $\Delta G_{\text{mix}}$ . In the case of positive  $\chi$ , the monomer segments of A and B repel each other in order to minimize the contacts between monomer A and monomer B and counteract the density fluctuations. The whole system conclusively reduces the mixing energy while on the other hand decreasing the entropy of the system. The two thermodynamic values  $\Delta G_{\text{mix}}$  and  $\Delta S_{\text{mix}}$  therefore compete and a mixing or demixing of the polymer blocks is dependent on the Flory-Huggins parameter  $\chi$ .<sup>126</sup>

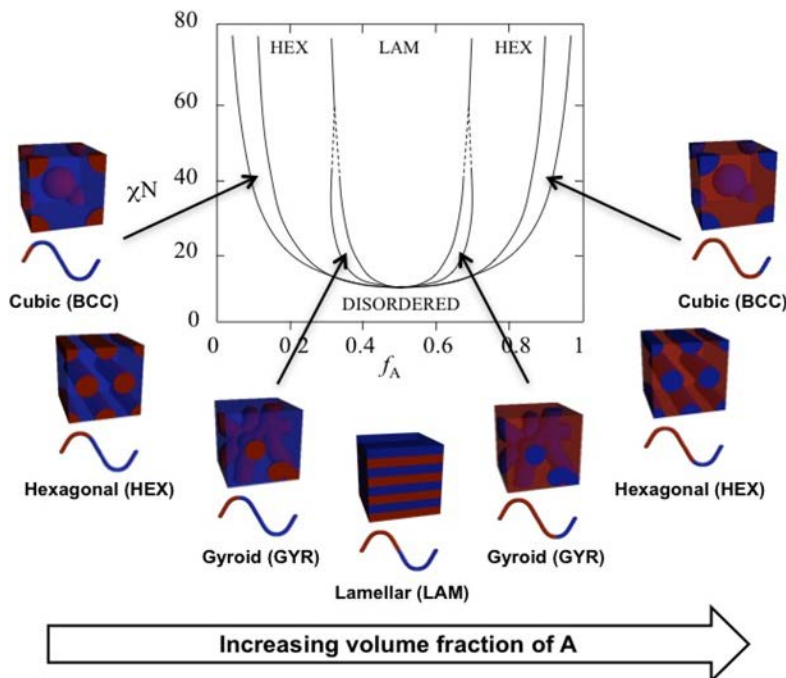
$$\chi = \frac{A}{T} + B$$

**Equation 4**

The constants  $A$  and  $B$  are system dependent constants and  $T$  is the temperature.

The morphology of these microphase domains after the demixing of the polymer blocks is strongly dependent on the demand of space of the specific polymer blocks. If the block A has the same spatial demand as block B ( $N_A = N_B$ ), the block copolymer aligns in alternating lamellar structures of segregated polymer fractions. The segment therefore usually consists of two layers of polymer due to the demand of tightest packing of the lamellar phases. As soon as the spatial demand of the polymer block A increases so that tightest packing does not fit into a lamellar phase any more, the phase deforms in order to maintain the tightest packing in a different domain structure (Scheme I.6). The morphological outcome of deformation is determined by the demand

of tightest packing of the polymer blocks and can be described with the Flory-Huggins theory.<sup>125,</sup>  
<sup>127</sup> In a simplified fashion, the theory describes that the alteration of the Gibbs energy  $\Delta G_{\text{mix}}$  for a block copolymer depends on the volume fraction  $f$  of one of the polymer blocks (Scheme I.6). For the given idealized model system of an A-B type linear block copolymer in Scheme I.6 with an exemplified value of  $\chi_N$  of 40, a movement from the y-axis from a volume fraction of block A  $f_A$  from 0 to 0.1, the phase system is still in a disordered state.<sup>126</sup> A further increase in  $f_A$  increases the tendency of the system to minimize the A-B contacts and spherical domains are observed as a result of the low volume fraction of A. The spherical phase at given  $\chi_N$  is present until  $f_A$  is increased to 0.15 and the volume fraction is too large to form spheres of polymer block A, the formation of hexagonal phases of block A in block B is observed. This microdomain phase is stable until an increase in  $f_A$  to 0.31 leads at first to the formation of a small bicontinuous gyroidal phase followed by the formation of lamellar domains at a volume fraction of 0.33. The lamellar domains are stable for a volume fraction between 0.33 and 0.66. As the phase diagram is symmetric, further increase leads to  $f_A$  being the predominant polymer fraction and first gyroidal followed by cylindrical domains of polymer block B in polymer block A are formed. A further increase in  $f_A$  subsequently results in spherical domains of B in A and finally a disordered phase of B in A is formed. The schematic phase diagram of an AB type block copolymer (Scheme I.6) nicely displays the immiscibility of two different polymer blocks in bulk and in a polymer melt. Altering the volume fraction of one block and therefore its spatial demand affects the morphology of the sample.



**Scheme I.6** Schematic phase diagram of an AB type block copolymer. With increasing volume fraction of block A the phase composition shifts from cubic to hexagonal to gyroid and to lamellar with increasing volume fraction of polymer block A  $f_A$ . Further increase in  $f_A$  inverts the morphology stepwise.<sup>a 126</sup>

This observation is already very captivating in terms of applications for material science.<sup>128, 129</sup> Moreover, the phase separation behavior is not only limited to bulk block copolymers but can be observed in block copolymer solutions as well. The most prominent examples for the phase separation in solution are amphiphilic block copolymers with their variety of structural morphologies.<sup>130</sup>

The phase separation of amphiphiles in solution has already been known for a very long time as it is the essential criterion for every single organism on earth. Starting from simple microorganisms to highly specialized mammals, the phase separation of amphiphilic phospholipids in aqueous solutions is the key element of life, e.g. the formation of bilayers, vesicles, and cell walls to separate and protect the interior from the environment. The ability of compartmentalization furthermore plays a crucial role for nutrient transport and DNA protection. Starting from the discovery in the 1960's that bio-membranes and

<sup>a</sup> Terms of use: The scheme adapted from "Design and Application of Nanoscale Actuators Using Block-Copolymers" by Joshua M. G. Swann; J. M. G. Swann and P. D. Topham, *Polymers*, 2010, 2, 454 is licensed under CC BY 3.0.

-vesicles are composed of lipids,<sup>131</sup> further investigation of the bilayer structures of lipids led to many advances in the fundamental understanding of liposomes and to various technological advances with respect to health care and drug delivery.<sup>24</sup>

The possibility of amphiphilic self-assembly in aqueous solution to mimic and investigate biological systems with synthetic and bio-derived amphiphiles and their transformation towards applications in biomedicine and material science had a large impact on polymer science. Amphiphiles are composed of a water soluble hydrophilic and a water insoluble hydrophobic part which are attached together *via* a single linkage. The most prominent example of amphiphiles in nature are phospholipids, i.e. trisubstituted esters of glycine containing two fatty acids as hydrophobic tail and a hydrophilic phosphoric acid head group. The driving force for the phase separation of amphiphiles in solution is the strong contrast in solubility between the different parts. The water insoluble hydrophobic part of the amphiphile attempts to minimize the contact with water molecules leading to a microphase separation where the hydrophobic part is shielded from the aqueous phase by the hydrophilic head groups. In analogy to the phase behavior of block copolymer melts, the structure of the phase separated amphiphiles is dependent on the volume fraction of the hydrophobic part  $v$ . Depending on  $v$ , structures such as spherical or cylindrical micelles, but also lamellar phases and vesicular structures can be observed.<sup>132</sup> Due to the amphiphilic system being in solution, further factors have to be taken into account in order to describe the structure of the phases. As the hydrophobic building block moieties aggregate in order to leave no area exposed to water, the length of the hydrophobic part and the volume it demands are important structure determining parameters. In order to estimate the shape of self-assembled structures of amphiphilic structures, the curvature of the hydrophobic-hydrophilic interface has to be known, which is related to the packing parameter of surfactants  $v/al$ :

$$p = \frac{v}{al} = 1 + Hl + \frac{Kl^2}{3}$$

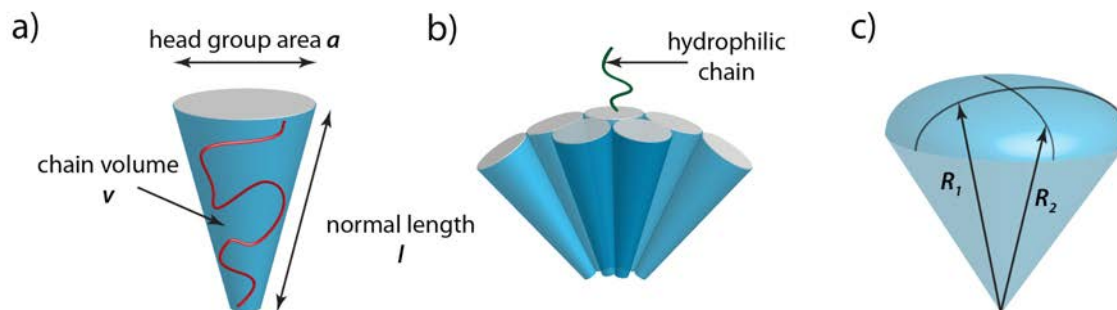
**Equation 5**

The equation reported by Hyde et al. implements the general geometric properties of the hydrophobic block to the interface description *via* the mean curvature  $H$  and the Gaussian curvature  $K$ , where  $v$  is the volume one hydrophobic chain occupies,  $l$  the length normal to the hydrophobic-hydrophilic interface and  $a$  the area that the hydrophilic head group is occupying (Scheme I.7a).<sup>130, 133</sup> Since the hydrophobic chains pack as dense as possible to exclude water

(Scheme I.7b), the separate curvatures can be summarized by applying  $H$  and  $K$ , which are given by two radii of curvature  $R_1$  and  $R_2$  (Scheme I.7c),

$$H = \frac{1}{2} \left( \frac{1}{R_1} + \frac{1}{R_2} \right) \text{ and } K = \frac{1}{R_1 \cdot R_2}$$

Equation 6



**Scheme I.7** Description of the amphiphile shape in terms of a) the volume fraction of the hydrophobic part, b) tightest packing of amphiphiles in order to minimize contact to water molecules, and c) the curvature model to describe the overall curvature of the self-assembled structure.

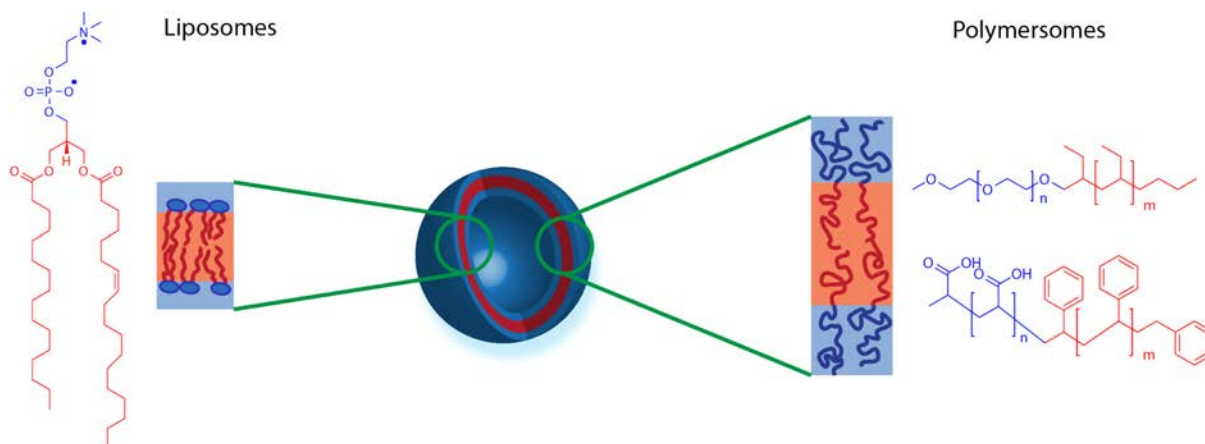
$p$  is related to different shapes of the amphiphilic aggregates. Whereas amphiphilic bilayers possess a  $p$  of 1, vesicles most likely form at  $1/2 \leq p \leq 1$  and micelles are observed for  $p \leq 1/3$ .<sup>23</sup>

The knowledge on the geometric requirements in order to form spherical aggregates from amphiphiles enabled the precise application of block copolymer synthesis to form amphiphilic micelles, bilayers, and vesicles of different size and shapes.

The general physical background for the phase separation of amphiphiles in solution can as well be transferred to amphiphilic block copolymers leading to a large amount of interesting structures. The development of controlled polymerization techniques led the way to precise amphiphilic block copolymers, e.g. polymers with a water soluble hydrophilic and an insoluble hydrophobic block. In contrast to bulk block copolymer self-assembly, the driving force for the phase separation of amphiphilic block copolymers in water is the insolubility of the hydrophobic block in the solvent in addition to the mutual immiscibility of the two different polymer blocks inside each other. In similarity to other amphiphiles such as lipids, the hydrophobic effect therefore leads to a phase separation where the hydrophobic block is expelled from the solvent.

Besides the formation of micelles, which can be used for templating of structures and frameworks,<sup>134, 135</sup> the formation of vesicles plays an important role in the investigation of amphiphilic molecules and block copolymers. Vesicles consisting of a self-assembled lipid bilayer structure (liposomes) attracted a lot of interest due to their broad range in applications as

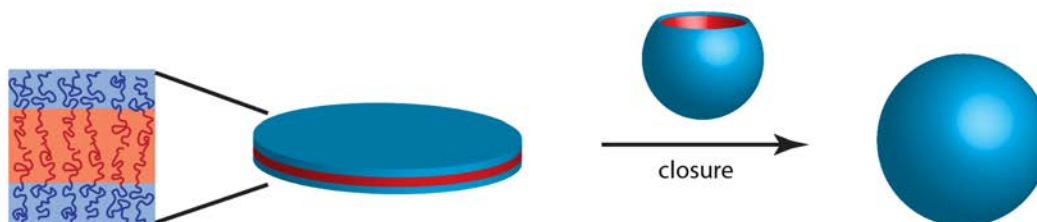
pharmaceutical carriers since their discovery by Alec Bangham.<sup>131, 136-138</sup> However, vesicles of amphiphilic block copolymers (polymersomes) were regarded to be a curiosum for a long time. The reason for that was the difference in the occurrence of bilayer structures in the phase diagrams of lipids and block copolymers.<sup>139</sup> Whereas lipids majorly form bilayer structures in their phase diagram, mostly micellar structures were observed in the phase diagram of amphiphilic block copolymers in solution.<sup>140</sup> The crucial value for successful polymersome formation lies in the chain length of the block copolymer,<sup>141</sup> i.e. the hydrophobic part has to possess a certain chain length in order to drive the self-assembly towards vesicular structures. The short lipids possess a strong contrast in hydrophilicity due to the polar and often charged head group and the short hydrocarbon tail, which displays strong hydrophobicity (Scheme I.8).



**Scheme I.8** Schematic differentiation between the double layer of self-assembled lipids and amphiphilic block copolymers to liposomes and polymersomes, respectively, emphasizing on the difference in the thickness of the double layer.

Amphiphilic block copolymers on the other hand possess two polymer chains of certain block lengths exceeding those of polar groups and fatty acids (Scheme I.8). As a result of this, the thickness of the bilayer and furthermore the corresponding structures can be varied *via* the length of the corresponding polymer blocks. However, vesicles do not form instantaneously as soon as the block copolymers are dissolved in a selective solvent. Since most amphiphilic block copolymers do not dissolve readily in water, e.g. polystyrene based block copolymers, a two-step procedure has to be applied: First the block copolymer is dissolved in a nonselective solvent for both blocks and subsequently water is added to encourage the aggregation of hydrophobic blocks.<sup>24, 141</sup> In the case of hydrophobic blocks with lower  $T_g$  such as poly(ethyl ethylene) (PEE), polymersomes can be obtained *via* direct preparation in water.<sup>25, 142</sup> The vesicle formation from

phase separated block copolymer layers occurs in both cases as follows.<sup>130-143</sup> The amphiphilic block copolymer first forms phase separated domains like spheres and rods to minimize the contact of the hydrophobic part with water. Subsequently lamellar areas are formed which close in the second step to form the vesicles (Scheme I.9).<sup>23</sup>



**Scheme I.9** Schematic illustration of the bilayer formation of amphiphilic block copolymers and their closure to polymersomes.

The radius of the lamellar phase is furthermore a key factor of the final size of the vesicle, determining the energy barrier which is required to bend the lamellar structure towards a spherical shape. The energy barrier can be overcome by applying several techniques of vesicle formation. As mentioned above, the addition of a co-solvent can drive phase separated layers to form vesicles. Moreover, the addition of charged surfactants or the introduction of very hydrophobic moieties such as fluorinated carbons can lead to the formation of polymersomes.<sup>144, 145</sup> A more frequently used technique of polymersome formation is the application of an electric field, i.e. the electroformation of vesicles.<sup>146-148</sup> Depending on the strength of the electric field and the applied amplitude, polymer vesicles of different sizes can be afforded. In addition, the  $T_g$  of the hydrophobic polymer blocks plays an important role on the structure of the polymersomes. Polymers with a high  $T_g$  such as polystyrene form rigid membranes whereas polybutadiene block copolymers possess a flexible membrane allowing further physical treatment of the vesicles such as extrusion for size adjustments.<sup>149</sup>

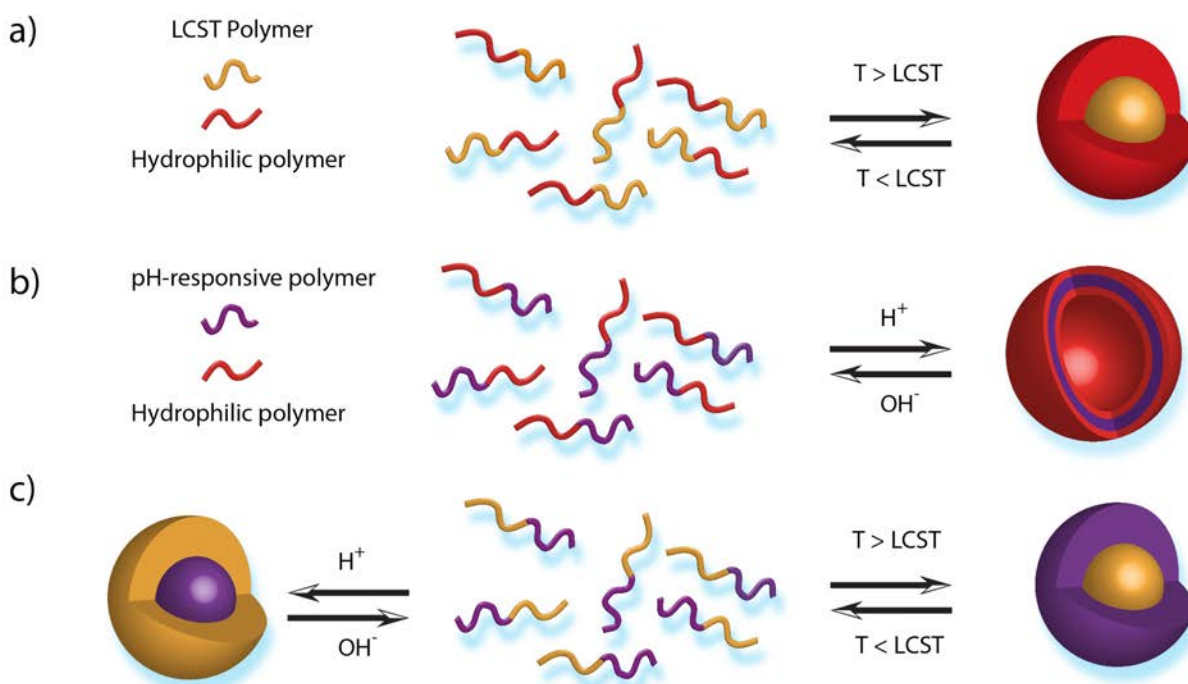
The impact of amphiphilic block copolymer vesicles has been increasing steadily since the early nineties, especially in terms of future applications. The hollow character of polymersomes immediately creates the desire to apply them as cargo system in medical fields as well as nanoreactors for material science. In order to be utilized as therapeutic component in medicine, polymersomes need to be composed of biodegradable or at least biocompatible polymer blocks, such as PEO, PVP, poly(*N*-(2-hydroxypropyl)methacrylamide) (PHPMA), and poly(ethylene-amine). Furthermore, bio(hybrid) polymers can be applied as an alternative to synthetic



polymers. In such way, oligo- and polypeptides, like poly(*L*-lysine) or poly(*L*-glutamate),<sup>150-152</sup> as well as carbohydrates and polysaccharides, e.g. dextran and hyaluronan,<sup>153, 154</sup> were already applied as blocks for amphiphilic polymersome preparation. Those polymer blocks which can be obtained from natural sources or are derived from natural building blocks, possess a high biocompatibility and are readily accessible towards functionalization increasing their versatility in biomedical applications.<sup>155, 156</sup> In contrast to liposomes, the polymersome membrane is denser and therefore more robust leading to a higher stability of the structures as well as decreased leaking probability. The increased stability is beneficial as it increases the circulation time of polymersomes in the blood stream but it also generates certain problematics with directed drug delivery. Being designed for drug delivery applications, the polymersomes have to release their target molecules at some point inside the body, either *via* disruption or controlled diffusion through the membrane. In order to address the issue of release, several approaches were developed. The most straightforward approach for the disruption of polymersomes with natural derived polymer blocks is the biodegradation. This can be carried out either by pH or enzymatic.<sup>157, 158</sup>

More advanced disruption techniques are conducted with redox<sup>159</sup> or UV light *via* the implementation of responsive polymers or the introduction of a UV-active protein to disrupt the membrane and release the target compounds.<sup>160, 161</sup> The second approach targets the controlled permeation of the incorporated substances by maintaining the polymersome structure. Therefore, pores need to be incorporated into the polymersome membrane. This can be either conducted *via* semi permeable membranes that form pores upon external triggers,<sup>162</sup> such as temperature,<sup>163</sup> pH,<sup>164</sup> or more sophisticated with the introduction of transmembrane proteins.<sup>165, 166</sup> In the case of enzyme therapy, the design of semi permeable membranes where reactants can enter and leave the vesicle, but the enzyme is kept inside is a very important topic in current research. The so called nanoreactors promise a versatile system for locally separated reaction systems. Lecommandoux and coworkers presented an interesting multicompartmentalized polymersome system, which can be regarded as a model cell mimic.<sup>167, 168</sup> The group showed a pathway to form a polymersome in polymersome system, where the encapsulated polymersome nanoreactors were able to conduct specific reactions in a cascade system simplifying reaction cascades in real cells.

A sub-type of amphiphilic block copolymer self-assembly is the application of pH or temperature sensitive blocks as the hydrophobic part. Polymers such as poly( $\epsilon$ -caprolactam) and poly(*N*-isopropyl acrylamide) (PNIPAM) possess a strong thermo-responsivity<sup>169</sup> being hydrophilic up to a certain temperature, the lower critical solution temperature (LCST). Below this temperature the polymer is capable of forming hydrogen bonds with the water molecules due to a positive contribution to the free energy of mixing  $\Delta G_{\text{mix}}$ . The antagonist of the positive contribution is the entropy term  $-T\Delta S_{\text{mix}}$ , which contributes negatively to  $\Delta G_{\text{mix}}$  due to the higher ordered state. As soon as  $T$  reaches the point where  $\Delta G_{\text{mix}}$  becomes positive, the hydrophilic polymer does not favor polymer-solvent contacts anymore but prefers polymer-polymer interactions leading to a phase separation of polymer blocks and water resulting in a clouding of the solution.<sup>170</sup> The second external trigger that can be applied to form structures such as micelles, vesicles, or particles is a change in pH if one block displays certain pH responsivity. Polymers like poly(*N,N*-dimethylaminoethyl methacrylate) (PDMAEMA) and poly(acrylic acid) (PAA), and additionally some synthetic peptides are commonly well soluble as ionic species, but turn insoluble as soon as their neutralized, either by base or by acid.<sup>171, 172</sup>



**Scheme I.10** Schematic behavior of a) a block copolymer with a thermo-responsive, b) a pH-responsive block upon the external trigger is applied and c) a schizophrenic block copolymer. The change in morphology is exemplified with a core shell particle for a) and a vesicular structure for b). The schizophrenic block copolymer displays an inversed aggregation behavior depending on the applied stimuli.

Various applications of these stimuli responsive block copolymers can be found in literature,<sup>170, 173, 174</sup> e.g. the formation of thermo-responsive functionalized surfaces and the preparation of “smart” particulate systems.<sup>173, 175, 176</sup> Especially PNIPAm is due to its LCST within the physiological range a frequently applied thermo-responsive polymer block in biomedical applications.<sup>177, 178</sup> Among the stimuli responsive block copolymer self-assemblies one very interesting type are dual responsive block copolymers, e.g. block copolymers that bear two different responses to external stimuli at the same time, such as a pH and temperature dependence, or pH, and redox responsivity.<sup>179</sup> Structures from these block copolymer types are of peculiar interest for biomedical applications since different levels of pH can be found in the human body as well as different enzymes or cells with a suitable redox potential for the targeted application.<sup>172, 179</sup> A more fascinating subspecies of the dual responsive hydrophilic block copolymers are schizophrenic block copolymers.<sup>180, 181</sup> Schizophrenic block copolymers for instance consist of two hydrophilic blocks where one shows LCST behavior and the second is pH responsive. If the block copolymer solution is heated above the LCST of the corresponding thermo-responsive block, aggregates such as micelles are formed to shield the now hydrophobic moiety of the block copolymer. A change in pH on the other hand results in the second pH-responsive block becoming hydrophobic (Scheme I.10c). This inverted aggregation is called schizophrenic behavior. Smith et al. demonstrated this principle very nicely with PDMAEMA-*b*-PNIPAm block copolymers.<sup>180</sup>

#### 1.4. *Purely Hydrophilic Block Copolymers*

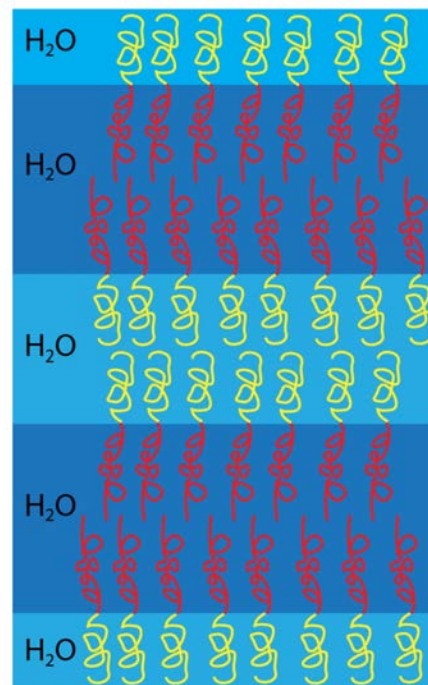
The structural diversity of amphiphilic block copolymers in solution opened a new pathway for biomedical applications.<sup>34, 182, 183</sup> The formation of amphiphilic micelles and vesicles for drug delivery with precisely synthesized block copolymers is still a very important topic in current research.<sup>184</sup> Nevertheless, there are some issues to be dealt with when applying amphiphiles as drug delivery agents. The self-assembly of commonly applied polymersomes is very efficient due to the hydrophobic effect and usually leads to the formation of a dense membrane structure. Therefore, several functionalization steps have to be applied to the vesicular or particle structure in order to trigger the disassembly of the structures and the release of the incorporated species. The introduction of degradable blocks and functionalities or channel pores is a challenging task and requires high synthetic skills and is time consuming and expensive. Furthermore, most

synthetic hydrophobic polymers are not very biocompatible and applications inside the body should be considered with caution.

Future applicability demands the development of a delivery system which is completely biocompatible or in the best case biodegradable and is able to be disassembled when the target compartment in the body is reached. Since the use of amphiphilic block copolymers for drug delivery applications requires high synthetic effort, a system containing two hydrophilic polymers attracts more and more attention. Moreover, a decent number of hydrophilic polymers is derived from biological structures and possesses good biocompatibility.

The main question arising now is how block copolymers formed by two hydrophilic blocks can act as transport system in aqueous solution. The answer is a strong difference in hydrophilicity. In contrast to common expectations, the incompatibility of two hydrophilic blocks in aqueous solution does exist and is already applied in science. A very important example is the demixing of concentrated aqueous dextran and PEO solutions. Thus, two phase systems of PEO and dextran are frequently used for the partitioning of proteins.<sup>185, 186</sup> The two hydrophilic and high molecular weight polymers do not mix with each other and therefore behave similar to polymer blends. Furthermore, the demixing of concentrated solutions as of two hydrophilic polymers was applied for stabilization of emulsions. Thus, it was possible to stabilize water in water pickering emulsions of microgels with in concentrated solutions of dextran and PEO.<sup>187-190</sup> Moreover, the demixing of two hydrophilic polymers should rely on the same fundamental concepts as it is the case for hydrophobic polymer mixtures and amphiphiles. A mixture of two different polymers in solution is due to the positive Gibbs free energy of mixing in most cases less favorable than a two phase system.<sup>188</sup> However, in the case of two hydrophilic polymers, the tendency of phase separation is in most cases less predominant and is usually observed for mixtures of high molecular weight polymers and highly concentrated solutions. A more interesting case is the study of aqueous systems containing double hydrophilic block copolymers (DHBC), i.e. block copolymers containing two different hydrophilic blocks. The two blocks therefore should fulfill the criteria of possessing no hydrophobic moieties since the self-assembly can consequently be driven by the insolubility of the hydrophobic part. Furthermore, thermo- and pH-responsivity should be avoided in order to obtain a pure hydrophilic self-assembly and study the interaction of the two hydrophilic block copolymers. By following the fundamentals of block copolymer self-assembly, it should be possible that this kind of block copolymers perform microphase

separation and self-assemble to structures due to their immiscibility similar to amphiphiles. The first observation in that regard was reported by Taubert et al. displaying a phase separation of PEO-*b*-PMeOx block copolymers in concentrated solutions.<sup>191</sup> The group investigated the presence of lyotropic mesophases of PEO-*b*-PMeOx at high concentrations of 60% to 70% in the nonselective solvent water. Taubert et al. attributed this microphase separation to the demixing of PEO and PMeOx blocks despite both being hydrophilic. As shown in Scheme I.11, a layer by layer stacking of water phases stabilized by PEO-*b*-PMeOx is assumed by Taubert and coworkers. Furthermore, PEO-*b*-PMeOx lyotropic mesophases possessed a structure directing platform for the formation of highly porous calcium phosphate (CaP). In contrast to previously applied hydrophilic block copolymers containing a polyelectrolyte block, such as PEO-*b*-PMAA and PEO-*b*-PSS as crystallization agent, the concentration of block copolymer had to be strongly increased in order to afford successful crystallization.<sup>192-194</sup> Nonetheless, this work was the first report of a phase separation of purely hydrophilic block copolymers. The aqueous self-assembly of purely hydrophilic DHBCs was rather neglected until 2009, when Ke et al. reported the findings of associates of the DHBC PEO-*b*-PDMA in the nonselective solvent water.<sup>195</sup> Ke and coworkers observed block copolymer aggregates with an apparent radius of 140 nm *via* DLS at concentrations between 0.3 mg·mL<sup>-1</sup> and 2.0 mg·mL<sup>-1</sup> in addition to the signal of free dissolved block copolymer. SLS measurements indicated that the structures of these aggregates are composed of a number of several associated polymer chains in a microdomain fashion and do not form micelles. Additionally, several factors that could possibly affect the self-assembly behavior, such as unreacted PEO chains, temperature, concentration, and block length of PDMA were investigated. The results suggested a self-assembly mechanism that is independent of temperature and other external stimuli. The extent of the associate formation slightly depends on the block copolymer concentration and on the block length of PDMA. Ke and coworkers attributed the self-assembly to the difference in interaction



**Scheme I.11** Schematic lyotropic mesophases of concentrated solutions of block copolymer as proposed by Taubert et al.

between the polymer block and the water molecules, which is the difference in hydrophilicity, respectively. This report was the first to state the possibility to form structures *via* the self-assembly of purely hydrophilic block copolymers at low concentrations.

In 2012, Casse et al. observed a similar self-assembly behavior with the DHBC PEO-*b*-PMeOx at low concentrations *via* DLS.<sup>196</sup> It was demonstrated that the block copolymer possesses a certain tendency to form aggregates with a hydrodynamic radius of approximately 100 nm that could be detected *via* DLS/SLS and furthermore observed in TEM micrographs in the form of collapsed structures. However, the amount of these aggregated structures was rather low in contrast to free dissolved block copolymer. Therefore, the results obtained from DLS and TEM were contradictory to the findings of the isothermal titration calorimetry (ITC), small angle X-ray scattering (SAXS), and analytical ultracentrifugation (AUC). The latter experiments could not confirm the presence of the observed aggregates. A certain confirmation and a rough quantification of the aggregated structures could be afforded *via* the application of diffusion NMR measurements resulting in approximately 2% of the block copolymer being self-assembled to the observed structures. Again, the authors attribute the formation of the self-assemblies to a difference in the water uptake and therefore hydrophilicity of the two different blocks with the self-assembly being governed by the Laplace pressure and the osmotic pressure between the two polymer domains, respectively.

A theoretical insight into DHBC microphase separation and self-assembly in aqueous solution was presented by Wu et al.<sup>197</sup> It was demonstrated, that the driving forces for phase transition is on the one hand depending on the volume fraction and concentration of the copolymer in similarity to amphiphilic block copolymers and on the other hand different hydrophilicities of the two blocks. The more hydrophilic polymer possesses a higher volume fraction due to increased swelling than the second, less hydrophilic block, which leads to a phase transition. For DHBCs with the same hydrophilicity on the other hand, the chain length is the substantial criteria for a phase transition. Thus, morphologies such as lamellar, gyroid, and cylindrical could be predicted, but also the presence of spheres in aqueous solution was shown from the calculations. This report further supports the observations of Taubert, Ke, and Casse on the self-assembly of DHBCs by giving this neglected block copolymer type a base for applications. An additional confirmation for the self-assembly of DHBCs in aqueous solution was reported by Blanzas and coworkers, who investigated the microphase separation behavior of PEO-*b*-poly[2-(methacryloyloxy)ethyl

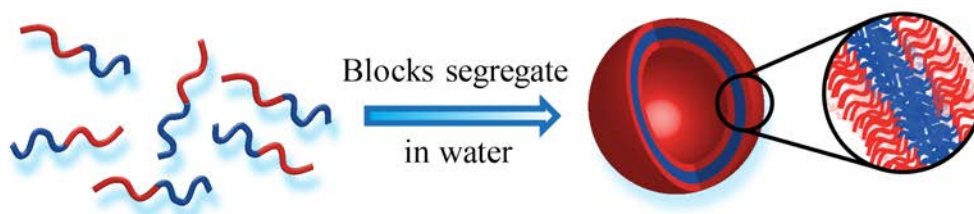
phosphorcholine] (PEO-*b*-PMPC) block copolymers.<sup>198</sup> The phase transitions of high concentrated block copolymer were monitored with SAXS and wide angle X-ray scattering (WAXS) showing that upon increased block copolymer concentration to 50 wt.% the prior present disordered phase forms hydrated lamellar structures. A further increase in concentration to 70 wt.% afforded hydrated hexagonally packed morphologies. Blanzas and coworkers attributed the microphase separation to the folding and unfolding of the PEO block at different hydration states. This report displays a nice proof of principle for aqueous DHBC self-assembly, despite one block being zwitterionic and the self-assembly being enhanced by the occurring ionic attractions.

Whereas the presence self-assembled aggregates observed by Ke et al. with PEO-*b*-PDMA and Casse et al. with PEO-*b*-PMeOx were rather difficult to confirm due to their low abundance in dilute solutions, Brosnan et al. displayed the possibility to form giant vesicles from DHBCs *via* self-assembly of PEO-polysaccharide and polysaccharide-poly(sarcosine) block copolymers.<sup>199</sup> Taking advantage of the well-known phase separation tendency of PEO and polysaccharides, PEO-*b*-dextran and PEO-*b*-pullulan block copolymers as well as dextran-*b*-poly(sarcosine) were synthesized. All three DHBCs applied the key features of purely hydrophilic self-assembly, i.e. both blocks were hydrophilic and not miscible with each other in solution, neither display pH- nor thermo-responsivity. Bimodal particle size distributions similar to the distributions reported by Casse et al. were observed *via* DLS for the different DHBCs at concentrations between 0.1 and 1.0 wt.%. In contrast to previous reports, two different techniques were applied in order to visualize the shape of the self-assembled structure, cryogenic SEM, and optical microscopy of a concentrated solution. In both cases it was possible to observe vesicular structures. In the first case vesicles with diameters of about one micrometer and in the case of concentrated solutions between 15% and 25% vesicles with diameters between 5 and 20  $\mu\text{m}$  were observed by simply dissolving the block copolymers in water. Furthermore, the observed vesicles behaved similar to the aforementioned polymersomes including fusion, bursting, and encapsulation of smaller vesicles, displaying the analogy of amphiphilic and double hydrophilic structures. This was indeed the first observation of large spherical structures self-assembled from purely hydrophilic block copolymers. In addition to the remarkable observations, PEO-*b*-polysaccharide block copolymers bear another important feature of interest, namely biocompatibility. Therefore, self-

assembled structures of biocompatible DHBCs possess a huge potential to act as future drug delivery devices.

These reports on self-assembly of DHBCs mark the current state of the art. In order to develop a starting point for the work of this thesis, it is noteworthy to summarize the key features novel DHBCs with the ability to perform self-assembly in water and carrying the potential to be applied in biomedical fields.

The first and most important criterion for future DHBCs is the pure hydrophilicity of both polymer blocks. The blocks should not possess hydrophobic moieties. Furthermore, the polymer blocks should not display a pH or temperature response within physiological ranges. Moreover, polymer blocks of the DHBC can even possess charged moieties unless no pH responsivity can be assigned turning them hydrophobic. Another criterion reported by Brosnan et al. is the immiscibility of the two blocks with each other in solution. Aqueous solutions of homopolymer should not mix with each other, which would encourage a phase separation of the block copolymer in aqueous solution and leads to the formation of organized structures such as particles or vesicles (Scheme I.12). Therefore, the difference in hydrophilicity has to be significant to ensure an efficient phase segregation of the two hydrophilic polymer blocks. The block copolymers can be synthesized with controlled polymerization techniques or derived from biomacromolecules such as polysaccharides.



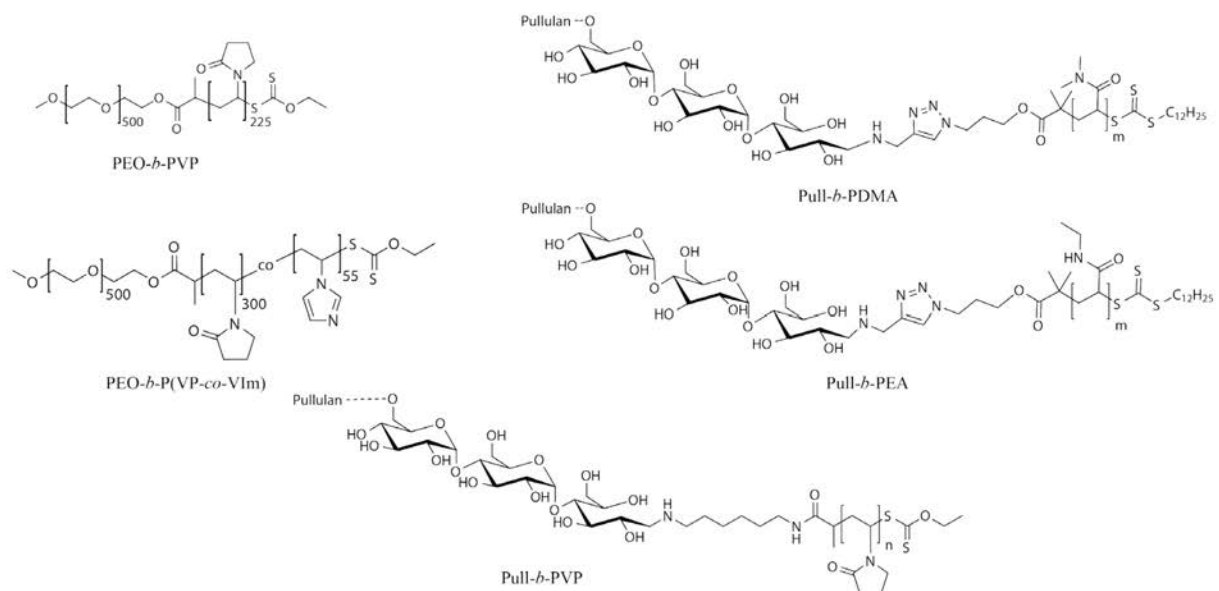
**Scheme I.12** Schematic self-assembly of DHBCs in water.

A potential benefit of the application of bio-derived polymer blocks is their biocompatibility. In combination with synthetic blocks of controlled size and functionality, potential drug delivery vehicles and nanoreactors could be generated from self-assembled DHBC vesicles.



## II. Outline

In order to investigate the general potential of DHBCs for biomedical and material science approaches, several combinations of hydrophilic polymer blocks were synthesized. The target blocks that should be investigated should fulfill the following criteria: The polymer block should be purely hydrophilic, meaning that no pH or temperature responsivity is present in a biological range. Hydrophilic polymers with a LCST between 20 and 50 °C such as PNIPAm can therefore not be applied. In terms of biocompatibility, ionic block copolymers without pH responsivity, such as PSS were not taken into account as well since the high charge density is regarded to be disadvantageous for drug delivery applications. Furthermore, the possibility to synthesize the polymer blocks with controlled polymerization techniques, such as RDRP or ROP techniques should be taken into account. The corresponding DHBCs were synthesized either by a block copolymerization or conjugated *via* CuAAC. Thus, the block copolymers containing PEO, pullulan, PVP, PDMA, and PEA were synthesized. The synthesis of the block copolymers was confirmed with SEC and <sup>1</sup>H-NMR measurements.



**Scheme II.1** DHBCs synthesized and analyzed during the investigations of the PhD thesis.

As the synthesized and investigated systems cover a broad spectrum of DHBCs and their self-assembly, only the aforementioned block copolymers are discussed in this thesis. Moreover, the emphasis of the current thesis was set to the block copolymer systems that led to a better

understanding of DHBC self-assembly or contributed to display the potential of DHBC particles and vesicles for future applications. Therefore, the first approach towards the investigation of DHBC self-assembly was conducted with a PEO-*b*-PVP block copolymer in Chapter III. The DHBC was synthesized *via* a RAFT/MADIX polymerization starting from a PEO macro RAFT chain transfer agent. The self-assembly behavior was studied with DLS and the according structures were visualized with LSCM and cryo SEM techniques. Furthermore, a crosslinker functionality in terms of the crosslinkable comonomer VIm was incorporated in order to preserve the self-assembled structures. The application bio-derived polymers and the use of conjugation chemistry to afford a DHBC were demonstrated in Chapter IV. Here, Pull-*b*-PDMA and Pull-*b*-PEA block copolymers were synthesized *via* CuAAC and the interesting novel self-assemblies were investigated *via* DLS, SLS, LSCM, and cryo SEM. The last chapter combines the achievements from the previous two systems by combining two biocompatible polymer blocks, i.e. pullulan and PVP. The DHBC was synthesized *via* RDRP and analyzed with the same techniques applied previously. Furthermore, a dual pH and redox responsive crosslinker was introduced in order to extend the applicability of the DHBC system. The structures self-assembled from Pull-*b*-PVP should therefore act as model compounds for future drug delivery vehicles with a responsive feature for disassembly.

### III. Organized Polymeric Submicron Particles *via* Self-Assembly and Crosslinking of Double Hydrophilic Poly(ethylene oxide)-*b*-Poly(*N*-vinylpyrrolidone) in Aqueous Solution

#### III.1. Preface<sup>a</sup>

The self-assembly behavior of DHBCs was mainly studied with block copolymers containing a PEO block with a variation of other synthetic polymers, such as poly(2-methyl-2-oxazoline),<sup>191, 200</sup> poly(*N,N*-dimethylacrylamide),<sup>195</sup> or polysaccharides, e.g. dextran and pullulan.<sup>199</sup> It turned out that all of these DHBCs formed aggregates ranging from particles to vesicular structures in dilute aqueous solutions. The key factor of the self-assembly to occur was attributed to a significant difference in the hydrophilicity of the two different hydrophilic blocks meaning that one polymer block has to possess a stronger hydrophilicity in contrast to the second hydrophilic block. Taking the possible applications of DHBCs in biomedicine into account, PEO is a viable and frequently referred choice. PEO is a hydrophilic biocompatible polymer which can be synthesized *via* controlled anionic ring opening polymerization (AROP) techniques.<sup>58, 59</sup> The interest in PEO occurs due to its stealth effect in the blood stream,<sup>201</sup> i.e. polymeric cargos containing PEO coatings are more difficult to be recognized by the immune system inside the blood stream and are therefore able to act as potential drug delivery carrier.<sup>20, 26, 28, 202</sup> Furthermore, PEO can be easily functionalized. Regular PEO and mono methylated PEO possess one or two hydroxyl groups respectively that can be functionalized with different molecules. Esterification for instance enables access to functional end groups with the ability to act as macro chain transfer agents for ATRP and RAFT polymerizations.<sup>99, 203</sup> Deprotonated terminal OH groups can act as initiators for oxyanionic polymerizations. In addition to this, derivatization of the hydroxyl groups can give access to alkyne and azide terminated PEO.<sup>204-206</sup>

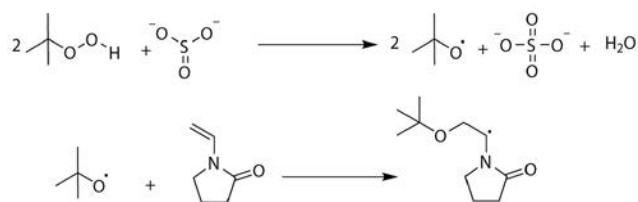
---

<sup>a</sup> Terms of use: This chapter was adapted with permission from J. Willersinn, M. Drechsler, M. Antonietti and B. V. K. J. Schmidt, "Organized Polymeric Submicron Particles *via* Self-Assembly and Cross-Linking of Double Hydrophilic Poly(ethylene oxide)-*b*-poly(*N*-vinylpyrrolidone) in Aqueous Solution"; *Macromolecules*, 2016, **49**, 5331-5341. Copyright 2016 American Chemical Society.

Those functionalized polymers can be used in cycloaddition reactions to synthesize a large number of block copolymers *via* copper catalyzed alkyne azide cycloaddition (CuAAC).<sup>207</sup>

Moreover, PEO is quite hydrophilic and has no lower critical solution temperature in a physiologic temperature range,<sup>208</sup> two key features in order to fulfill the criteria of a purely double hydrophilic self-assembly process, as it should be achieved in here. It has no hydrophobic moieties and readily dissolves in water up to high concentrations of more than 50%.<sup>191</sup>

Another interesting polymer fulfilling the demanded criteria of purely hydrophilic self-assembly is poly (*N*-vinylpyrrolidone) (PVP). PVP is a hydrophilic polymer with a vinyl backbone attached to a five membered lactone ring. PVP can be produced by free radical and RDRP techniques, such as ATRP and RAFT processes starting from a suitable initiator or chain transfer agent. Recent developments in RAFT/MADIX polymerizations improved the polymerization of *N*-vinylpyrrolidone (VP) to aqueous polymerizations at ambient temperatures.<sup>97, 209</sup> In contrast to RAFT polymerizations performed in organic solvents where AIBN and other thermal initiators were used, the system was transferred to a redox pair initiation system using the water soluble *t*-butyl peroxide (*t*-BuOOH) and sodium sulfite. The sulfite anion is oxidized to a sulfate anion and generates a *t*-butoxy radical in a sufficient rate. The *t*-butoxy radical can attack a monomer in the common radical polymerization fashion. The radical generating redox reaction takes place at ambient temperature and therefore allows running polymerizations at lower temperatures compared to commonly utilized systems (Scheme III.1).

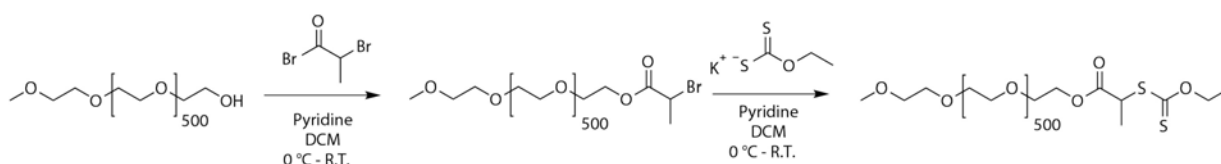


**Scheme III.1** Schematic radical generation with *t*-BuOOH/Na<sub>2</sub>SO<sub>4</sub> and radical addition to a VP monomer.

Due to the rather basic character, Na<sub>2</sub>SO<sub>3</sub> prevents the hydrolysis of VP, which occurs in acidic media. Furthermore, the redox potential of the oxidizing agent *t*-BuOOH is low enough to prevent direct VP oxidation. Therefore, the *t*-BuOOH/Na<sub>2</sub>SO<sub>3</sub> redox pair is well suitable for VP polymerizations in aqueous media.<sup>97</sup>

Pound et al. demonstrated the possibility to polymerize VP onto a PEO macro chain transfer agent using RAFT/MADIX polymerization techniques.<sup>99</sup> The monomethylated PEO chain was

functionalized with a xanthate end group capable of undergoing a chain transfer polymerization. These two important developments of the last decade allow a facile tunable synthesis of a DHBC in aqueous media, using less toxic reactants in comparison to common polymerization techniques (Chapter I.2). Furthermore, PVP offers two important properties that contribute to the conceptional idea of DHBC self-assembly. PVP shows no LCST behavior within the temperature region of 15 °C to 50 °C. The lack of a lower critical solution temperature is necessary in order to ensure a temperature independent self-assembly of the corresponding DHBC. In addition, PVP displays a good biocompatibility and is therefore already used in food additives and in biomedical fields, especially as blood plasma substitute and in drug delivery.<sup>210-213</sup> Recent reports by the group of Caruso lead to the application of PVP-*b*-poly(methacrylic acid) (PVP-*b*-PMAA) copolymers as carrier systems for DNA.<sup>214, 215</sup> In order to synthesize a DHBC that fulfills the requirements of a strong difference in hydrophilicity and containing no charged and thermo-responsive units, as well as a certain biocompatibility, PEO-*b*-PVP block copolymers are a viable choice. Starting from the abovementioned concept, this chapter contains the synthesis of a PEO-*b*-PVP block copolymer that possesses the ability to self-assemble to spherical structures. In order to synthesize the PEO-*b*-PVP block copolymer, 20 000 g·mol<sup>-1</sup> poly(ethylene oxide)-monomethyl ether was functionalized with a xanthate group in a two-step reaction (Scheme III.2).<sup>99</sup>



**Scheme III.2** Synthesis of PEO-macro xanthate chain transfer agent.

Recent reports by Casse et al. and Ke et al. employed PEO initiators with lower molecular weight ranging from 2000 g·mol<sup>-1</sup> to 5000 g·mol<sup>-1</sup> in order to synthesize PEO based DHBCs. In contrast to them, Brosnan et al. used a PEO with 20 000 g·mol<sup>-1</sup> as one DHBC building block. Regarding the resulted self-assembled DHBC structures from Ke et al. and Casse et al., where loose aggregates of PEO-*b*-PMOXA and PEO-*b*-PDMA block copolymer assemblies within the  $R_h$  range of 100 nm to 200 nm were found, Brosnan et al. were able to form giant vesicles with PEO-*b*-Pull and PEO-*b*-Dex block copolymers using a PEO block with a higher molecular weight. For that reason, the length of the single polymer chains should be taken into account and it appears that in the case of PEO chains with a higher molecular weight perform better in DHBC

self-assembly processes. Therefore, PEO with a molecular weight of 20 000 g·mol<sup>-1</sup> was employed.

As visible from the <sup>1</sup>H-NMR spectrum in Figure III.1b, monomethylated PEO was successfully functionalized with a xanthate end group. Furthermore, the SEC traces display a narrow *D* with an average number weighted molecular weight of 20 000 g·mol<sup>-1</sup> (Figure III.1c).

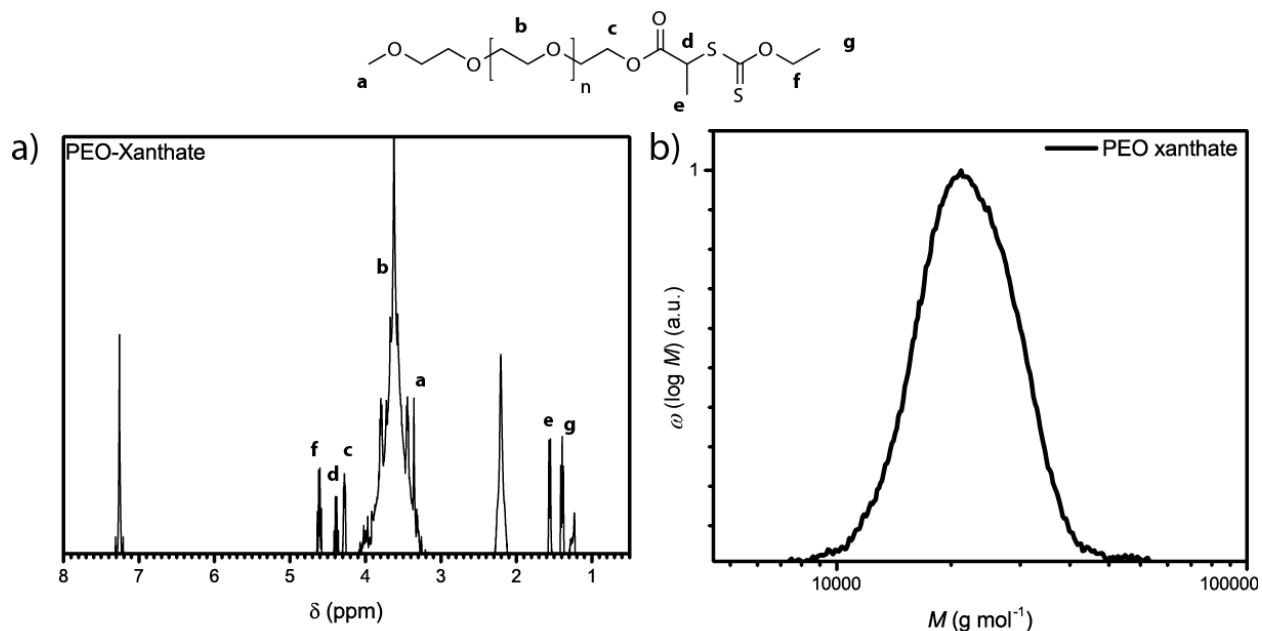
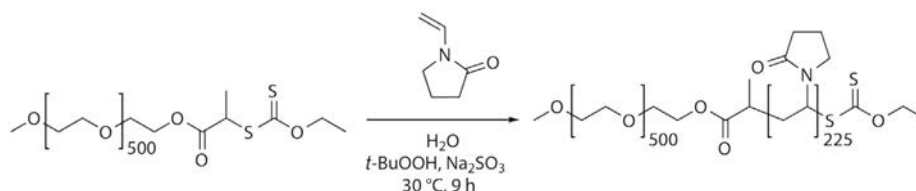


**Figure III.1a)** Scheme of PEO-xanthate; **b)** <sup>1</sup>H-NMR of PEO-xanthate recorded at 400 MHz in CDCl<sub>3</sub>; and **c)** corresponding apparent molecular weight distribution determined *via* SEC in NMP at 70 °C using a PEO calibration.

### III.2. Synthesis of PEO-*b*-PVP Block Copolymer

Starting from the aforementioned PEO macro RAFT chain transfer agent, block copolymerization of VP onto the PEO block was performed. As known from literature, controlled polymerization of VP is a challenging task. Even though Pound et al. reported a successful block copolymerization of VP with a short PEO-xanthate using AIBN in toluene at 70 °C, attempts to synthesize a PEO-*b*-PVP block copolymer with a longer PEO chain in a controlled synthesis were not successful. In fact, controlled polymerization of VP with standard techniques such as ATRP and RAFT/MADIX is still difficult. The occurrence of undesired side reactions of VP such as hydration of the C-C double bond or the irreversible dimerization of VP are known to terminate the active polymer chain in RDRP reactions in addition to general termination processes.<sup>99, 216, 217</sup> A detailed examination of different side reactions in VP

polymerization processes with xanthates was done by Pound et al. and Huang et al. showing that various factors, such as choice of xanthate, halogen impurities, and acidic conditions can lead to side reactions and irreversible termination reactions.<sup>216, 218</sup> For that reason, the polymerization procedure was changed to a redox based aqueous system described by Guinaudeau et al.<sup>209</sup>



**Scheme III.3** Redox initiated aqueous RAFT/MADIX polymerization of VP with a PEO-macro xanthate as chain transfer agent.

In order to optimize the block copolymerization of VP with a long chain PEO-macro CTA, the reported procedure had to be adjusted. As visible from Scheme III.3, the temperature was increased from 25 °C to 30 °C and reaction time decreased from 24 h to 9 h, respectively. It turned out that a longer PEO chain as macro chain transfer agent requires slightly elevated temperatures due to increased viscosity of polymerization solutions and less accessible chain ends. With proceeding reaction time, increased tailing due to termination reactions were observed. Therefore, it was decided to terminate the polymerization after a set time of 9 h in order to prevent side reactions and maintain a low  $\mathcal{D}$ . With the adjusted conditions, it was possible to afford PEO-*b*-PVP block copolymers with a good  $\mathcal{D}$  and acceptable monomer conversion.

**Table III.1** SEC and NMR summary of synthesized PEO-*b*-PVP block copolymers.

Block copolymer	$M_{n,app,SEC}$ ( $\text{g}\cdot\text{mol}^{-1}$ ) <sup>a</sup>	$\mathcal{D}$	VP incorporation ( <sup>1</sup> H-NMR) <sup>b</sup>	$M_{n,NMR}$ ( $\text{g}\cdot\text{mol}^{-1}$ )
PEO <sub>500</sub> -Xanthate	20 000	1.1	-	22 000
PEO <sub>500</sub> - <i>b</i> -PVP <sub>225</sub>	42 000	1.3	52%	47 000

<sup>a</sup> SEC apparent average weight distributions were obtained in NMP using a PEO calibration. <sup>b</sup> <sup>1</sup>H NMR were recorded in CDCl<sub>3</sub> at 400 MHz and 25 °C.

As shown in Table III.1, a PEO-*b*-PVP block copolymer containing 225 VP units was synthesized applying the abovementioned conditions. SEC traces display an apparent number weighted molecular mass of 42 000  $\text{g}\cdot\text{mol}^{-1}$  and a polydispersity of 1.3. Moreover, the SEC elugram in Figure III.2 displays a successful chain extension. Only slight tailing of the elugram

in Figure III.2a was observed. The broadening of the elution curve is a result of the aforementioned side reactions occurring during the RAFT polymerization of PVP. As visible from the corresponding number weighted molecular weight distribution curves in Figure III.2b and Table III.1, the molecular weight increased by  $22\,000\text{ g}\cdot\text{mol}^{-1}$ . The VP incorporation into the block copolymer determined by  $^1\text{H-NMR}$  was 52%. This value is rather low in comparison to reported VP polymerizations but can be attributed to the short reaction time. The resulted low  $D$  of 1.3 is a strengthening argument for the shorter reaction time as well since the probability of side reactions was reduced, too.

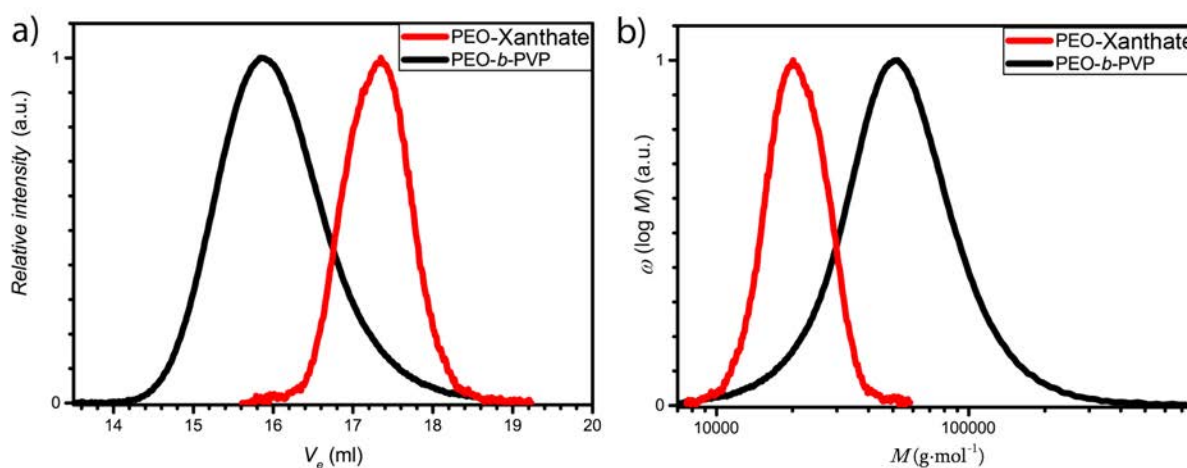


**Figure III.2** a) SEC elution curves of PEO-X and the corresponding PEO-*b*-PVP; b) corresponding SEC apparent molecular weight distributions of the polymers obtained in NMP at 70 °C using PEO calibration.

When comparing the determined molecular weight of  $M_{n,\text{NMR}}$  and  $M_{n,\text{app,SEC}}$ , it can be seen that the weight determined *via* NMR exceeds the one determined *via* SEC by  $5000\text{ g}\cdot\text{mol}^{-1}$ . A possible explanation for the difference is the use of a PEO calibration in SEC affording a lower molecular weight. The calibration curve only affords an apparent value since the calibration was conducted with pure PEO standards. Furthermore, the determination *via*  $^1\text{H-NMR}$  does not afford a weight distribution, but an apparent average number weighted polymer mass.

After the synthesis of a suitable PEO-*b*-PVP block copolymer, the focus on the further examinations was set to the investigation of the self-assembly behavior.



### III.3. Self-Assembly of PEO-*b*-PVP Block Copolymers in Aqueous Solution

In order to investigate if double hydrophilic PEO-*b*-PVP block copolymers are able to self-assemble to organized structures in aqueous solution without any external triggers, the synthesized PEO<sub>500</sub>-*b*-PVP<sub>225</sub> block copolymer was dissolved in Millipore water. Concentrations of 0.1, 0.5, 1.0, 2.5, 5.0, and 7.5 wt.% were prepared by precisely weighing polymer into vials and adding Millipore water. After filtration with 0.45  $\mu\text{m}$  CA syringe filters, the solutions were examined *via* DLS at ambient temperature.

As visible from the DLS size distribution curves in Figure III.3a, an increase in block copolymer concentration affects the size distribution already at low concentrations. The lowest amount of block copolymer of 0.1 wt.% results in a unimodal size distribution with an apparent hydrodynamic radius of 11 nm. The peak can be attributed to the size of free dissolved block copolymer in a random coil conformation. The concentration is therefore too low to cause any phase segregation effect with PEO-*b*-PVP.

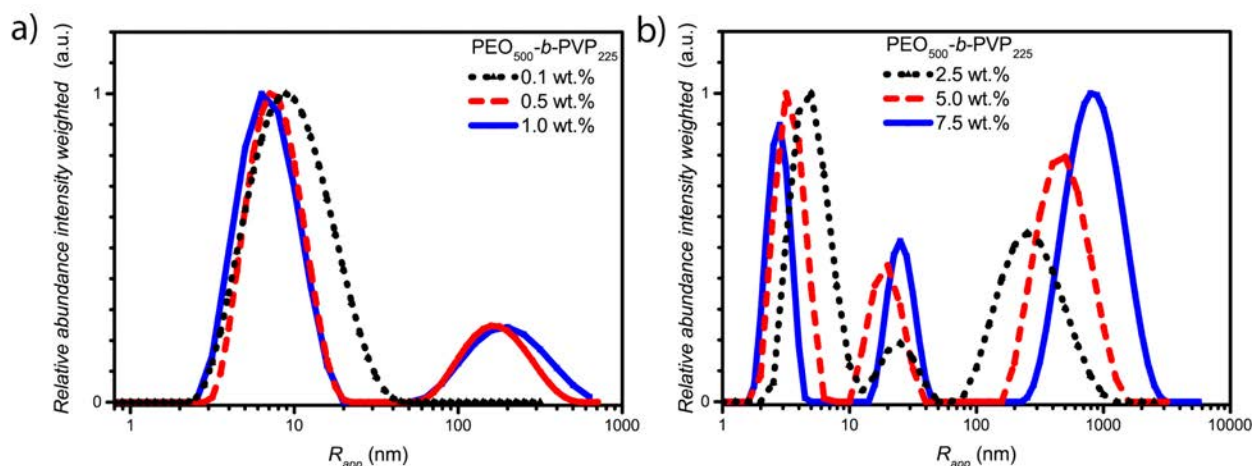


**Figure III.3** Intensity weighted particle size distribution of PEO<sub>500</sub>-*b*-PVP<sub>225</sub> at a) 0.1, 0.5, and 1.0 wt.% and b) 2.5, 5.0, and 7.5 wt.% in water measured *via* DLS at 25 °C.

A fivefold increase in the block copolymer concentration to 0.5 wt.% already causes a drastic change in the shape of the apparent size distribution curve. The major peak at 8 nm can still be attributed to free dissolved block copolymer chains, but the standard deviation of the peak decreased by approximately 50%. Furthermore and more outstanding, a second peak with a  $R_{app}$  of 180 nm and a relative abundance of 0.27 is present. This surprising observation of an

---

aggregation effect of PEO-*b*-PVP block copolymers even at low concentrations already strongly supports our postulation of a DHBC self-assembly with PEO-*b*-PVP. However, it has to be taken into account, that the particle size distribution is intensity weighted. As a result of this, the actual abundance of the large species is significantly lower than it appears in Figure III.3a.<sup>b</sup> The two fold increase of concentration to 1.0 wt.% causes no drastic change in the intensity weighted apparent particle size distribution and can be compared to the one of 0.5 wt.%.

A further change in the particle size distribution composition occurred with a further increase of block copolymer concentration to 2.5 wt.% (Figure III.3b). Here, a trimodal particle size distribution is present. The first peak at 8 nm can again be attributed to free dissolved block copolymers in random coil conformation. The new peak at 25 nm possesses a relative abundance of 0.2 and can be attributed to small undefined block copolymer aggregates. The small size is approximately three times larger than a single chain. Therefore, the possibility of a loose aggregation of a few polymer chains is quite likely.

In contrast to the 1.0 wt.% sample, the relative abundance of the peak corresponding to the large particles increased to 0.55 and the average apparent radius increased by 100 nm to 315 nm. The increase of the average apparent radius of the large species can be attributed to an increase in its aggregation number. Due to more polymer chains being present in the solution, more polymer chains can be incorporated into these aggregates. This effect can be attributed to a decrease in osmotic repulsion, too meaning that polymer solvent contacts and solvation of single block copolymer chains becomes slightly less predominant with increasing concentration. Further increase in the concentration to 5.0 wt.% enhances the described effects even more. The second drastic change in the apparent particle size distribution occurs with a concentration of 7.5 wt.%. Here, the relative abundance of the large species with an average apparent radius of 927 nm exceeds the one of free dissolved block copolymer chains by 0.1 and is shifted to the maximum of 1.0 in relative abundance. The average apparent hydrodynamic radii and corresponding relative abundances are further summarized in Table III.2.

---

<sup>b</sup> According to Equation 22, the actual abundance is about  $10^{-5}$  lower than displayed in intensity weighted particle size distributions.

**Table III.2** Summary of average apparent hydrodynamic radii and relative abundances of PEO-*b*-PVP obtained *via* DLS at 25 °C.

Concentration (wt.%)	Peak 1 $R_{h,app}$ (nm)	Rel. abund.	Peak 2 $R_{h,app}$ (nm)	Rel. abund.	Peak 3 $R_{h,app}$ (nm)	Rel. abund.
0.1	11	1.0	-	-	-	-
0.5	8	1.0	-	-	180	0.27
1.0	6	1.0	-	-	215	0.28
2.5	8	1.0	25	0.2	315	0.55
5.0	3	1.0	20	0.44	501	0.79
7.5	3	0.9	25	0.52	927	1.0

A problem resulting in the use of higher block copolymer concentrations is an increase in viscosity of the solution as well as increased density fluctuations in the solution. Since the actual viscosities of the corresponding samples were not determined, the results obtained from DLS cannot be taken into strict account. The real hydrodynamic radii of the observed species should deviate from the determined ones because  $R_{app}$  was calculated according to the viscosity and refractive index of water, an assumption which is only valid for diluted solutions. In the case of 5.0 wt.% and more concentrated solutions, the deviant self-diffusion and density fluctuations of the solution drive the autocorrelation function to the limit of decent evaluation of the self-diffusion coefficient. Therefore, only apparent hydrodynamic values can be obtained of these high DHBC concentrations with conventional DLS techniques.<sup>c</sup>

In order to visualize the formed PEO<sub>500</sub>-*b*-PVP<sub>225</sub> aggregates in aqueous solution, the block copolymer solution containing 7.5 wt.% was stained with Rhodamine B followed by examination *via* LSCM. The corresponding confocal images in Figure III.4a, b, and c display large spherical circular structures with Rhodamine B stained outer surface.

<sup>c</sup> A range of new light scattering techniques and setups that may possibly be capable of measuring hydrodynamic radii of highly viscous or turbid samples are under development. The most important of those systems is fiber optic quasi elastic scattering (FOQELS).<sup>219</sup>

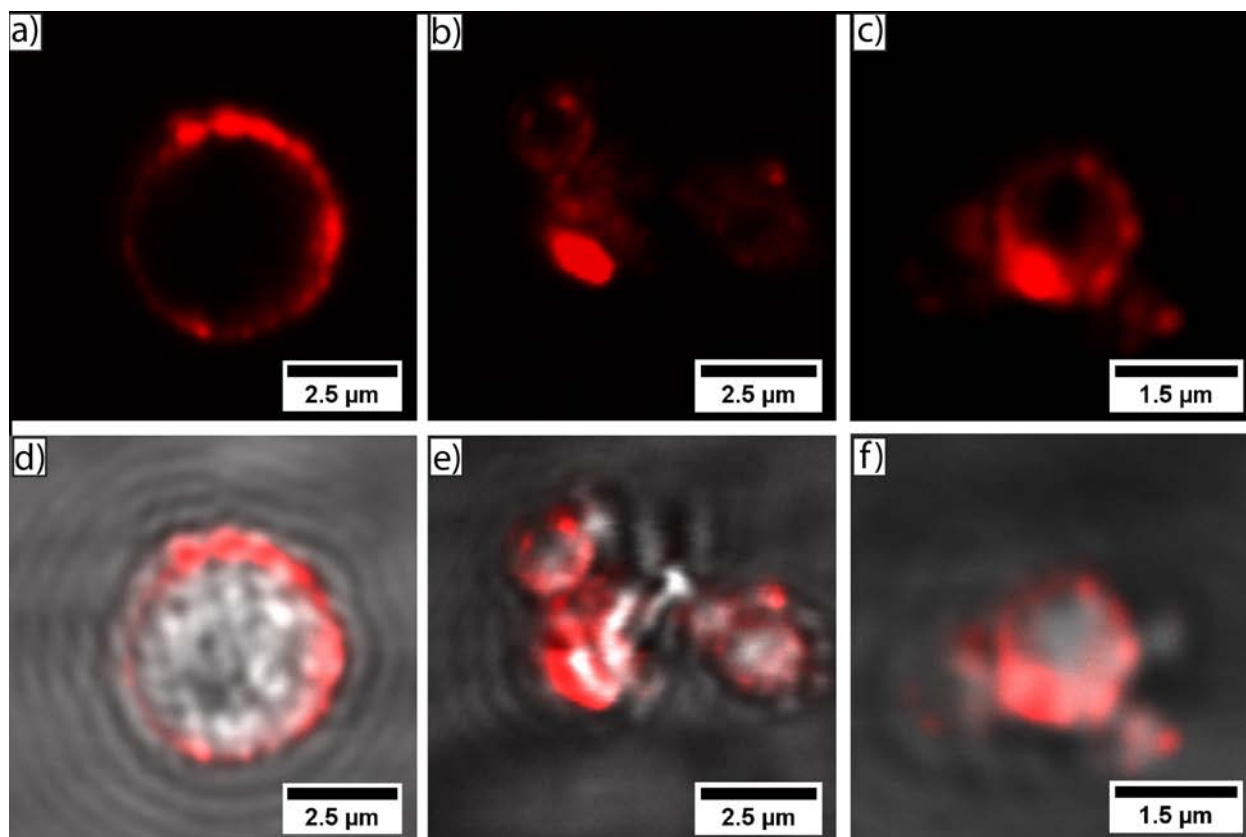


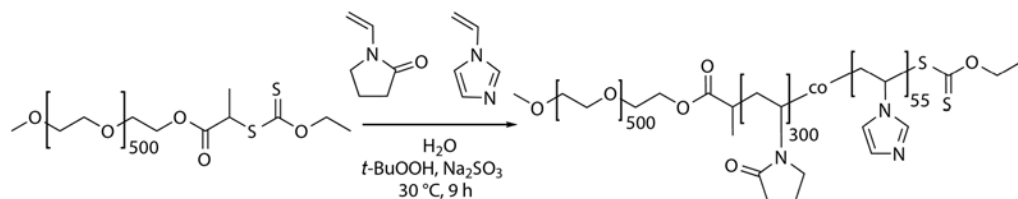
**Figure III.4** a), b) & c) Confocal micrographs of spherical particles of PEO<sub>500</sub>-*b*-PVP<sub>225</sub> at 7.5 wt.% stained with Rhodamine B; d), e) & f) corresponding DIC images with fluorescence overlay displaying the particle structure.

The diameters of these structures range from 700 nm in Figure III.4c to almost 5 μm in Figure III.4a. Compared to the average apparent diameters of the large species obtained from DLS for the 7.5 wt.% block copolymer solution (Figure III.3b), the diameters of the structures observed *via* LSCM are in a comparable range. The confocal/interference contrast (DIC) micrographs corresponding to the confocal micrographs (Figure III.4d, e and f) display spherical particles where Rhodamine B is highly concentrated at the outer membranes of the particles. Rhodamine B appears to enrich in spherical speckles around the structures. Due to the low resolution level of LSCM at these length scales and particle motion inside the solution, it was not possible to further examine these speckles. The DIC micrographs give the impression of rather dense, structured particles being present since Rhodamine B is only able to visibly enrich in the outer surface of these particles. In contrast to the vesicular structures reported by Brosnan et al.,<sup>199</sup> PEO<sub>500</sub>-*b*-PVP<sub>225</sub> forms smaller, structured submicron sized particles. The occurrence of large particle structures is a novel observation for self-assembled DHBC structures.

However, the self-assembly itself is not as efficient compared to the reported systems and requires highly concentrated solutions. A reason for the less efficient self-assembly is the lower difference in hydrophilicity between PEO and PVP resulting in a diminished phase separation tendency in comparison to PEO and polysaccharides, for instance. The lower phase separation tendency can only be overcome by a decrease in osmotic repulsion, i.e. an increase in block copolymer concentration. To improve the observed DHBC system towards a better self-assembly tendency at lower concentrations, one of the polymer blocks has to become more hydrophilic. Therefore, the block copolymer was further functionalized.

#### *III.4. Synthesis of PEO-*b*-P(VP-co-VIm) Block Copolymers*

In order to improve the hydrophilicity difference of the block copolymer, one polymer building block has to become significantly more hydrophilic. A facile step to accomplish this requirement is the incorporation of a more hydrophilic comonomer to one of the homopolymer blocks. Since the PEO block of the former investigated PEO-*b*-PVP DHBC was afforded commercially and functionalized to act as macro RAFT chain transfer agent, the functionalization of the PVP block appeared to be more versatile. The most straight forward approach of functionalization would be a copolymerization with a more hydrophilic polymer. A second opportunity that can be achieved with a copolymerization is the introduction of functionalities into the polymer block that gives access to possible crosslinking strategies. Crosslinking of the afforded self-assembled particles would preserve the structures from disassembly upon dilution, a very beneficial concept taking a possible application of the structures into account. Therefore, *N*-vinylimidazole (VIm) was chosen as comonomer for the VP block copolymerization. VIm possesses several beneficial properties that fulfill the criteria to enhance the self-assembly. The basic imine in the five membered ring increases the hydrophilicity compared to the less polar lactone group of VP. Furthermore, the imine nitrogen can be protonated or undergo addition reactions that result in imidazolium cations, this circumstance can even further increase the hydrophilicity of a PVP block in which VIm is incorporated and enhance the self-assembly ability. The possibility to form quaternary nitrogen atoms in the imidazole ring furthermore enables access to crosslink the block copolymer chains as soon as self-assembled to spherical particles. In order to synthesize a block copolymer containing a certain amount of VIm, the polymerization procedure of PEO-*b*-PVP was modified in a rather simple way (Scheme III.4).



**Scheme III.4** Block copolymerization of VP and VIm.

Regarding the  $Q$ - $e$  scheme by Alfrey and Price<sup>220</sup>, VP and VIm possess values that are located in the same region (VP:  $Q = 0.088$ ,  $e = -1.62$ ; VIm:  $Q = 0.11$ ,  $e = -0.68$ ; region III, respectively).<sup>221, 222</sup> The neighboring location of VP and VIm in the  $Q$ - $e$  scheme is a very beneficial circumstance, because neither of both monomers is incorporated with higher priority only due to its reactivity. Since the monomers are incorporated arbitrarily at the beginning of the polymerization, only concentration effects play a role in the distribution of VIm inside the copolymer. However, the basic character of the nitrogen in *N*-vinylimidazole can lead to a cleavage of the PEO macro RAFT CTA's *O*-ethyl xanthate group. For that reason the molar ratio between VP and VIm was kept at 9/1 for the block copolymerizations and the polymerization conditions were maintained similar to previous polymerizations.

As visible from Table III.3, the copolymerization of VP and VIm was successful. The apparent average molecular mass determined *via* SEC was 30 000 g·mol<sup>-1</sup> and with a  $\mathcal{D}$  of 1.4. When comparing the SEC and <sup>1</sup>H-NMR results of the different block copolymers in Table III.3, two important differences can be seen. The SEC apparent average mass of PEO-*b*-P(VP-*co*-VIm) differs by 30% from the one of PEO-*b*-PVP whereas the polydispersity is in a similar range.

**Table III.3** SEC and <sup>1</sup>H-NMR summary of synthesized PEO-*b*-PVP and PEO-*b*-P(VP-*co*-VIm) block copolymers.

Block copolymer	$M_{n,app,SEC}$ (g·mol <sup>-1</sup> ) <sup>a</sup>	$\mathcal{D}$	VP incorporation ( <sup>1</sup> H-NMR) <sup>b</sup>	$M_{n,NMR}$ (g·mol <sup>-1</sup> )
PEO <sub>500</sub> -Xanthate	20 000	1.1	-	22 000
PEO <sub>500</sub> - <i>b</i> -PVP <sub>225</sub>	42 000	1.3	52%	47 000
PEO <sub>500</sub> - <i>b</i> -P(VP <sub>300</sub> - <i>co</i> -VIm <sub>55</sub> )	30 000	1.4	40%	60 300

<sup>a</sup> SEC apparent average weight distributions were obtained in NMP using a PEO calibration. <sup>b</sup> <sup>1</sup>H NMR were recorded in CDCl<sub>3</sub> at 400 MHz and 25 °C.

Since the copolymerization conditions were kept equal to the homopolymerization of VP, the possibility of a retarding effect of VIm in the RAFT polymerization is one possibility. In contrast to the SEC results,  $^1\text{H-NMR}$  results propose the opposite, with PEO-*b*-P(VP-*co*-VIm) possessing a 22% higher apparent average molecular mass of  $60\,300\text{ g}\cdot\text{mol}^{-1}$ . The difference between SEC and  $^1\text{H-NMR}$  of 50% probably results from the PEO calibration of the SEC, giving lower apparent number weighted molecular masses for the more hydrophilic, VIm incorporated block copolymer compared to PEO-*b*-PVP.

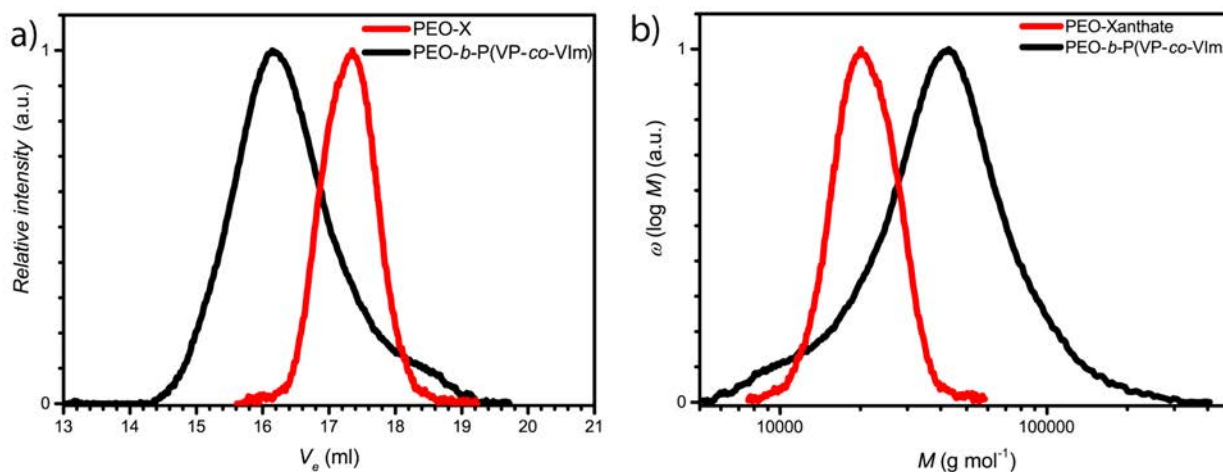


**Figure III.5** a) SEC elution curves of PEO-X and the corresponding PEO-*b*-P(VP-*co*-VIm); b) corresponding SEC apparent molecular weight distributions of the polymers obtained in NMP at 70 °C using a PEO calibration.

As visible from the SEC elution curves and molecular weight distributions in Figure III.5, a visible tailing of the elution curve towards lower molecular weights of the synthesized block copolymer is visible. The tailing occurred due to the abovementioned degradation processes of the *O*-ethyl xanthate end groups caused by VIm. Since the polydispersity is still rather low with 1.4, the copolymerization can be still assumed to be controlled and the majority of PEO-macro chain transfer agent is actually polymerized to PEO-*b*-P(VP-*co*-VIm). A comparison of the incorporated monomer units of PEO-*b*-P(VP-*co*-VIm) and PEO-*b*-PVP determined via  $^1\text{H-NMR}$  displays that 58% more monomer units were incorporated into the VIm functionalized block copolymer. The incorporation of VP increased by 33% from 225 incorporated units to 300. According to  $^1\text{H-NMR}$ , 55 monomer units and therefore 15% of the incorporated monomer units can be assessed to *N*-vinylimidazole. This amount is five percent higher than the attempted

incorporation, but a higher incorporation could possibly improve the hydrophilicity and therefore the self-assembly behavior of the corresponding block copolymer.

### III.5. Self-Assembly of PEO-*b*-P(VP-co-VIm)

In order to assess the self-assembly of PEO<sub>500</sub>-*b*-P(VP<sub>300</sub>-*co*-VIm<sub>55</sub>) in water, the DBHC was dissolved in Millipore water in a similar fashion as PEO<sub>500</sub>-*b*-PVP<sub>225</sub>. The corresponding solutions containing 0.1, 0.5, 1.0, 2.5, 5.0, and 7.5 wt.% were then examined *via* DLS at 25 °C. As visible from Figure III.6a, the self-assembly of PEO<sub>500</sub>-*b*-P(VP<sub>300</sub>-*co*-VIm<sub>55</sub>) is already improved at low concentrations of 0.1 wt.%. In contrast to PEO-*b*-PVP self-assembly, a second peak with an average apparent radius of 232 nm with a relative abundance of 0.15 is present for PEO-*b*-P(VP-*co*-VIm) in addition to the major peak at 8 nm. The increased self-assembly tendency is already an improvement compared the initial DHBC. A further increase in the concentration to 0.5 wt.% results in an increase in relative abundance of the particle species by 86% to 0.28 and a decrease in the average apparent radius to 184 nm. The decrease in the average apparent radius is a result of the broad distribution of the peak. According to the particle size distribution graph in Figure III.6a, the maximum of the particle species peak is in the same range as the particle species of the 0.1 wt.% solution.

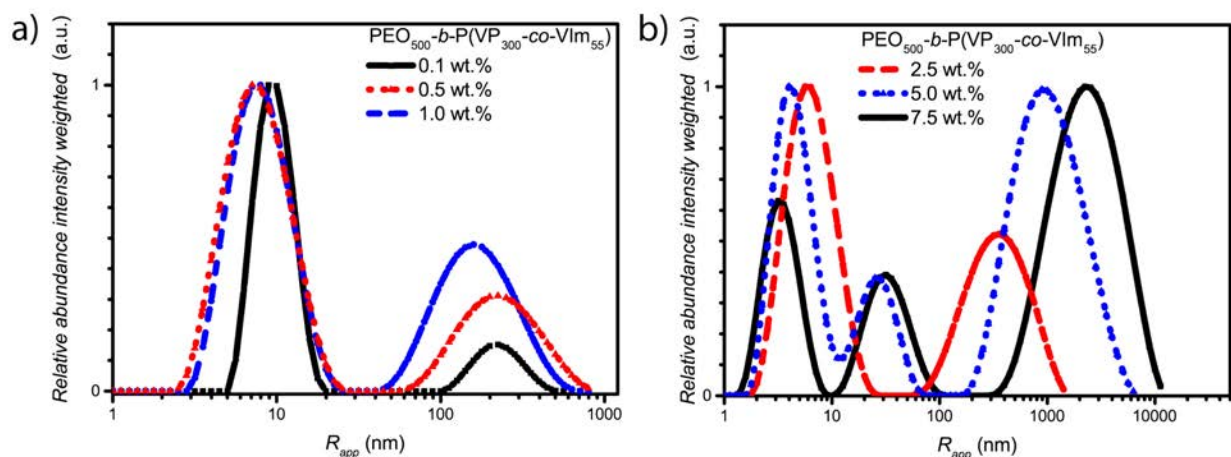


**Figure III.6** Intensity weighted particle size distribution of PEO<sub>500</sub>-*b*-P(VP<sub>300</sub>-*co*-VIm<sub>55</sub>) at **a)** 0.1, 0.5, and 1.0 wt.% and **b)** 2.5, 5.0, and 7.5 wt.% in Millipore water measured *via* DLS at 25 °C.

In contrast to the first two concentrations, apparent particle maximum of the 1.0 wt.% sample is shifted to a smaller radius of 200 nm, whereas the average apparent hydrodynamic radius



increased to 255 nm. The relative abundance further increased by 82% to 0.51 (see Table III.4 for details).

When comparing the particle size distributions of the first three concentrations of PEO-*b*-PVP with the ones of PEO-*b*-P(VP-*co*-VIm), not only the improved self-assembly tendency visible by the relative abundance of the functionalized block copolymer but also an increased average apparent hydrodynamic radius can be seen. The effect was observed for high concentrations of PEO-*b*-PVP, too. Increasing the PEO-*b*-P(VP-*co*-VIm) concentration to 2.5 wt.% results in an increase in the average apparent radius of the large species to 406 nm. Compared to PEO-*b*-PVP, no aggregates with an average apparent radius between 20 and 25 nm were observed until a concentration of 5.0 wt.% was reached. As visible from Figure III.6b the particle size distribution of the 5.0 wt.% solution indeed displays a drastic change compared to lower concentrations. The most striking difference is the increase in the average apparent radius of the particle species by 200% to 1200 nm with an increase in relative abundance to 0.99. The drastic increase in average apparent hydrodynamic radius even exceeds the one of the 7.5 wt.% solution of PEO-*b*-PVP and possesses a relative abundance almost as high as the free dissolved block copolymer chains.

**Table III.4** Summary of average apparent hydrodynamic radii and relative abundancies of PEO-*b*-PVP obtained *via* DLS at 25 °C.

Concentration (wt.%)	Peak 1 $R_{h,app}$ (nm)	Rel. abund.	Peak 2 $R_{h,app}$ (nm)	Rel. abund.	Peak 3 $R_{h,app}$ (nm)	Rel. abund.
0.1	8	1.0	-	-	232	0.15
0.5	8	1.0	-	-	184	0.28
1.0	8	1.0	-	-	255	0.51
2.5	6	1.0	-	-	406	0.52
5.0	5	1.0	29	0.37	1200	0.99
7.5	4	0.63	35	0.39	2789	1.0

Furthermore, the second peak corresponding to the not specified small block copolymer aggregates appears with a relative abundance of 0.37 and a larger average apparent hydrodynamic radius of 29 nm, compared to PEO-*b*-PVP.

The apparent particle size distribution of the final increase in concentration from 5.0 to 7.5 wt.% displays the particle species to possess the highest relative abundance and a high average

apparent hydrodynamic radius of 2789 nm. It turned out that PEO-*b*-P(VP-*co*-VIm) possesses an increased aggregation tendency upon higher concentrations compared to PEO-*b*-PVP. The average apparent hydrodynamic radii of the last two concentrations are almost three times larger than the non-functionalized block copolymer. These observations not only display an improved self-assembly behavior of PEO-*b*-P(VP-*co*-VIm), but an increased preference to form larger aggregates too. It still has to be taken into account, that solutions with high block copolymer content possess a higher viscosity. Therefore, the values of the apparent hydrodynamic radii have to be taken with care because the abovementioned errors strongly influence the DLS autocorrelation function.

In order to visualize the particles formed by the self-assembly of PEO-*b*-P(VP-*co*-VIm), cryogenic SEM (cryo SEM) measurements were conducted. Since the 7.5 wt.% solution afforded the highest relative abundance of self-assembled particles in DLS particle size distributions, this sample was investigated *via* cryo SEM.

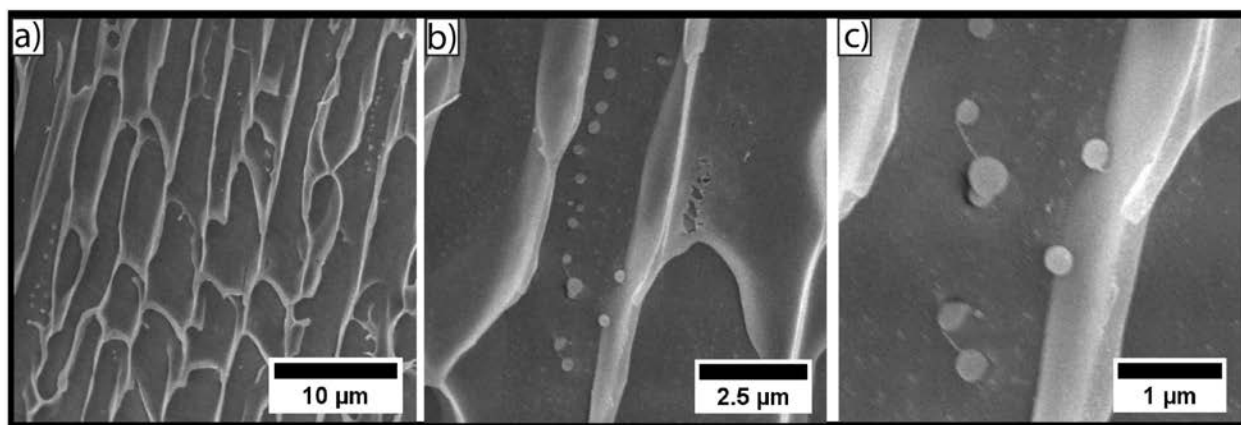


**Figure III.7** Cryo SEM micrographs of PEO-*b*-P(VP-*co*-VIm) in Millipore water at 7.5 wt.%, displaying a) an overview of the sample; b), and c) a magnification of the observed particles.

As visible from the micrograph in Figure III.7a, two different structural species were obtained from cryo SEM measurements, tubular oriented structures, and spherical particles. The tubular oriented structures being present as the majority of the sample can be attributed to free dissolved block copolymer. As mentioned before, intensity weighted particle size distributions afford higher intensities for larger structures. The “actual” abundance of large particles is presumably  $10^{-5}$  times lower than expected from DLS. For that reason, the majority of block copolymer is still present as free dissolved chains in a high concentration. During the freezing process of the sample in liquid nitrogen, ice crystals are formed and grow in tubular directions pushing the

block copolymer to the outer crystal borders.<sup>223</sup> Upon fracturing and sputtering, the block copolymer structures remain as walls of the corresponding ice crystals. Within those tubular structures, the larger particle structures can be found. Due to their slower diffusion, the particles remain inside or at the interface of the ice crystals and do not merge with the block copolymer phase upon freezing in liquid nitrogen. The small amount of particles observed in Figure III.7b and Figure III.7c possess diameters within the range of less than one micrometer and can be found in the interior of the tubular oriented structures. Furthermore, the particles with averages sizes exceeding 1  $\mu\text{m}$  as predicted from DLS were not observed. The lack of the large spherical particles in the cryo SEM micrographs can be attributed to the enhanced block copolymer immobilization at high concentrations leading to higher local viscosities. Since the local viscosity of the sample was not determined, DLS affords higher apparent radii due to the simplification of the viscosity to be close to the one of Millipore water. Another possibility for the missing of larger self-assembled block copolymer particles could be the bursting of large particles during the freezing process. However, no particle fragments indicating the presence of large spherical particles were found in the cryogenic samples.

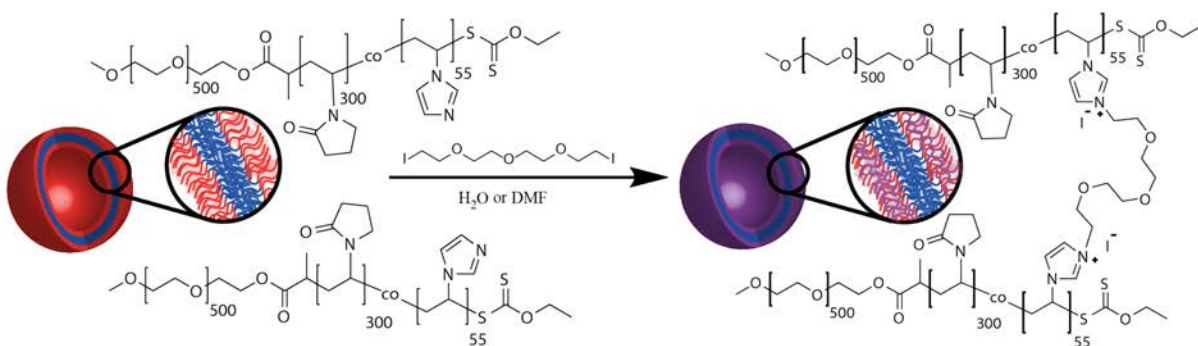
The incorporation of the more hydrophilic comonomer VIm to the PVP block improved the self-assembly behavior of the double hydrophilic block copolymer. Larger spherical aggregates could be observed at low concentrations *via* DLS and the overall relative abundance of these particles could be increased. Despite these improvements, the abundance of free dissolved block copolymer chains in the samples is still significantly high and the amount of spherical particles observed relatively low. Furthermore, the self-assembled particles cannot be extracted separately from the block copolymer solution because dilution or dialysis drives the spherical self-assemblies towards disassembly. A possible pathway towards a preservation of the formed self-assemblies is a crosslinking strategy allowing the self-assembled DHBC particles to maintain their structure upon dilution and change of the solvent.

### ***III.6. Crosslinking of Self-Assembled PEO-*b*-P(VP-co-VIm)***

#### ***Submicron Particles***

The basic nitrogen of *N*-vinylimidazole not only improves the hydrophilicity of the PVP block, but also gives access to crosslinking approaches *via* protonation or quaternization reactions. Quaternized *N*-vinylimadazolium polymers and derivatives are already widely explored in the

field of poly(ionic liquids) (PILs).<sup>224, 225</sup> Here, quaternization occurs *via* alkylation reactions of suitable alkyl halides that readily form the desired ionic structures. Taking advantage of the facile quaternization reaction of *N*-vinylimidazole, the use of a bifunctional crosslinker in order to interconnect the self-assembled DHBC chains would be of high benefit. Alkyl halide compounds for instance show a good reactivity towards nucleophilic tertiary amines to form quaternary imidazolium cations and are frequently used as alkylation agents.<sup>226</sup> In order to maintain the hydrophilic character of the DHBC a diiodo compound with a certain hydrophilicity, namely diethylene glycol bis(2-iodoethyl) ether was synthesized. Furthermore, the crosslinker possesses a certain chain flexibility allowing to maintain the high permeability of the double hydrophilic membrane structure.



**Scheme III.5** Reaction scheme of the crosslinking procedure using diethylene glycol bis(2-iodoethyl) ether.

By forming imidazolium linkages, the crosslinker should ensure the preservation of the self-assembled particles (Scheme III.5).

In order to assess the effect of crosslinker addition to the self-assembled particles and examine a possible crosslinking effect, solutions of PEO-*b*-P(VP-*co*-VIm) containing 1.0, 2.5, and 5.0 wt.% were prepared and examined *via* DLS before and after crosslinker addition. The amount of crosslinker added to the solution was adjusted to the theoretical VIm content incorporated in the block copolymer, 10 mol% respectively. When comparing the apparent particle size distributions of the 1.0 wt.% solution in Figure III.8a before and after the addition of diethylene glycol bis(2-iodoethyl) ether, a strong increase in the relative abundance of the particle species by 50% and a broadening of the peak resulting in a higher apparent average radius of 25% to 320 nm could be observed. Additionally, a third signal with an apparent average radius of 7900 nm was visible in

the particle size distribution. The particle size distributions of the 2.5 wt.% and 5.0 wt.% samples in Figure III.8b and Figure III.8c display a similar signal at large apparent radii.

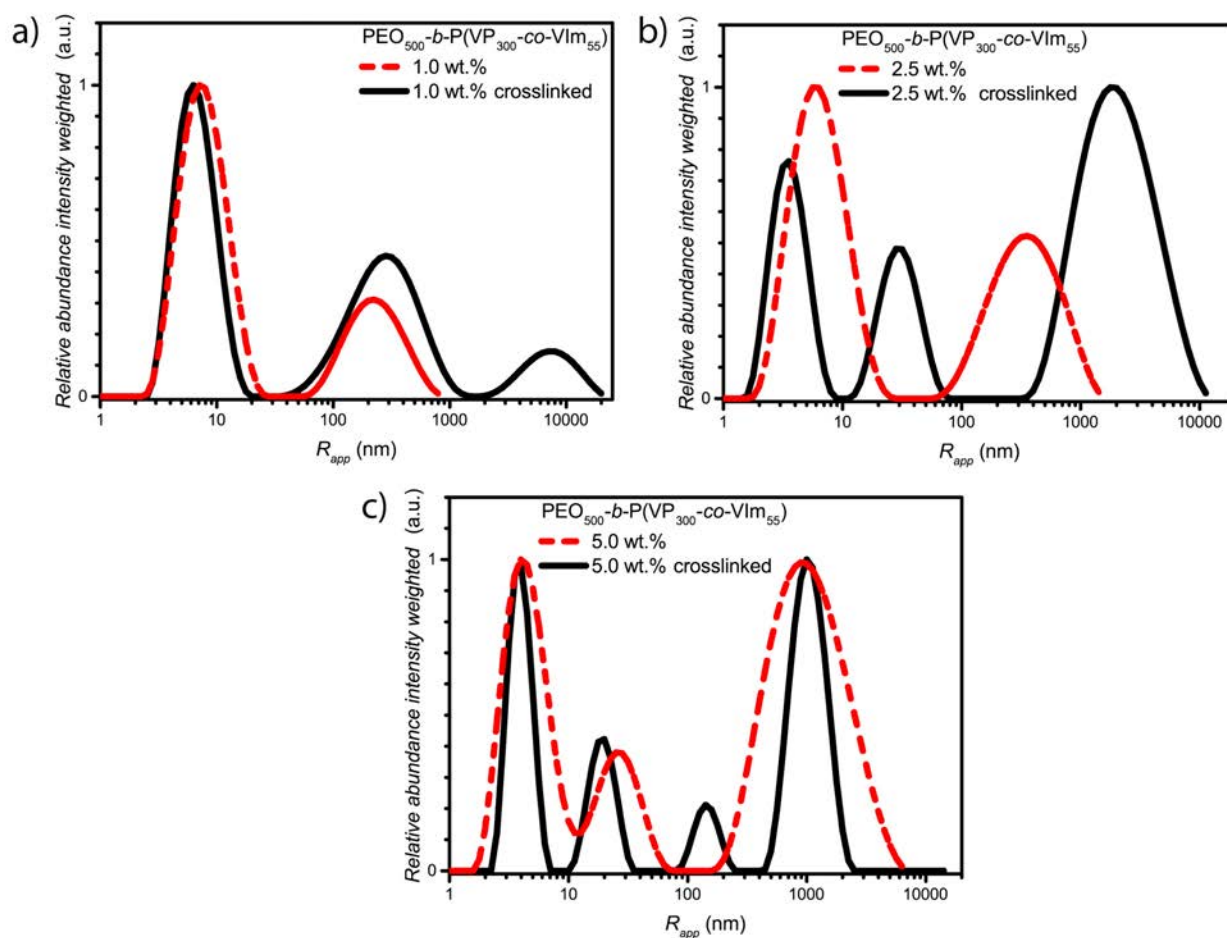


**Figure III.8** Intensity weighted particle size distribution of  $\text{PEO}_{500}\text{-}b\text{-P}(\text{VP}_{300}\text{-}co\text{-VIm}_{55})$  at **a)** 1.0 wt.%, **b)** 2.5 wt.%, and **c)** 5.0 wt.% in Millipore water before and after addition of crosslinker measured *via* DLS at 25 °C.

The addition of crosslinker to the 2.5 wt.% solution changed the particle size distribution to a trimodal one with a decreased relative abundance of free dissolved block copolymer chains and the appearance of a peak with an apparent average radius of 37 nm. The peak attributed to the particle structures broadened and was shifted to an average apparent radius of 2250 nm. In contrast to the more diluted solutions, the appearance of the 5.0 wt.% solution did not change drastically. The occurrence of these extremely large structures even at rather low concentrations might indicate the formation of aggregates of several particles *via* interparticle crosslinking. Particles in close contact to each other possess a certain probability to be crosslinked to each other. Interparticle crosslinking can result in the formation of large particle aggregates.

The circumstance of interparticle crosslinking could be observed *via* LSCM with a crosslinked 7.5 wt.% solution of PEO-*b*-P(VP-*co*-VIm) stained with Rhodamine B. As visible from the micrograph in Figure III.9a and Figure III.9c, multiparticle aggregates with a length exceeding 20  $\mu\text{m}$  were formed. A magnification of another aggregated particle structure of several micrometers in Figure III.9d visualizes several submicron sized particles connected together.

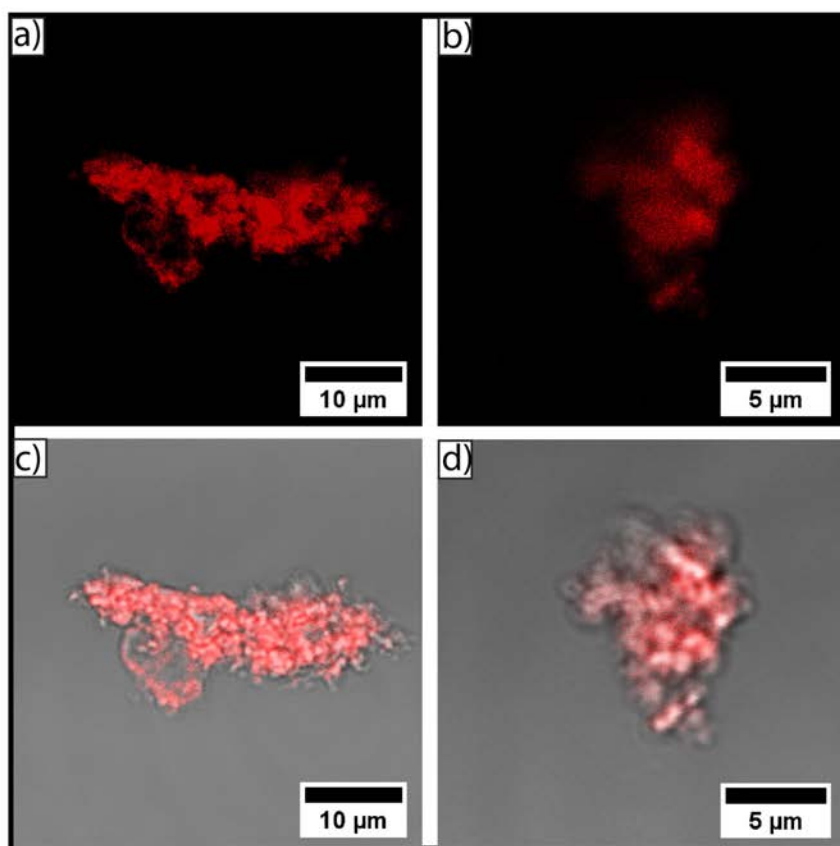


**Figure III.9** a) & b) Confocal micrographs of aggregated crosslinked particles of PEO<sub>500</sub>-*b*-P(VP<sub>300</sub>-*co*-VIm<sub>55</sub>) at 7.5 wt.% stained with Rhodamine B; c) & d) corresponding DIC images with fluorescence overlay displaying the aggregate structure.

**Table III.5** Zeta potential values of 0.1 wt.% block copolymer solutions.

Entry	Block copolymer	Zeta potential [mV]
1	PEO <sub>500</sub> - <i>b</i> -PVP <sub>225</sub>	-6.74
2	PEO <sub>500</sub> - <i>b</i> -P(VP <sub>300</sub> - <i>co</i> -VIm <sub>55</sub> )	0.44
3	PEO <sub>500</sub> - <i>b</i> -P(VP <sub>300</sub> - <i>co</i> -VIm <sub>55</sub> ) (crosslinked in water)	1.09

The drastic increase in average apparent radius of the particle species and the formation of aggregates lead to the conclusion, that diethylene glycol bis(2-iodoethyl) ether efficiently forms linkages between block copolymer chains. Furthermore, an increase in the zeta potential of

0.65 mV (Table III.5) for 0.1 wt.% solutions of PEO-*b*-P(VP-*co*-VIm) after addition of crosslinker underlines the formation of ionic species corresponding to the quaternization of the imidazolium nitrogen. In order to further compare the effect of crosslinker addition to PEO-*b*-P(VP-*co*-VIm) solutions, a 2.5 wt.% solution of the block copolymer in DCM was prepared and investigated before and after crosslinker addition.

As visible from Figure III.10a, PEO-*b*-P(VP-*co*-VIm) possesses a broad size distribution with an average apparent radius of 60 nm in DCM and a broad signal with low relative abundance in the micrometer range. Upon treatment with crosslinker two new signals appear in the particle size distribution curve, one with an apparent radius of 350 nm and a second with 150  $\mu$ m. The formation of large structures can be attributed to the formation of charges due to the crosslinking resulting in a decreased solubility of the P(VP-*co*-VIm) block in the organic solvent DCM. The formation of large structures in DCM displays a certain stability of the crosslinked particles in organic solvents. A second and more important demand on the crosslinked DHBC particles is the stability towards dilution. The self-assembled and crosslinked PEO-*b*-P(VP-*co*-VIm) submicron particles need to proof stability towards dilution in order to fulfill the criteria to perform in any possible applications. Therefore, a 2.8 wt.% block copolymer solution was crosslinked and subsequently diluted to 1.0, 0.5, and 0.1 wt.% (Figure III.10b).

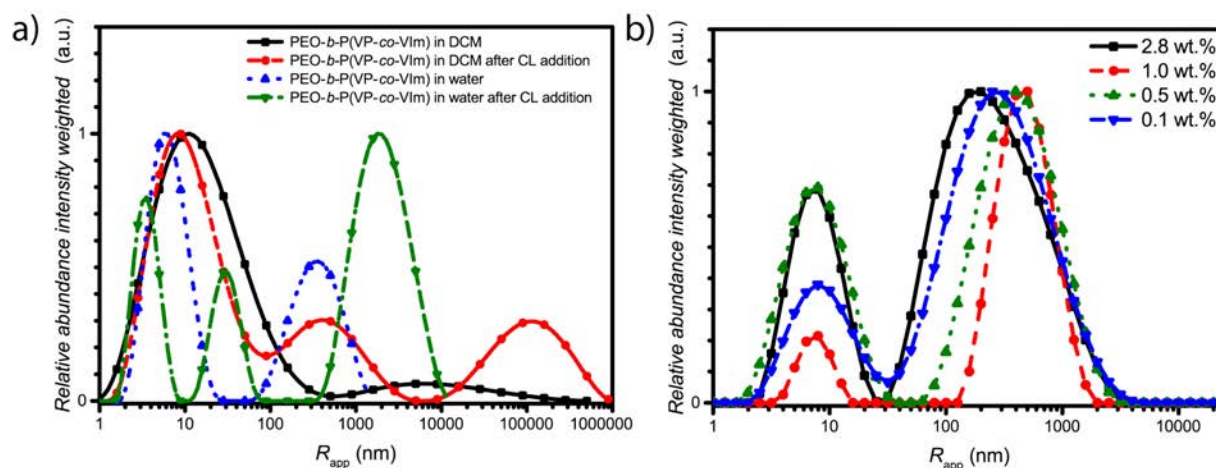


**Figure III.10** a) Intensity weighted apparent particle size distribution of a 2.5 wt.% solution of PEO-*b*-P(VP-*co*-VIm) in DCM and Millipore water before and after crosslinking determined *via* DLS at 25 °C; b) DLS dilution experiment of crosslinked PEO-*b*-P(VP-*co*-VIm) particles in Millipore water determined *via* DLS at 25 °C.

The particle size distributions in Figure III.10b display two significant differences in comparison to the non-crosslinked particle size distributions in Figure III.6. On the one hand, the maximum

in relative abundance maintains with the particle species even upon high dilution to 0.1 wt.%. Therefore, it can be assumed that the crosslinked submicron particles are still present after dilution and no drastic decrease in the average apparent radius was observed in the particle size distribution. Furthermore, the relative abundance of the peak corresponding to the free dissolved block copolymer chains maintains at a lower level below 0.7 and decreases to 0.4 for the highly diluted sample. Summarizing the results of the crosslinking examinations in DCM and the dilution row of a solution of crosslinked submicron particles in Millipore water, it can be stated that the afforded crosslinked particles are stable in organic solvents and upon dilution.

The micrographs of the conducted cryogenic SEM experiments of a 7.5 wt.% solution with addition of crosslinker in Figure III.11 display spherical particles in between the tubular structures formed by free dissolved block copolymer (Figure III.11a). The crosslinked particles possess diameters between 200 nm and approximately 1  $\mu\text{m}$  (Figure III.11b). A further magnification of the sample reveals string shaped connections between separated particles (Figure III.11c). However, it cannot be distinguished if these interconnections are formed due to the crosslinking and therefore are a cause for the particle aggregation or if the strings are artifacts of the sample preparation (especially of the sputtering process). Although the overall content of particles in the solution was determined to be higher according to DLS, the cryogenic SEM samples did not show an increased amount of particles only by crosslinking. In analogy to the non-crosslinked particle samples, no particles with diameters exceeding 2  $\mu\text{m}$  could be observed within the crosslinked samples.

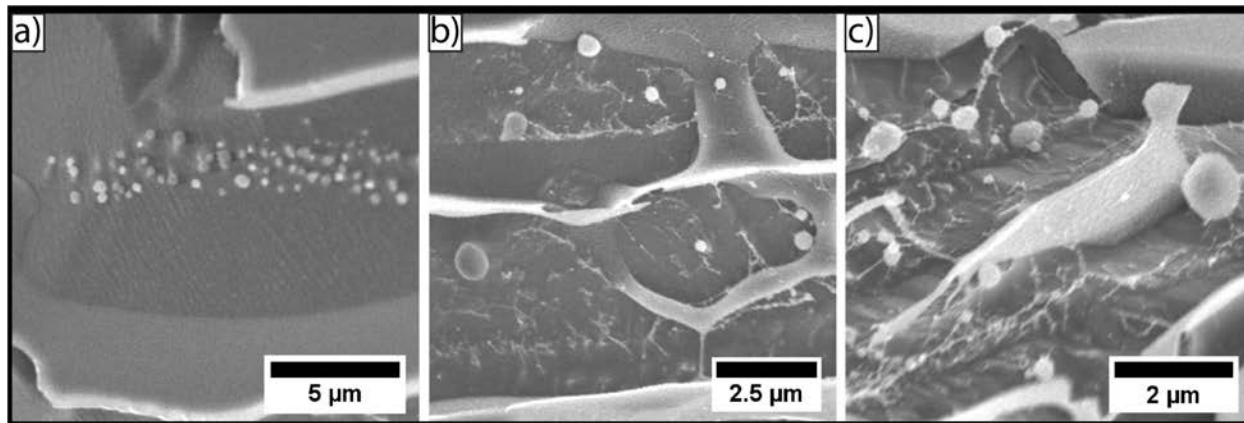


**Figure III.11** Cryo SEM micrographs of a 7.5 wt.% solution of crosslinked PEO-*b*-P(VP-*co*-VIm) particles.



Therefore, the large species observed *via* DLS can be attributed to the formation of aggregated particles and to the decreased diffusion of block copolymer in a concentrated solution with high viscosity. The broadening of the DLS peaks in Figure III.6 and Figure III.8 can be attributed to these concentration effects.

Regarding the results obtained from the dilution experiments of crosslinked particles in Figure III.10b, i.e. the ability to maintain the particles upon high dilution, a strategy towards the removal of free dissolved block copolymers and undesired particle aggregates to afford a solution only containing particles should be possible. In order to remove free dissolved block copolymer chains from the crosslinked particles, a dialysis approach was conducted. A 5.0 wt.% PEO-*b*-P(VP-*co*-VIm) block copolymer solution was crosslinked and dialyzed against Millipore water using a 1 000 000 MWCO dialysis tube for several days. The average pore size of the applied dialysis tube should be large enough to ensure a diffusion of free dissolved block copolymer chains, dimers, and larger aggregates to the surrounding exterior but preserve crosslinked particles with a diameter exceeding 100 nm inside the tube. The solution was dialyzed for several days in order to remove the majority of free dissolved block copolymer chains and examined *via* DLS. As visible from the particle size distribution in Figure III.12a, the crosslinked and dialyzed sample displays a strong contrast to the block copolymer solution at 1.0 wt.% with and without crosslinking (Figure III.8). Whereas crosslinking only increases the relative abundance of the particle species by two fold with the free dissolved block copolymer chains still being the most abundant species, dialysis of the 5.0 wt.% solution and dilution to 1.0 wt.% displays a drastic increase in the relative abundance of the crosslinked particle species. The relative abundance of the free dissolved block copolymer chains decreased to 0.35 and the abundance of the particles increased by 0.52 being the most abundant species. Furthermore, the polydispersity of the particle species increased drastically to an apparent average diameter of 877 nm in contrast to 260 nm for the crosslinked species.

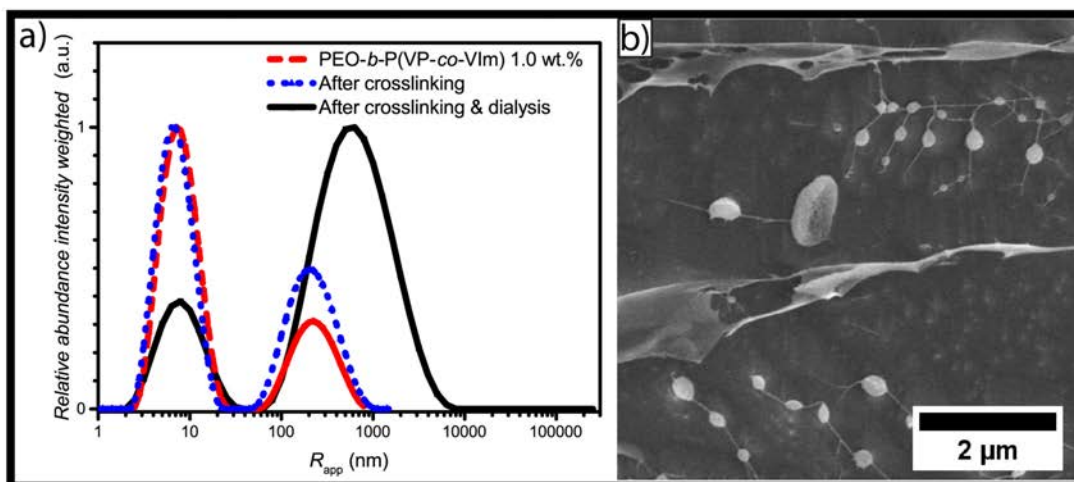


**Figure III.12** a) Intensity weighted particle size distributions of 1.0 wt.% solutions of PEO-*b*-P(VP-*co*-VIm) before crosslinking, after crosslinking and after dialysis determined *via* DLS at 25 °C in Millipore water and b) corresponding cryo SEM micrographs of dialyzed PEO-*b*-P(VP-*co*-VIm) particles.

The cryo SEM micrographs obtained from the crosslinked and dialyzed block copolymer solution in Figure III.12b display that a high content of the sample now contains of spherical particles with average diameters between 100 nm and 1 μm. Larger block copolymer aggregates could be observed too, but only in a small amount. The presence of free dissolved block copolymer is still visible from the micrographs as thin and more sheet-like tubular structures. Furthermore, the strings connecting crosslinked particles with each other are still present, too. The thin slings of block copolymer are aligned between the submicron particles giving the appearance of pearls lined up on a string. With the crosslinking and dialysis in aqueous solution applied the self-assembly of PEO-*b*-P(VP-*co*-VIm) could already be improved and a majority in the solution could be transferred to spherical particles. But the amount of free dissolved block copolymer chains is still too high for future applications. Since the crosslinked particles tend to be stable in organic solutions, an approach towards solutions only containing crosslinked particles was conducted.

### III.7. Self-Assembly and Crosslinking of PEO-*b*-P(VP-*co*-VIm) in DMF

A rather unexpected finding occurred during the search for an organic solvent to proof the formation of ionic charges within the crosslinking procedure with the almost complete self-assembly of PEO-*b*-P(VP-*co*-VIm) to particle structures in the organic solvent DMF. Despite both homo blocks being well soluble in DMF, 2.5 wt.% solutions of PEO and PVP in DMF only

display average apparent radii of 6 nm and 11 nm (Figure III.13a), the connection of both polymers to a block copolymer results in an interesting aggregation of the block copolymer chains to larger structures.

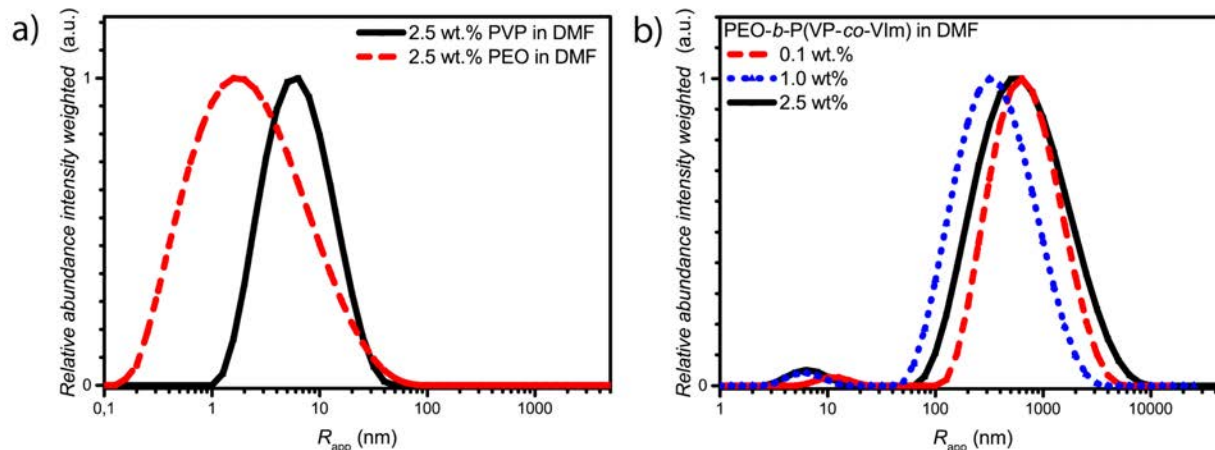


**Figure III.13** Intensity weighted particle size distributions of **a)** 2.5 wt.% solutions of PEO and PVP in DMF and **b)** PEO-*b*-P(VP-*co*-VIm) solutions of 0.1, 1.0 and 2.5 wt.% in DMF determined *via* DLS at 25 °C.

As visible from Figure III.13b, PEO-*b*-P(VP-*co*-VIm) forms structures with an apparent average radius of 852 nm being the most abundant species. The peak corresponding to free dissolved block copolymer chains at 10 nm only possesses a very low relative abundance of 0.03. The tenfold increase in concentration to 1.0 wt.% decreases the average apparent hydrodynamic radius 472 nm and the relative abundance of the free dissolved block copolymer increases slightly to 0.04. Regarding the increase in average apparent radius for the large species to 928 nm for an increase in concentration to 2.5 wt.% while maintaining the low relative abundance of the free dissolved species, the decrease in  $R_{app}$  of the 1.0 wt.% sample may be caused by the data treatment and the actual average apparent radius is in the same range as the two other concentrations. The almost exclusive self-assembly of PEO-*b*-P(VP-*co*-VIm) in DMF to large aggregates proves a significantly more efficient self-assembly behavior compared to aqueous solutions. The enhanced self-assembly tendency can be attributed to a better solvent contrast of PEO and P(VP-*co*-VIm) pointing out that the difference in the interaction of the different polymer block with DMF molecules is significantly stronger compared to water. The minor amount of free dissolved block copolymer can probably be attributed to unreacted macro RAFT chain transfer agent present in the block copolymer behaving similar to pure PEO in DMF.

Having found a suitable system in order to obtain a significant amount of particles, the particles self-assembled in DMF were crosslinked to maintain the structure upon transfer to aqueous systems. Therefore, addition of diethylene glycol bis(2-iodoethyl) ether crosslinker to a 5.0 wt.% block copolymer solution in DMF and subsequent dilution was applied to investigate the effects of crosslinking *via* DLS. As visible from the apparent particle size distribution in Figure III.14, the addition of crosslinker decreases the self-assembly efficiency of PEO-*b*-P(VP-*co*-VIm) in DMF. The formation of ionic structures drives the self-assembly slightly towards highly aggregated structures containing ionic structures on the one hand and a decent amount of small structures on the other hand.

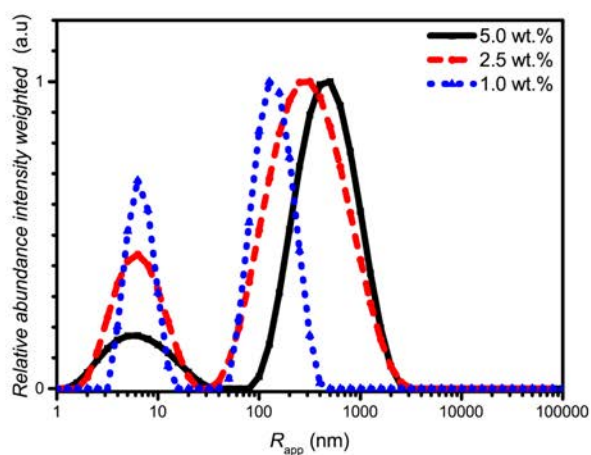


**Figure III.14** Intensity weighted particle size distributions of a 5.0 wt.% solution of crosslinked PEO-*b*-P(VP-*co*-VIm) in DMF diluted to 2.5 and 1.0 wt.% determined *via* DLS at 25 °C.

The average apparent diameter of the main peak corresponding to 5.0 wt.% decreases from 565 nm to 414 nm at 2.5 wt.% and to 150 nm at 1.0 wt.%. Additionally, the relative abundance of the free dissolved species increases with decreasing block copolymer concentration. In contrast to the crosslinking in DCM in Figure III.10a, no large aggregates of particles were observed *via* DLS. Therefore, a combination of crosslinking in DMF followed by a transfer to aqueous systems and dialysis as demonstrated before was applied. A 5.0 wt.% solution of PEO-*b*-P(VP-*co*-VIm) in DMF was crosslinked with a diethylene glycol bis(2-iodoethyl) ether solution (5% *v/v*) in DMF. The solution of crosslinked particles was then slowly added to Millipore water to afford a 0.1 wt.% solution. The mixture of water/DMF containing crosslinked particles was then dialyzed against Millipore water with a 1 000 000 MWCO dialysis tube for two days in order to ensure complete removal of DMF and free dissolved block copolymer

chains leading to a resulting aqueous solution of crosslinked particles with an approximate polymer content of 0.07 wt.%. The apparent particle size distribution in Figure III.15a displays the dialysis succeeded in an almost complete removal of free dissolved block copolymer chains. The relative abundance decreased to 0.04. The self-assembled and crosslinked particles amount the majority of the sample as observed for PEO-*b*-P(VP-*co*-VIm) in DMF with an average apparent radius of 150 nm. Furthermore, the particle size distribution strongly differs from the one of PEO-*b*-P(VP-*co*-VIm) crosslinked in water (Figure III.8c and Figure III.10b) resulting in a strong point towards successful crosslinking in DMF and a possible transfer to aqueous systems. A slight drawback can be seen in the formation of large particle aggregates. As no aggregates were detected in the crosslinked DMF sample, an aggregation during the transfer to Millipore water is quite likely.

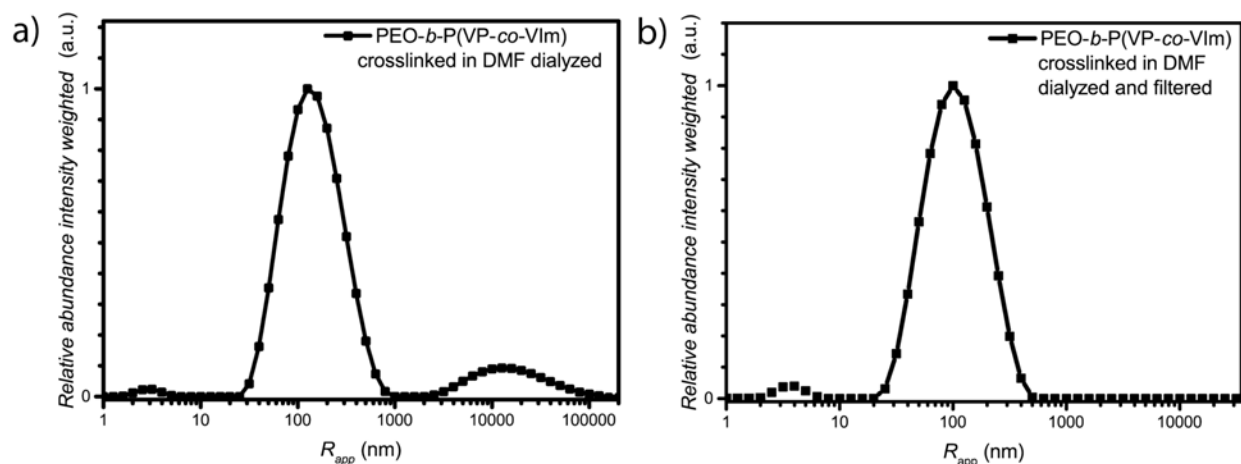


**Figure III.15** Intensity weighted particle size distributions of **a)** PEO-*b*-P(VP-*co*-VIm) particles crosslinked in DMF, transferred to Millipore water, and dialyzed determined *via* DLS at 25 °C; **b)** Corresponding particle size distribution after filtration with 1.2 μm CA filters.

In order to remove the aggregates formed due to solvent transfer, the sample was filtered over a 1.2 μm CA syringe filter. Aggregates exceeding the diameter of 1.2 μm should therefore remain inside the filter membrane. The particle size distribution in Figure III.15b displays a successful quantitative removal of the aggregated species.

The successful transformation of crosslinked submicron particles from a DMF to an aqueous solution proves two major postulates of our work. Since the DLS apparent size distribution shows almost no difference when comparing DMF and aqueous system for very low concentrations after crosslinking and transformation, the success of the crosslinking attempt can

---

be stated. Non-crosslinked solutions of the block copolymer would have shown the apparent size distribution similar to those shown in Figure III.13b. The second more unexpected fact is the similarity in self-assembly behavior of PEO-*b*-P(VP-*co*-VIm) in Millipore water and DMF. The small difference in average apparent particle size before and after transformation confirms that the structure of crosslinked submicron particles is maintained during the change of solvent.

Cryogenic SEM investigations of the crosslinked and dialyzed unfiltered PEO-*b*-P(VP-*co*-VIm) particles in Figure III.16a and Figure III.16b display a large amount of spherical particles within the submicron range. The particles possess a rather broad size distribution between 100 nm and almost one micrometer. In contrast to SEM investigations of the previous samples, no tubular structures containing free dissolved block copolymer could be detected. The magnification in Figure III.16c displays two particles with a diameter of almost one micrometer and one small particle to visualize the samples polydispersity. As visible from Figure III.16b, some string-like structures that appear to form interparticle connections are still present in the sample. The string like connections could cause the appearance of large structures with several micrometers in the DLS size distribution curve in Figure III.15a. Furthermore, a small amount of non-spherical structures can be seen. Since the solution was not filtered previous to investigation, it cannot be determined whether these structures are caused by the preparation of the cryo sample or if these structures are actually present in the solution.

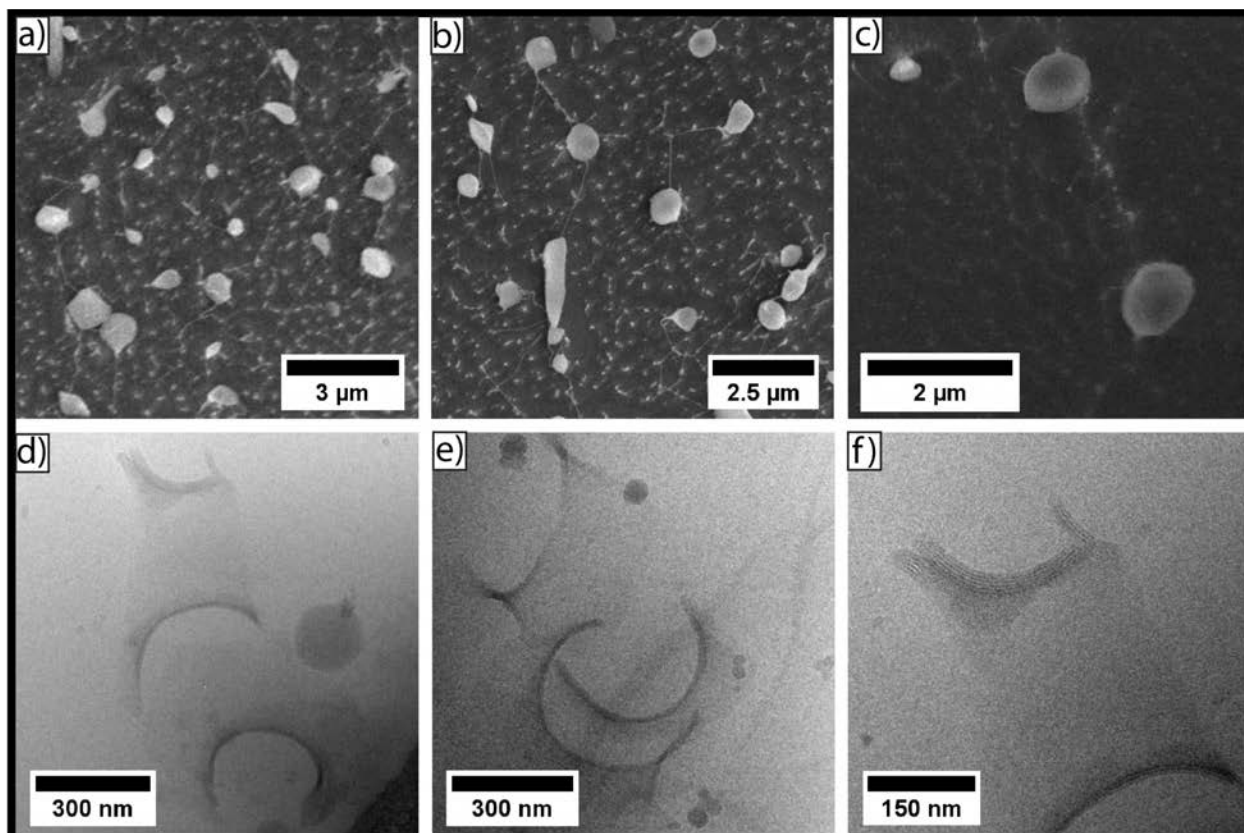


**Figure III.16** a) & b) Cryo SEM micrographs of PEO-*b*-P(VP-*co*-VIm) particles crosslinked in DMF after transfer to Millipore water and dialysis displaying spherical particles; c) magnification of corresponding submicron particles; d) & e) cryo TEM micrographs of the corresponding solution displaying spherical particles and complex membrane structures; f) magnification of a membrane structure.

In order to gather more information about the intrinsic structure of the self-assembled PEO-*b*-P(VP-*co*-VIm) particles, cryo TEM was applied. The micrographs in Figure III.16d and Figure III.16e display spherical particles with average diameters between 50 nm and almost 300 nm. In contrast to cryo SEM, the average particle diameters visible from cryo TEM are smaller, but still match with the particle size distribution obtained *via* DLS. In addition to spherical particles, a large amount of complex membrane structures were observed, where the membrane consists of several layers of phase separated block copolymer (Figure III.16f). Due to a higher atom number of iodide in close environment, the phase with stronger contrast can possibly be attributed to crosslinked P(VP-*co*-VIm) blocks. The shape of the complex membrane structures appears as a folded sheet or ruptured tube. Unfortunately, it cannot be determined if the membrane structures originate from ruptured particles. But the presence of phase separated layers additionally supports the postulated structure of DHBC particles and vesicles.

### III.8. Labelling of PEO-*b*-P(VP-co-VIm) Submicron Particles with Rhodamine B

Since it is not clear up to this point how these particles aggregates are built on a molecular level, it was decided to investigate the structure of the particle shells with LSCM, which is widely used in pharmaceutical and medical research. Benefitting from the fact that PEO-*b*-P(VP-co-VIm) block copolymers form persistent spherical particles by crosslinking, the particles were labelled with Rhodamine B by taking advantage of residual iodides within the crosslinked structures. The amine groups of Rhodamine B can possibly attach to these free crosslinker arms and be incorporated into the structures. For that, a 5.0 wt.% block copolymer solution in DMF containing 0.1 mg of dye was prepared and crosslinked with diethylene glycol bis(2-iodoethyl) ether according to the previous description. Performing the block copolymer self-assembly in dye enriched DMF should ensure reaction of Rhodamine B with the particles, which are then fixed by crosslinking and the dye is covalently attached to the particles.

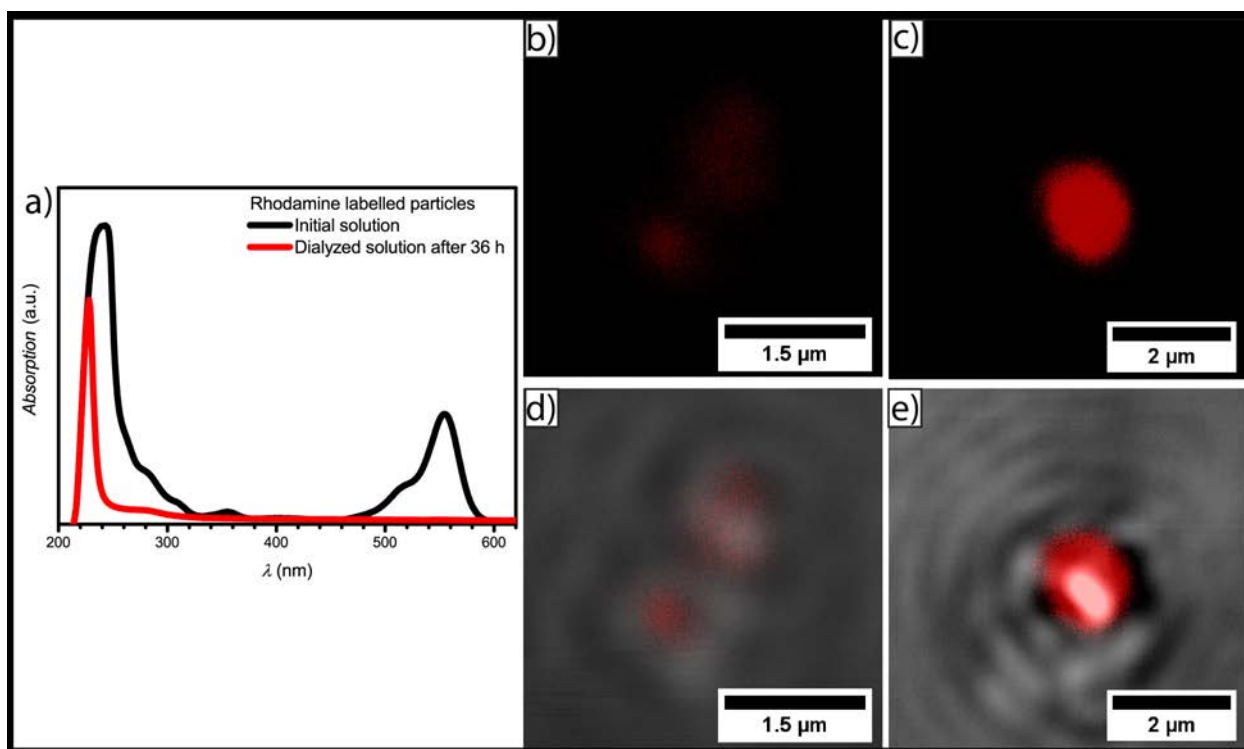


**Figure III.17** a) UV-Vis spectra of Rhodamine B labelled crosslinked PEO-*b*-P(VP-co-VIm) before and after dialysis against Millipore water; b) and c) Confocal micrographs of the dialyzed particle solution displaying a high concentration of Rhodamine B inside the particles; d) and e) corresponding DIC micrographs with fluorescence overlay.



As evident from UV-Vis spectra (Figure III.17a), the absorption peaks corresponding to Rhodamine B at 580 nm, 510 nm, and 330 nm disappeared almost completely after dialysis for 36 h with a 1 000 000 MWCO dialysis tube. It can therefore be assumed that free Rhodamine B was completely removed from the solution. LSCM measurements of the dialyzed solution (Figure III.17c and Figure III.17d) display that Rhodamine B was indeed successfully attached to the submicron sized particles. In the micrographs, an enriched spherical shaped area of Rhodamine B is present at the same area where the corresponding DIC signal displays a spherical structure. Furthermore, the exterior solution shows almost no fluorescence in the confocal signal. With average diameters ranging from 500 nm to 1.5  $\mu\text{m}$ , the observed particles are larger than the average size determined *via* DLS. As a result of the lower resolution limit of the used confocal objective, no smaller particles could be observed. The presence of dye labelled block copolymer throughout the complete structure of the crosslinked spherical structures supports the observations *via* cryo TEM and cryo SEM of particles being present. Furthermore, the dye was able to interpenetrate through the complete particle and covalently attach to residual crosslinker groups leading to the assumption that self-assembled P(VP-*co*-VIm) phases are distributed throughout the entire particle structure as well. For that reason, the crosslinked particle structures should be composed of microphase separated domains.

### III.9. Conclusion

In summary, we were able to demonstrate the self-assembly of a purely hydrophilic block copolymer poly(ethylene oxide)-*b*-poly(*N*-vinylpyrrolidone) in an aqueous system. The block copolymers self-assembled to spherical shaped submicron structures. DLS and LSCM/DIC measurements displayed the presence of these structures in concentrated block copolymer solutions. With the introduction of a small amount of slightly more hydrophilic *N*-vinylimidazole into the poly(*N*-vinylpyrrolidone) block the self-assembly behavior was improved and a method to preserve the spherical structures by cross-linking the incorporated *N*-vinylimidazole moieties with diethylene glycol bis(2-iodoethyl) ether was developed. The crosslinked submicron sized particles maintained their apparent radii upon dilution and in organic solvents. Furthermore, imaging with cryo SEM and LSCM/DIC was possible. The organic non-selective solvent DMF enhanced the self-assembly to almost quantitative amounts of submicron particles. These particles could be successfully crosslinked and transferred to an aqueous solution without a

---

change in their apparent size. Finally the particles were labeled with the dye Rhodamine B and the structure could be visualized *via* LSCM/DIC after dialysis. Taking the positive particle charge into account, a significant effect on the applicability of the studied particles for biomedical applications and has to be considered for future studies.

## IV. Vesicles of Double Hydrophilic Pullulan and Poly(acrylamide) Block Copolymers: A Combination of Synthetic- and Bio-derived Blocks

### IV.1. Preface<sup>a</sup>

In the previous chapter it was proven that double hydrophilic block copolymers are able to self-assemble to organized structures in pure water. However, organized particles of PEO-*b*-PVP suffer from a low and concentration dependent self-assembly tendency which affords further treatment in order to preserve these structures. As discussed in Chapter III, crosslinking strategies were able to preserve the particular structures from disassembly upon dilution.<sup>227</sup> In order to improve the self-assembly, a different system has to be applied to achieve efficient micro phase separation. For that reason, a combination of different species of purely hydrophilic polymer blocks that were already reported to perform improved self-assembly was applied.<sup>195, 199</sup> In the case of this chapter the focus was set to a combination of the polysaccharide pullulan with the poly(acrylamides) poly(*N,N*-dimethylacrylamide) (PDMA) and poly(*N*-ethylacrylamide) (PEA).

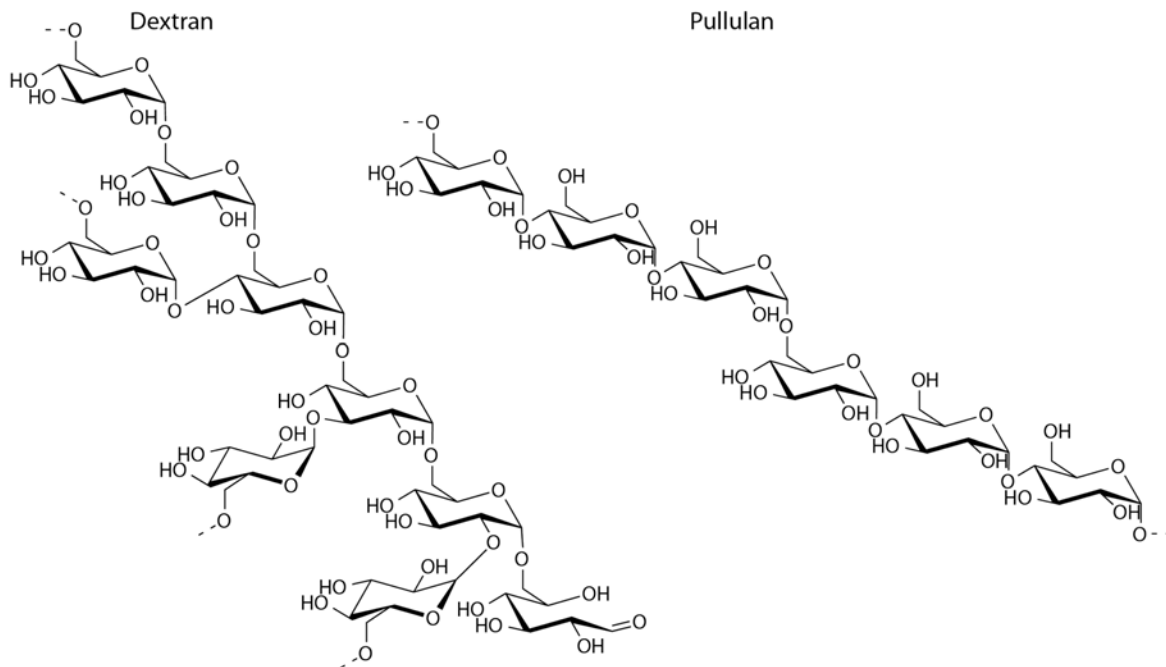
Polysaccharides, such as dextran, pullulan, and chitosan are prominent examples of biopolymers used in polymer science and in biomedical fields. Dextran, a polysaccharide consisting of a linear  $\alpha$ -(1,6) linked glucose chain with various branchings at  $\alpha$ -(1,2),  $\alpha$ -(1,3), and  $\alpha$ -(1,4) positions (Scheme IV.1), is produced by the bacterium *Leuconostoc mesenteroides*, which can be found in plant sources.<sup>228-230</sup> The biodegradable and biocompatible biopolymer possesses a good solubility in common solvents such as water and DMSO. Moreover, dextran is already widely applied in medical,<sup>229, 231</sup> biomedical,<sup>232, 233</sup> and food industry applications<sup>228</sup> - most commonly as blood plasma replacement.<sup>230</sup> A potential problem with the use of dextran for DHBC self-

---

<sup>a</sup> Terms of use: This chapter was adapted with permission from J. Willersinn, A. Bogomolova, M. B. Cabré and B. V. K. J. Schmidt, “Vesicles of double hydrophilic pullulan and poly(acrylamide) block copolymers: A combination of synthetic- and bio-derived blocks”; *Polym. Chem.*, 2017, **8**, 1244-1254 and is licensed under CC BY 3.0.

assembly is its branched nature. In order to use linear dextran chains for the desired application, the biopolymer has to be degraded prior to functionalization.<sup>234</sup> Initial experiments with dextran depolymerization displayed a certain difficulty to afford the desired structure. Therefore, pullulan was set to be in focus of a polysaccharide containing DHBC.

The linear polysaccharide pullulan consists of maltotriose units, 3  $\alpha$ -(1,4) connected glucose units that are linked *via*  $\alpha$ -(1,6) glycosidic bonds (Scheme IV.1). The polysaccharide is produced by the yeast like fungus *Aureobasidium pullulans*, in order to protect itself from external threats.<sup>235</sup> In analogy to dextran and derivatives, pullulan is a prominent example of the use of biopolymers and has a broad spectrum of applications, such as blood plasma substitutes,<sup>236</sup> food manufacturing,<sup>237</sup> and pharmaceutical applications.<sup>238</sup>

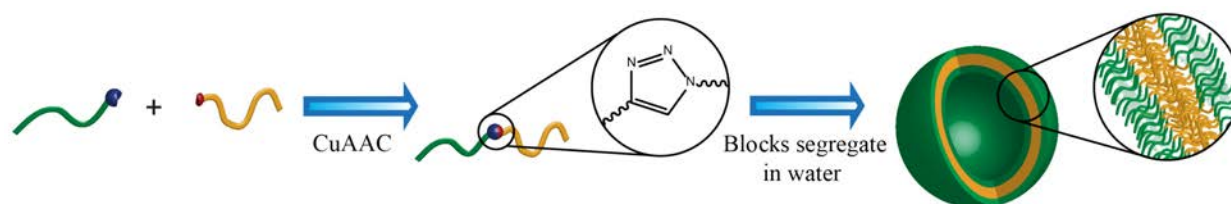


**Scheme IV.1** Chemical structures of two commonly used polysaccharides, dextran and pullulan.

The functionalization of pullulan is extensively studied.<sup>239</sup> Whereas biomedical applications mainly address to the functionalization of the hydroxyl groups, such as acetylation to change the properties of pullulan towards the desired fashion, end group functionalization of polysaccharides is a more frequent task in polymer science. In order to afford defined polysaccharide block copolymers, the exchange of terminal aldehyde or alcohol groups ( $\alpha$ -C1 groups) to functional groups bearing the possibility to act as permanent connection point for the

second block of choice.<sup>240, 241</sup> The polysaccharide can therefore be functionalized with terminal alkene or alkyne groups to be accessible to conjugation reactions, such as CuAAC or thiol-ene conjugations.<sup>118</sup> Furthermore, chain transfer groups such as xanthates can be attached allowing reversible deactivation radical polymerizations (RDRP).<sup>118</sup> The various possibilities of polysaccharide functionalization result in a broad spectrum of applications in polymer science. Furthermore, the well biocompatible dextran and moreover pullulan enlarge the scope of DHBCs capable to act as future drug delivery systems.

The functionalization of biomacromolecules and synthetic polymers to act as building blocks for CuAAC conjugations is a viable extension for synthesis of novel double hydrophilic block copolymers. The application of a facile conjugation procedure allows the construction of a broad variety of novel double hydrophilic block copolymers bearing interesting self-assembly features in aqueous media.



**Scheme IV.2** Conjugation and self-assembly scheme of double hydrophilic block copolymers in water.

The benefit of a DHBC synthesis *via* CuAAC conjugation is the high flexibility in the choice of polymer building blocks. Hydrophilic blocks which promote a good self-assembly tendency due to a high difference in hydrophilicity can be easily combined without long lasting examinations of the synthesis procedure of the block copolymer using conventional polymerization techniques. This allows scientists to efficiently adjust the block copolymer components depending on their demand, and create self-assembled DHBC structures such as particles and vesicles.

This chapter exemplarily describes the synthesis of suitable hydrophilic building blocks of pullulan and poly(acrylamides) that were conjugated to a double hydrophilic block copolymer. The self-assembly behavior of the block copolymers was investigated and the block copolymers were further functionalized with a fluorescent dye to demonstrate the adaptability of the DHBC system to perform in various ways. The self-assembled structures were investigated using SEC, DLS, SLS, cryo SEM, and LSCM techniques.

---

## IV.2. Synthesis of Alkyne Functionalized Pullulan

Pullulan is a linear polysaccharide produced from the yeast like fungus *Aureobasidium pullulans*. Since the fungus produces pullulan from starch by fermentation to act as a protective layer, pullulan is a biopolymer with no defined molecular mass. Therefore, custom pullulan possesses a broad molecular mass weight distribution with  $D$  between 2.1 and 4 and high average molecular masses ranging from a  $M_w$  between 300 000  $\text{g}\cdot\text{mol}^{-1}$  and 500 000  $\text{g}\cdot\text{mol}^{-1}$ .<sup>238</sup> In order to afford pullulan with a more defined  $D$  below 2.0 and an average molecular weight in the range of 20 000  $\text{g}\cdot\text{mol}^{-1}$ , technical grade pullulan has to be depolymerized to a certain degree prior to use. Since pullulan predominantly consists of maltotriose units (three glucose units linked *via*  $\alpha$ -(1,4) glycosidic bonds) that are connected *via*  $\alpha$ -(1,6) linkages, the most accessible point for depolymerization is the cleavage of  $\alpha$ -(1,6) bonds between the maltotriose units. A controlled method for pullulan depolymerization using 0.025 M hydrochloric acid solution and elevated temperatures was described by Ilic et al.<sup>242</sup> (Figure IV.1a) Following that procedure, commercial pullulan was depolymerized to a  $M_n$  of 14 000  $\text{g}\cdot\text{mol}^{-1}$  with  $D$  of 1.8 (see Figure IV.1b). In comparison to the commercial pullulan, that possesses a  $M_n$  of 35 0000  $\text{g}\cdot\text{mol}^{-1}$  and a polydispersity of 19.0, the employed depolymerization was successful. Further attempts to optimize the polydispersity without decreasing the molecular weight of the obtained pullulan were not successful due to the broad molecular mass distribution of the starting material. Since effective self-assembly of DHBCs containing pullulan with a similar  $D$  around 1.8 was reported by Brosnan et al.,<sup>199</sup> further efforts to optimize the pullulan block were not attempted.

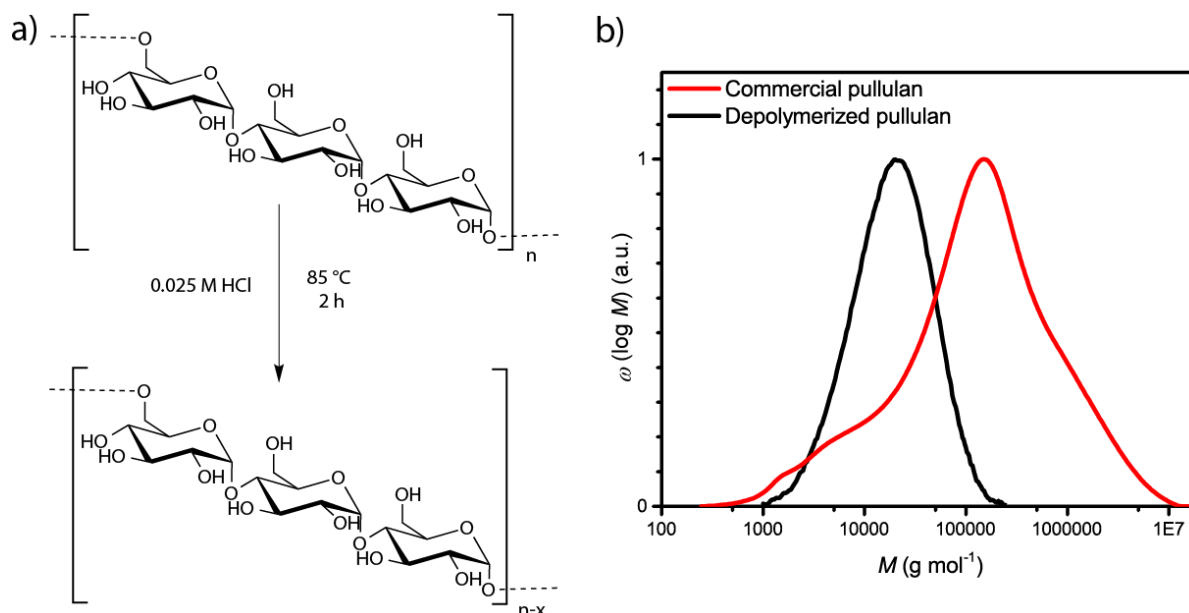


**Figure IV.1** a) Reaction scheme of pullulan depolymerization; b) apparent molecular mass distributions of commercial pullulan and depolymerized pullulan against a pullulan calibration curve determined *via* SEC in acetate buffer solution.

In order to act as building block for a conjugation reaction, pullulan has to be further functionalized with an alkyne group. The alkyne functionalization was conducted in acetate buffer at  $50^\circ\text{C}$  *via* reductive amination (see Figure IV.2a). To afford full conversion of the aldehyde corresponding to the  $\omega$ -glucose unit to an amine, the reaction was conducted in acetate buffer to ensure the open acetal form of the  $\omega$ -glucose. Furthermore, a 100-fold excess of propargylamine and  $\text{NaCNBH}_3$  was applied to ensure full conversion. The utilization of a high excess of reactants compared to pullulan should diminish undesired side reactions, such as further depolymerization.

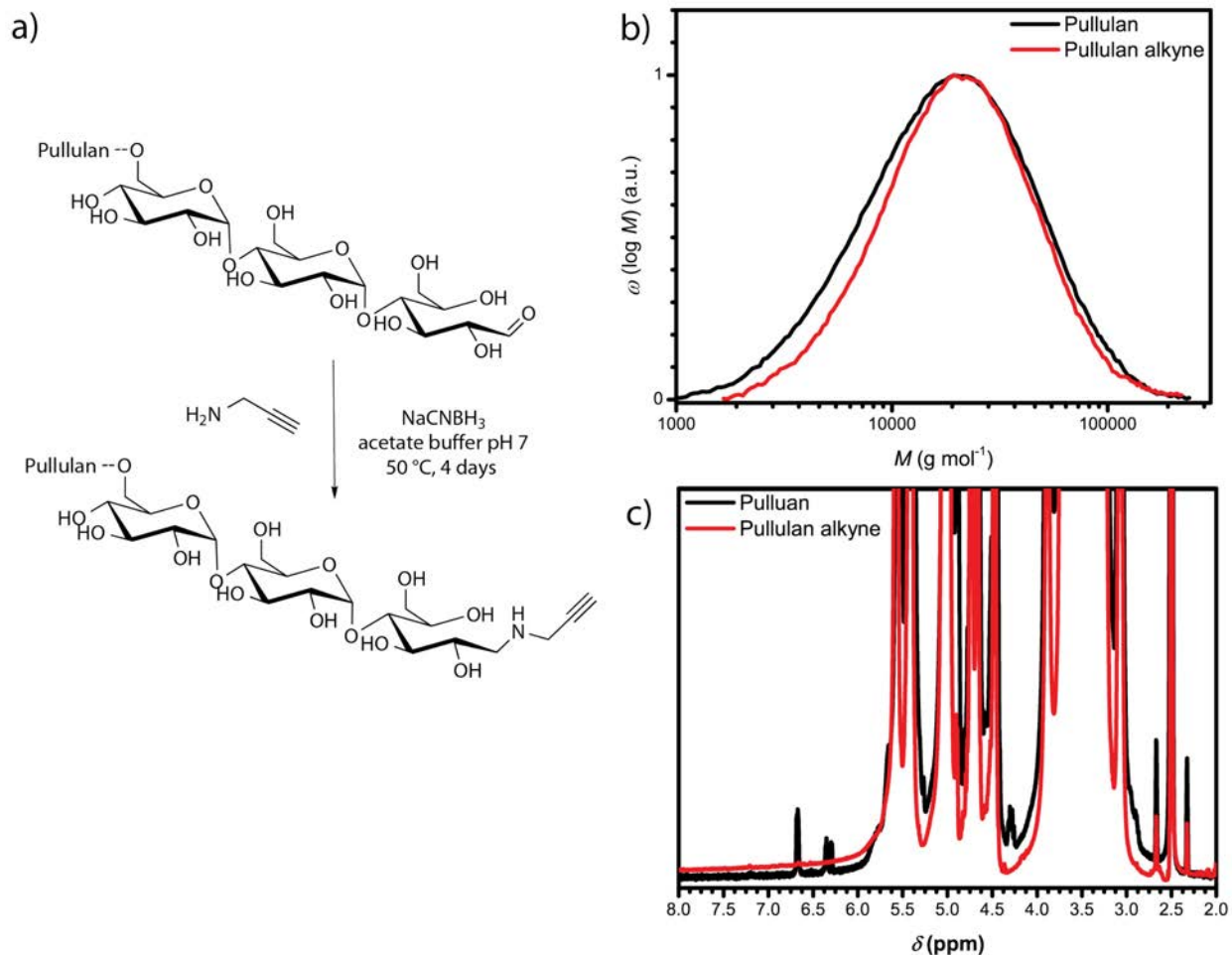


**Figure IV.2** a) Synthesis scheme of pullulan-alkyne; b) corresponding molecular mass distribution curves determined *via* SEC against a pullulan calibration curve in acetate buffer solution; c) <sup>1</sup>H-NMR comparison of anomeric proton area of pullulan and pullulan alkyne recorded at 400 MHz in DMSO-d<sub>6</sub>.

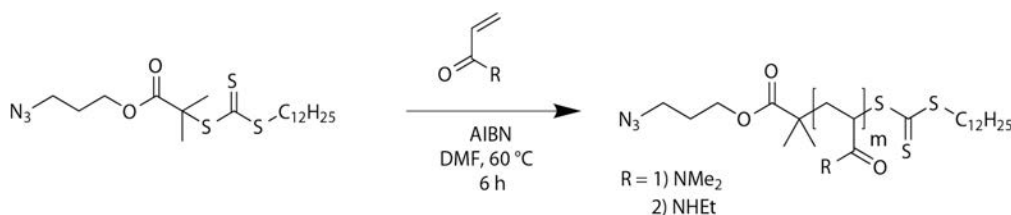
When comparing the SEC elution curves of depolymerized pullulan with the alkyne functionalized in Figure IV.2b only a very slight decrease in the average molecular weight was observed. For that reason it can be stated, that the reaction conditions for the reductive amination of pullulan do not promote depolymerization and the predominant reaction pathway is the reductive amination of the  $\alpha$ -1 aldehyde corresponding to the  $\omega$ -glucose unit. However, the presence of the alkyne group cannot be directly detected *via* <sup>1</sup>H-NMR due to an overlap of the propargyl proton with signals corresponding to pullulan. Therefore, different signals corresponding to the anomeric protons of the terminal glucose unit have to be investigated. In case of full conversion of the  $\alpha$ -1 aldehyde to the corresponding amine, the anomeric proton signals ( $\alpha$ -centered at 6.7 ppm and  $\beta$ -centered at 6.3 ppm) should disappear completely. As



displayed in Figure IV.2c, both proton signals disappeared after the reductive amination and a complete conversion can therefore be assumed.

### IV.3. Synthesis of Azide Terminated Acrylamide Homopolymers

The introduction of a terminal alkyne functionality to the polysaccharide pullulan introduces a pathway to synthesize a variety of DHBCs by employing CuAAC as conjugation reaction. In order to conjugate a second block to pullulan, the polymer has to possess an azide group. Therefore, poly(acrylamide) polymers were synthesized *via* RDRP reactions starting from a chain transfer agent bearing an azide functionality. Thus, poly(*N,N*-dimethylacrylamide) (PDMA- $N_3$ ) and poly(*N*-ethylacrylamide) (PEA- $N_3$ ) were synthesized with dodecylthiocarbonylthio-2-methylpropanoic acid 3'-azidopropylester as chain transfer agent according to a known procedure.<sup>89, 105</sup>



**Scheme IV.3** RAFT polymerization procedure for the synthesis of azido terminated poly(acrylamides).

The synthesized poly(acrylamides) PDMA- $N_3$  and PEA- $N_3$  possess a narrow size distribution and molecular masses of 16 800 g·mol<sup>-1</sup> and 13 900 g·mol<sup>-1</sup> (Table IV.1). Furthermore, the afforded homopolymers were well soluble in water, even without the removal of the RAFT group. However, a certain presence of aggregates or associates was observed for all conjugation blocks *via* DLS (Figure IV.3a).

**Table IV.1** Summary of SEC results of PDMA- $N_3$  and PEA- $N_3$  measured in NMP at 70 °C against PS calibration.

Polymer	$M_{n,app,SEC}$ (g·mol <sup>-1</sup> )	$\mathcal{D}$
PDMA- $N_3$	16 800	1.26
PEA- $N_3$	13 900	1.37

PEA- $N_3$  and pullulan display bimodal size distributions with average apparent radii of 7 nm and 10 nm for the small species and 100 nm for the second species, respectively. In contrast to this, PDMA- $N_3$  possesses a very broad monomodal size distribution. The presence of these homopolymer aggregates gives rise to a certain interaction of the homopolymers inside the aqueous solution, probably due to the RAFT groups in the case of the poly(acrylamide) polymers and presumably due to hydrogen bonding in the case of pullulan, respectively. It has to be taken into account, that the particle size distribution is weighed by intensity and the absolute abundance of the aggregates is relatively low. However, size and shape of the aggregates origin from the conformation of single polymer chains in aqueous solution were not determined.<sup>243</sup> Assuming a flexible coil conformation, the interaction of polymer chains occurs already at low concentration, presumably leading to the observed aggregates or associates.<sup>121, 244</sup>

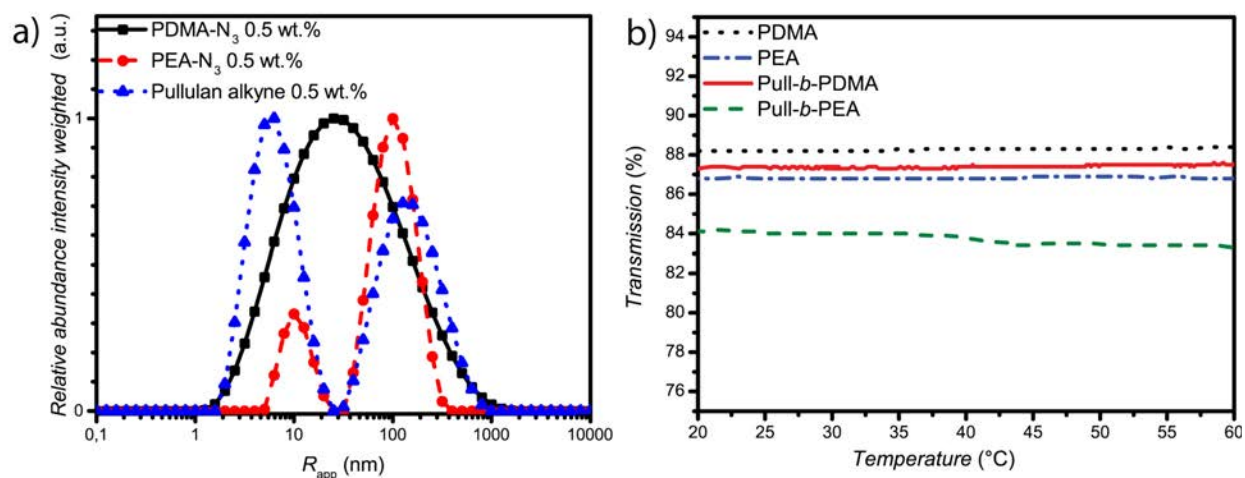
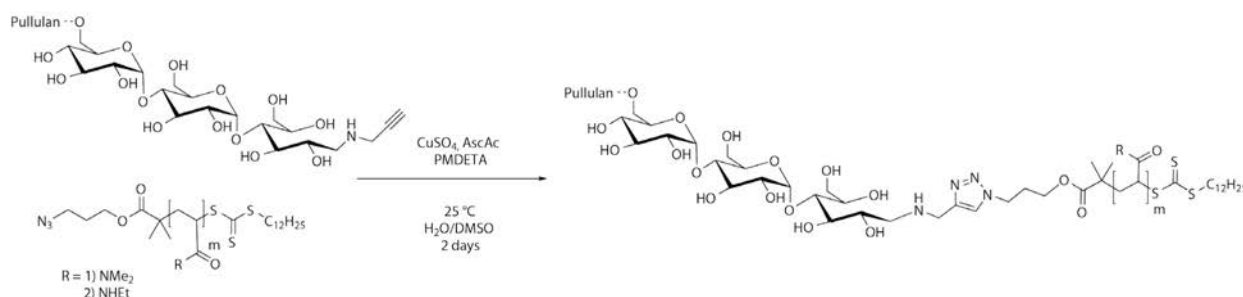


**Figure IV.3** a) Intensity weighted size distributions of pullulan, PDMA- $N_3$  and PEA- $N_3$  in Millipore water measured *via* DLS at 25 °C; b) Turbidimetry measurements of PDMA and PEA homopolymers and the block copolymers pullulan-*b*-PDMA and pullulan-*b*-PEA.

In addition, turbidimetry measurements of PDMA- $N_3$  and PEA- $N_3$  in water proved the solubility of the homopolymers up to 60 °C. Therefore, any temperature dependent aggregation of polymer chains can be excluded as well.

#### IV.4. Conjugation of Block Copolymers via Copper Catalyzed Azide Alkyne Cycloaddition

After the synthesis of the corresponding alkyne and azide functionalized homopolymer blocks, the conjugation towards the DHBCs *via* CuAAC was attempted. CuAAC is a versatile tool for the facile synthesis of block copolymers. The conjugation can be carried out at ambient temperature in various solvents, such as toluene, DMSO, and water. In order to conjugate two hydrophilic polymers to a DHBC, a mixture of water and DMSO was employed to ensure complete solubility of all reagents (Scheme IV.4).



**Scheme IV.4** CuAAC conjugation reaction scheme of pullulan alkyne and azide terminated poly(acrylamides).

As displayed in Scheme IV.4, the conjugation appears to be a 1:1 reaction. However, the absolute molecular masses of the two polymer blocks were not determined and only apparent average molecular weight distributions were assessed. The determination of the correct molar ratio between both polymers would only be possible with the conduction of several conjugation experiments with varying compositions. Due to the difficulty of a removal of unreacted polymer blocks and therefore a recovery of homopolymer, a different approach was assessed. In order to ensure a full conversion of one polymer block, namely the azide functionalized poly(acrylamides), a 1.2 molar excess of pullulan alkyne was used. The excess of pullulan was then removed by the application of an azidomethyl polystyrene resin, which was added to the reaction mixture after the conjugation. Thus, the resin azide groups conjugate with remaining pullulan alkyne and the resin particles with a mesh size of 100 to 200 can be easily removed after the cycloaddition reaction by filtration, which facilitates the purification of the block copolymers. A summary of the apparent average number weighted molecular masses determined *via* SEC displays the outcome of the conjugation reactions and the corresponding values of the homopolymers (Table IV.2). As visible from the SEC results, the apparent average number

weighted molecular masses of the conjugated block copolymers differ strongly from the ones of the corresponding homopolymers. Despite increased molecular masses, no clear indication of a successful conjugation and removal of unreacted homopolymer can be given by a separate consideration of the SEC result only. For that reason, the block copolymers were further investigated by  $^1\text{H-NMR}$  and precise comparison with the homopolymer blocks was conducted *via* SEC.

**Table IV.2** Summary of SEC results corresponding to the conjugation reactions.

Polymer	SEC System	$M_{n,app,SEC}$ ( $\text{g}\cdot\text{mol}^{-1}$ )	$D$
<b>Pullulan depolymerized</b>	Water, pullulan calib.	14 000	1.8
<b>Pullulan alkyne</b>	Water, pullulan calib.	16 000	1.8
<b>PDMA-<math>N_3</math></b>	NMP PS calib.	16 800	1.3
<b>PEA-<math>N_3</math></b>	NMP PS calib.	13 700	1.4
<b>Mixture Pull &amp; PDMA</b>	Water, pullulan calib.	17 300	1.9
<b>Mixture Pull &amp; PEA</b>	Water, pullulan calib.	6000	3.5
<b>Pull-<i>b</i>-PDMA</b>	Water, pullulan calib.	21 500	1.9
<b>Pull-<i>b</i>-PEA</b>	Water, pullulan calib.	26 500	1.6

### Conjugation of Pull-*b*-PDMA

With an apparent average number weighted molecular mass of  $21\,500\text{ g}\cdot\text{mol}^{-1}$  and a  $D$  of 1.9, Pull-*b*-PDMA does not differ significantly from both homopolymers. A significant issue is the determination in different elution solvents. In order to afford comparable values to distinguish a successful conjugation, pullulan, PDMA, a mixture of both blocks, and Pull-*b*-PDMA were examined *via* SEC in acetate buffer. Figure IV.4b displays the comparison of the different polymers showing that the block copolymer elutes at a lower volume than the different polymer blocks and the corresponding mixture. This is already a good indication for the successful conjugation of pullulan and PDMA. Regarding that pullulan elutes at a higher volume than the mixture and the block copolymer, a complete removal of unreacted pullulan alkyne can be stated as well. The application of an equimolar amount of resin ensured a full conversion of PDMA.

When comparing the conjugated block copolymer with the homopolymer mixture, only a small increase in the apparent average molecular mass by 25% from 17 300 g·mol<sup>-1</sup> to 21 500 g·mol<sup>-1</sup> with similar  $D$  of 1.9 was detected. The comparison between block copolymer and polymer mixture is only indicative due to further consideration of the separated homopolymer blocks allowing distinguishing whether the conjugation afforded the desired block copolymer. The comparison of the elution curves directs towards a successful conjugation of pullulan and PDMA, but the <sup>1</sup>H-NMR spectrum of the block copolymer underlines the successful conjugation by displaying proton signals originating from the anomeric protons of pullulan between 5.0 and 5.3 ppm as well as the signals of the methyl side groups corresponding to PDMA between 2.7 and 3.1 ppm (Figure IV.4c).

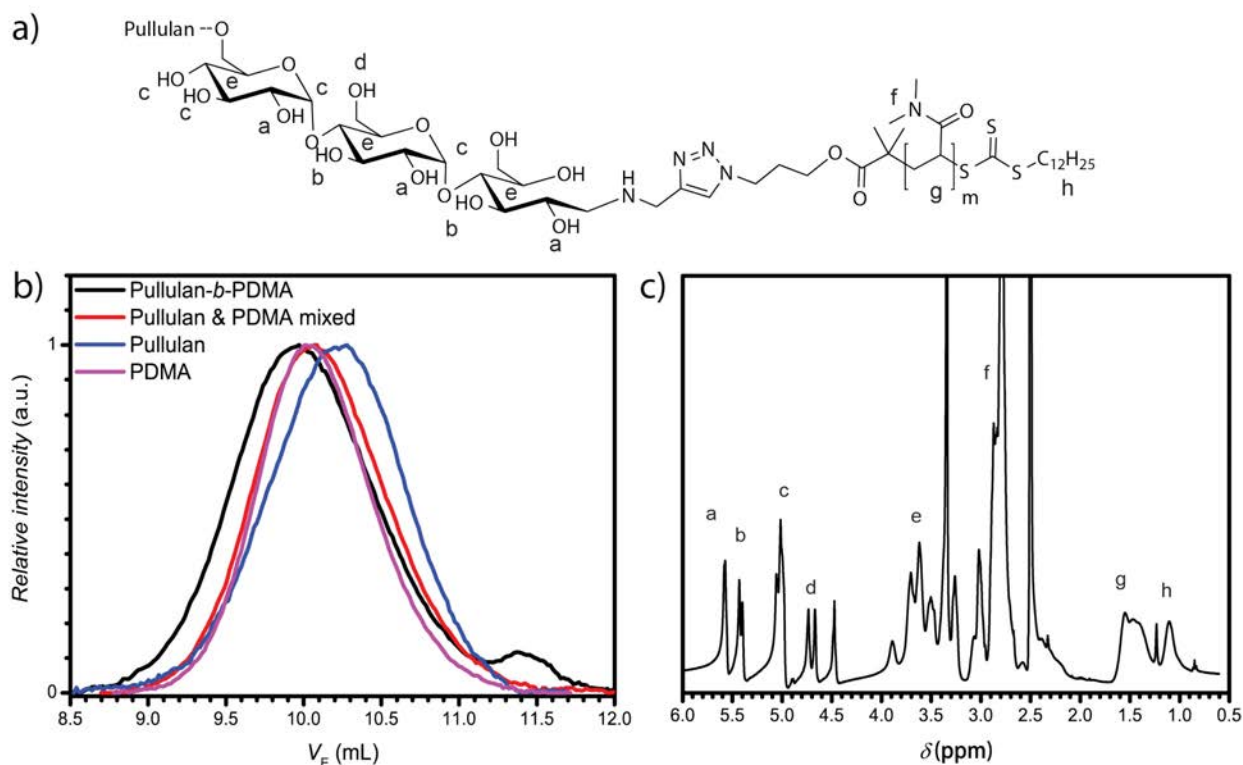


**Figure IV.4** a) Chemical structure of Pull-*b*-PDMA; b) SEC traces of conjugated Pull-*b*-PDMA, a homopolymer mixture and the homopolymers in acetate buffer and c) corresponding <sup>1</sup>H-NMR spectrum of the block copolymer in DMSO-*d*<sub>6</sub> at 400 MHz.

## Conjugation of Pull-*b*-PEA

In order to assess a successful conjugation of pullulan and PEA, the approach was conducted similar to Pull-*b*-PDMA. In contrast to the SEC elution curves corresponding to Pull-*b*-PDMA the SEC results of the conjugation of Pull-*b*-PEA in Figure IV.5b display a larger difference in the elution volumes. Pull-*b*-PEA possesses the lowest elution volume with an apparent average number weighted molecular mass of  $26\,500\text{ g}\cdot\text{mol}^{-1}$  and a polydispersity of 1.6 and the homopolymers elute significantly after the block copolymer. The most striking difference is the SEC curve of the polymer mixture with a  $M_{n,\text{app}}$  of  $6000\text{ g}\cdot\text{mol}^{-1}$  and broad  $D$  of 3.5 (Table IV.2). The strong contrast between block copolymer and mixture indicates a completely different structure and therefore states the conjugation of pullulan and PEA. Furthermore, the mixture broadly elutes in between the single polymer blocks indicating a certain separation of the different polymers on the column.

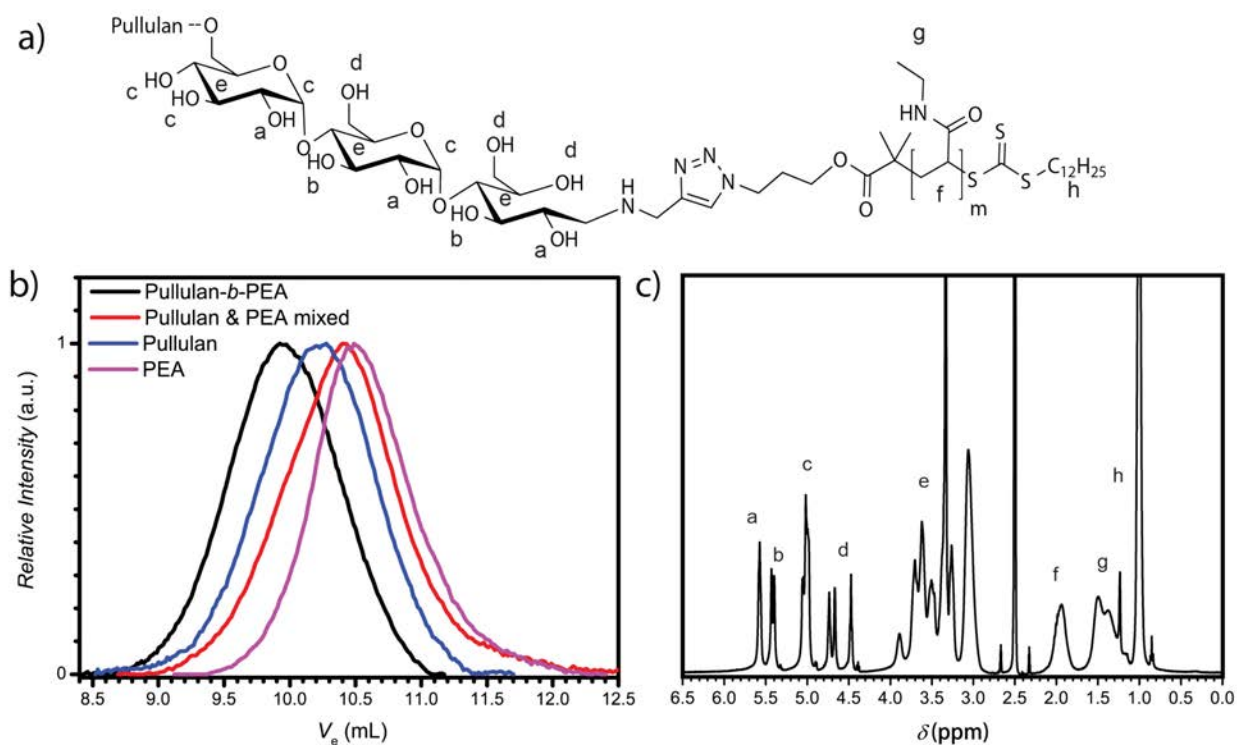


**Figure IV.5** a) Chemical structure of Pull-*b*-PEA; b) SEC traces of conjugated Pull-*b*-PEA, a homopolymer mixture and the homopolymers in acetate buffer and c) corresponding  $^1\text{H-NMR}$  spectrum of the block copolymer in DMSO- $d_6$  at 400 MHz.

The  $^1\text{H-NMR}$  spectrum of the block copolymer displays the presence of both blocks as well, e.g. the signals of anomeric protons in the pullulan block between 5.0 and 5.3 ppm and the signals of

the methyl side groups in the PEA block between 0.9 and 1.1 ppm (Figure IV.5c). A full conversion of PEA to the block copolymer can be stated here as well as for Pull-*b*-PDMA.

The evaluation of SEC and  $^1\text{H-NMR}$  results of Pull-*b*-PEA display a clearer outcome compared to Pull-*b*-PDMA. Whereas  $^1\text{H-NMR}$  shows full conversion for both DHBCs, the corresponding SEC traces of Pull-*b*-PDMA are rather ambiguous. A possible explanation of this behaviour can be given in a lower difference in hydrophilicity causing pullulan and PDMA mixtures to elute in a similar fashion as the conjugated block copolymer. In contrast to PEO-*b*-PVP block copolymers examined in chapter III, where the block copolymer was synthesized *via* RAFT polymerization starting from a PEO macro RAFT chain transfer agent, successful synthesis of the conjugated pullulan block copolymers could not be as easily determined *via* SEC. With the use of the azidomethyl polystyrene resin, an effective and versatile pathway for CuAAC reactions was introduced. The self-assembly behaviour of the novel double hydrophilic block copolymers Pull-*b*-PDMA and Pull-*b*-PEA has to be investigated now.

#### IV.5. Aqueous Self-Assembly of Pull-*b*-PDMA and Pull-*b*-PEA

DHBC self-assembly without influence of external stimuli such as pH or temperature requires certain properties of the block copolymer composition. In previous reports, a strong difference in hydrophilicity i.e. the interaction of the polymer with water molecules was regarded as the key role for successful self-assembly.<sup>197, 199</sup> Regarding this assumption, a comparison of the second virial coefficient  $A_2$  of the homopolymers should be further taken into account. The  $A_2$  factor which can be determined via SLS can be seen as a quantitative measure for solvent solute interactions.<sup>245</sup> The second virial coefficients for pullulan and PDMA in the molecular weight range were already studied in literature and determined to be  $3.2 \cdot 10^{-4} \text{ mol} \cdot \text{cm}^3 \cdot \text{g}^{-2}$  for pullulan,<sup>246</sup> and  $8.0 \cdot 10^{-4} \text{ mol} \cdot \text{cm}^3 \cdot \text{g}^{-2}$  for PDMA, respectively.<sup>247</sup> When comparing these two values, PDMA appears to possess a stronger interaction with the solvent water than pullulan. Since PEA is a quite similar polymer, its  $A_2$  factor should be in the same range as the one of PDMA. (It is assumed that phase separation of the different hydrophilic polymer blocks occurs, when the difference in hydrophilicity is large enough.) Furthermore, chain rigidity is assumed to influence the self-assembly behavior, too. Hydrogen bonding and the corresponding thermo-responsivity

as well as phase separation of the backbone it was observed for homopolymer self-assembly play only a minor role.<sup>248, 249</sup> Furthermore, the functional groups of pullulan and both polyacrylamide polymer blocks are not known to show any thermo-responsive behavior (Figure IV.3b) in the investigated temperature range, which allows the formation of purely hydrophilic self-assembly. Nevertheless, PEA is known for its LCST behavior at elevated temperatures above 70 °C.<sup>250</sup> Actually, PEA was chosen as a block due to this fact because the comparison between a block without LCST and a block with LCST at elevated temperatures should give some insights into fundamentals of DHBC aggregate formation. Since the mechanism of DHBC self-assembly is not completely understood yet, investigations of the dissolved DHBCs via DLS were conducted first.

### Self-assembly of Pull-*b*-PDMA

In order to investigate the self-assembly behaviour of Pull-*b*-PDMA, aqueous solutions of the block copolymer containing 0.1, 0.5, and 1.0 wt.% were prepared and examined *via* DLS at 25 °C. The average apparent radii of the prepared block copolymer solutions are summarized in Table IV.3. As visible from the intensity weighted particle size distribution in Figure IV.6a, Pull-*b*-PDMA self-assembles to aggregated structures with an apparent average radius of 80 nm at low concentration of 0.1 wt.%. A small amount with relative abundance of 0.04 and an average apparent radius of 4 nm can be observed as well in the particle size distribution. The peak can be attributed in similarity to PEO-*b*-PVP block copolymers (Chapter III) to a very small amount of free dissolved block copolymer in the solution.

**Table IV.3** Summary of apparent average hydrodynamic radii of Pull-*b*-PDMA and derivatives determined *via* DLS at 25 °C.

Polymer	Concentration (wt.%)	Peak 1 $R_{h,app}$ (nm)	Rel. abund.	Peak 2 $R_{h,app}$ (nm)	Rel. abund.
Pull- <i>b</i> -PDMA	0.1	4.0	0.04	79.4	1.0
	0.5	5.0	0.04	79.4	1.0
	1.0	5.0	0.04	100.0	1.0
Pull- <i>b</i> -PDMA-OH	0.1	5.0	0.1	170.0	1.0
Pull- <i>b</i> -PDMA-RhB	0.1	-	-	100.0	1.0

The fivefold increase in concentration to 0.5 wt.% does not affect the apparent particle size distribution. Only a slight increase in the apparent average radius of the free dissolved block



copolymer species to 5 nm can be detected. An increase in concentration to 1.0 wt.% results in an increase in the average apparent radius of the aggregate species by 20% to 100 nm. The increase in the radius can be attributed to the higher amount of Pull-*b*-PDMA abundant to be incorporated into these structures. When comparing the particle size distribution of Pull-*b*-PDMA with the one of the previously investigated PEO-*b*-PVP (Figure III.3), a drastic difference can be stated in the relative abundance of self-assembled species. Whereas PEO-*b*-PVP only self-assembles in a very low amount at concentration below 1.0 wt.%, Pull-*b*-PDMA block copolymers almost exclusively self-assemble to higher ordered structures. Moreover, the self-assembly can be regarded as quite efficient in comparison to similar systems reported in literature.<sup>195, 196, 199, 227</sup>

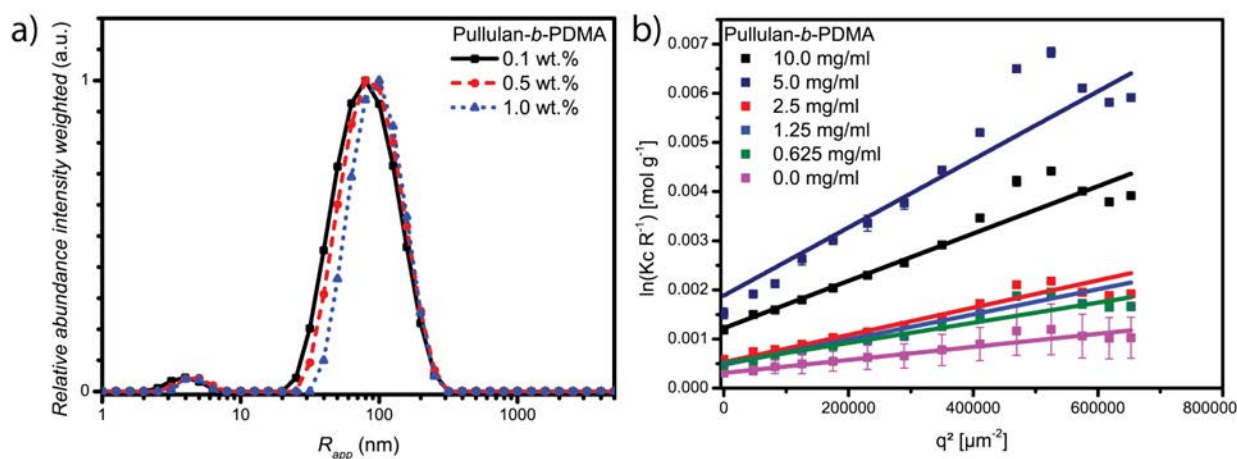


**Figure IV.6** a) Intensity weighted particle size distributions of Pullulan-*b*-PDMA in Millipore water measured *via* DLS at 25 °C; b) SLS Guinier plot of Pull-*b*-PDMA with extrapolation of  $c \rightarrow 0$ .

Again, it should be emphasized that the particle size distributions are calculated *via* the average intensity of the detected signals. Therefore, the quantity of the larger species is overestimated in a decent amount and the actual species of self-assembled structures is significantly lower as depicted. Concerning the apparent average size distribution of the homopolymers in Figure IV.3a, a direct connection with the intensity weighted particle size distribution of Pull-*b*-PDMA cannot be stated. In contrast to the homopolymers, the relative abundance of free dissolved species can be neglected. Furthermore, the broad size distribution of the PDMA cannot be seen in the size distribution of the block copolymer as well. Therefore, it can be stated that the observed aggregates correspond to self-assembled block copolymer structures.

The confirmation of a significant amount of self-assembled structures in Pull-*b*-PDMA solution leads to the opportunity to determine the structure of these species. In order to determine the radius of gyration ( $R_g$ ) of Pull-*b*-PDMA, static light scattering experiments were conducted with concentration a row of  $10 \text{ mg}\cdot\text{mL}^{-1}$ ,  $5 \text{ mg}\cdot\text{mL}^{-1}$ ,  $2.5 \text{ mg}\cdot\text{mL}^{-1}$ ,  $1.25 \text{ mg}\cdot\text{mL}^{-1}$ , and  $0.63 \text{ mg}\cdot\text{mL}^{-1}$ . The data obtained from the light scattering experiments at scattering angles between  $30^\circ$  and  $150^\circ$  were plotted via a Guinier plot in Figure IV.6b. The calculated values for Pull-*b*-PDMA are listed in Table IV.4.

**Table IV.4** Calculated values of the quantities of Pull-*b*-PDMA determined *via* the Guinier plot.

Entry	Quantity	Value (unit)	Error (%)
1	$M_w$ (c)	$3.239\text{e}+06 \text{ (g}\cdot\text{mol}^{-1})$	$\pm 27.9$
2	$M_w$ ( $q^2$ )	$3.239\text{e}+06 \text{ (g}\cdot\text{mol}^{-1})$	$\pm 8.35$
3	$A_2$	$6.684\text{e}-08 \text{ (mol}\cdot\text{dm}^3\cdot\text{g}^{-2})$	$\pm 42.2$
4	$R_g$	$1.081\text{e}+02 \text{ (nm)}$	$\pm 7.1$

As displayed in Figure IV.6b, the Guinier plot extrapolation afforded some discrepancies for high  $q^2$  values resulting in larger errors. The nonlinear increase in  $\ln(Kc\cdot R^{-1})$  can be attributed to the presence of free dissolved block copolymer chains that affect the intensity function. Nonetheless, it was possible to evaluate the obtained data and determine  $R_g$  with 108 nm and a low error of 7%. This value is in the range of  $R_{app}$  determined via DLS measurements. Moreover, a direct comparison of both values in analogy to the  $\rho$ -ratio *via* the quotient of  $R_g$  and the average apparent radius  $R_{app}$  afforded a value of 0.98, which corresponds to hollow spheres and therefore indicates the presence of vesicular structures.<sup>245</sup>

In order to exclude external effects such as the hydrophobic effect of the trithiocarbonate RAFT group attached to the PDMA chain end to direct the self-assembly towards vesicular structures, a block copolymer with the PDMA RAFT group removed was synthesized and investigated *via* DLS. The comparison of the intensity weighted particle size distributions of Pull-*b*-PDMA before and after the removal of the RAFT group reveals that the hydrophobic end group of the trithiocarbonate function does not enhance the self-assembly behaviour of the block copolymer in water (Figure IV.7a). Moreover, a shift to a larger average apparent radius by 100% from 79 nm to 170 nm was observed. It has to be noted, that the relative abundance of free dissolved block copolymer increased as well, but the driving force for the self-assembly can be clearly attributed to the difference in hydrophilicity of the two polymer blocks.

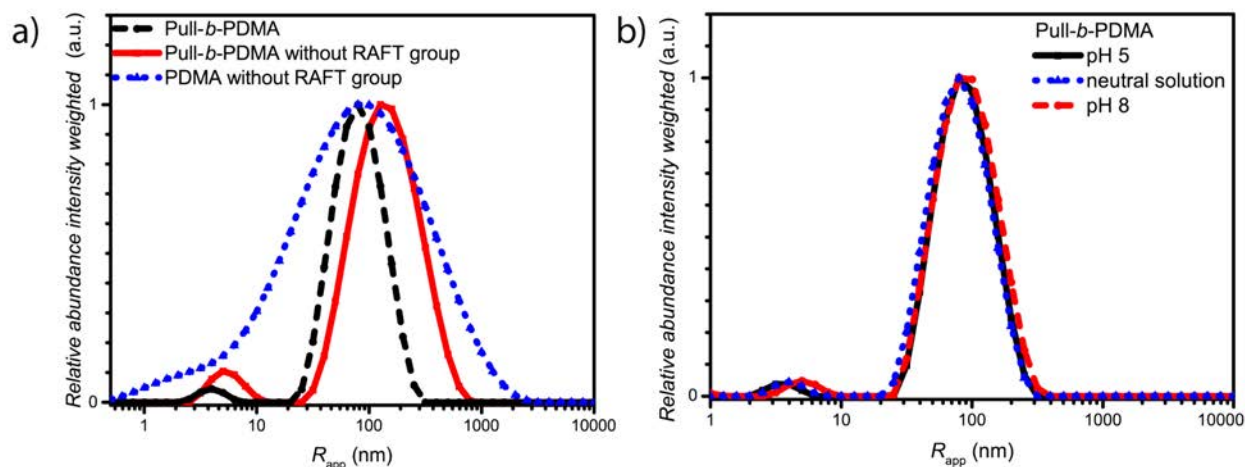


**Figure IV.7** a) Intensity weighted particle size distributions of 0.1 wt.% solutions of Pull-*b*-PDMA with and without RAFT group attached to PDMA; b) intensity weighted particle size distribution of 0.5 wt.% solutions of Pull-*b*-PDMA at different pH values in Millipore water measured *via* DLS at 25 °C.

The effect of the pH value of the Pull-*b*-PDMA solution on the self-assembly behaviour was studied as well to exclude the influence of charges or pH driven forces. Therefore, 0.5 wt.% solutions of the block copolymer in pH 5 and pH 8 buffer were prepared and investigated *via* DLS. Higher acidic or basic conditions were not investigated as decomposition of pullulan might occur. As seen in Figure IV.7b, neither slightly acidic nor basic conditions cause an effect to the particle size distribution of Pull-*b*-PDMA. This further supports the concept of purely hydrophilic block copolymer self-assembly.

With DLS and SLS experiments indicating the presence of spherical vesicular structures, cryo SEM microscopy was applied to confirm the light scattering results.

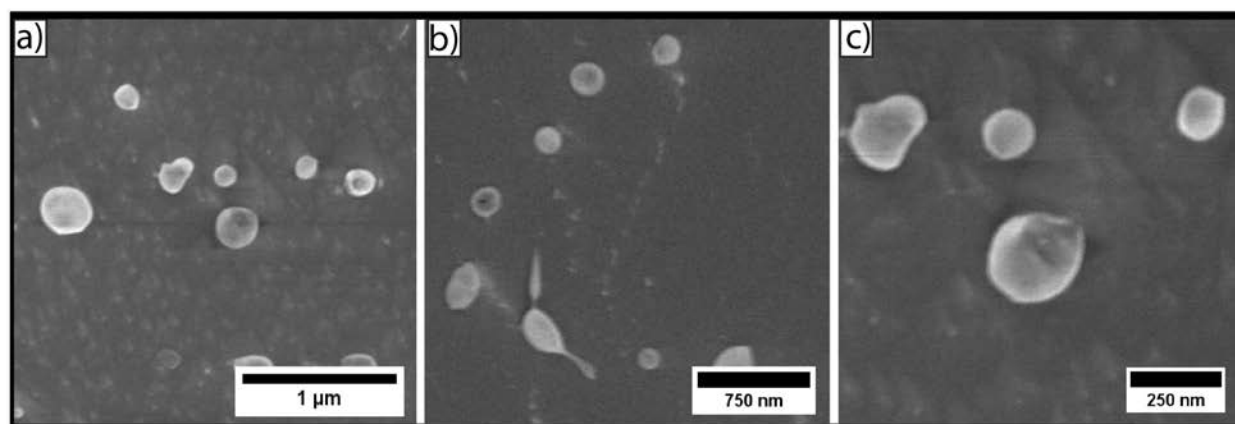


**Figure IV.8** Cryo SEM micrographs of 0.5 wt.% solutions of self-assembled Pull-*b*-PDMA vesicles.

As visible from the micrographs in Figure IV.8a and Figure IV.8b, spherical structures of Pull-*b*-PDMA with diameters in a range between 80 nm and 250 nm were observed. The estimated particle size distribution obtained from cryo SEM is in a comparable range with the average particle size distribution afforded by DLS measurements. This result underlines the initial assumption that the structures observed *via* DLS correspond to spherical structures. However, no clearly ruptured particles were observed in the cryo SEM micrographs. Therefore, it cannot be distinguished, if vesicular structures are present or not. In order to gain deeper insight into the particle morphology, a 2.5 wt.% solution of Pull-*b*-PDMA was directly stained with 10  $\mu$ L of a 0.08 mM Rhodamine B solution and investigated with LSCM/DIC microscopy.

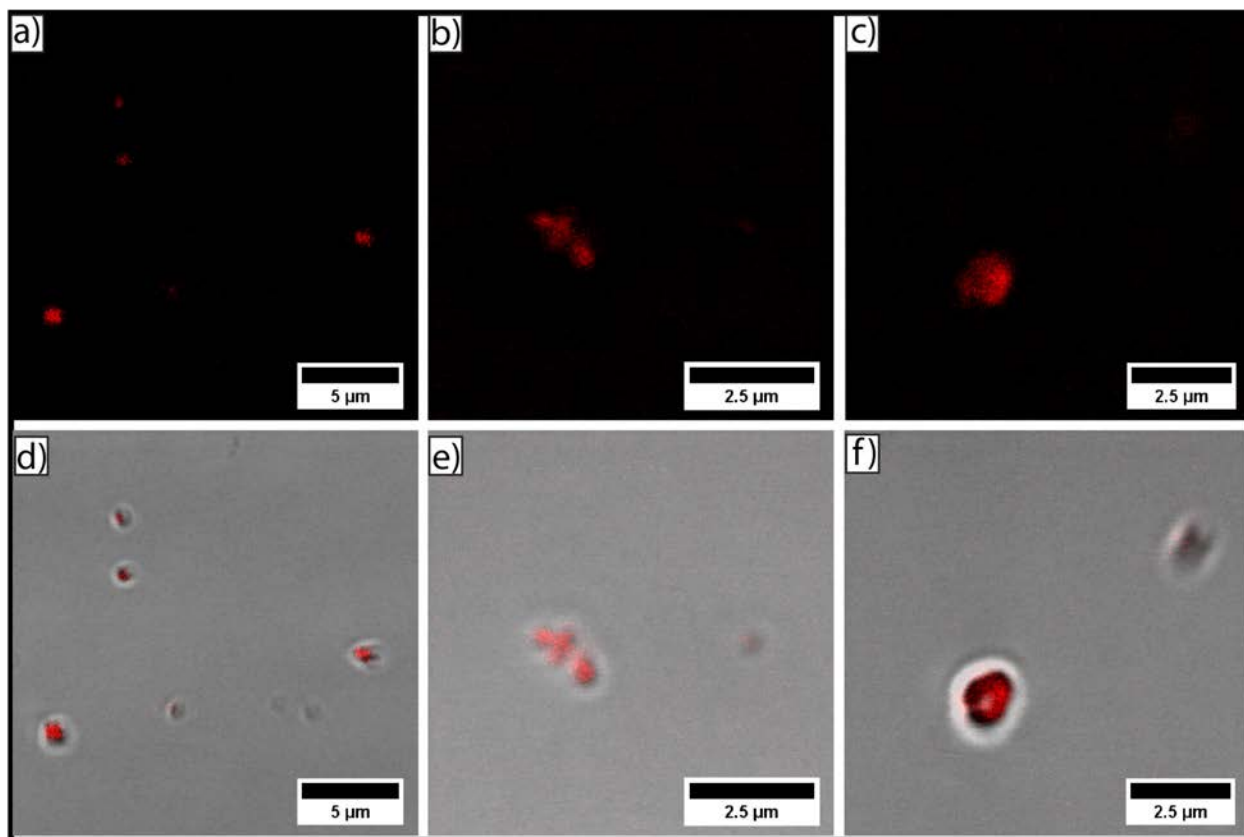


**Figure IV.9** a), b) & c) Confocal micrographs of spherical particles of Pull-*b*-PDMA at 2.5 wt.% stained with 0.08 mM Rhodamine B; d), e) & f) corresponding DIC images with fluorescence overlay displaying the particle structure.

As displayed in Figure IV.9 the confocal micrographs show spherical structures with enriched Rhodamine B content. Since the dye was added to the block copolymer solution after the dissolution and therefore after the self-assembly occurred, the enrichment inside the structures can be attributed to permeation into the spherical structures. However, interactions of the block

copolymer membrane with Rhodamine B seem to prevent diffusion back to the external media. Consequently, the observed enrichment inside the particles may occur. As visible from the LSCM micrographs, the average diameter of the observed spherical particles exceeds the determined one from DLS and cryo SEM with more than one micrometer by almost five fold. The increase in the diameter can be attributed on the one hand to the higher concentration of Pull-*b*-PDMA and on the other hand to the particle motion inside the solution resulting in an uncertainty of the image. Furthermore, the lower resolution level of LSCM instruments within the range of the determined particle size prevents a clear resolution and broadens the signal. Therefore, the size of the depicted spherical particles has to be handled with care. Moreover, the resolution of the LSCM instrument prevents imaging of particles with smaller size. Besides the spherical structures within the micrometer size, smaller spherical particles without increased Rhodamine B concentration are visible in Figure IV.9d. These particles were observed quite frequently but could not be resolved efficiently due to the fast particle motion inside the solution. In order to exclude interactions between the self-assembled particles and the dye inside solution and to obtain a higher resolution, PDMA- $N_3$  was labelled with Rhodamine B isothiocyanate and subsequently conjugated to pullulan *via* CuAAC to afford a dye labelled block copolymer (Figure IV.10a). Since attaching a charged end group to the block copolymer that might affect the self-assembly, DLS was performed with a 0.1 wt.% solution of Pull-*b*-PDMA-RhB to investigate the effect of the dye. As visible from Figure IV.10b, the labelling with the dye results in a monomodal apparent average size distribution.

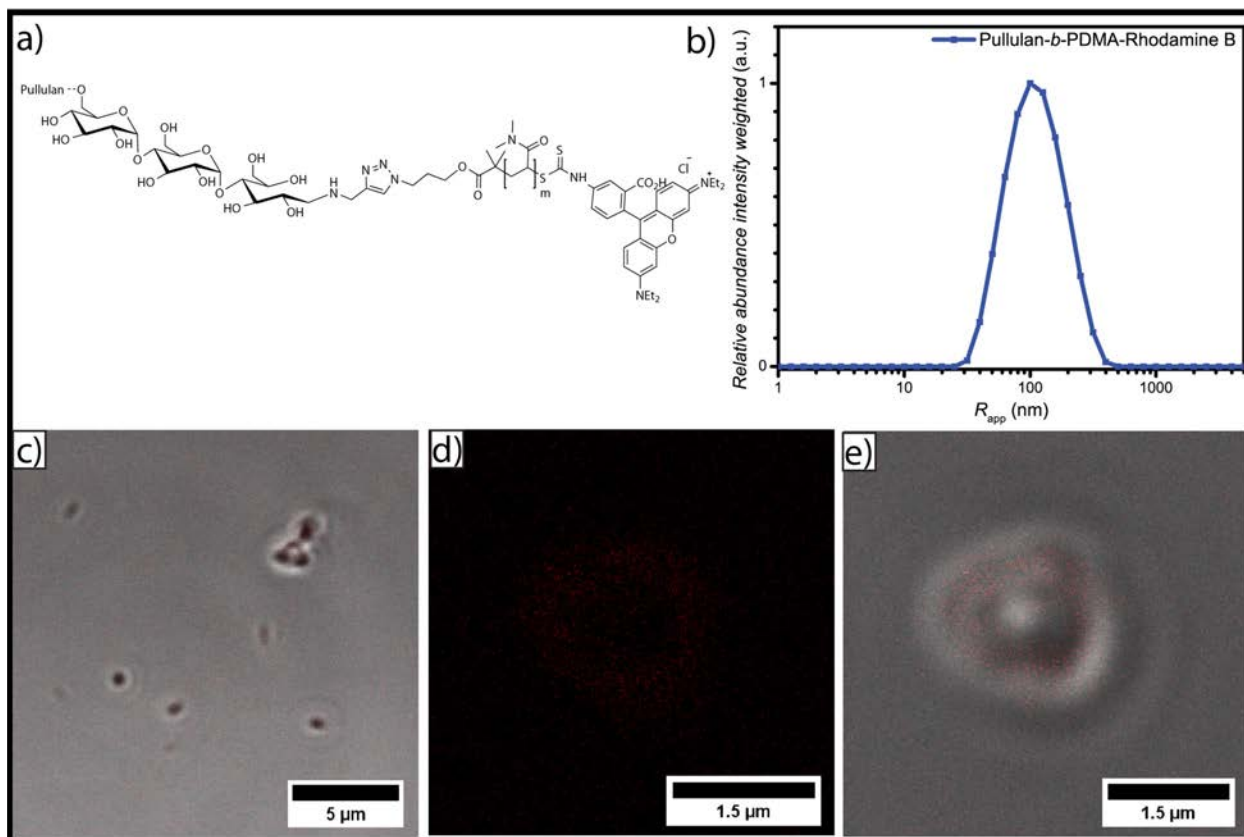


**Figure IV.10** a) Scheme of the Rhodamine B functionalized Pull-*b*-PDMA block copolymer; b) corresponding intensity weighted particle size distribution at 0.1 wt.%; c) LSCM micrographs of a 2.5 wt.% 9:1 solution of Pull-*b*-PDMA / Pull-*b*-PDMA-RhB and d) and e) magnification of Pull-*b*-PDMA / Pull-*b*-PDMA-RhB based particles.

The average apparent radius of self-assembled Pull-*b*-PDMA-RhB was determined to be 100 nm (Table IV.3). The fact that no free dissolved block copolymer was observed for the dye labelled block copolymer gives rise to the assumption that the dye incorporation has a certain effect on the self-assembly. Most probably ionic charges generated by Rhodamine B lead to an enhanced self-assembly. With having a dye labelled block copolymer that can be added to Pull-*b*-PDMA solutions, more insight into the particle structure could possibly be obtained by LSCM measurements. The fluorescent dye directly attached to the block copolymer should on the one hand ensure that only spherical structures which self-assembled from the DHBC were investigated. On the other hand, the proposed membrane structure should be further examined because the dye can only be present in areas where the block copolymer is expected to concentrate. For that reason, 10% of the block copolymer mass corresponding to a 2.5 wt.% solution was replaced by Pull-*b*-PDMA-RhB and the solution was investigated *via* LSCM/DIC microscopy. As visible from the micrographs in Figure IV.10c and Figure IV.10e, the amount of

fluorescent material is conclusively decently lower in comparison to the stained samples. Furthermore, spherical structures with a vesicular morphology and average diameters of 1 to 2  $\mu\text{m}$  could be observed, where the fluorescent membrane can be clearly attributed to the labelled Pull-*b*-PDMA block copolymer (Figure IV.10d). This is a strong indication that the predicted vesicular structure is present in the case of larger particles. However, particle motion and resolution limit of LSCM prevent a closer look on the observed submicron sized structures. Structures in the submicron-size range were observed, but could only be resolved as fluorescent spheres because the volume excited by the laser is too small to be resolved by the detector. In conclusion, it can be stated that Pull-*b*-PDMA forms self-assembled particular structures in aqueous solution with high abundance. Moreover, SLS and LSCM measurements indicate that hollow structures are formed.

### Self-assembly of Pull-*b*-PEA

The investigation of the self-assembly behaviour of Pull-*b*-PEA was carried out in a similar fashion as for Pull-*b*-PDMA. Solutions containing 0.1, 0.5, and 1.0 wt.% of block copolymer were prepared and investigated *via* DLS. As visible from the intensity weighted particle size distribution in Figure IV.11a, the self-assembly of Pull-*b*-PEA is slightly superior to Pull-*b*-PDMA.

**Table IV.5** Summary of apparent average hydrodynamic radii of Pull-*b*-PEA determined *via* DLS at 25 °C.

Polymer	Concentration (wt.%)	Peak 1 $R_{h,app}$ (nm)	Rel. abund.	Peak 2 $R_{h,app}$ (nm)	Rel. abund.
Pull- <i>b</i> -PEA	0.1	5.0	0.02	125.9	1.0
	0.5	5.0	0.02	125.9	1.0
	1.0	4.0	0.03	158.5	1.0

The bimodal intensity weighted apparent particle size distribution displays with 0.02 a 50% lower relative abundance of free dissolved block copolymer compared to Pull-*b*-PDMA. The average apparent radius of the free dissolved species was with 5 nm in the same range (compare Table IV.3 and Table IV.5). The average apparent radius of the second species corresponding to the aggregated structures was with 126 nm for the 0.1 wt.% solution 56% larger than the self-assemblies of Pull-*b*-PDMA at the same concentration. Increasing the block copolymer concentration to 0.5 wt.% results in slight broadening of the average apparent particle size distribution. The peak broadening is a similar observation as for the PDMA containing block

copolymer. The increase in concentration to 1.0 wt.% results in an increase in the average apparent radius by 33% to 160 nm. Compared to Pull-*b*-PDMA the self-assemblies possess an 80% larger average apparent radius and the relative abundance of the free dissolved species is in general lower. For that reason, the self-assembly of Pull-*b*-PEA can be regarded as more efficient. This improved self-assembly behaviour can be attributed to an increased tendency of microphase separation of the block copolymer due to a lower hydrophilicity of PEA in contrast to PDMA. The secondary amide side groups of *N*-ethylacrylamide interact in a different fashion with water than the tertiary amide of *N,N*-dimethylacrylamide. This difference can be seen as well in the intensity weighted particle size distributions of the corresponding homopolymers in Figure IV.3.

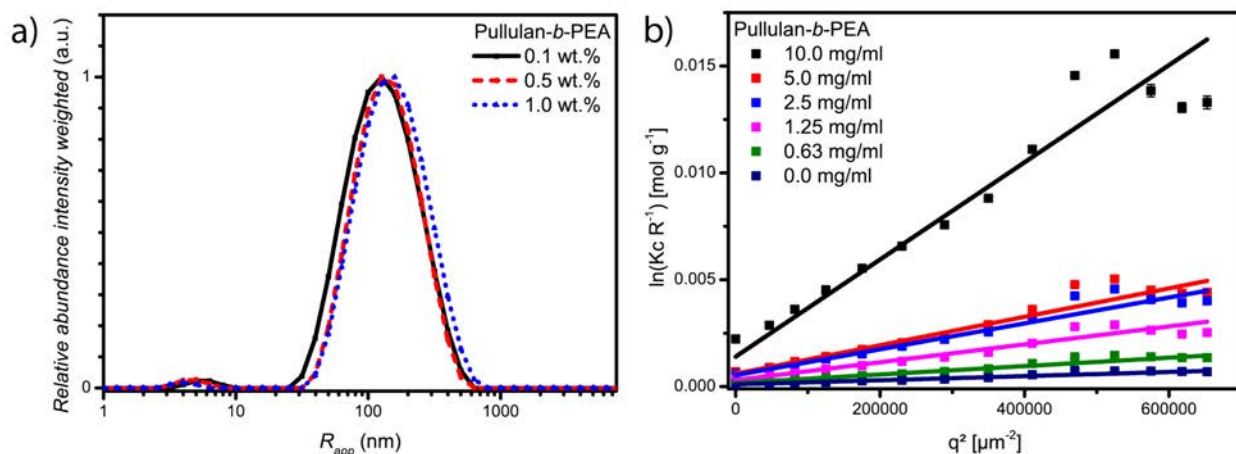


**Figure IV.11** a) Intensity weighted particle size distributions of Pull-*b*-PEA in water measured *via* DLS at 25 °C; b) SLS Guinier plot of Pull-*b*-PEA with extrapolation of  $c \rightarrow 0$ .

Due to the further improved self-assembly of Pull-*b*-PEA, SLS was performed in order to assess the structure of the aggregates observed in DLS. In analogy to the SLS evaluation of Pull-*b*-PDMA, the obtained data from SLS measurements at angles between 30° and 150° were evaluated using a Guinier plot (Figure IV.11b). As visible from the graph, the extrapolation of  $c \rightarrow 0$  *via* the Guinier plot affords more linear increasing data sets. Moreover, the errors of the separately assessed data points are significantly smaller when compared to Pull-*b*-PDMA. A possible explanation of the improved evaluability of the SLS Guinier plot of Pull-*b*-PEA could be the decreased amount of free dissolved species. However, the evaluation becomes less precise when approaching high  $q^2$  values as it was shown before with Pull-*b*-PDMA. These discrepancies origin from the high absolute amount of free dissolved block copolymer. As



explained before, the DLS average apparent size distributions are intensity weighted and therefore only suggest a very low amount of free dissolved block copolymer because large structures scatter with a higher intensity. The evaluation of the data obtained from SLS displayed in Table IV.6 affords a  $R_g$  of 129 nm for the Pull-*b*-PEA assemblies. The determined radius of gyration is in good agreement with the  $R_{app}$  determined *via* DLS for a concentration of 0.5 wt.%. The corresponding quotient of  $R_g$  and  $R_{app}$  is with 1.03 in the range of hollow spheres as it is the case for Pull-*b*-PDMA. Again, a strong indication for the presence of vesicular structures can be given from SLS investigations.

**Table IV.6** Calculated values of the quantities of Pull-*b*-PEA determined *via* the Guinier plot.

Entry	Quantity	Value (unit)	Error (%)
1	$M_w$ (c)	9.117e+06 (g·mol <sup>-1</sup> )	± 23.2
2	$M_w$ (q <sup>2</sup> )	9.117e+06 (g·mol <sup>-1</sup> )	± 5e-12
3	$A_2$	7.029e-08 (mol·dm <sup>3</sup> ·g <sup>-2</sup> )	± 29.6
4	$R_g$	1.293e+02 (nm)	± 3e-12

Regarding the obtained values of  $M_w$  for Pull-*b*-PDMA and Pull-*b*-PEA from Table IV.4 and Table IV.6, the low molecular weight of the structures comes to attention. When relating the average apparent molecular mass determined *via* SEC of the two block copolymers with the  $M_w$  determined *via* DLS, the number of polymer molecules incorporated into the structures is with approximately 150 for Pull-*b*-PDMA and 350 for Pull-*b*-PEA fairly low. It has to be considered that either the amount of free dissolved block copolymers inside the solution generates such high errors, that the value of  $M_w$  can only be regarded as a mean number between aggregates and chains or that the aggregates are at a highly swollen state in low concentrated solutions and form the observed aggregates as soon as the solution possesses the necessary concentration of block copolymer.

In order to confirm the vesicular structures postulated by SLS and DLS, cryo SEM measurements of an aqueous solution containing 0.5 wt.% of Pull-*b*-PEA were conducted. The corresponding micrographs in Figure IV.12a, Figure IV.12c, and Figure IV.12d display the presence of spherical particles with diameters ranging from approximately 50 nm to 300 nm as well as of larger particles with ruptured membrane structures with diameters between 200 nm and 500 nm. According to the average apparent particle size distribution obtained from DLS (Figure IV.11), the particle size distribution of the observed particles from the cryo SEM

micrographs is in close proximity. The fact that only large spherical structures show ruptures may be explained by two different possibilities. First, the sample could possess two types of spherical structures, small particle like structures below a diameter of 200 nm, and larger vesicular structures with membranes that rupture due to the freezing process in liquid nitrogen.

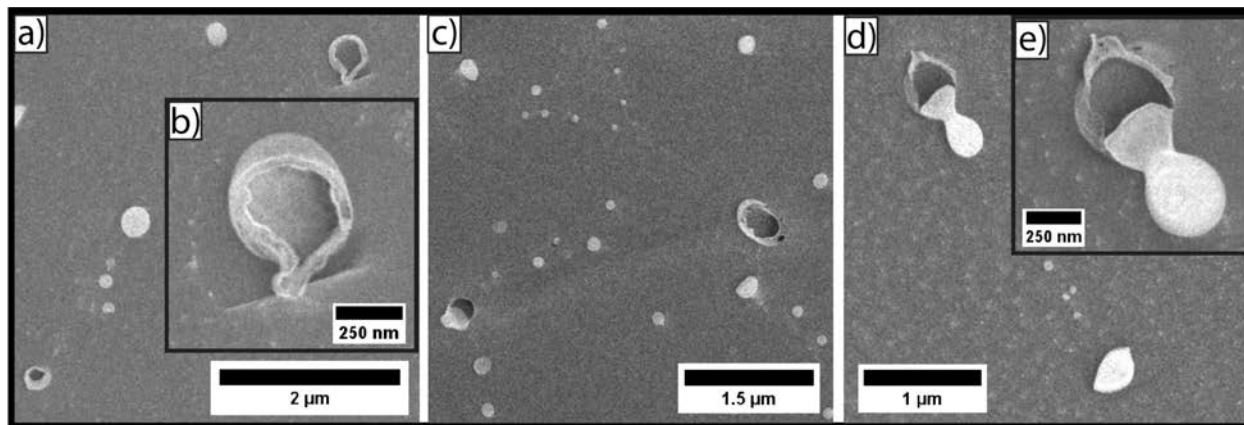


**Figure IV.12** Cryo SEM micrographs of 0.5 wt.% Pull-*b*-PEA displaying a), c), and d) spherical particles and hollow vesicular structures; b) & e) magnifications of the vesicular self-assemblies.

The second and more likely explanation is that only vesicular structures are present, but in order to generate ruptures of the membrane, the water content inside the vesicles has to be high enough that the ice crystals formed during the freezing process can break the membrane. The expansion of water inside the smaller vesicular structures is not strong enough to rupture the membrane and therefore, smaller vesicles appear as intact. Regarding the magnifications of ruptured structures in Figure IV.12b show a rather thick membrane structure that can be compared to the complex membrane structures observed *via* cryo TEM microscopy of crosslinked PEO-*b*-P(VP-*co*-VIm) structures in the previous chapter (Figure III.16). Furthermore, the magnified structure in Figure IV.12e displays a large ruptured vesicle attached or in close proximity to a smaller spherical structure. This particle pair strengthens the explained assumption. The outstanding result of the investigations of Pull-*b*-PEA is the relatively small size of these vesicles, compared to the dextran-*b*-PEO vesicles reported by Brosnan et al.<sup>199</sup>

LSCM/DIC measurements were employed with a Rhodamine B stained 2.5 wt.% Pull-*b*-PEA solution in order to obtain more insight to the vesicular structures. The confocal micrographs in Figure IV.13 display spherical particles with an average diameter of approximately 1 μm and an enriched Rhodamine B content. Most of the structures were observed directly in solution causing a diminished resolution due to particle motion and a certain density fluctuation and distortion

(Figure IV.13e and Figure IV.13f). Furthermore, it was possible to image vesicular shaped structures which were adsorbed to the glass surface (Figure IV.13d). Compared to the Rhodamine B stained structures of Pull-*b*-PDMA, the amount of Rhodamine B incorporated into the structures was significantly lower. The magnification of a single spherical structure in Figure IV.13c and Figure IV.13f displays only a low amount of counts, whereas Figure IV.9c displays a large fluorescence signal. In addition, more structures without or with a very low Rhodamine B content could be observed in the DIC micrographs causing no signal in the fluorescence channel (compare Figure IV.13a and Figure IV.13d). The spherical structures are clearly visible in DIC, but the resolution limit prevents a further investigation of the dye content of these structures.

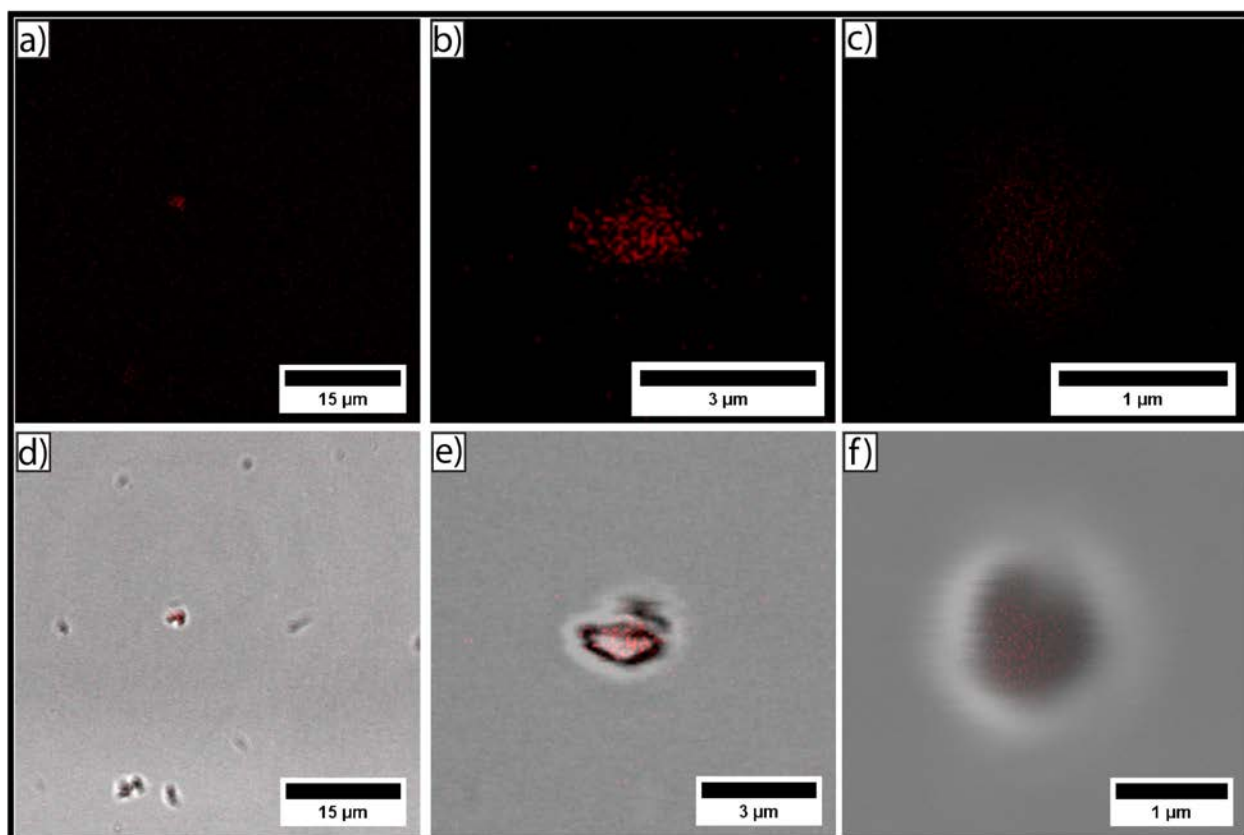


**Figure IV.13** a), b) & c) Corresponding fluorescence images of a d) LSCM overview of Rhodamine B stained Pullulan-*b*-PEA vesicles in water; e) a magnification of a vesicular structure. The distortion originates from the particle motion through the solution; f) magnified spherical particle.

Summarizing the results obtained *via* LSCM/DIC measurement, it has to be stated that no further information could be obtained from the investigation of Rhodamine B stained Pull-*b*-PEA solutions. In analogy to Pull-*b*-PDMA investigations, spherical structures with enriched dye content were observed and some of the structures indicate a vesicular structure. However, the

lack of resolution prevents a clear statement of the sample composition. SLS and cryo SEM measurements on the other hand afford a clearer indication towards vesicular structures.

### On the choice of filters

DLS and SLS are very sensitive techniques regarding the presence of dust inside the investigated samples. In order to remove all dust from the sample, 0.45  $\mu\text{m}$  CA filters were used for all investigations shown previously in this chapter. Especially the presence of aggregates exceeding the size of 1  $\mu\text{m}$  in the LSCM micrographs generates the question if larger aggregates were removed by filtration. To investigate the effect of filter sizes on the intensity weighted particle size distribution of Pull-*b*-PDMA and Pull-*b*-PEA, two larger filter variants, 0.8  $\mu\text{m}$  and 1.2  $\mu\text{m}$  CA syringe filters, were applied and the filtered solutions containing 0.5 wt.% of polymer were investigated *via* DLS.

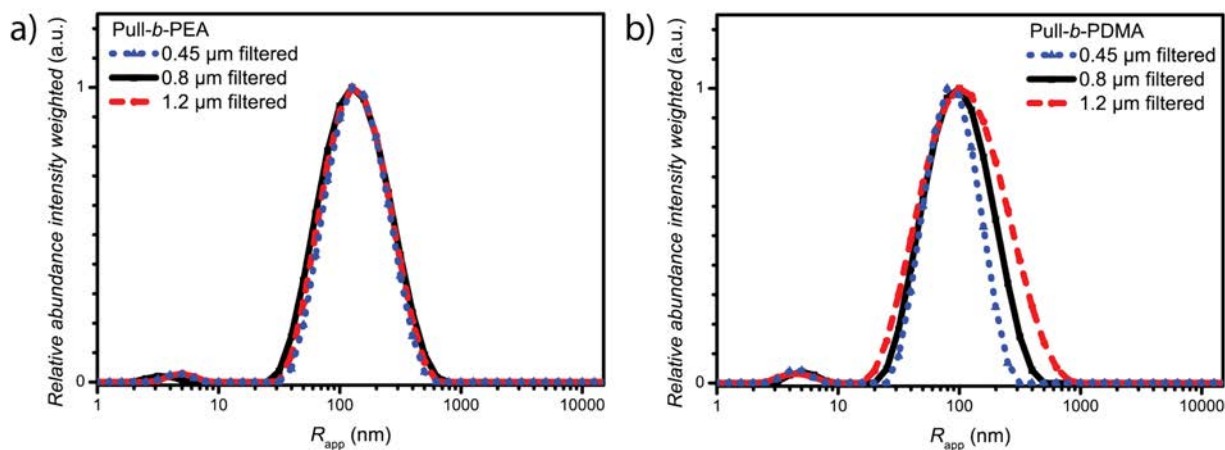


**Figure IV.14** Intensity weighted particle size distributions of a) Pull-*b*-PEA and b) Pull-*b*-PDMA in Millipore water filtered with different CA filters, e.g. 0.45  $\mu\text{m}$ , 0.8  $\mu\text{m}$ , and 1.2  $\mu\text{m}$  measured *via* DLS at 25  $^{\circ}\text{C}$ , showing that no aggregates were removed by using 0.45  $\mu\text{m}$  CA filters.

As visible from the particle size distributions of Pull-*b*-PDMA in Figure IV.14a, no effect was observed for a variation of the filter size. The average apparent radii of the three filtered samples are in the same range of approximately 80 nm. The intensity weighted particle size distributions of Pull-*b*-PEA in Figure IV.14b only show a slight peak broadening towards larger radii, the average apparent radii maintain with 125 nm in the same range as the 0.45  $\mu\text{m}$  filtered samples. The explanation of the peak broadening is not an easy task because it is not clear up to this point,

if the observed structures are squeezed or disrupted during the filtration process. Therefore, a different reorganization of the polymer chains to new aggregates cannot be excluded. This question is furthermore a probe into the still not completely understood directive forces of DHBC self-assembly, especially concerning the mechanical stability of the self-assembled spherical DHBC aggregates. Since the presence of large aggregates was not observed in the intensity weighted particle size distribution, it can be stated that the use of filters does not remove any aggregates. This statement is only valid for these systems and no generalization. A different interaction with the filter material or crosslinked structures can be prevented from passing the filter membrane and clearly affect the composition of the solution.

#### *IV.6. Conclusion*

To conclude, the investigations on the novel pullulan-*b*-poly(acrylamide) block copolymers and their self-assembly, more insight into the criteria of DHBC self-assembly was afforded. The synthesis of double hydrophilic block copolymers was extended from block copolymerization techniques such as the RAFT process and ATRP to a more versatile CuAAC conjugation approach allowing combining a variety of polymer building blocks suitable to form DHBCs. The successful block copolymer conjugation was confirmed *via* SEC and <sup>1</sup>H-NMR techniques. In contrast to PEO-*b*-PVP block copolymers, Pull-*b*-PDMA and Pull-*b*-PEA self-assemble to spherical structures with average diameters between 200 nm and 500 nm at very low concentrations. Whereas the confirmation of vesicular structures could not completely be stated for Pull-*b*-PDMA, cryo SEM investigations of Pull-*b*-PEA visualized vesicular structures. In addition LSCM was utilized using Rhodamine B staining or Rhodamine B labelled block copolymers.

---

# V. pH and Redox Responsive Vesicles from Double Hydrophilic Pullulan-*b*-Poly(vinylpyrrolidone) Block Copolymers

## V.1. Preface

The previous chapter discussed the synthesis and self-assembly of pullulan-*b*-poly(acrylamide) block copolymers in aqueous solution. In contrast to PEO-*b*-PVP (Chapter III), the self-assembly of Pull-*b*-PEA as such was already superior in water without additional supports such as crosslinkers or a solvent change (Chapter IV). However, poly(acrylamides) only display poor biocompatibility, which limits their application in drug delivery processes. Furthermore, utilization of CuAAC conjugations with polysaccharides is slightly controversial for biomedical applications as well. Since the complete removal of copper after the conjugation cannot be guaranteed due to the good interaction of copper ions and the hydroxyl groups of the sugar building blocks,<sup>118</sup> a different pathway for polysaccharide derived systems should be applied.

Therefore, the synthesis of a block copolymer consisting of pullulan and PVP as a novel double hydrophilic block copolymer could be advantageous. In order to avoid the presence of transition metals, the pullulan block was end group functionalized to act as a macro RAFT/MADIX chain transfer agent. Employing the knowledge obtained on the aqueous polymerization of *N*-vinylpyrrolidone in Chapter III, the synthesis of a double hydrophilic pullulan-*b*-PVP block copolymer is accessible. The change in the second polymer block should overcome the biocompatibility issues of CuAAC and poly(acrylamides). Nonetheless, the problem of disassembly upon infinite dissolution of the self-assemblies still hinders the system to be a potential drug delivery vehicle and a crosslinking strategy is necessary in order to preserve the self-assembled structures. Due to the positive charges that were introduced during the crosslinking of self-assembled PEO-*b*-P(VP-*co*-VIm) particles with diiodo compounds, the crosslinked particles would not act as the best possible way for biomedical applications. Therefore, a crosslinking strategy for the pullulan blocks would be more beneficial. Moreover, the implementation of reversible crosslinking in order to guarantee a sufficient disassembly and a targeted potential release of drugs inside the body is achieved. In such way, two external triggers

that possess the potential of being utilized in the body are pH and redox can be applied. Thus, a potential crosslinker could bear pH sensitivity or redox responsive, cleavable groups.

The following chapter contains the synthesis of a novel Pull-*b*-PVP block copolymer *via* RAFT/MADIX techniques. Subsequently, the self-assembly of the block copolymer in water was investigated. Furthermore, a potentially dual responsive crosslinking strategy was developed and the self-assembly was investigated *via* DLS measurements.

## V.2. Synthesis of $\omega$ -functionalized Pullulan-xanthate

In analogy to Chapter IV, commercially available high molecular weight pullulan with a broad polydispersity has to be depolymerized prior to any functionalization. The depolymerization was carried out similar to Chapter IV.<sup>242, 251</sup> Commercial pullulan was treated with a 0.025 M HCl solution for 2.5 h, followed by dialysis in order to afford depolymerized pullulan (Figure V.1a). The depolymerization afforded pullulan with an average molecular weight of 22 400 g·mol<sup>-1</sup> and *D* of 2.0. The polydispersity is slightly higher than the one of pullulan utilized for CuAAC conjugations with poly(acrylamides) in Chapter IV, but still in an acceptable range to proceed with a further functionalization as the polydispersity narrowed from 19 to 2.0 through a removal of low molecular weight pullulan and depolymerization of high molecular weight pullulan (Figure V.1b).

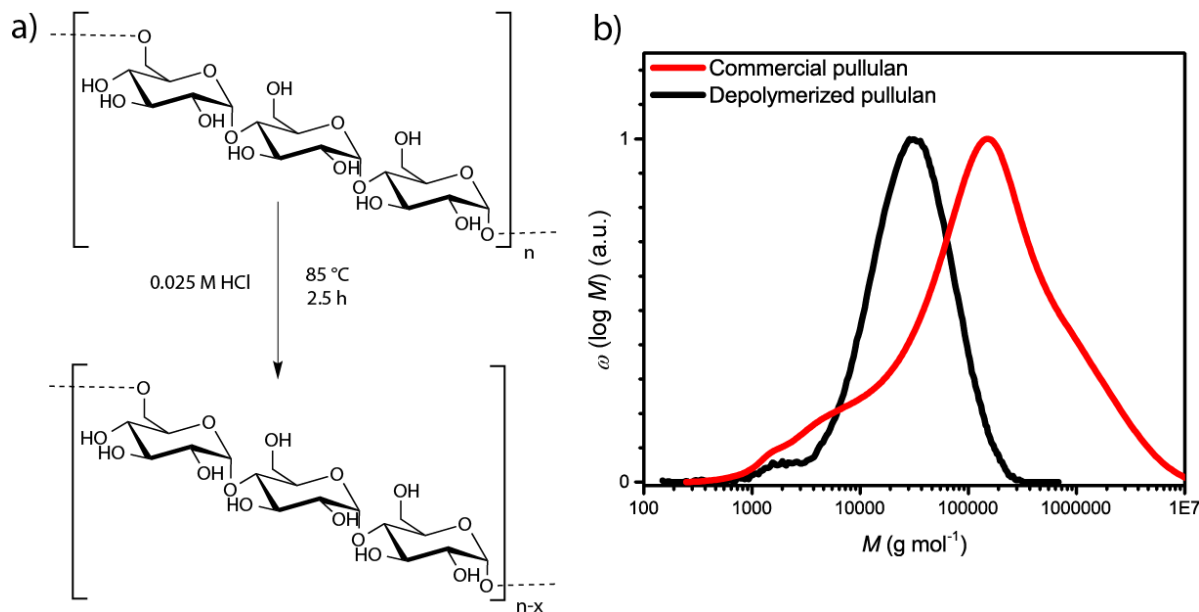


**Figure V.1** a) Reaction scheme of pullulan depolymerization; b) molecular mass distributions of commercial pullulan and depolymerized pullulan against a pullulan calibration curve determined *via* SEC in acetate buffer solution.

---

Due to the emphasis on more biocompatible synthesis routes, a conjugation reaction of functionalized pullulan and PVP could not be conducted as well as an attachment of a RAFT/MADIX chain transfer agent *via* CuAAC.<sup>118</sup> Therefore, a novel functionalization pathway had to be established. A pathway to attach chain transfer groups to primary amines of proteins by applying *N*-succinimidyl functionalized as transfer agents was presented by Lecolley et al. in 2004.<sup>252</sup> Furthermore, a transition to terminal amine groups for chain ends of synthetic polymers was demonstrated some years later by Hasegawa et al.<sup>253</sup> These reports lead to a pathway for the synthesis of a pullulan bearing a RAFT/MADIX chain transfer agent as end group. Therefore, depolymerized pullulan was functionalized with an amine group by reductive amination in the first step. Perez et al. reported a successful reductive amination of dextran with hexamethylenediamine.<sup>241</sup> However, the previous satisfying results that were obtained with the utilization of the reductive amination procedure reported by Schatz et al. support a derivatization of the procedure (Figure V.2a).<sup>153, 251</sup> In analogy to the reductive amination to an alkyne, a 100-fold excess of NaCNBH<sub>3</sub> and hexamethylenediamine was applied to ensure complete conversion and more importantly prevent a reductive linking between two pullulan chains *via* the bifunctional diamine.



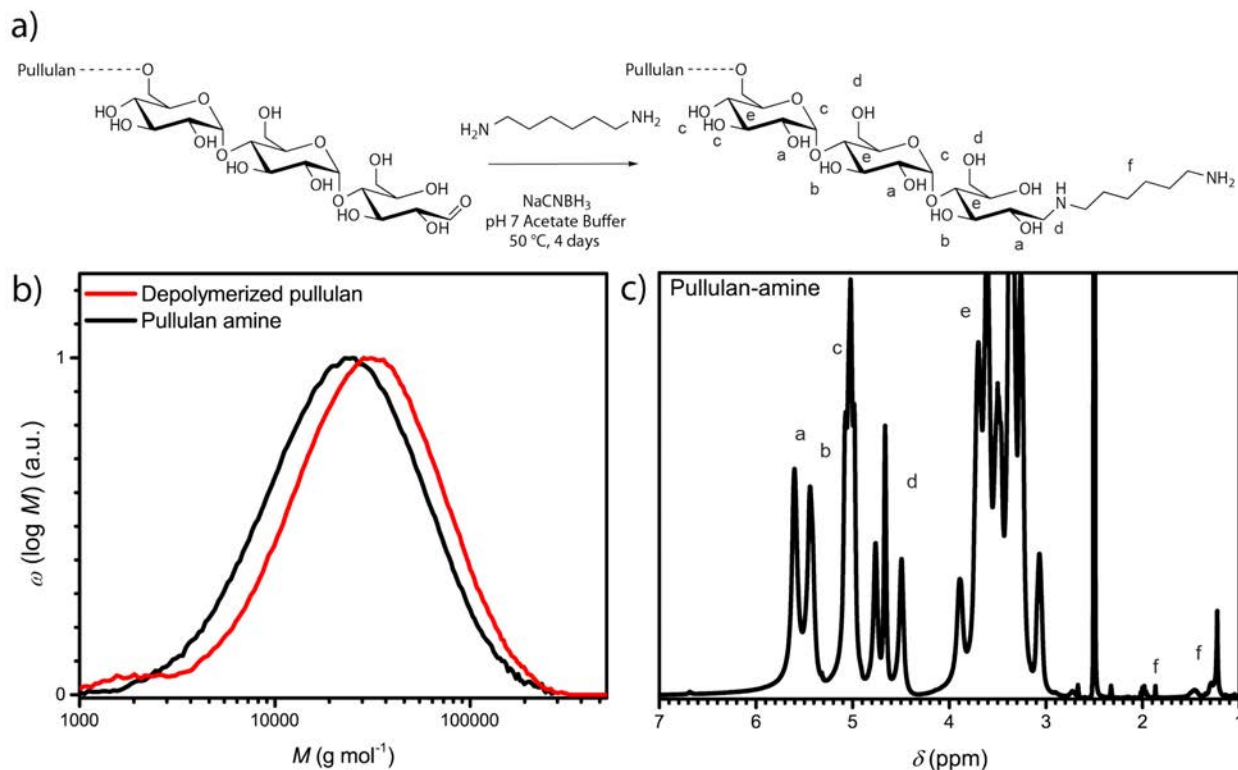


**Figure V.2** a) Reductive amination scheme of pullulan with hexamethylenediamine; b) apparent molecular mass distributions of depolymerized pullulan and amine functionalized pullulan against a pullulan calibration curve determined *via* SEC in acetate buffer solution; c) corresponding  $^1\text{H-NMR}$  of pullulan amine recorded at 400 MHz in  $\text{DMSO-d}_6$ .

As visible from the SEC curves in Figure V.2b, the reductive amination resulted in a slight decrease in the average molecular mass of pullulan by 20% from  $22\,000\ \text{g}\cdot\text{mol}^{-1}$  to  $16\,000\ \text{g}\cdot\text{mol}^{-1}$  with an increase in  $D$  from 2.0 to 2.1. The decrease in the apparent average molecular mass can be attributed to a different behavior of the pullulan amine on the SEC column due to a different chemical behavior. Furthermore, a slight depolymerization is possible as well, which leads to a broadening of the SEC molecular mass distribution. Nonetheless, the reductive amination to introduce a terminal amine can be regarded as successful because signals corresponding to the hexamethylenediamine protons at 1.29 ppm and 1.87 ppm are present in the  $^1\text{H-NMR}$  spectrum in Figure V.2c. Furthermore, the disappearance of the anomeric proton signals of the  $\omega$ -glucose unit ( $\alpha$ -centered at 6.7 ppm and  $\beta$ -centered at 6.3 ppm) could be confirmed with  $^1\text{H-NMR}$  (Figure V.3) and a complete conversion can be stated again in similarity to the reductive amination to a pullulan alkyne in chapter IV.

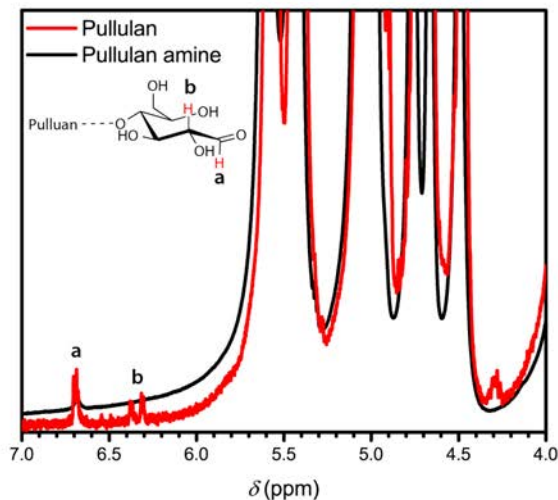


**Figure V.3**  $^1\text{H-NMR}$  comparison of depolymerized pullulan and amine functionalized pullulan recorded at 400 MHz in  $\text{DMSO-d}_6$  displaying the disappearance of the anomeric proton signals.

After the successful transformation of the  $\omega$ -aldehyde to a primary amine, the attachment of a RAFT/MADIX chain transfer agent was attempted in the next step. Therefore, a *N*-succinimidyl xanthate, namely 2,5-dioxopyrrolidin-1-yl 2-((ethoxycarbonothioyl)thio)propanoate was synthesized *via* literature known procedures of Lecolley et al. and a derived procedure by Pound et al. (see appendix for details).<sup>99, 252</sup> The xanthate transfer agent was synthesized starting from *N*-hydroxysuccinimide, which was esterified with 2-bromopropionyl bromide in DCM. The intermediate was subsequently reacted with potassium *O*-ethyl xanthate to afford the transfer agent (Figure V.4a). In contrast to Hasegawa et al., the xanthate had to be attached prior to the functionalization of the pullulan amine in order to avoid side reactions, such as multiple chain transfer agents attached to one polymer. Furthermore, the application of an additional synthetic step with the pullulan macro agent was considered to be not beneficial due to possible incomplete conversion. The amide formation with *N*-hydroxysuccinimide derivatives occurs almost quantitatively with primary amines. Moreover, the transformation is selective towards amide formation next to hydroxyl groups. Therefore, an attachment of the RAFT/MADIX chain transfer agent to the  $\omega$ -glucose amine of pullulan should occur with the highest selectivity. The synthesis of the pullulan chain transfer agent was carried out in DMSO at ambient temperature to ensure complete dissolution of pullulan amine and the xanthate transfer agent. The xanthate functionalized pullulan was dialyzed and lyophilized after the reaction to remove DMSO and unreacted xanthate transfer agent from the solution (Figure V.4b). When comparing SEC results

of the amine functionalized pullulan with the pullulan xanthate, an increase in average molecular weight by almost 60% from 16 000  $\text{g}\cdot\text{mol}^{-1}$  to 26 500  $\text{g}\cdot\text{mol}^{-1}$  can be seen. Furthermore, the polydispersity decreased by 25% to 1.7 (Table V.1). Compared to the depolymerized pullulan, the pullulan xanthate possesses a 20% higher average molecular weight and an 18% lower  $D$  (Figure V.4c). This can be attributed to a further purification of the pullulan due to several dialysis processes resulting in a more efficient removal of small pullulan chains below the MWCO of the dialysis tube.

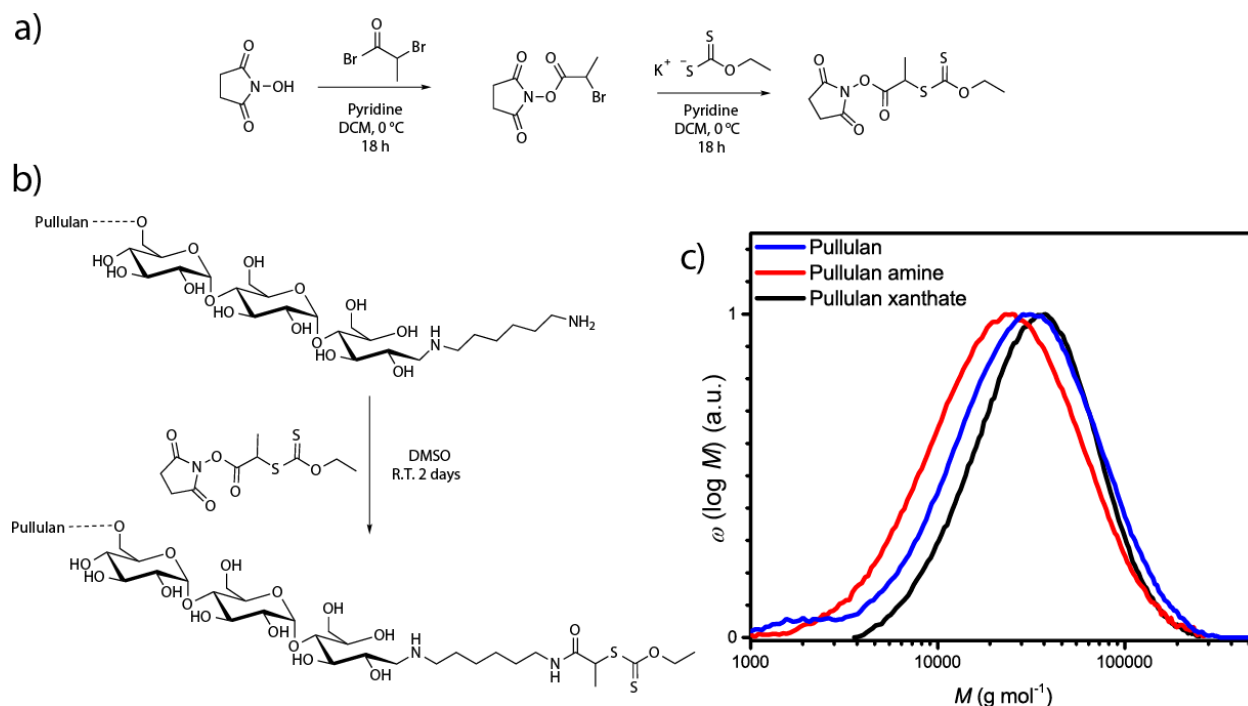


**Figure V.4** a) Schematic synthesis of the *N*-succinimidyl xanthate; b) schematic transfer of the xanthate group to pullulan amine; c) apparent molecular mass distributions of the reaction cascade of pullulan recorded *via* SEC in acetate buffer against a pullulan calibration curve.

The  $^1\text{H-NMR}$  spectrum in Figure V.5b displays the successful attachment of the xanthate group to pullulan amine. The proton signals corresponding to the xanthate and the hexamethylene group could be assigned *via* the magnification of the area with a low chemical shift in Figure V.5c.

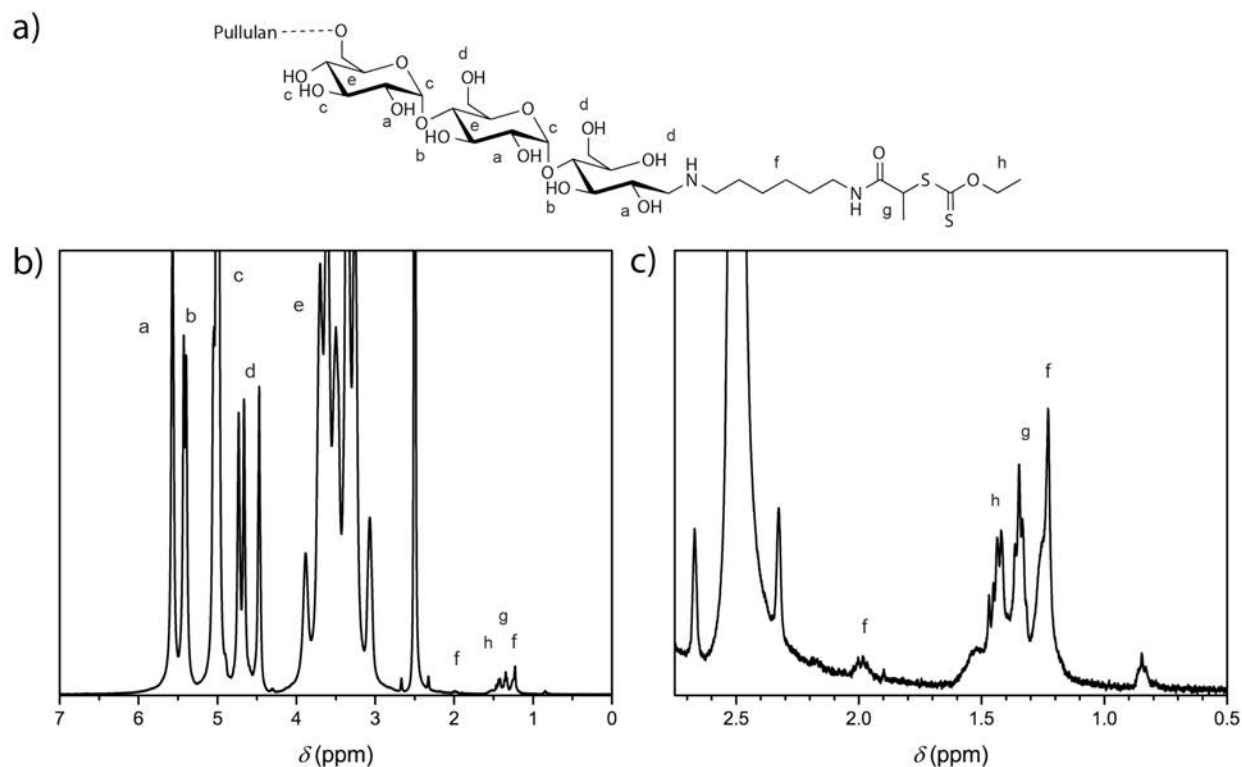


**Figure V.5** a) Scheme of pullulan xanthate; b)  $^1\text{H-NMR}$  spectrum of pullulan xanthate and c) a magnification of the location corresponding to the protons of the functional group recorded at 400 MHz in  $\text{DMSO-d}_6$ .

Moreover, a difference in elution behavior of the three different pullulans can also result in the observed discrepancies. The chemical properties of depolymerized pullulan, pullulan amine, and pullulan xanthate differ quite distinctly resulting in different elution times and therefore apparent molecular masses.

**Table V.1** Summary of SEC results of the pullulan functionalization recorded in acetate buffer against a pullulan calibration curve.

Polymer	$M_{n, \text{SEC}} (\text{g}\cdot\text{mol}^{-1})$	$\mathcal{D}$
Pullulan	22 000	2.0
Pullulan amine	16 000	2.1
Pullulan xanthate	26 500	1.7

Nonetheless, it was possible to design a xanthate end functionalized pullulan as a macro RAFT/MADIX chain transfer agent. The next step to be attempted should therefore be the block copolymerization of VP onto the pullulan block.

### V.3. Block Copolymerization of Pull-*b*-PVP

The controlled synthesis of a Pull-*b*-PVP block copolymer *via* RDRP turned out to be a challenging task. The adaption of the aqueous redox pair initiated RAFT/MADIX polymerization as described in Chapter III with the block copolymerization of PEO-*b*-PVP emerged several problems that had to be overcome. The first problem arose in terms of solubility. Applying the previously described procedure caused a highly viscous solution already before the polymerization was initiated. In contrast to PEO, pullulan forms more viscous solutions with water as such and especially with water-*N*-vinylpyrrolidone mixtures. Since a key factor of controlled radical polymerizations is the homogeneity of the reaction mixture *via* stirring, the solution had to be diluted drastically to decrease the viscosity. Despite decreased viscosity, the dilution with water affected concentration of sodium sulfate in the solution and therefore the pH value. As reported by Guinaudeau et al., a certain basicity is necessary to prevent side reactions of *N*-vinylpyrrolidone and maintain control over the polymerization.<sup>97, 209</sup> Indeed, increased tailing towards low molecular weight and a broad *D* between 2.2 and 2.7 were observed from SEC for the initial experiments without and with diluted systems (Figure V.6b). It has to be mentioned that it was necessary to record the SEC measurements in NMP due to the high interaction of the PVP block on the SEC column in aqueous acetate buffer solution. The number weighted molecular masses can therefore only be regarded as apparent masses since a PEO calibration was applied. The molecular weight with the block copolymerization was determined to be 50 000 g·mol<sup>-1</sup>. Therefore, the reaction was terminated after 8 hours in order to prevent side reactions.

**Table V.2** Summary of apparent average number weighted molecular masses of Pull-*b*-PVP block copolymers against PEO calibration curve recorded in NMP at 70 °C.

Polymer	$M_{n,app,SEC}$ (g·mol <sup>-1</sup> )	<i>D</i>
Pullulan xanthate	11 700	2.0
Pull- <i>b</i> -PVP standard procedure (Chapter III)	73 500	2.7
Pull- <i>b</i> -PVP diluted with H <sub>2</sub> O to 50%	59 600	2.2
Pull- <i>b</i> -PVP water/DMSO	58 800	1.8

As visible from Table V.2, the apparent molecular masses differ tremendously because of the dilution of the system. Whereas the conventional non-diluted sample possesses a high apparent

$M_{n,app}$  and a very broad  $D$  of 2.7, the diluted polymerization indicates a better control over the reaction. A higher viscosity indeed leads to a decreased control over the polymerization. Despite a narrower molecular weight distribution in the case of the diluted polymerization in contrast to the control polymerization,  $D$  exceeds the usual values for controlled polymerization systems and complicates the determination of the molecular mass even further. Therefore, the system was diluted with another polar but aprotic solvent, namely DMSO. DMSO is a good solvent for monomer and macro RAFT/MADIX chain transfer agent and should have less influence on the pH value of the reaction mixture (Figure V.6a).

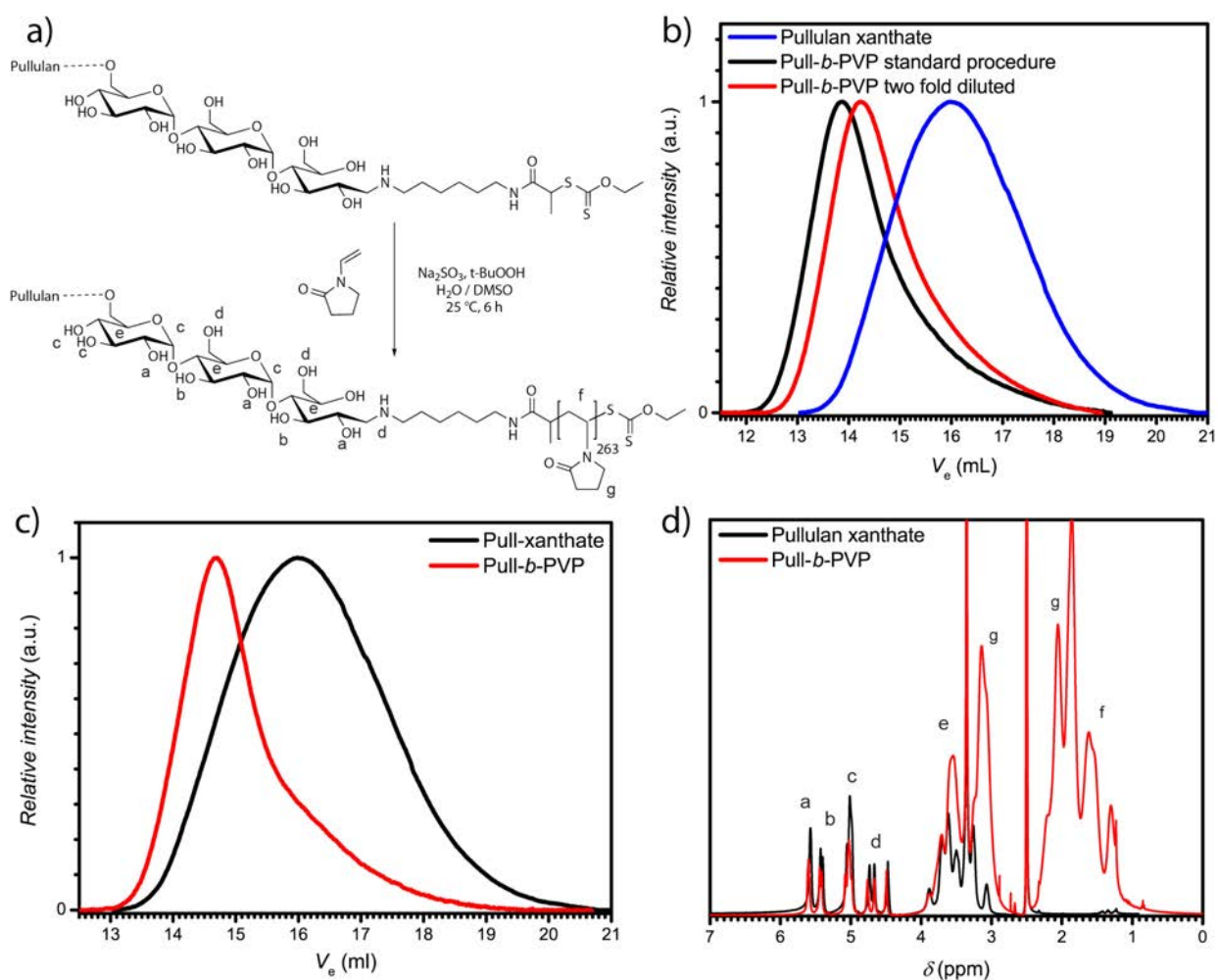


**Figure V.6** a) Polymerization scheme of Pull-*b*-PVP block copolymers in water/DMSO mixture; b) SEC traces of pullulan xanthate and initial polymerization attempts recorded in NMP at  $70\text{ }^\circ\text{C}$ ; c) SEC traces of pullulan xanthate and Pull-*b*-PVP block copolymer synthesized in water/DMSO mixtures recorded in NMP at  $70\text{ }^\circ\text{C}$ ; d)  $^1\text{H-NMR}$  of pullulan xanthate and Pull-*b*-PVP recorded at  $400\text{ MHz}$  in  $\text{DMSO-d}_6$ .

As visible from Table V.2, the application of a mixture of water and DMSO as solvent for the block copolymerization of PVP resulted in a Pull-*b*-PVP block copolymer with an apparent number weighted molecular mass of 58 800 g·mol<sup>-1</sup> and a decrease in  $\bar{D}$  by 10% from 2.0 to 1.8. The improvement of the polydispersity compared to the previous polymerizations indicates increased control during the polymerization. Figure V.6c displays slight tailing though, which can be explained with the broad molecular weight distribution of pullulan. Additionally, increased interactions with the SEC column as well as the occurrence of dead chains during the polymerization can play a role for the observed tailing. In contrast to the block copolymerization of PEO-*b*-PVP, the polymerization time was further decreased to avoid a drastic increase in viscosity and therefore a loss of control over the polymerization resulting in side reactions of VP and recombinations of active chain ends. The <sup>1</sup>H-NMR in Figure V.6d furthermore displays the successful block copolymerization with the proton signals of both polymer blocks between 4.4 ppm and 5.7 ppm for pullulan and from 1.2 ppm to 2.1 ppm for PVP, respectively present in the spectrum. Integration of the protons corresponding to the **a**-OH group of Pullulan (Figure V.6a) and the relation to the integral of the protons corresponding to the PVP backbone, indexed as **f** (Figure V.6a) in the <sup>1</sup>H-NMR spectrum in Figure V.6d resulted in a VP incorporation of 263 units into the block copolymer. The block copolymer composition was therefore assessed to be Pull<sub>124</sub>-*b*-PVP<sub>263</sub>.

Further improvement of redox initiated aqueous RAFT/MADIX polymerization allowed to synthesize a Pull-*b*-PVP block copolymer. The addition of the co-solvent DMSO not only decreased the viscosity of the polymerization mixture but also improved the control over the RDRP process. The successful synthesis of the block copolymer could be confirmed by a combination of SEC and <sup>1</sup>H-NMR spectroscopy. The next step to be attempted was the investigation of the self-assembly behavior of Pull-*b*-PVP in diluted aqueous solutions.

#### V.4. Self-Assembly of Pull-*b*-PVP Block Copolymers in Aqueous Solution

After the successful synthesis of Pull<sub>124</sub>-*b*-PVP<sub>263</sub>, the self-assembly behavior was investigated. Therefore, solutions containing 0.1, 0.5, 1.0, and 2.5 wt.% of Pull<sub>124</sub>-*b*-PVP<sub>263</sub> in Millipore water were prepared, filtered with 0.45 μm CA syringe filters, and analyzed *via* DLS. In order to

compare the block copolymer with the pullulan homopolymer, a pullulan solution containing 0.1 wt.% in Millipore water was prepared as well and investigated *via* DLS.

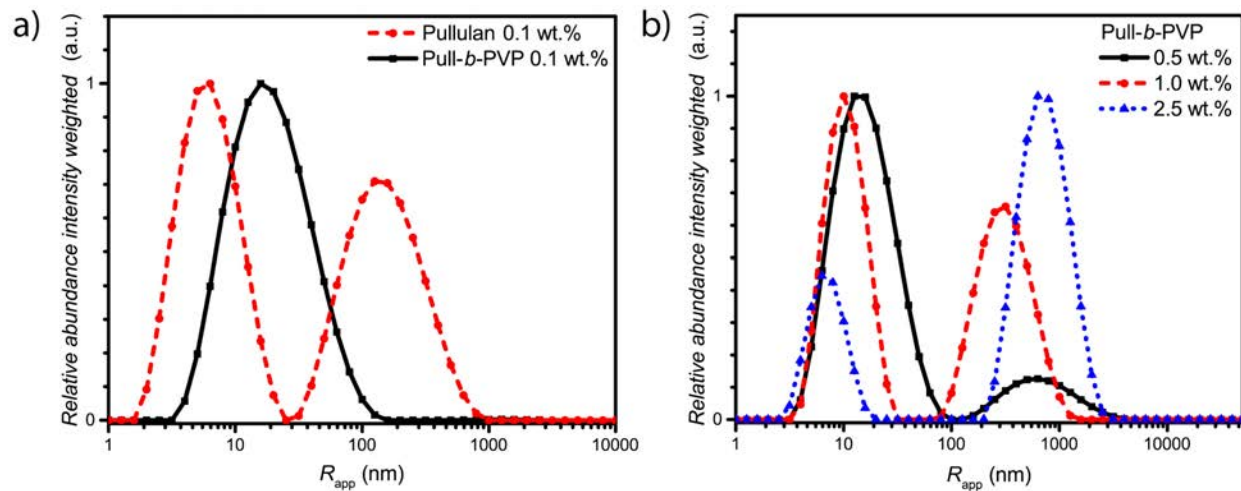


**Figure V.7** a) Intensity weighted size distributions of pullulan and Pull-*b*-PVP at 0.1 wt.%; b) intensity weighted size distributions of Pull-*b*-PVP at higher concentrations in Millipore water measured *via* DLS at 25 °C.

The intensity weighted size distributions of pullulan and Pull<sub>124</sub>-*b*-PVP<sub>263</sub> at 0.1 wt.% in Figure V.7a display a strong difference. Pullulan displays a bimodal particle size distribution with the first peak being the most abundant species with an average apparent radius of 7 nm. The peak can be attributed to free dissolved pullulan macromolecules. The second peak possesses an average apparent radius of 180 nm with a relative abundance of 0.7. As discussed before in Chapter IV, the second peak corresponds to weak aggregates of pullulan chains. The aggregates presumably form because of hydrogen bonding between hydroxyl groups and entanglement of the pullulan chains. Due to the intensity weighted particle size distribution, the actual abundance of these aggregates is 10<sup>-5</sup> times lower compared to the free dissolved polymer. In contrast to free pullulan, the block copolymer only displays a unimodal particle size distribution with an average apparent radius of 25 nm. This is a further indication of the successful block copolymerization as the self-assembly behavior in solution is significantly different from the pullulan homopolymer. Despite this fact, the self-assembly of Pull<sub>124</sub>-*b*-PVP<sub>263</sub> block copolymers is not as efficient as expected for low concentrations. Instead of large structures that would indicate the presence of particles or vesicular structures, only one signal corresponding either to free dissolved block copolymer or small aggregates could be observed. Since the average apparent radius is with 25 nm quite large for free dissolved block copolymer chains, the presence of small aggregates of a low amount of block copolymer chains is more conceivable.



**Table V.3** Summary of apparent average hydrodynamic radii of pullulan and Pull-*b*-PVP determined *via* DLS at 25 °C.

Polymer	Concentration (wt.%)	Peak 1 $R_{h,app}$ (nm)	Rel. abund.	Peak 2 $R_{h,app}$ (nm)	Rel. abund.
Pullulan	0.1	7	1.0	180	0.7
Pull <sub>124</sub> - <i>b</i> -PVP <sub>263</sub>	0.1	25	1.0	-	-
	0.5	16	1.0	750	0.12
	1.0	11	1.0	350	0.66
	2.5	7	0.42	800	1.0

An increase in concentration to 0.5 wt.% already has a decent effect on the self-assembly behavior of the block copolymer (Figure V.7b). In contrast to the 0.1 wt.% sample, a bimodal particle size distribution is present with a second peak with an apparent average radius of 750 nm and a relative abundance of 0.12. The average apparent radius of the small species still being the most abundant decreased by 36% to 16 nm. The decrease in the average apparent radius of the small species and the formation of very large aggregates indicates a concentration dependent tendency to form larger structures. A similar behavior was already observed for PEO-*b*-PVP block copolymers in Chapter III, however with a lower tendency of self-assembly. An increase in the block copolymer concentration to 1.0 wt.% further decreases the average apparent radius of the free dissolved block copolymer species by 31% to 11 nm. The average apparent radius of the second species decreased as well by 53% to 350 nm, but the relative abundance is increased by 550% to 0.66. The narrower apparent particle size distribution of the second species could indicate the formation of a single species, such as particles. A last increase in the block copolymer content to 2.5 wt.% resulted in the second species of the intensity weighted apparent particle size distribution being the most abundant by intensity weighting. Moreover, the average apparent radius of the large species increased to 800 nm. Regarding the change in  $R_{app}$  of the different concentrations, the radius of the 1.0 wt.% sample does not match with the radii of the 0.5 wt.% and 2.5 wt.% concentrations. A possible explanation of this discrepancy can be the lack of a larger amount of structures with a higher scattering intensity leading to a less over pronounced intensity weighted particle size distribution for the large species. Moreover, the self-assembly of Pull<sub>124</sub>-*b*-PVP<sub>263</sub> displays an even stronger dependency on the concentration as assumed resulting in a low amount of aggregates for low concentrations. More precise but smaller structures are formed as soon as the concentration is increased to 1.0 wt.% and a further increase in concentration results in a swelling of the structures due to a higher abundance of free

dissolved polymer present supporting the stabilization of these assemblies. The decrease in free block copolymer abundance supports this assumption, however only slightly due to the intensity weighing of the abundance.

Since the abundance of self-assembled structures at low concentrations was quite low in contrast to the pullulan-poly(acrylamide) block copolymers, LSCM measurements with a Rhodamine B stained 2.5 wt% solution of Pull<sub>124</sub>-*b*-PVP<sub>263</sub> were conducted prior to cryo SEM measurements in order to support the probability for the observation of the structures postulated by DLS.

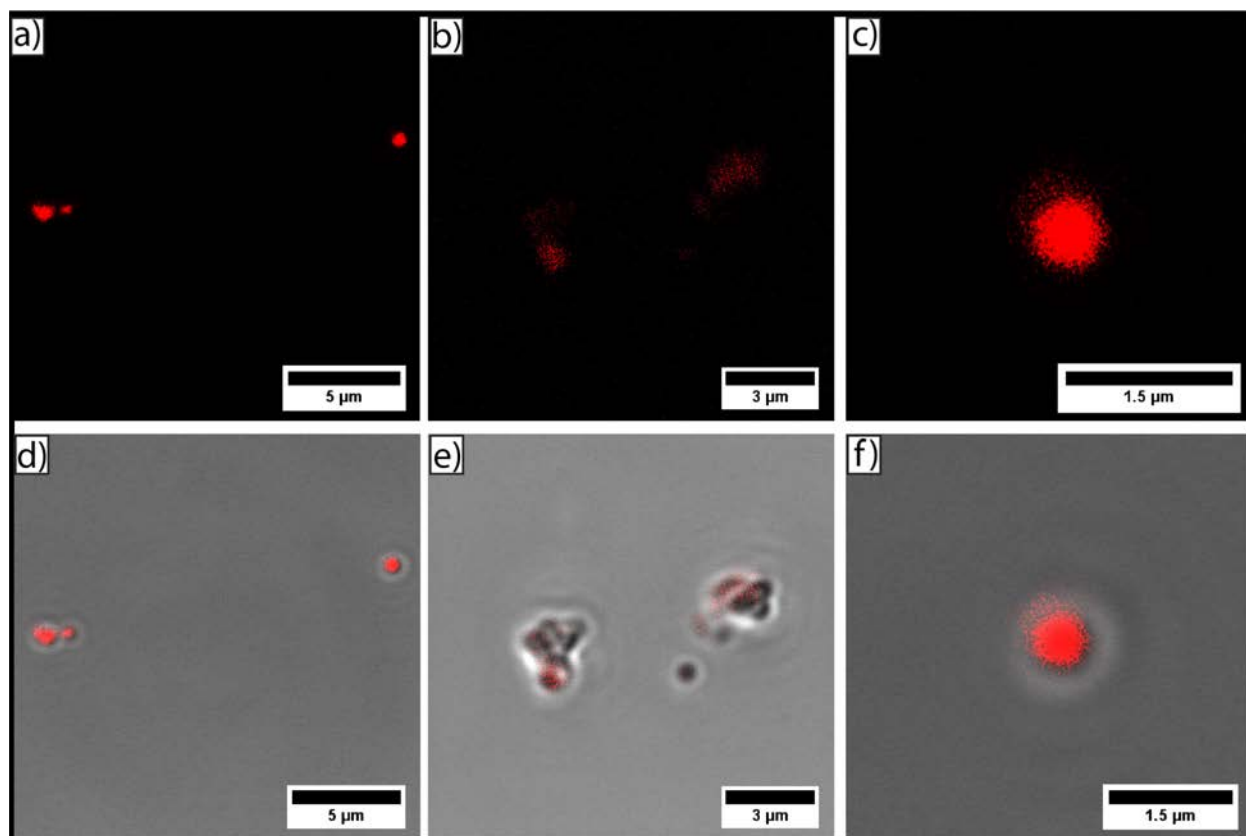


**Figure V.8** a), b) & c) Confocal micrographs of spherical particles of Pull-*b*-PVP at 2.5 wt.% stained with 0.08 mM Rhodamine B; d), e) & f) corresponding DIC images with fluorescence overlay displaying the particle structure.

In order to investigate the structures observed *via* DLS in 2.5 wt.% Pull-*b*-PVP solutions, the solution was stained with a 0.08 mM Rhodamine B solution and investigated with LSCM techniques. As displayed in Figure V.8, spherical particles with a diameter between 600 nm and 1 μm could be observed in the confocal micrographs. The DIC micrographs with the fluorescence overlay show that the particles are highly enriched with Rhodamine B (Figure V.8d and Figure V.8f). In addition to observed single particles, agglomerates of several particles as shown in Figure V.8e could be observed as well. Since the structures were imaged directly at the

surface of the glass slide in order to decrease blurring effects due to increased particle motion, the occurrence of the particle agglomerates can be explained by a continuous sinking of particles from the solution onto the same area of the glass surface.

The highly increased amount of dye inside the spherical structures compared to the surrounding solution can be attributed to the same phenomenon as described with Pull-*b*-PDMA and Pull-*b*-PEA block copolymer solutions.<sup>251</sup> Rhodamine B can permeate through the membrane structure inside the self-assembled particles, but remains inside the structure due to an increased interaction between dye molecules and block copolymer.

The cryo SEM measurements of a 0.5 wt.% solution of Pull-*b*-PVP Figure V.9 display a sample composition which is quite similar to the one obtained from PEO-*b*-P(VP-*co*-VIm) block copolymers in the Chapter III.<sup>227</sup> Alongside with an increased amount of spherical particles with average diameters between 150 nm and almost 1  $\mu\text{m}$ , the presence of tubular structures containing free dissolved block copolymer can be observed (Figure V.9a). The structures form due to the growth of ice crystals during the freezing process in liquid nitrogen pushing the free dissolved block copolymers to the crystal border, where they concentrate and form tubular alignments.<sup>223</sup>

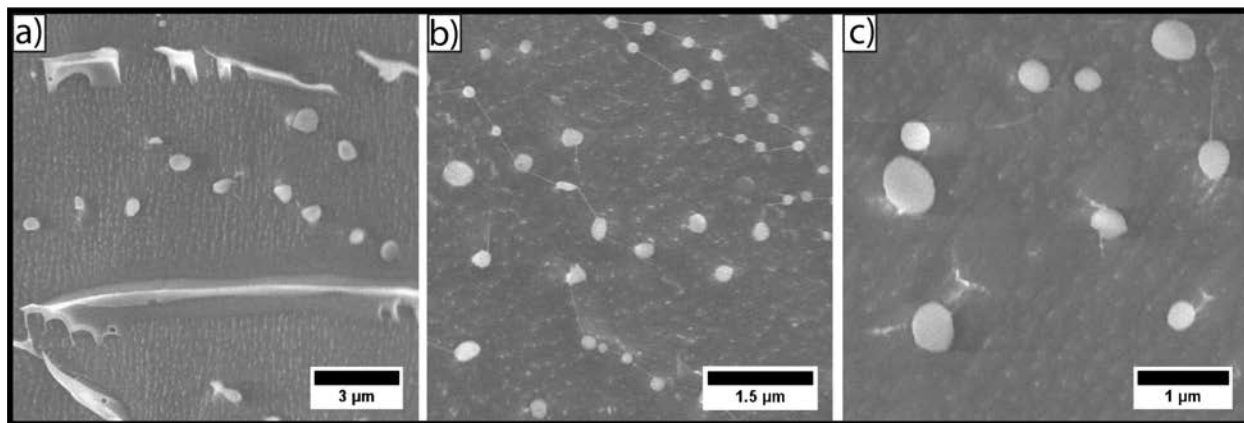


**Figure V.9** Cryogenic SEM micrographs of a 0.5 wt.% Pull<sub>124</sub>-*b*-PVP<sub>263</sub> solution displaying spherical particles and tubular alignments of free dissolved block copolymer due to the formation of ice crystals during the preparation process.

Furthermore, string-like connections between a larger number of smaller particles could be observed. As shown in Figure V.9b, the particles are aligned in the fashion of pearls that are lined up on a string composed of block copolymer. The occurrence of these interparticle connections is not completely understood yet and is possibly an artifact of the cryo SEM process, such as drying artifacts can occur in conventional SEM measurements. Nonetheless, a high

---

amount of spherical particles could be confirmed *via* cryo SEM measurements. In agreement to the intensity weighed particle size distribution of the 0.5 wt.% solution from DLS, the amount of free dissolved block copolymer is significantly present in the cryo SEM sample as tubular shaped structures.

When comparing the average diameters from LSCM/DIC and cryo SEM with the average apparent radii obtained from DLS at the corresponding concentrations, it can be stated that the average apparent diameters from DLS exceed the diameters determined *via* microscopy. In case of the 0.5 wt.% solution, the average diameter obtained from DLS is with 1500 nm 50% larger than the size of the largest particles observed in the cryo SEM micrographs in Figure V.9. Again, the intensity weighted particle size distribution could give an explanation by the overexpression of larger particles in contrast to smaller ones in the distribution curve. The same conclusion arises with the comparison of the diameters obtained from LSCM at 2.5 wt.%. The average diameters observed are almost 30% larger than the ones from cryo SEM, but still not in the range of the average apparent particle size determined *via* DLS.

### V.5. Oxidation and Crosslinking of Pull-*b*-PVP Vesicles

The confirmation of spherical particles self-assembled from Pull-*b*-PVP block copolymers already displays the potential of this system. However, the problem of disassembly upon dilution of the system is an ongoing struggle of DHBC based systems. In order to preserve the structures and generate more applicable systems for future drug delivery utilizations, a crosslinking strategy has to be developed. Due to the formation of positive charges with the previously shown crosslinking of *N*-vinylimidazoles in Chapter III,<sup>227</sup> the application of this crosslinking system for biomedical applications is very restricted. Therefore, a different crosslinking strategy was developed. Since the application of polysaccharides in biomedical and pharmaceutical field as hydrogel components is well studied, several techniques to crosslink polysaccharide hydrogels with or without the application of reversible crosslinking agents were reported to the best of our knowledge.<sup>254-258</sup>

The reversibility of the crosslinking was usually enabled *via* crosslinkers bearing redox responsive groups such as dithiols or a pH sensitive linkage with the polysaccharide, such as imines.<sup>257</sup> To make the polysaccharides such as dextran or pullulan available for imine formation, the cyclic hexoses need to be oxidized to aldehydes. The most frequently reported

pathway to accomplish a mild oxidation of polysaccharides without the destruction of the backbone is carried out with sodium (meta)periodate in aqueous solutions.<sup>254, 255</sup> Maia et al. reported a facile oxidation and crosslinking method for dextran,<sup>256</sup> but up to this point no oxidation procedures corresponding to pullulan were reported.

In order to investigate the possibility of selective pullulan oxidation to a pullulan dialdehyde, test oxidations with depolymerized pullulan with different percentages of NaIO<sub>4</sub> as oxidizing agent were conducted (Figure V.10a). The state of oxidation was characterized *via* <sup>1</sup>H-NMR spectroscopy. Furthermore, SEC measurements should indicate possible depolymerization or degradation of oxidized pullulan. As shown in the <sup>1</sup>H-NMR spectra in Figure V.10b, new signals are arising in the area between 6.1 ppm and 7.5 ppm which increase in intensity and the area below the curve with increasing theoretical oxidation state. These peaks can be attributed to the increasing number of aldehydes formed by the oxidation of a hexose to a dialdehyde. In parallel to the increase in aldehyde peaks, the signals corresponding to the hydroxyl groups and the  $\alpha$ -3-centered protons between 4.5 ppm and 5.6 ppm decrease significantly with increasing amount of oxidized glucose units. The <sup>1</sup>H-NMR affords a qualitative measure for the increasing amount of oxidized groups, but in order to quantify the amount of aldehydes an internal standard had to be applied. Therefore, 0.013 mmol DMF was added to a solution of 0.005 g of oxidized pullulan in 0.7 mL DMSO-d<sub>6</sub>. The low amount of DMF should ensure a distinguishable proton signal which can be used as an internal standard peak. DMF was chosen because of the singlet amide proton signal in a chemical region, where no signals from pullulan and its oxidized species occur. The corresponding amide peak at 8.0 ppm was integrated, normalized to one, and the area below the signals between 6.1 ppm and 7.5 ppm was integrated.

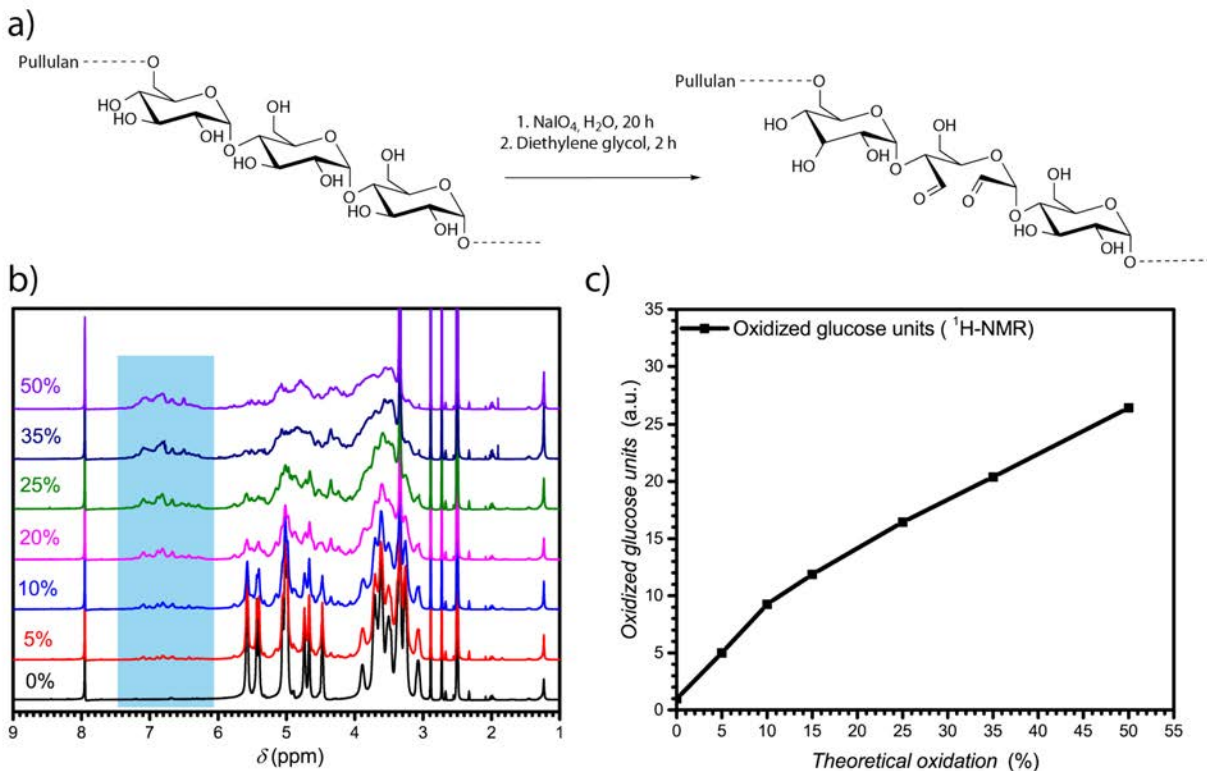


**Figure V.10** a) Schematic oxidation of pullulan with NaIO<sub>4</sub>; b) <sup>1</sup>H-NMR spectra of oxidized pullulans emphasizing on the anomeric proton peaks of the oxidized glucose units recorded at 400 MHz in DMSO-d<sub>6</sub>; c) line plot of oxidized pullulan units against the theoretical oxidation.

The integral of the 0% oxidation was set to be 1 oxidized unit (ω-aldehyde) and the oxidized glucose were calculated from integrals corresponding to higher oxidations as follows. With an apparent average number weighted molecular weight of 14 400 g·mol<sup>-1</sup>, the non-oxidized pullulan possesses approximately 80 glucose units. This pullulan already features one aldehyde group at its terminal glucose unit with an integral of 0.42 in correspondence to the integral of the internal standard. By relating the integrals of higher theoretical oxidations with these values, the number of oxidized units can be determined (Table V.4). The line graph in Figure V.10c displays a linear increase in oxidized units with increasing theoretical oxidation. However, the increase becomes less predominant for theoretical oxidations above 25%. Whereas the actual oxidation matches quite nicely with the theoretical one for attempted oxidations below 25%, higher oxidized samples do show significant discrepancies, i.e. the actual percentage is significantly lower than the theoretical one.

**Table V.4** Summary of  $^1\text{H-NMR}$  oxidation experiments of a pullulan homopolymer.

Theoretical oxidation (%)	Integral	Oxidized units	Oxidation (%)
0	0.42	1	1
5	2.12	5	6.3
10	3.89	9.3	11.6
15	4.98	11.9	14.8
25	6.91	16.5	20.6
35	8.56	20.4	25.5
50	11.11	26.5	33.1

The decrease in oxidized groups with increasing amount of  $\text{NaIO}_4$  can be explained by taking the SEC elution curves in Figure V.11 into account. As visible from the elution curves in Figure V.11a, the elution curves shift to a higher elution volume upon increasing oxidation indicating a decrease in the size of the pullulan. The apparent average molecular weight distribution in Figure V.11b further states this observation leading to the assumption that pullulan fractures upon higher oxidation.

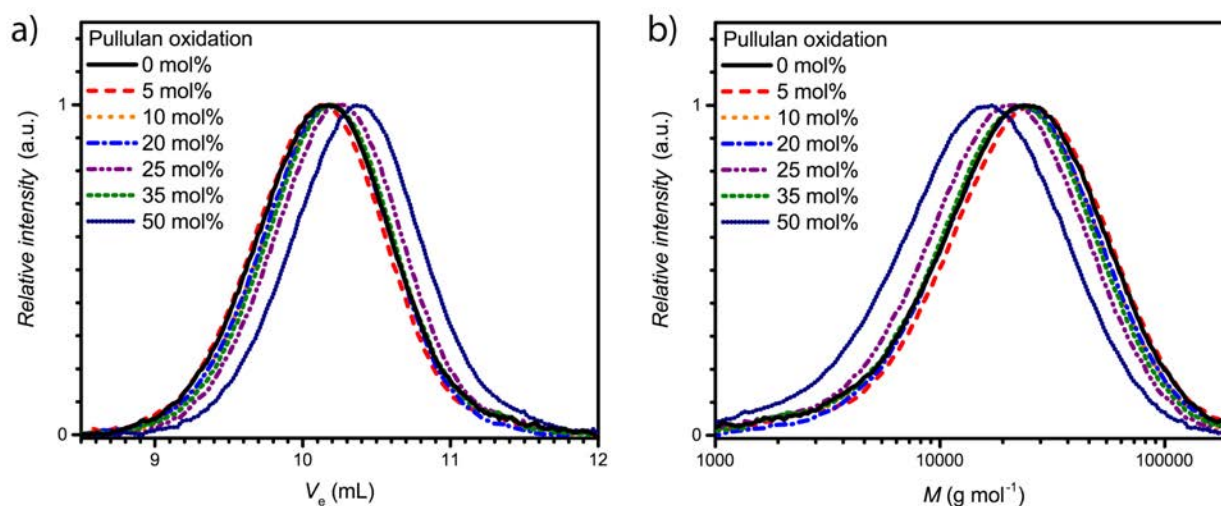


**Figure V.11** a) SEC traces of oxidized pullulan at different oxidation percentages and b) corresponding apparent molecular weight distributions recorded in acetate buffer solution against a pullulan calibration curve.

This fracture or depolymerization of pullulan is not beneficial for the targeted block copolymer self-assembly since it drastically affects block copolymer structure and could even lead to the destruction of the block copolymer connection. For that reason, oxidations exceeding 10% were not conducted with the Pull-*b*-PVP block copolymers.

---

In order to oxidize the pullulan moieties of a Pull-*b*-PVP block copolymer, the DHBC was dissolved in Millipore water and the corresponding amount of NaIO<sub>4</sub> was added to oxidize 5% and 10% of the pullulan units to dialdehydes (Figure V.12a). As visible from the <sup>1</sup>H-NMR spectra in Figure V.12b, the oxidation of glucose units of Pull<sub>124</sub>-*b*-PVP<sub>263</sub> can be regarded as successful. The appearance of the anomeric aldehyde protons in the area between 6.1 ppm and 7.5 ppm confirms a successful oxidation procedure. The integrals normalized to the internal standard DMF display an increase from the control sample with an integral of 0.04 to 0.67 and 1.35 for the 5% and 10% oxidation, respectively. However, absolute values of oxidized units cannot be determined *via* the previous method because the exact molecular mass of the block copolymer is unknown and only the apparent average number weighted molecular masses were determined. Therefore, no clear statement on the actual oxidation state can be given, but from the comparison of the integrals corresponding to 5% oxidation and 10% oxidation a two fold increase in the absolute value of anomeric aldehyde protons can be stated.

The SEC elution curves in Figure V.12c display a decent change of the elution curves upon oxidation with NaIO<sub>4</sub>. The oxidized block copolymers elute with a significantly broader curve compared to the initial block copolymer. Furthermore, a shoulder appeared at an elution volume of approximately 13 mL for both oxidized block copolymers. The drastic change in the appearance of the elugrams can be attributed to a different interaction of the oxidized block copolymer with the solvent NMP resulting in a peak broadening towards higher elution volumes and a slightly more pronounced tailing. Moreover, no clear indication of a polymer chain fracture or depolymerization could be stated from the elugrams indicating a successful oxidation of pullulan. The appearance of the anomeric proton signals in the <sup>1</sup>H-NMR spectrum and the SEC results both point towards a successful oxidation.



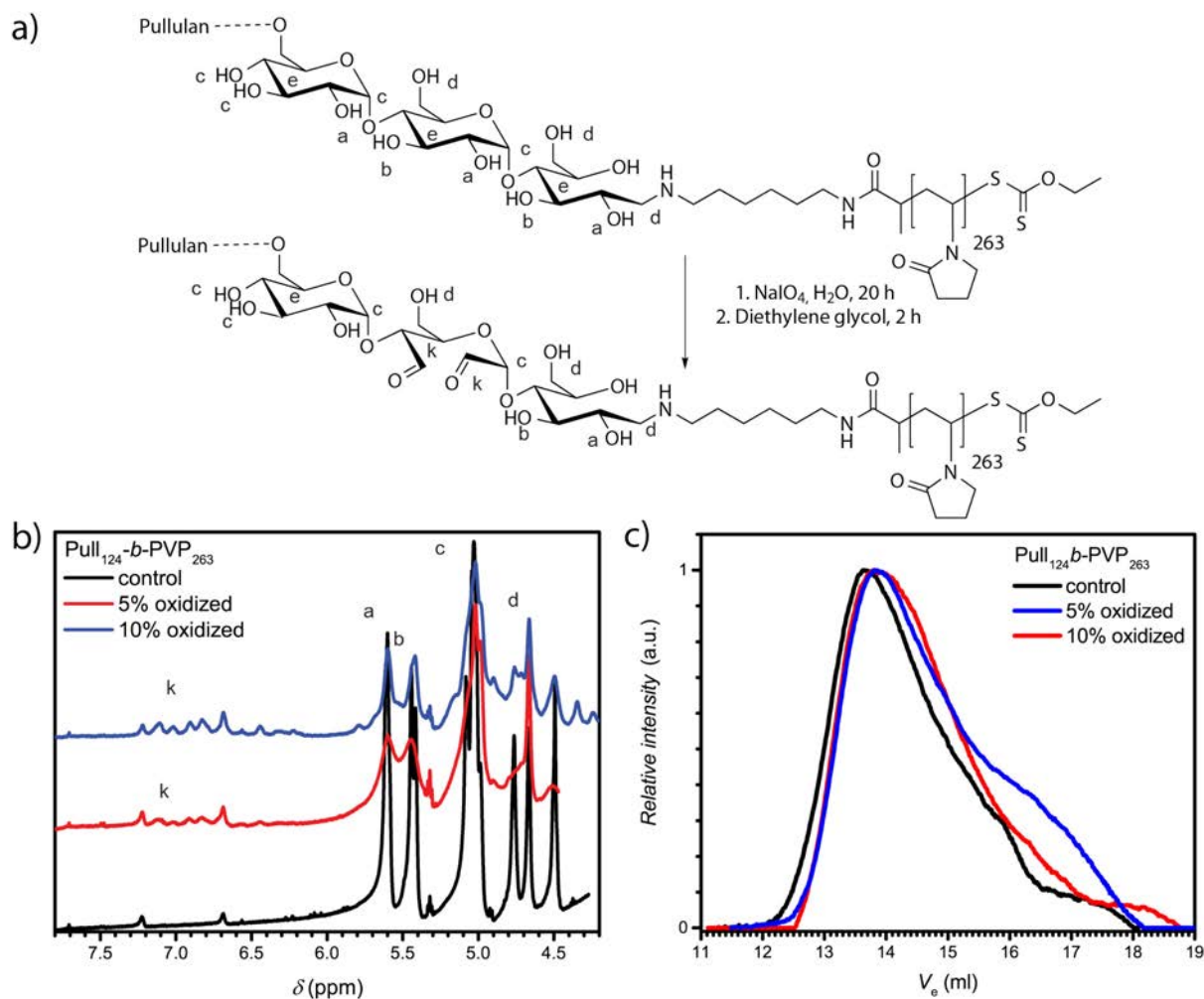


**Figure V.12** a) Schematic oxidation of Pull<sub>124</sub>-*b*-PVP<sub>263</sub> with NaIO<sub>4</sub>; b) <sup>1</sup>H-NMR spectra of oxidized Pull-*b*-PVP emphasizing on the anomeric proton peaks of the oxidized glucose units recorded at 400 MHz in DMSO-*d*<sub>6</sub>; c) corresponding SEC elution curves recorded in NMP at 70 °C.

The SEC elugrams furthermore indicate a change in the chemical behavior of the block copolymer. This change can be seen as well in the average particle size distribution of 0.1 wt.% solutions of Pull<sub>124</sub>-*b*-PVP<sub>263</sub> and its oxidized derivatives.

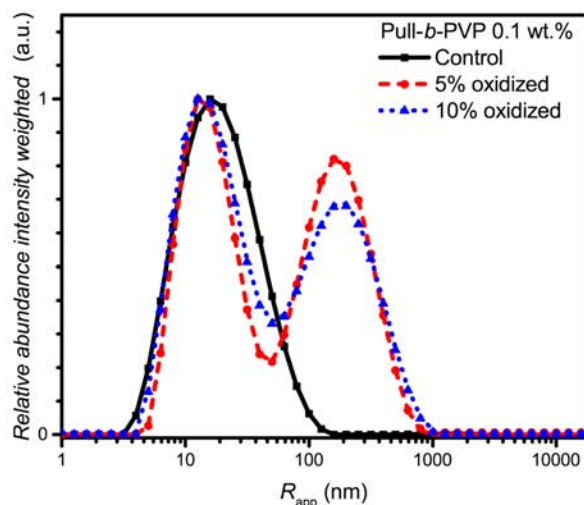
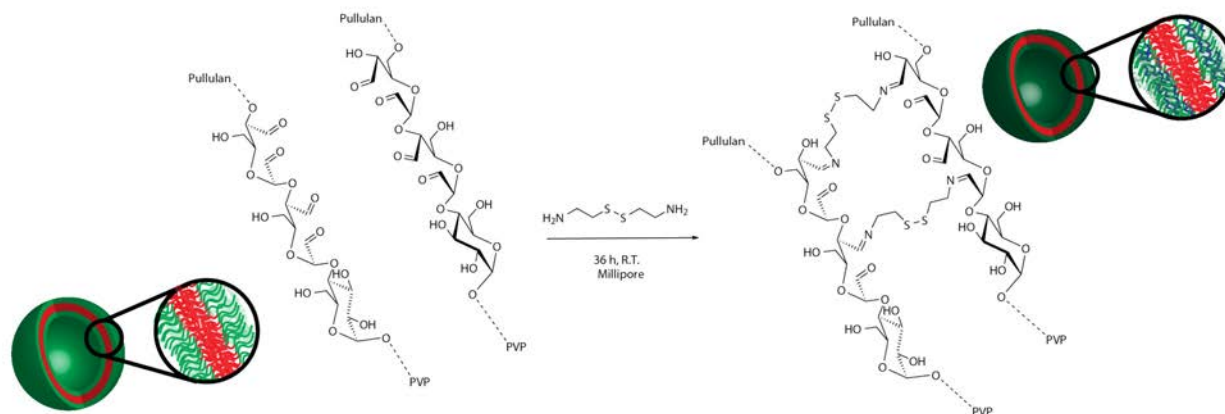


**Figure V.13** Intensity weighted particle size distributions of 0.1 wt.% Pull-*b*-PVP and its oxidized species with 5% and 10% pullulan oxidation in Millipore water measured *via* DLS at 25 °C.

As visible from the particle size distribution in Figure V.13 the unimodal average apparent particle size distribution of Pull-*b*-PVP at 0.1 wt.% turned to a bimodal distribution for both oxidized species. The two different peaks are not completely separated, but overlap at an apparent radius of approximately 50 nm. The first peak of the sample with a theoretical oxidation of 5% possesses an average apparent radius of 11 nm and is the most abundant species. The second peak with an average apparent radius of 200 nm possesses a relative abundance of 0.8. The sample with a theoretical oxidation of 5% displays similar apparent average radii for the separate species, but the relative abundance of the larger one is with 0.7 12.5% lower. The apparent average particle size distributions of the oxidized block copolymers show an increased tendency for self-assembly already at low concentrations in contrast to Pull-*b*-PVP. The origin of the increased tendency can be referred to a change in the hydrophilicity of pullulan. The oxidation of alcohols to aldehyde causes a decrease in the hydrophilicity of pullulan which encourages the microphase separation. Furthermore, the probability of hydrogen bonding between the pullulan blocks could be increased. This observation is very beneficial for the attempted crosslinking step. As shown for higher concentrated solutions of Pull-*b*-PVP in Figure V.7b, the tendency to form structures such as particles increases with raising concentration. Conclusively, a higher amount of self-assembled structures should be present for the oxidized species at more concentrated solutions than it was the case for general Pull-*b*-PVP. For that reason, the crosslinking procedure was conducted at a highly concentrated state of 5.0 wt.%.



**Scheme V.1** Schematic crosslinking procedure of oxidized Pull-*b*-PVP self-assemblies with cystamine in Millipore water.

Cystamine dihydrochloride was selected as crosslinking agent. The crosslinker can reversibly attach to the oxidized glucose units of the pullulan block *via* imine formation with aldehyde groups. Furthermore, the disulfide bridge can be cleaved redox chemically by the application of suitable reducing agents, such as ascorbic acid and tricarboxyethyl phosphine (TCEP). Thus, two different triggers for release and disassembly can possibly be applied, pH and redox responsivity. But prior to the disassembly reaction of the crosslinked Pull-*b*-PVP structures, the crosslinking itself has to be investigated. Therefore, an aqueous solution containing 5 wt.% of block copolymer was prepared and a  $0.044 \text{ mmol} \cdot \text{mL}^{-1}$  cystamine dihydrochloride solution was added. The mixture was shaken for 36 hours in order to achieve a high crosslinking density (Scheme V.1). In order to remove free dissolved block copolymer as well as dimers and lower aggregates, the crosslinked solution was diluted to 0.1 wt.% and dialyzed for three days with an 1 000 000 MWCO dialysis tube against Millipore water. The high MWCO of the dialysis membrane and the long dialysis time should ensure a complete removal of smaller species, but trap the larger crosslinked aggregates inside the tube.

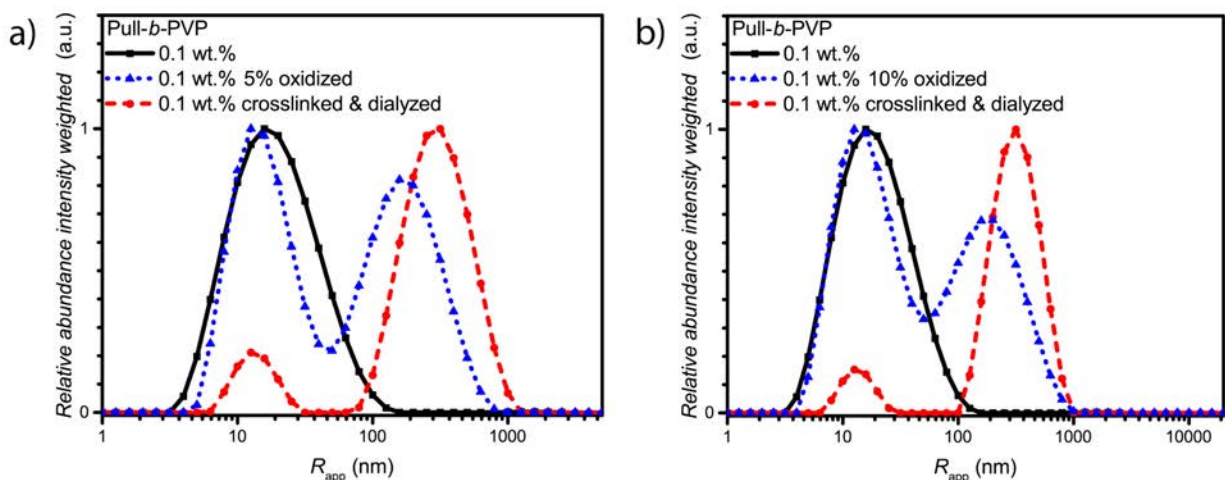


**Figure V.14** Intensity weighted particle size distributions of 0.1 wt.% solutions of initial Pull-*b*-PVP, oxidized block copolymer before and after crosslinking and dialysis with **a)** 5% of oxidized pullulan and **b)** 10% of oxidized pullulan in Millipore water measured *via* DLS at 25 °C.

As visible from the intensity weighted particle size distributions of the oxidized Pull-*b*-PVP block copolymer before and after crosslinking and dialysis in Figure V.14, crosslinking and dialysis drastically shifted the average apparent particle size distribution towards the large species. The relative abundance of the free dissolved 5% oxidized block copolymer species decreased by 80% from 1.0 to 0.2 while maintaining the average apparent radius of 14 nm. Moreover, the average apparent radius of the large particle species increased by 70% to 340 nm being the most abundant species by intensity weighting. The certain separation of the two peaks in contrast to the non-crosslinked block copolymer indicates a successful removal of all intermediates such as crosslinked dimers and smaller aggregates. However, free dissolved block copolymer is still present in the solution. Due to the intensity weighted size distribution, the abundance of the free dissolved block copolymer species appears to be significantly lower than it is the case in reality. Therefore, it can be stated that dialysis was not able to completely remove all free dissolved species. One explanation for this inability could be the reversibility of the imine formation due to concentration and entropic reasons leading to slight disassembly with time. This may result in free dissolved block copolymer still being abundant in the solution of crosslinked structures. The crosslinked and dialyzed sample of Pull<sub>124</sub>-*b*-PVP<sub>263</sub> oxidized to 10% displays the same bimodal intensity weighted particle size distribution with average apparent radii of 14 nm for the free dissolved block copolymer and 340 nm for the crosslinked structures is present. The difference in the two oxidized and crosslinked distributions is a 25% lower relative abundance of the free dissolved oxidized Pull-*b*-PVP of 0.15.

The cryo SEM micrographs of the crosslinked and dialyzed sample of Pull<sub>124</sub>-*b*-PVP<sub>263</sub> oxidized to 5% in Figure V.15 display spherical particles and a small amount of vesicular structures. Moreover, no tubular alignments of free dissolved block copolymer as they were present in the cryo SEM samples of the initial block copolymer in Figure V.9 were observed. As displayed in the micrograph in Figure V.15a, the crosslinked and dialyzed particles possess average diameters between 250 nm and 700 nm.

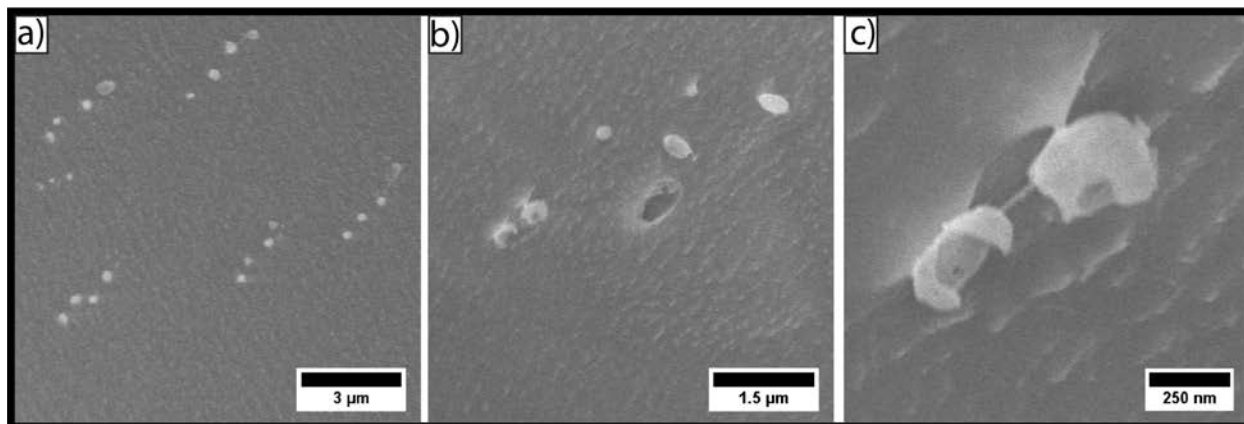


**Figure V.15** Cryo SEM micrographs of 5% oxidized Pull-*b*-PVP particles after crosslinking and dialysis displaying a) spherical particles and b) & c) hollow vesicular structures of with different diameters.

Larger spherical structures with diameters between 700 nm and 1.2 μm as displayed in Figure V.15b are often ruptured and show a hollow interior similar to the vesicles observed for Pull-*b*-PEA block copolymers. Moreover, some ruptured smaller particles with diameters around 250 nm could be observed (Figure V.15c) which indicate a hollow structure as well. This is an astonishing observation because it reveals the vesicular structure of oxidized and crosslinked Pull-*b*-PVP structures in Chapter V.4. In contrast to this observation, the spherical particles of the predeceasing untreated Pull-*b*-PVP do not show any indication of a vesicular character. Therefore, it can be assumed that the pullulan oxidation and crosslinking lead to this interesting morphological change.

The presence of vesicular structures furthermore increases with a higher oxidation state of pullulan at 10%. The cryogenic SEM micrographs in Figure V.16 display a high amount of vesicular structures with average diameters ranging between 250 nm and 1.2 μm. Only a small amount of small structures without vesicular shape could be observed in Figure V.16a and Figure V.16b. An even more impressive observation can be seen in Figure V.16b with the presence of anisotropic structures, which could possibly origin from two structures that merged during the crosslinking process. The probability of this occurrence is not unlikely since the high

concentration of 5.0 wt.% during the crosslinking procedure results in the spherical structures being in close proximity to each other and an entanglement of block copolymer chains can result in a merging of two spherical structures.

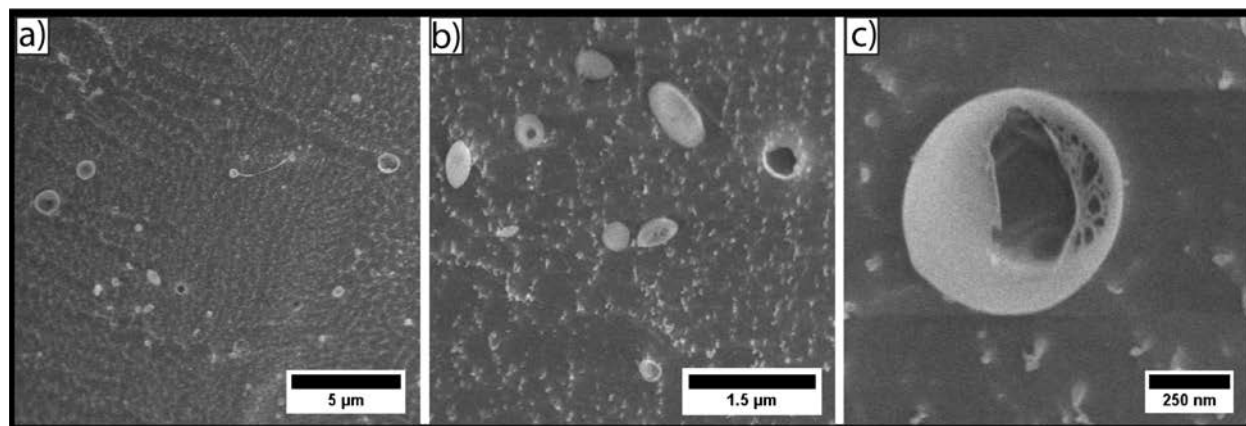
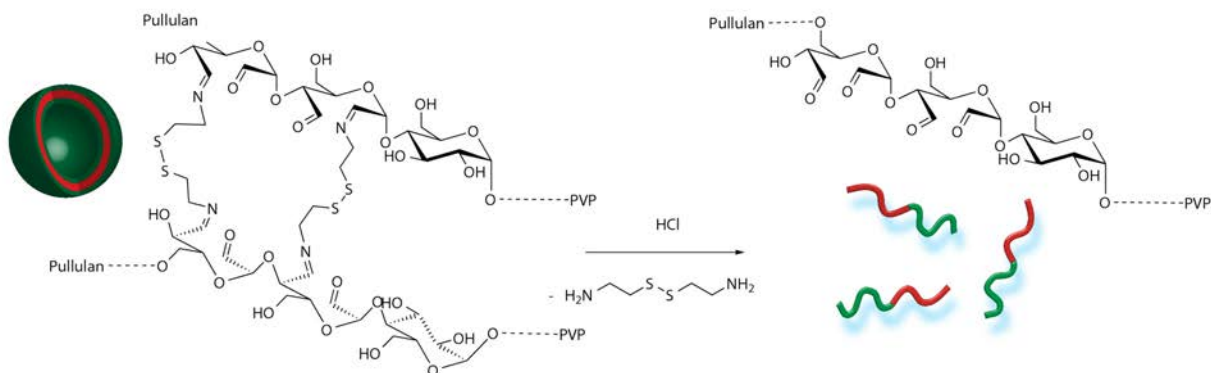


**Figure V.16** Cryo SEM micrographs of 10% oxidized Pull-*b*-PVP particles after crosslinking and dialysis displaying a) spherical vesicular structures and a minor amount of small spherical particles; b) & c) a magnification of a crosslinked Pull-*b*-PVP vesicle.

The magnification of a crosslinked Pull-*b*-PVP vesicle in Figure V.16c gives some more insight into its interior displaying an interpenetrating network of crosslinked block copolymer which increases in density towards the outer border to form a closed shell. Despite the insight into the vesicular structure, the cryo SEM technique prevents a clear postulation about the origin of the observations. These network structures can either be an intrinsic feature of the vesicles or be artifacts of the sample preparation, especially during the freezing and sputtering process.

Despite the uncertainties regarding their interior vesicle structure, the self-assembled and crosslinked vesicles already mark a significant step towards a model drug delivery cargo system. The vesicular structures encourage an encapsulation of target molecules. The last step to be attempted would be the pH induced disassembly of the imine linkages and the redox cleavage of the disulfide bridges. Since the cleavage of disulfide bridges requires a more precise study of the reaction conditions, the more facile pH induced disassembly *via* the destruction of imine bonds under acidic conditions was favored (Scheme V.2). However, tricarboxyethyl phosphine (TCEP) was utilized to demonstrate the general possibility of the disulfide cleavage of self-assembled and crosslinked Pull-*b*-PVP vesicles, too.



**Scheme V.2** pH induced disassembly of crosslinked Pull-*b*-PVP vesicles.

In order to assess the stimuli responsive disassembly of self-assembled and crosslinked Pull-*b*-PVP vesicles, 2.0 mL of 0.1 wt.% solutions of the 5% oxidized and crosslinked samples were treated with 20 mg TCEP for the cleavage of the disulfide bridges. Therefore, the solution containing the crosslinked vesicles was placed in a DLS vial and argon was bubbled through to remove the oxygen inside the solution. Subsequently, TCEP was added and the sealed vial was heated in a water bath at 40 °C overnight. The assessment of the pH responsivity was carried out *via* the addition of 150  $\mu\text{L}$  of a 0.1  $\text{mol}\cdot\text{L}^{-1}$  HCl solution to 2 mL of the crosslinked vesicle solution to set the pH value to 3, followed by heating the sealed sample at 40 °C overnight. The heat treatment was necessary to generate a certain activation energy which is required in both cases to accelerate the desired reaction pathway and encourage the disassembly process.

After the addition of the disassembly agent and heat treatment, the two samples were investigated *via* DLS and compared with the particle size distribution of the oxidized and the crosslinked samples (Figure V.17).

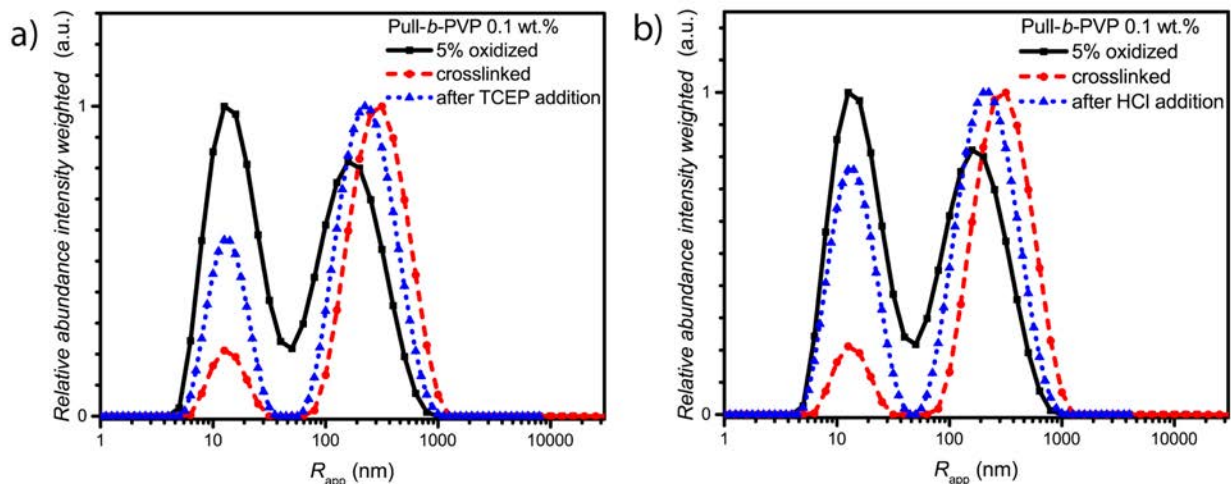


**Figure V.17** Comparison of intensity weighted particle size distributions of **a)** crosslinked Pull-*b*-PVP after treatment with TCEP; **b)** after treatment with 0.1 M HCl solution in Millipore water measured *via* DLS at 25 °C.

As visible from the intensity weighted apparent average particle size distribution in Figure V.17a, the addition of TCEP to the crosslinked vesicle solution resulted in a partial disassembly of the vesicular structures. The relative abundance of the peak corresponding to the free dissolved block copolymer increased by three fold from 0.2 to 0.57. Taking the intensity weighing into account, the increase in relative abundance is already quite large and a decent success in disassembly can be stated. Furthermore, the average apparent radius decreased by 21% from 340 nm to 268 nm (Table V.5). When comparing the average apparent particle size distribution of the oxidized species with the crosslinked one after TCEP addition, a complete disappearance of the aggregated species can probably not be achieved because the oxidized species displays a certain tendency to form aggregates as well.

**Table V.5** Summary of DLS results of the oxidation, crosslinking and disassembly of Pull-*b*-PVP at 0.1 wt.%.

Polymer	Peak 1 $R_{h,app}$ (nm)	Rel. abund.	Peak 2 $R_{h,app}$ (nm)	Rel. abund.
<b>Pull-<i>b</i>-PVP 5% oxidized</b>	13	1.0	160	0.8
<b>Pull-<i>b</i>-PVP crosslinked</b>	14	0.2	340	1.0
<b>Pull-<i>b</i>-PVP after TCEP addition</b>	14	0.57	268	1.0
<b>Pull-<i>b</i>-PVP after HCL addition</b>	15	0.77	250	1.0

The DLS results of the acid treatment of the crosslinked Pull-*b*-PVP vesicles in Figure V.17b display a more significant disassembly of the crosslinked structures. The relative abundance of the free dissolved species increased by four-fold to 0.77 and the average apparent radius decreased by 27% from 340 nm to 250 nm. The more pronounced increase in relative abundance



compared to the cleavage of the disulfide bridges with TCEP can be attributed to two factors. First, the cleavage of imine groups is acid catalyzed meaning that the disassembly agent is not consumed over time as it is the case for redox agents. Furthermore, traces of oxygen or other redox active species inside the solution can react with the redox agent as well, or reoxidize the thiols leading to new linkages that can possibly form.

Nonetheless, the TCEP addition displays a second pathway towards the disassembly of the crosslinked DHBC vesicles. However, the disassembly conditions have to be further optimized in order to improve the disassembly of the crosslinked vesicles towards completion.

## V.6. Conclusion

This chapter demonstrated the versatility of DHBC self-assembly. A novel block copolymer Pull-*b*-PVP was synthesized *via* RAFT/MADIX techniques starting from a pullulan macro RAFT/MADIX CTA. The block copolymer self-assembled to spherical structures with an average apparent radius of 800 nm at increased concentrations. Furthermore, spherical structures could be observed with cryo SEM and LSCM techniques. The pullulan block could be successfully functionalized with aldehyde groups to act as anchor point for crosslinker attachments. It was demonstrated, that the oxidized self-assembled particles could be crosslinked *via* the bifunctional crosslinker cystamine forming imine linkages with the aldehyde groups. The afforded vesicles with an average diameter of 700 nm were stable upon high dilution and could be observed *via* cryo SEM. Furthermore, it was possible to cleave the crosslinking bonds to a certain degree with the treatment of acid or the application of the reducing agent TCEP. Despite no complete disassembly could be afforded, the disassembly experiments obtained from DLS proof the stimuli responsivity of crosslinked Pull-*b*-PVP DHBC vesicles. The responsivity is a key feature taking future applications in the biomedical sector into account.

## VI. Conclusion and Perspectives

The fundamental motivation of the elaborated investigations of the synthesis and the self-assembly behavior of double hydrophilic block copolymers was to explore a new pathway towards novel transport vehicles that could possibly be applied in drug delivery. The benefits of DHBCs and the corresponding particles and vesicles, such as biocompatibility, high permeability towards water, and hydrophilic compounds as well as the large amount of possible functionalizations that can be addressed to the block copolymers make the application of DHBC based structures a viable choice in biomedicine. To examine the potential of DHBCs and propose examples that direct to a theoretical practical application, five different block copolymers were synthesized and investigated in within the scope of this thesis, PEO-*b*-PVP, PEO-*b*-P(VP-*co*-VIm), Pull-*b*-PDMA, Pull-*b*-PEA, and Pull-*b*-PVP focusing on the self-assembly behavior of these DHBCs and the introduction of functionalities.

The first topic (Chapter III) addressed the investigation of the literature known DHBC PEO-*b*-PVP, which was synthesized by applying aqueous RAFT/MADIX techniques. The block copolymer containing two FDA approved hydrophilic polymer blocks was a promising candidate in order to assess the self-assembly behavior. The self-assembly behavior of PEO<sub>500</sub>-*b*-PVP<sub>225</sub> was determined *via* DLS and despite a lower tendency for self-assembly in contrast to other reported DHBCs, spherical structures of self-assembled block copolymer could be observed *via* cryo SEM and LSCM at higher concentrations. The observation of the concentration dependency of PEO<sub>500</sub>-*b*-PVP<sub>225</sub> is a very important insight into the self-assembly behavior and gives rise to two conclusions. First, the difference in hydrophilicity is a crucial value for the extent of the microphase separation of DHBC self-assemblies. A high difference leads to a stronger aggregation tendency at lower concentrations, whereas a smaller difference requires a higher concentration of block copolymer to afford similar structures. What appears to be a drawback for pure self-assemblies can actually be an advantage for drug delivery. The second conclusion regarding the concentration dependent tendency of self-assembly is that formed structures can be preserved from disassembly upon dilution *via* crosslinking. Therefore, the comonomer VIm was introduced to the PVP block to increase the difference in hydrophilicity and provide a functional monomer where crosslinkers can be addressed, too. PEO<sub>500</sub>-*b*-P(VP<sub>300</sub>-*co*-VIm<sub>55</sub>) displayed an improved self-assembly in contrast to PEO<sub>500</sub>-*b*-PVP<sub>225</sub> which could be determined with DLS

and cryo SEM. The application of the crosslinker diethylene glycol bis(2-iodoethyl) ether could indeed successfully crosslink the structures with an average diameter of 300 nm and preserve them from disassembly upon dilution. Furthermore, a crosslinking pathway in the polar solvent DMF followed by the transfer into an aqueous system and dialysis led to spherical particles which could be observed in cryo SEM and cryo TEM. In addition, it was possible to label the particles with Rhodamine B *via* free crosslinker attachments. The introduction of a second monomer possessing a functional group that can be addressed to crosslinkers and functional molecules such as dyes displays a significant improvement of DHBC self-assemblies towards possible applications. Moreover the increased self-assembly tendency after the addition of a comonomer afforded a deeper insight into the driving forces of DHBC self-assembly.

The second block copolymer system containing the double hydrophilic Pull-*b*-PDMA and Pull-*b*-PEA in Chapter IV should give a deeper insight into DHBC self-assembly. In contrast to PEO-*b*-PVP based block copolymers, the pullulan and poly(acrylamide) polymer blocks were synthesized separately and connected *via* a CuAAC reaction to the corresponding block copolymers. The self-assembly of the pullulan containing block copolymers surpassed the one of the previous chapter by far with only a very small amount of free dissolved block copolymer being visible from DLS measurements even at a low concentration of 0.1 wt.%. Furthermore, the structure of the self-assemblies differed from the one of the PEO-*b*-P(VP-*co*-VIm) block copolymers. Cryo SEM investigations of Pull-*b*-PEA self-assemblies clearly displayed the presence of vesicular structures with average diameters between 200 and 500 nm at a low concentration. The occurrence of vesicular structures self-assembled from DHBCs was already confirmed by Brosnan et al., but the presence at very low concentrations underlines that DHBC vesicles are a substantial part of the phase diagram. The determination of the structure of Pull-*b*-PDMA self-assemblies was more challenging. Cryo SEM measurements of the block copolymer with a slightly diminished self-assembly tendency from DLS directed towards the presence of particle structures. The functionalization of the RAFT group of PDMA attaching Rhodamine B ITC followed by the conjugation reaction with pullulan and the investigation with LSCM on the other hand pointed towards the presence of vesicular structures, subsequently observing structures with a red corona. Since the dye is exclusively present permanently attached to the block copolymer, the hollow structures have to be attributed to Pull-*b*-PDMA self-assemblies. The two different block copolymers display a clear tendency towards the formation of vesicular

structures. The introduction of a functional end group of the block copolymer, Rhodamine B respectively, furthermore displays the applicability of DHBCs towards functionalization. However, the poly(acrylamide) blocks are not biocompatible which decreases the spectrum of possible applications. Nonetheless, the pullulan-*b*-poly(acrylamide) block copolymers display an outstanding self-assembly behavior and afforded deeper insight into the morphological appearance of DHBC structures. Additionally, the transition of CuAAC reactions to DHBCs broadens the scope for the possible synthetic pathways of novel block copolymers.

The last chapter (Chapter V) can be regarded as a profound probe into possible applications of DHBC vesicles. Pull-*b*-PVP was synthesized *via* RAFT/MADIX techniques starting from a pullulan macro RAFT chain transfer agent. The block copolymerization appeared to be more challenging compared to PEO-*b*-PVP due to the higher viscosity of the reaction solution, which was overcome by the addition of the co-solvent DMSO. Aqueous solutions of the block copolymer displayed a self-assembly behavior that can be situated between the ones observed in Chapter III and Chapter IV. The apparent average particle size distributions of different concentrations display two key properties, which are appealing for further proceedings, the lack of aggregates at a very low concentration, and the intensive formation of aggregates upon increasing concentration, pointing towards a high abundance of aggregates. The aggregates could be assessed to be spherical particles with cryo SEM and LSCM techniques. Subsequently, glucose units corresponding to the pullulan block of the block copolymer were oxidized to aldehydes to form functional units for crosslinking. The self-assembled structures were then crosslinked with cystamine, a bifunctional crosslinker containing a disulfide bridge and two amine groups to form imine linkages with the block copolymer. The crosslinked solution was diluted and dialyzed to remove remaining free dissolved block copolymer in similar fashion to PEO-*b*-P(VP-*co*-VIm). The decent amount of crosslinked structures that were displayed in the particle size distribution of DLS could be visualized as vesicles *via* cryo SEM measurements. The observation of crosslinked DHBC vesicles with a block copolymer composition that is regarded to be fully biocompatible and in the case of pullulan even biodegradable displays an enormous step towards a possible applicability of these structures. Furthermore, the introduction of a bifunctional crosslinker that can be cleaved in acidic media or by reduction can lead to the disassembly of the vesicles. The DLS results obtained after the treatment of the crosslinked vesicles with acid and the reduction agent TCEP at a slightly elevated temperature display that a

disassembly can be achieved. The observations of the last chapter afforded biocompatible crosslinked DHBC vesicles which can be disassembled *via* external triggers, such as pH and redox agents. As a future perspective, these vesicles can be loaded with a target molecule, e.g. a dye, and the release properties can be studied depending on the external trigger applied.

In conclusion, the investigations of the DHBCs PEO-*b*-PVP, PEO-*b*-P(VP-*co*-VIm), Pull-*b*-PDMA, Pull-*b*-PEA, and Pull-*b*-PVP contributed to a high extend to the increased understanding of double hydrophilic self-assembly. Starting from the investigation of the possibilities of DHBC self-assembly in the first chapter going on to the confirmation of vesicles and the application of a versatile DHBC synthesis in addition to the dye functionalization of the block copolymer in the second chapter, the third chapter dealing with the synthesis and analysis of dual responsive crosslinked Pull-*b*-PVP vesicles displays a very promising spectrum for DHBC self-assembly. A significant number of new block copolymers can be easily synthesized by applying the reported conjugation process. Furthermore, novel drug delivery approaches can be developed with the concept of the displayed DHBC vesicles addressing to the delivery of hydrophilic drugs or providing confinements for enzymes, to name two examples.

For future applications on the hand and out of scientific curiosity on the other hand, the structure of the membrane or vesicle wall of the DHBC self-assemblies has to be investigated more precisely. The work carried out in this thesis displays that a multilammelar structure could be present for the particle shaped structures, but this could not be confirmed for the vesicular structures with the applied methods. Therefore, more advanced techniques such as STED and cryo TEM measurements should be applied for future systems for a thorough investigation. Moreover, DHBCs with a superior self-assembly compared to the ones presented here should be applied for these investigations since the amount of free dissolved block copolymer is still decent and could possibly hinder precise measurements. The exchange of one hydrophilic block with a hydrophilic polymer brush for example could already improve the self-assembly behavior.

Nonetheless, DHBC self-assemblies show a strong potential to generate an impact on biomedicine and nanotechnologies.

## VII. Appendix

### VII.1. Abbreviations

$^{13}\text{C}$ -NMR	carbon nuclear magnetic resonance
$^1\text{H}$ -NMR	proton nuclear magnetic resonance
AIBN	azobis(isobutyronitrile)
app	apparent
AROP	anionic ring opening polymerization
CA	cellulose acetate
CL	crosslinker
cryo	cryogenic
CTA	chain transfer agent
CuAAC	copper(I) catalyzed azide alkyne cycloaddition
$D$	polydispersity index
DCM	dichloromethane
DHBC	double hydrophilic block copolymer
DIC	differential interference contrast
DLS	dynamic light scattering
DMF	<i>N,N</i> -dimethylformamide
DMSO	dimethylsulfoxide
FDA	US Food and Drug Administration
IR	infra red
LCST	lower critical solution temperature
LSCM	laser scanning confocal microscopy
M	$\text{mol L}^{-1}$
MADIX	macromolecular design <i>via</i> the interchange of xanthates
$M_n$	average number weighted molecular weight
$M_w$	average mass weighted molecular weight
MWCO	molecular weight cut off
$\text{N}_3$	azide termination
$\text{NaCNBH}_4$	sodium cyanoborohydride
PDMA	poly( <i>N,N</i> -dimethylacrylamide)
PEA	poly( <i>N</i> -ethylacrylamide)
PEO	poly(ethylene oxide)
pH	$-\log c(\text{H}^+)$
Pull	pullulan
PVP	poly( <i>N</i> -vinylpyrrolidone)

---

RAFT	reversible addition fragmentation transfer
RDRP	reversible deactivation radical polymerization
redox	reduction-oxidation reaction
$R_{app}$	apparent radius
$R_g$	radius of gyration
$R_h$	hydrodynamic radius
DNA	deoxyribonucleic acid
RT	room temperature
SEC	size exclusion chromatography
SEM	scanning electron microscopy
SLS	static light scattering
TEM	transmission electron microscopy
$T_g$	glass transition temperature
UV	ultra violet
UV-vis	ultra violet to visible light
wt.%	weight %

## VII.2. Applied Methods

### VII.2.1. Nuclear Magnetic Resonance (NMR) Spectroscopy

NMR spectroscopy is a versatile technique to determine the chemical structure of a molecule in solution. The technique is frequently used to determine the number and the chemical environment of hydrogen ( $^1\text{H}$ -NMR) or carbon ( $^{13}\text{C}$ -NMR) atoms within a molecule. The fundamental concept behind NMR spectroscopy is the Zeeman Effect, i.e. the spins of the atom nuclei split into distinct energy levels upon the application of an external magnetic field. In the case of  $^1\text{H}$  and  $^{13}\text{C}$  the nuclei spins split into two energy levels for example. As soon as the dissolved molecule is placed in a strong magnetic field (between 2 and 10 T) the spins of the nuclei align in the magnetic field and precess around the magnetic field direction. The sample can be subsequently irradiated with a short pulse of radiofrequency energy characteristic to the nucleus of interest in order to disturb the equilibrium balance between two energy levels. Some nuclei absorb the energy and are promoted to a higher energetic level. Upon termination of the radiofrequency, the nuclei spins fall back to the equilibrium state at a lower energy level and this energy can be detected and processed by a radiofrequency detector. The electronic surrounding of the nucleus, such as electron distribution affects the strength of the applied magnetic field, affects the frequency at which the corresponding nucleus resonates. The difference in the resonance energy can be observed as a chemical shift in comparison to a reference.

$^1\text{H}$ -NMR and  $^{13}\text{C}$ -NMR spectra were recorded at ambient temperature at 400 MHz for  $^1\text{H}$  and 100 MHz for  $^{13}\text{C}$  with a Bruker Ascend400.

### VII.2.2. Size Exclusion Chromatography (SEC)

SEC is a relative method to determine the molecular weight and the polydispersity of a polydisperse polymer. A solution of the polymer is fractionated through a column containing highly crosslinked polystyrene resin with defined pore sizes between 10 and 1000 Å. Depending on the hydrodynamic volume of the polymer, the residence time inside the column varies due to interaction with pores of different sizes. For that reason the elution of polymers with large hydrodynamic volumes occurs before the ones of a small hydrodynamic volume. The elution of the polymer can be detected with a refractive index or an UV detector in dependence of the



elution volume. The corresponding molecular weight of the elugrams corresponding to the investigated polymer can be determined *via* a calibration curve of a polymer standard with a defined molecular weight distribution.

Size exclusion chromatography (SEC) for poly(acrylamides), poly(ethylene oxides), PEO-*b*-PVP block copolymers, and Pull-*b*-PVP block copolymers were conducted in NMP (Fluka, GC grade) with 0.05 mol L<sup>-1</sup> LiBr and BSME as internal standard at 70 °C using a column system by PSS GRAM 100/1000 column (8 x 300 mm, 7 µm particle size) with a PSS GRAM precolumn (8 x 50 mm) and a Shodex RI-71 detector and a PS calibration for poly(acrylamides) and a PEO calibration for the other block copolymers, respectively, with standards from PSS. Pullulan samples were analyzed in acetate buffer containing 20% MeOH at 25 °C using a PSS NOVEMA Max analytical system XL (pre column size 50 mm x 8 mm – 10 µm, main column size 300 mm x 8 mm - 10 µm) using a pullulan calibration with standards from PSS.

### VII.2.3. Static light scattering (SLS)<sup>245</sup>

Static light scattering is generally used to determine the weight average of the molecular mass  $M_w$  of completely dissolved polymers. In addition, it is possible to determine the radius of gyration  $R_g$  of particles, such as polymer aggregates, polymersomes and polymeric particles. The theoretical background of SLS will be explained in the following section.

In a light scattering experiment, the scattered intensity  $I_s$  is the most important value, which is the resulting intensity that is detected by a detector at a certain angle  $\theta$ . Variation of  $\theta$  results in a difference in the scattering volume  $V$  and therefore in the scattered intensity  $I_s$ . For that reason, it is necessary to normalize the detected scattered intensity to an angle and volume independent value. In practice, the scattered intensity is normalized to an absolute scattered intensity  $R$ , also called the Rayleigh ratio, which summarizes the experimental setup parameters (wavelength  $\lambda_0$ , sample detector distance  $r_D^2$  and scattering volume  $V$ ), the scattered intensities of the solvent  $I_{\text{solvent}}$  with the refractive index  $n_{D,0}$ , the particle or polymer solution  $I_{\text{solution}}$  with the corresponding refractive index increment  $\left(\frac{\partial n_D}{\partial c}\right)$ , concentration  $c$  and molar mass  $M$ .

$$R = b^2 \cdot \frac{cM}{N_L} = \frac{4\pi^2}{\lambda_0^4} n_{D,0}^2 \left(\frac{\partial n_D}{\partial c}\right)^2 \frac{cM}{N_L} = (I_{\text{solution}} - I_{\text{solvent}}) \frac{r_D^2}{V}$$

Equation 7

In standard experimental setup, the absolute scattered intensity is determined by the direct measurement of  $I_{\text{solvent}}$ ,  $I_{\text{solution}}$ , the scattered intensity of a standard solvent (typically toluene)  $I_{\text{std}}$ , all with the same setup, normalized by a literature reference absolute intensity of the standard  $I_{\text{std,abs}}$ .

$$R = (I_{\text{solution}} - I_{\text{solvent}}) \cdot \frac{I_{\text{std,abs}}}{I_{\text{std}}}$$

**Equation 8**

The Rayleigh ratio removes all dependencies of the scattering intensity towards experimental conditions, such as scattering volume or detector distance. Therefore, the Rayleigh ratio is necessary in order to afford comparative results for different experimental setups with static light scattering.

Since the scattered intensity of small particles is determined by the particle mass and the number of particles in the scattering volume, the scattering power of a single dissolved particle  $b$ , Equation 10 can be rewritten by using a derivation of the van't Hoff equation for real solutions,

$$\frac{\partial \pi}{\partial c} = kT \left( \frac{1}{M} + 2A_2c + \dots \right)$$

**Equation 9**

to afford the basic equation for static light scattering of small particles (size < 10 nm),

$$\frac{Kc}{R} = \frac{1}{M} + 2A_2c + \dots$$

**Equation 10**

where the contrast factor  $K$  is the squared scattering power  $b^2$  and  $A_2$  the second virial coefficient as a quantitative measure of solvent-solute interactions.

In general, particle sizes exceeding 10 nm are examined. Here, the scattering intensity is no longer independent of the scattering angle and an experimentally determined scattering vector  $\vec{q}$  has to be introduced.  $\vec{q}$  is a quantitative measure for the length scale of an SLS experiment and contains the scattering vector  $\theta$ , the wavelength  $\lambda$  of the incident laser beam and the refractive index of the solvent  $n_D$ .

$$|\vec{q}| = q = \frac{4\pi n_D \sin\left(\frac{\theta}{2}\right)}{\lambda}$$

Equation 11

The dependence of the scattering intensity on the scattering vector leads to the summation of all scattering centers  $Z$  of a single particle and the relative distance  $\vec{r}_{i,j}$  between these centers. The scattering of a single particle can therefore be described via the so called particle form factor  $P(q)$ .

$$P(q) = \frac{1}{Z^2} \sum_{i=1}^Z \sum_{j=1}^Z \left( 1 - \frac{1}{6} q^2 r_{i,j}^2 + \dots \right)$$

Equation 12

Since the relative distances between the separate scattering centers are only attributed to the selected particle, the coordinate origin can be assessed to the particle's center of mass, assuming a homogenous mass distribution throughout the particle. Conclusively, replacement of  $\vec{r}_{i,j}$  with  $\vec{s}_j - \vec{s}_i$  changes the appearance of the particle form factor  $P(q)$  to

$$P(q) = \left( 1 - \frac{1}{3} q^2 s^2 + \dots \right)$$

Equation 13

where  $s^2$  is the squared radius of gyration ( $R_g$ ). The insertion of the particle form factor into the basic light scattering equation (Equation 10) affords the important Zimm equation

$$\frac{Kc}{R} = \frac{1}{M_w} \left( 1 + \frac{1}{3} q^2 s^2 \right) + 2A_2c$$

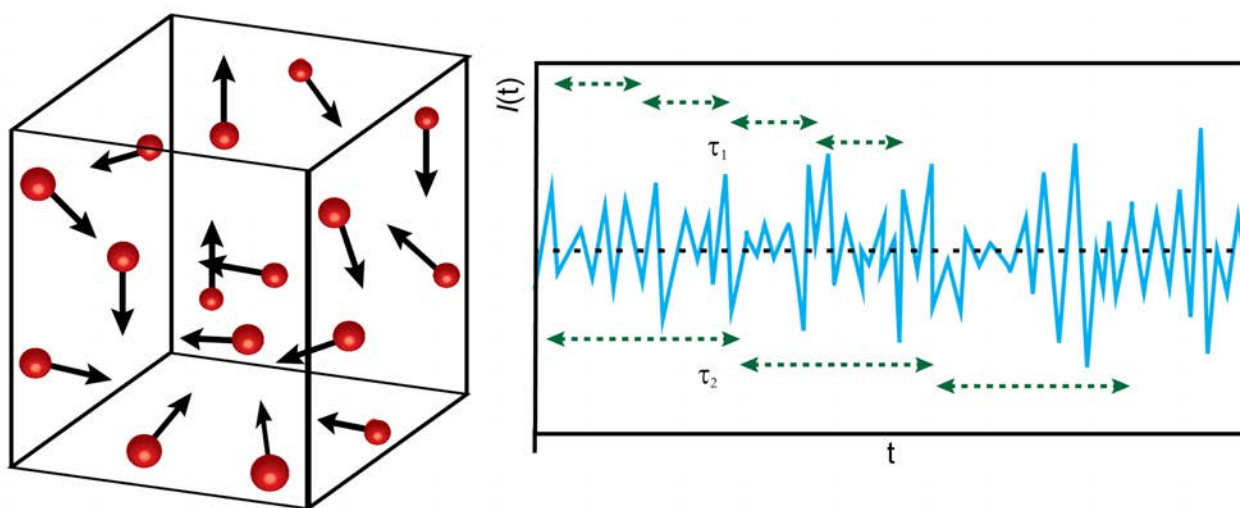
Equation 14

The Zimm equation enables the determination of several important values, such as  $M_w$ ,  $A_2$ , and  $R_g$  by the examination of the solution's scattered intensity. Static light scattering is therefore a measure for the interaction of the examined (polymeric) species with the solvent (second virial coefficient  $A_2$ ), its average molecular weight ( $M_w$ ) and the average radius of gyration ( $R_g$ ). It is therefore a direct method to afford the average molecular weight distribution for polymers, which do not have a proper calibration curve, e.g. polymer brushes. Furthermore, the second virial provides an insight in polymer solvent interactions. The values are typically assessed by a so called Zimm plot. The determined values of all angles are plotted on  $Kc/R$  against  $q^2 \cdot c$  and extrapolated to  $c = 0$ . In this fashion, the x-axis distance corresponds to  $M_w$  and the extrapolation

slope to  $A_2$  and  $s^2$ , respectively. A problem occurs with samples containing two different fractions, such as free dissolved polymer chains and aggregates. Typical SLS experimental setups only afford the average values of a combination of both species, resulting in a difficult to impossible deconvolution of the Zimm plot.

#### VII.2.4. Dynamic light scattering (DLS)<sup>245</sup>

Dynamic light scattering (DLS) is a versatile technique in order to determine aggregate sizes and shapes. The key feature of DLS is the detection of intensity fluctuations in the sample with light scattering techniques. Intensity fluctuations origin from thermal density fluctuations of the solvent molecules, causing the particles inside the solution to diffuse through the solvent in a random fashion (Scheme VII.1a). The so called Brownian motion of a solute particle is an isotropic diffuse particle motion and is strongly dependent on its mobility inside the solvent, i.e. its self-diffusion coefficient  $D_s$ .



**Scheme VII.1** a) Schematic view of the Brownian motion of particles in a cubic box; b) Schematic view of the intensity function and the different correlation times  $\tau$ .

The self-diffusion coefficient  $D_s$  can be expressed via the Stokes-Einstein Relation for a hard sphere.

$$D_s = \frac{kT}{f} = \frac{kT}{6\pi\eta R_H}$$

**Equation 15**

Hence, the Brownian motion of the scattering particles is depending on the particle mobility, the intensity fluctuation can be correlated with the self-diffusion of the particles. Inside the scattering volume,  $n$  particles are moving towards or away from each over a certain time ( $n(\vec{r}, t)$ ). This movement can be expressed via the van Hove self-correlation function  $G_s(\vec{r}, \tau)$ ,

$$G_s(\vec{r}, \tau) = \langle n(\vec{0}, t)n(\vec{r}, t + \tau) \rangle_{V,T}$$

**Equation 16**

The van Hove self-correlation function describes the probability of finding a particle at the position  $\vec{r}$  after a time period of  $t + \tau$ , if the same particle was located at  $\vec{0}$  coordinate at the time  $t$ . Since the particle movement is completely arbitrary, the absolute distances and times do not matter, but the relative vector  $\vec{r} - \vec{0}$  and time difference  $\tau$ . Because average over the whole scattering volume and the measuring is taken,  $G_s(r, \tau)$  only depends on the travelled distance of the particle  $r = |\vec{r}|$ ,

$$G_s(r, \tau) = \left[ \frac{2\pi}{3\langle \Delta R(\tau)^2 \rangle} \right]^{3/2} \exp\left( -\frac{3r(\tau)^2}{2\langle \Delta R(\tau)^2 \rangle} \right)$$

**Equation 17**

with the mean-square displacement  $\langle \Delta R(\tau)^2 \rangle$  of the scattering particle. As the particle is pushed through the volume by Brownian motion, the mean square displacement can be related to the self-diffusion coefficient  $\langle \Delta R(\tau)^2 \rangle = 6D_s\tau$ .

In similarity to SLS experiments, the experimental setup parameters, such as scattering angle and laser wavelength can be summarized to the scattering vector  $q$ . The information of the particle motion can therefore be summarized in the dynamic structure  $F_s(q, \tau)$ , the primary quantity measured in a DLS experiment:

$$F_s(q, \tau) = \left( -q^2 \langle \Delta R^2(\tau) \rangle_T \tau / 6 \right) = \exp(-D_s q^2 \tau)$$

**Equation 18**

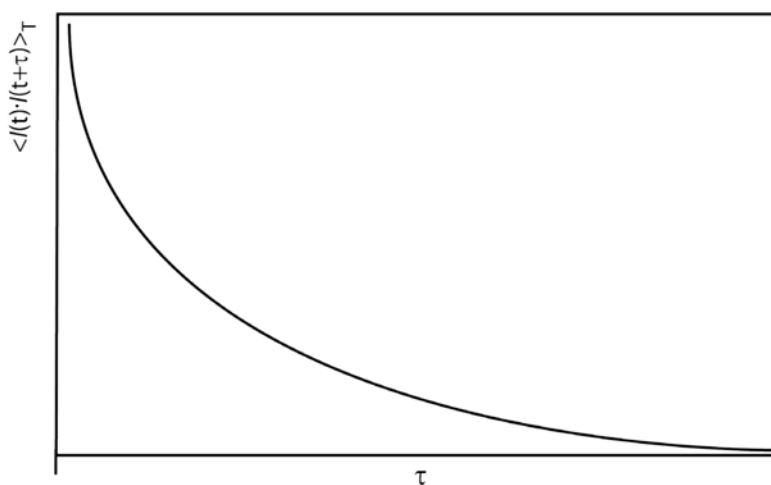
In a DLS experiment, fluctuations of the detected intensity at a fixed angle of a certain time period  $\tau$  (Scheme VII.1b) are measured. In contrast to SLS, where only the average detected intensity  $\langle I(q, t) \rangle_T$  is detected (dashed line in Scheme VII.1b), DLS requires detailed analysis of the fluctuating intensity. Therefore, the fluctuation has to be translated mathematically via an autocorrelation function. In principle, the measured time dependent intensity  $I(q, t)$  is multiplied with itself after a time shift of  $\tau$ ,  $\langle I(q, t)I(q, t + \tau) \rangle$ , divided by the squared average intensity

$\langle I(q, t)^2 \rangle$ , with  $\tau$  ranging in a scale of 100 ns to several seconds. In order to relate the detected time dependent scattering intensity with the dynamic structure factor  $F_s(q, \tau)$ , the Siegert relation  $g_2(q, \tau) = 1 + g_1(q, \tau)^2$  is used. In this case,  $F_s(q, \tau)$  is formally replaced by  $g_1(q, \tau)$ , and  $g_2(q, \tau)$  the normalized scattered intensity autocorrelation function. The relation is rewritten in order to afford  $g_1(q, \tau)$  ( $F_s(q, \tau)$ , respectively):

$$F_s(q, \tau) = \exp(-D_s q^2 \tau) = \sqrt{\frac{\langle I(q, t) I(q, t + \tau) \rangle}{\langle I(q, t)^2 \rangle}} - 1$$

Equation 19

The determination of the dynamic structure factor is accomplished by the measurement and the mathematical translation of the intensity autocorrelation function. With the knowledge of  $q$ , the solvent properties and  $\tau$ , it is possible to determine the average hydrodynamic radius  $R_h$  of the solute particle. For monodisperse samples,  $g_2(q, \tau)$  is a single exponential decay from 2 to 1 (Scheme VII.2).



Scheme VII.2 Schematic depiction of an autocorrelation function.

In the case of polydisperse samples with different hydrodynamic radii and therefore different particle masses  $M_i$ , particle form factors  $P_i(q)$  and the species' number density  $n_i$ . The intensity of the particle  $i$  is therefore given as  $I_i \sim n_i \cdot M_i^2 \cdot P_i(q)$ . The average self-diffusion coefficient is conclusively defined via a distribution function  $P(D_s)$ . Therefore, the dynamic structure factor is a superposition of single exponentials weighted by  $P(D_s)$  instead of a single exponential decay function.

$$F_s(q, \tau) = \int_0^{\infty} P(D_s) \exp(-q^2 D_s \tau) dD_s$$

Equation 20

The more complicated polydisperse systems require a different evaluation approach, the so called cumulant analysis, a series expansion of  $F_s(q, \tau)$  has to be applied.

$$\ln F_s(q, \tau) = \Gamma_0 - \Gamma_1 \tau + \frac{1}{2!} \Gamma_2 \tau^2 - \frac{1}{3!} \Gamma_3 \tau^3 + \dots$$

Equation 21

The cumulant  $\Gamma_1 = \langle D_s \rangle q^2$  yields the average diffusion coefficient and  $\Gamma_2 = (\langle D_s^2 \rangle - \langle D_s \rangle^2) q^4$  delivers a quantitative measure of the polydispersity of the diffusion coefficient distribution

$$\text{function } (\sigma_D) = \sqrt{\frac{\Gamma_2}{\Gamma_1^2}}.$$

The cumulant analysis affords a resolution of two particle species being present in the same solution. This feature makes the cumulant analysis very important for polymer science since presence of two or more species can be determined independently.

### Rayleigh scattering

An important value for the calculation of the DLS particle size distribution is the intensity. The particle size distribution is therefore usually represented as intensity weighted distribution. Since light scattering of particles in solution is mainly dependent on elastic Rayleigh scattering, the intensity is strongly correlating with the size of the particles.

$$I = \frac{I_0}{R^2} \frac{1 + \cos^2(\theta)}{2} \left(\frac{2\pi}{\lambda}\right)^4 \left(\frac{n_D^2 - 1}{n_D^2 + 2}\right)^2 r^6$$

Equation 22

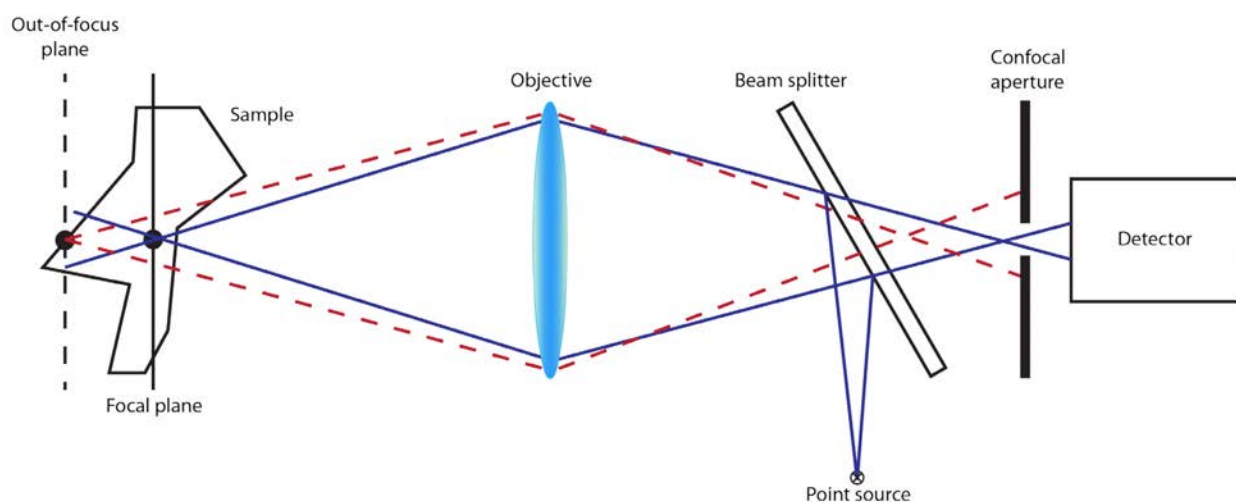
Therefore, the scattered intensity of larger particles scales with the power of  $10^6$  compared to smaller particles. This results in an increased pronunciation of larger particles in contrast to smaller ones. Therefore, the afforded intensity weighted particle size distributions have to be taken with care since they differ from the actual composition in the solution.

Dynamic light scattering (DLS) and static light scattering (SLS) was performed using an ALV-7004 Multiple Tau Digital Correlator in combination with a CGS-3 Compact Goniometer and a HeNe laser (Polytec, 34 mW,  $\lambda = 633$  nm at  $\theta = 90^\circ$  setup for DLS and  $30^\circ$  to  $150^\circ$  with step of  $10^\circ$  for SLS). Sample temperatures were adjusted to  $25^\circ\text{C}$ . Toluene (Sigma Aldrich, HPLC

grade) was used as immersion liquid. Apparent hydrodynamic radii ( $R_{app}$ ) have been determined from fitting autocorrelation functions by using REPES algorithm. Radii of gyration ( $R_g$ ) were determined via SLS with ALV Stat ALV-5000 using a Guinier plot.

### VII.2.5. Laser Scanning Confocal Microscopy (LSCM)

Confocal microscopy is a technique for the imaging of thin lateral sections of a sample without the detection of out-of-focus light. The principle of an optical sectioning microscope applying the confocal principle is displayed in Scheme VII.3. The illumination of the sample from a point source such as a laser is focused on a spot inside the sample.



**Scheme VII.3** Schematic view of a point scanning confocal microscope. The blue rays exemplify the rays in focus, whereas the red rays display the out-of-focus rays rejected from the pinhole.

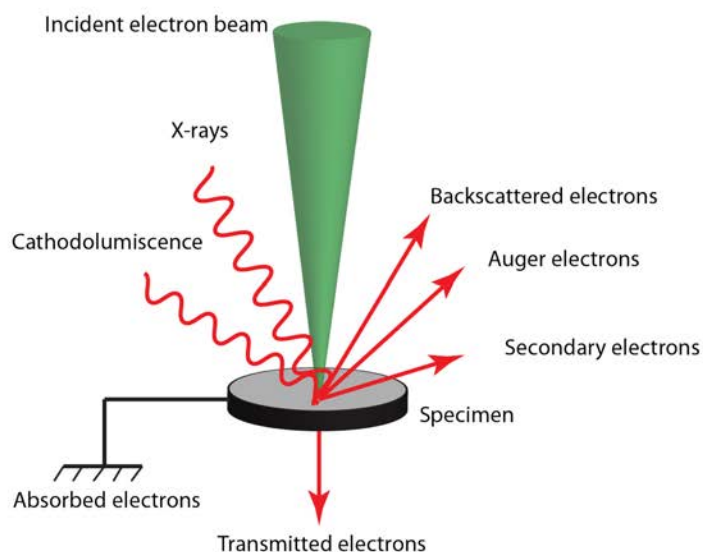
In order to improve the acquisition rate, the confocal principle can be extended with a line-scanning microscope. In this case a line is used to illuminate the sample and fluorescence is collected through a slit. As all points in the line are detected at once, acquisition times are greatly improved but this comes at the expense of reduced sectioning strength.

LSCM measurements were conducted with a Leica TCS SP5 (Wetzlar, Germany) confocal microscope, using a 63x (1.2 NA) water immersion objective. The dye stained samples were excited with a diode pumped solid-state laser at 561 nm. The emission bands were collected at 640 nm.



### VII.2.6. Electron microscopy

When electrons enter the surface of a specimen, the electrons are scattered within the specimen due to interaction with other electrons and atomic nuclei. Therefore, they gradually lose their energy and become absorbed by the sample. The extent of the scattering is therefore dependent on the atomic composition of the specimen, i.e. samples with atoms of a higher atom number result in less intense scattering than low atom number samples. As displayed in Scheme VII.4, the signals that can be emitted from a sample that is irradiated with an electron beam. The electrons penetrating the sample can either be directly backscattered, transmitted through the sample or interact with the specimen to release secondary electrons, Auger electrons or energy in terms of X-rays of a certain energy which is depending on the specimen composition. Depending on the applied technique, the specific interaction of the electron beam with the specimen can be detected. In order to generate and detect electrons, the sample and the electron beam path have to be under high vacuum to avoid interaction of electrons with air. Two techniques will be briefly explained in the following section, TEM and SEM, respectively.



**Scheme VII.4** Schematic view of the interaction of an electron beam with a specimen.

### Transmission Electron Microscope (TEM)<sup>259</sup>

Standard TEM measurements detect the electrons that are transmitted through the specimen, resulting in two dimensional images. In order to afford an image with sufficient contrast, the specimen has to be very thin to allow transmittance through the sample. The sample is therefore casted on a thin copper grid which is covered with a conductive layer, such as carbon. The

electron beam penetrates through the specimen and the corresponding transmitted electrons are detected on a screen or a camera system. Depending on the thickness of the specimen and its atomic composition, the intensity of the detected transmitted electrons is different. Thicker sections of the specimen or areas with atoms of a higher atom number transmit a smaller amount of electrons than thinner areas or areas with atoms of a low atom number.

Cryo TEM is a technique that enables the observation of specimen in solution. The specimen is therefore frozen in liquid ethane and examined at a low temperature and a low voltage to avoid destruction of the sample.

Cryogenic transmission electron microscopy (cryo TEM) was performed utilizing a Zeiss EM922 Omega EFTEM (Zeiss Microscopy GmbH, Jena, Germany) with a cryotransfer holder (CT3500, Gatan, Munich, Germany). Samples were frozen with the help of an automatic plunge freeze device Leica GP (Wetzlar, Germany). Examinations were carried out at temperatures around 90 K with an acceleration voltage of 200 kV. Zero-loss filtered images ( $\Delta E = 0$  eV) were taken under reduced dose conditions (100–1000 e/nm<sup>2</sup>).

### **Scanning Electron Microscope (SEM)<sup>260</sup>**

Standard SEM techniques apply a detection of secondary and backscattered electrons to visualize the sample surface. The electron beam is therefore scanning over the sample surface and suitable detectors detect and process the amount and energy of the corresponding electrons to afford an image of the specimen morphology. The detection of secondary and backscattered electrons gives insight into the specimen topology and structures due to their intrinsic properties. Secondary electrons are produced from the emission of valence electrons from the specimen atoms which interact with the electron beam. Due to the small energy of these electrons, they are quickly adsorbed and only secondary electrons generated in close proximity to the surface possess the ability to be emitted from the specimen. Therefore, the occurrence of secondary electrons is closely related to the surface morphology of the specimen, representing the topology of the sample. Backscattered electrons on the other hand represent those electrons that are scattered from the atoms and emitted out of the specimen. They possess a higher energy than secondary electrons and contain information from deeper regions of the specimen, respectively. The number of backscattered electrons correlates directly with the atomic number of the specimen atoms, resulting in a brighter appearance of areas with atoms of higher atom number.

In order to visualize structures which are sensitive to vacuum or only present in solution, a cryogenic process has to be applied in order to visualize those structures with SEM techniques. In a cryogenic SEM (cryo SEM) measurement, the sample is frozen in liquid nitrogen and placed into a special cryo-preparation chamber. Inside the chamber, the sample gets fractured in order to expose its interior structure. Sputtering with gold preserves the structure from vaporization through the electron beam. The examination of the structure can be carried out similar to standard SEM measurements.

Cryogenic scanning electron microscopy (cryo SEM) was performed with a Jeol JSM 7500 F and the cryo-chamber from Gatan (Alto 2500).

#### **VII.2.7. FT-IR spectrometry**

All FT-IR spectra were recorded with a Varian 600 FTIR spectrometer from Agilent Technologies.

#### **VII.2.8. UV-Vis Measurements**

UV-Vis measurements were conducted with a T70+ UV/Vis Spectrometer (PG Instruments Ltd).

#### **VII.2.9. Turbidimetry measurements (LCST)**

Turbidimetry measurements to obtain the lower critical solution temperature (LCST) were conducted with a T70+ UV/Vis Spectrometer (PG Instruments Ltd) at a wavelength of 660 nm and a temperature control system consisting of a Peltier Temperature Controller PTC-2 and a Manson Switching Mode Power Supply 1-36VDC-10A. Typically, 0.5 wt.% solutions were investigated with a heating rate of 1 K min<sup>-1</sup> and the transmission values were detected within a 5 second interval.

## VII.3. Chemicals

Chemical Name	Abbreviation	Purity	Vendor
2-bromo-2-methylpropanoic acid		98%	Sigma Aldrich
2-bromopropionyl bromide		97%	Sigma Aldrich
3-bromo-1-propanol		97%	Sigma Aldrich
acetone		99%	J.T. Baker
aluminium oxide		neutral	Sigma Aldrich
aluminium oxide		basic Brockman I	Sigma Aldrich
ammonium chloride	NH <sub>4</sub> Cl	99%	Roth KG
ascorbic acid	Asc Ac	98%	Alfa Aesar
Azobis(isobutyronitrile)	AIBN	99%	Sigma Aldrich
carbon disulfide	CS <sub>2</sub>	anhydrous 99%	Sigma Aldrich
chloromethyl polystyrene resin		2.4 mmol g <sup>-1</sup>	TCI
copper sulfate	CuSO <sub>4</sub>	99%	Roth KG
cystamine dihydrochloride		96%	Sigma Aldrich
dichloromethane	DCM	99%	Acros Organics
diethylene glycol		99%	Fischer Chemical
diethylether	Et <sub>2</sub> O	analytical grade	Sigma Aldrich
dimethylsulfoxide	DMSO	analytical grade	VWR Chemicals
dodecanethiol		98%	Alfa Aesar
ethyl acetate	EAtOAc	analytical grade	Chem Solute
hexamethylene diamine		96%	Sigma Aldrich
hexane		analytical grade	Fluka
hexylamine		>99%	Fluka
hydrochloric acid	HCl	fuming	Roth KG
magnesium sulfate	MgSO <sub>4</sub>	dried	Fischer Scientific
methanol	MeOH	analytical grade	Fischer Scientific
<i>N,N,N',N'',N'''</i> -pentamethyldiethylenetriamine	PMDETA	98%	Sigma Aldrich
<i>N,N'</i> -dicyclohexylcarbodiimide	DCC	99%	Sigma Aldrich
<i>N,N</i> -Dimethylacrylamide	DMA	99%	TCI
<i>N,N</i> -dimethylaminopyridine	DMAP	99%	Sigma Aldrich
<i>N,N</i> -dimethylformamide	DMF	analytical grade	Sigma Aldrich
<i>N</i> -Ethylacrylamide	EA	99%	TCI
<i>N</i> -hydroxy succinimide	NHS	98%	Sigma Aldrich
<i>N</i> -methylpyrrolidone	NMP	GC grade	Fluka

<b><i>N</i>-Vinylimidazole</b>	VIm	99%	Alfa Aesar
<b><i>N</i>-Vinylpyrrolidone</b>	VP	99%	Sigma Aldrich
<b>poly(ethylene oxide)-monomethyl-ether</b>	PEO 20000 g mol <sup>-1</sup>		Sigma Aldrich
<b>potassium phosphate</b>	K <sub>3</sub> PO <sub>4</sub>		Sigma Aldrich
<b>potassium-<i>O</i>-ethyl xanthate</b>		98%	Alfa Aesar
<b>propargylamine</b>		98%	Sigma Aldrich
<b><i>p</i>-toluenesulfonyl chloride</b>		99%	Fluka
<b>pullulan</b>	Pull	pure	TCI
<b>pyridine</b>		99% extra dry	Acros Organics
<b>Rhodamine B</b>	RhB	99%	Sigma Aldrich
<b>Rhodamine B isothiocyanate</b>	RhB ITC	99%	Sigma Aldrich
<b>sodium (meta) periodate</b>	NaIO <sub>4</sub>	pure	VWR Chemicals
<b>sodium azide</b>		>99.5%	Fluka
<b>sodium bicarbonate</b>	NaHCO <sub>3</sub>	>99%	Fluka
<b>sodium cyanoborohydride</b>	NaCNBH <sub>3</sub>	95%	Sigma Aldrich
<b>sodium iodide</b>		anhydrous	Acros Organics
<b>sodium sulfite</b>	Na <sub>2</sub> SO <sub>3</sub>	97%	Acros Organics
<b><i>t</i>-butyl peroxide</b>	<i>t</i> -BuOOH	70% solution in water	Acros Organics
<b>tetraethylene glycol</b>		99.5%	Acros Organics
<b>tetrahydrofuran</b>	THF	extra dry	Acros Organics
<b>triethylamine</b>	Et <sub>3</sub> N	99.5%	Sigma Aldrich
<b>tris(2-carboxyethyl)-phosphinohydrochloride</b>	TCEP	>98%	Roth KG

All chemicals were used as received except following:

*N*-Vinylpyrrolidone was dried over anhydrous magnesium sulfate and purified by distillation under reduced pressure. *N*-Vinylimidazole was passed over a basic aluminum oxide column prior to use. Acetone and dichloromethane were stored over molecular sieves (3 Å) prior to use. Azobis(isobutyronitrile) was recrystallized twice from methanol. *N,N*-Dimethylacrylamide was passed over neutral aluminum oxide prior to use. *N*-Ethylacrylamide was distilled under vacuum prior to use. Millipore water was obtained from an Integra UV plus pure water system by SG Water (Germany).

## VII.4. Experimental Part

### VII.4.1. General procedure for the preparation of solutions for DLS investigation

The preparation of the aqueous block copolymer solutions with different concentrations are listed in Table VII.1. The according masses were weighed precisely into vials and filtered with 0.45  $\mu\text{m}$  CA syringe filters into DLS vials unless not otherwise stated.

**Table VII.1** Preparation assessment for block copolymer solutions according to the attempted weight percentage.

Entry	Weight percentage	m (block copolymer) [g]	m (Millipore water) [g]
1	0.1	0.002	1.998
2	0.5	0.01	1.990
3	1.0	0.02	1.980
4	2.5	0.05	1.950
5	5.0	0.1	1.900
6	7.5	0.15	1.850

### VII.4.2. Organized polymeric submicron particles via self-assembly and crosslinking of double hydrophilic poly(ethylene oxide)-*b*-poly(*N*-vinylpyrrolidone) in aqueous solution

**Synthesis of PEO<sub>500</sub>-Macro CTA: 2-((Ethoxycarbonothioyl)thio)propionic acid [poly(ethylene oxide)methyl ether] ester**

The PEO macro chain transfer agent was synthesized according to a procedure reported in literature.<sup>99</sup>

*2-Bromopropionic acid [poly(ethylene oxide)-methyl-ether]-ester (PEO-Br):* Poly(ethylene oxide)monomethyl-ether (PEO-OH, 10.0 g, 0.5 mmol, 1.0 eq.) was placed in a dry, argon purged 100 mL two neck round bottom flask and dissolved in dry DCM (40.0 mL). Dry pyridine (0.11 mL, 1.35 mmol, 2.7 eq.) was added under stirring and the mixture was cooled with an ice water bath to 0 °C. 2-Bromopropionyl bromide (0.13 mL, 1.17 mmol, 2.33 eq.) was slowly

added to the cooled reaction mixture. The reaction mixture was allowed to warm to ambient temperature and stirred overnight. A white precipitate was filtered off and the reaction mixture was diluted with DCM (200 mL). The solution was washed with aqueous saturated ammonium chloride solution (4 x 40 mL), aqueous saturated sodium hydrogen carbonate solution (4 x 40 mL), deionized water (2 x 40 mL) and dried over anhydrous magnesium sulfate. The solution was filtered and the solvent was evaporated. The residue was re dissolved in a small amount DCM. The product was obtained by precipitation into ice cold diethyl ether, filtered and dried under reduced pressure. 2-Bromopropionic acid [poly(ethylene oxide)methyl ether] ester (PEO-Br) was obtained as a white solid (12.3 g, 0.62 mmol, 83% recovery).  $^1\text{H}$  NMR (400 MHz,  $\text{CDCl}_3$   $\delta$ ): 4.38 (q,  $^3J = 6.9$  Hz, 1H, CH), 4.30 (t, 2H,  $\text{CH}_2\text{OC}(\text{O})$ ), 3.62 (s), 3.85-3.4 (m,  $\text{CH}_2\text{CH}_2\text{O}$  PEO-backbone), 3.36 (s, 3H  $\text{CH}_3$ ), 1.81 (d,  $^3J = 6.9$  Hz, 3H,  $\text{CH}_3$ ).  $M_{n,\text{SEC}} = 26\,000\text{ g}\cdot\text{mol}^{-1}$  (PEO equivalents in NMP),  $\mathcal{D} = 1.1$ .

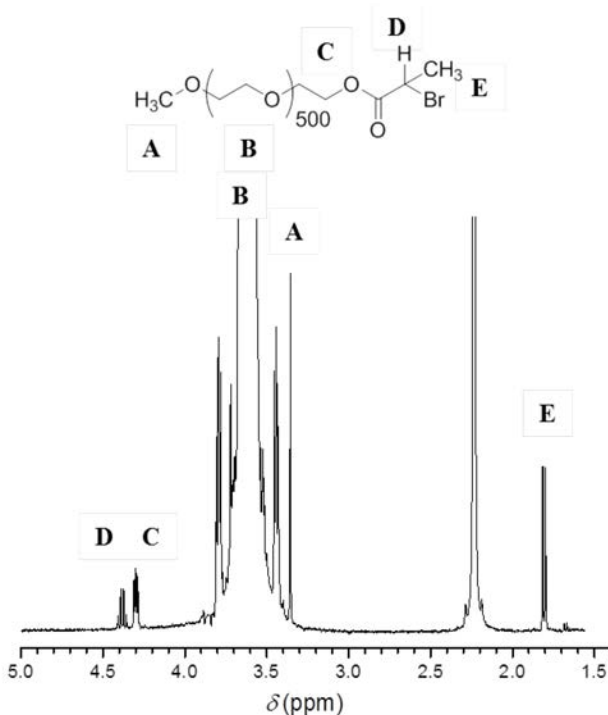


**Figure VII.1**  $^1\text{H}$ -NMR of PEO-Br recorded in  $\text{CDCl}_3$  at 400 MHz at 25  $^\circ\text{C}$ .

*2-((Ethoxycarbonothioyl)thio)propionic acid [poly(ethylene oxide)methyl ether] ester (PEO-X):* 2-Bromopropionic acid [poly(ethylene oxide)methyl ether] ester (PEO-Br, 8.0 g, 0.4 mmol, 1.0 eq.) was dissolved in dry DCM (45 mL) in a dry, argon purged 100 mL two neck round bottom flask. Dry pyridine (1.88 mL, 21.2 mmol, 53 eq.) was added and the reaction mixture was

cooled to 0 °C. Potassium *O*-ethyl xanthate (1.96 g, 12.0 mmol, 30 eq.) was added slowly in portions. The reaction mixture was allowed to warm to ambient temperature and stirred for 16 hours. A white precipitate was filtered off and DCM (150 mL) was added. The solution was washed with aqueous saturated ammonium chloride solution (5 x 75 mL), aqueous saturated sodium hydrogen carbonate solution (5 x 75 mL), deionized water (1 x 75 mL) and dried over anhydrous magnesium sulfate. The solution was filtered and the solvent was evaporated under reduced pressure. The residue was purified by Soxhlet extraction with diethyl ether overnight. 2-((Ethoxycarbonothioyl)thio)propionic acid [poly(ethylene oxide)methyl ether] ester (PEO-X) was obtained (7.5 g, 0.4 mmol, 93 % recovery).  $^1\text{H NMR}$  (400 MHz,  $\text{CDCl}_3$   $\delta$ ): 4.61 (q,  $^3J = 7.1$  Hz, 2H  $\text{OCH}_2\text{CH}_3$ ), 4.39 (q,  $^3J = 7.4$  Hz, 1H, CH), 4.28 (t, 2H,  $\text{CH}_2\text{OC}(\text{O})$ ), 3.62 (s), 3.85-3.4 (m,  $\text{CH}_2\text{CH}_2\text{O}$  PEO-backbone), 3.36 (s, 3H  $\text{CH}_3$ ), 1.56 (d,  $^3J = 7.4$  Hz, 3H,  $\text{CH}_3$ ), 1.39 (t,  $^3J = 7.1$  Hz, 3H,  $\text{OCH}_2\text{CH}_3$ ).  $M_{n,\text{SEC}} = 20\,000\text{ g}\cdot\text{mol}^{-1}$  (PEO equivalents in NMP),  $\mathcal{D} = 1.1$ .

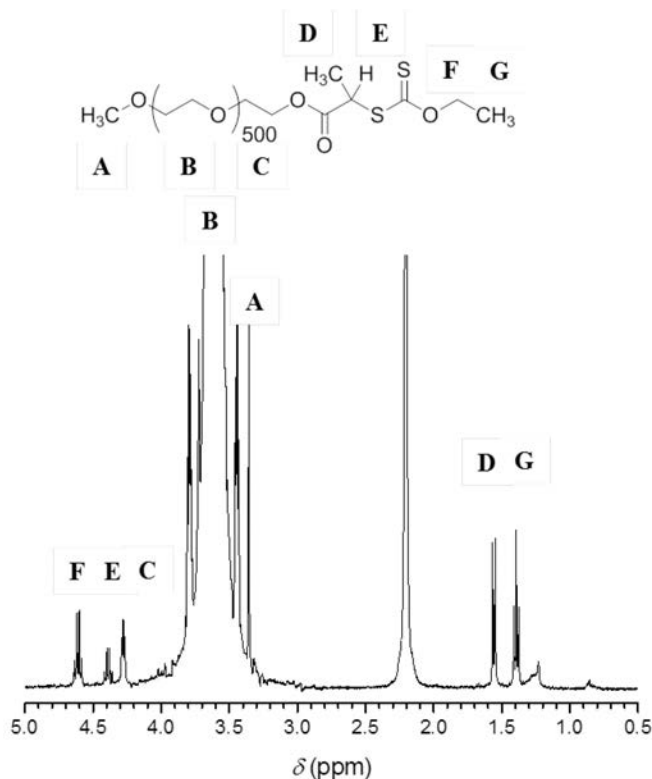


Figure VII.2  $^1\text{H-NMR}$  of PEO-X recorded in  $\text{CDCl}_3$  at 400 MHz at 25 °C.

### Synthesis of the crosslinker diethylene glycol bis(2-iodoethyl) ether

Diethylene glycol bis(2-iodoethyl) ether was synthesized according to the literature.<sup>261</sup>



*Diethylene glycol bis(2-tosylethyl) ether*: In a dry argon purged 250 ml round bottom Schlenk flask, tetraethylene glycol (5.0 g, 25.7 mmol, 1.0 eq.) was dissolved in dry triethyl-amine (200 ml). 4-toluenesulfonyl chloride (11.0 g, 57.9 mmol, 2.25 eq.) was added to the solution. The reaction mixture was stirred overnight at ambient temperature. Triethyl-amine was removed under reduced pressure. The resulting residue was extracted with ethyl acetate (4 x 30 ml) and a white salt was filtered off. The organic phase was washed with saturated brine solution (1 x 80 ml), dried over anhydrous magnesium sulfate and the solvent was removed under reduced pressure. The crude product was purified by column chromatography (EtOAc/ Hexane = 1:1,  $R_f$  = 0.28) to afford diethylene glycol bis(2-tosylethyl) ether as a white solid (9.0 g, 70%, 17.92 mmol).  $^1\text{H NMR}$  (400 MHz,  $\text{CDCl}_3$   $\delta$ ): 7.79 (d,  $^3J = 8.3$  Hz, 4H), 7.31 (d,  $^3J = 8.0$  Hz, 4H), 4.15 (t,  $^3J = 4.8$  Hz, 4H,  $\text{CH}_2\text{-O-Tos}$ ), 3.67 (t,  $^3J = 4.9$  Hz, 4H,), 3.55 (m, 8H,  $\text{CH}_2\text{-CH}_2\text{-}$ ), 2.44 (s, 6H,  $\text{CH}_3$ ).

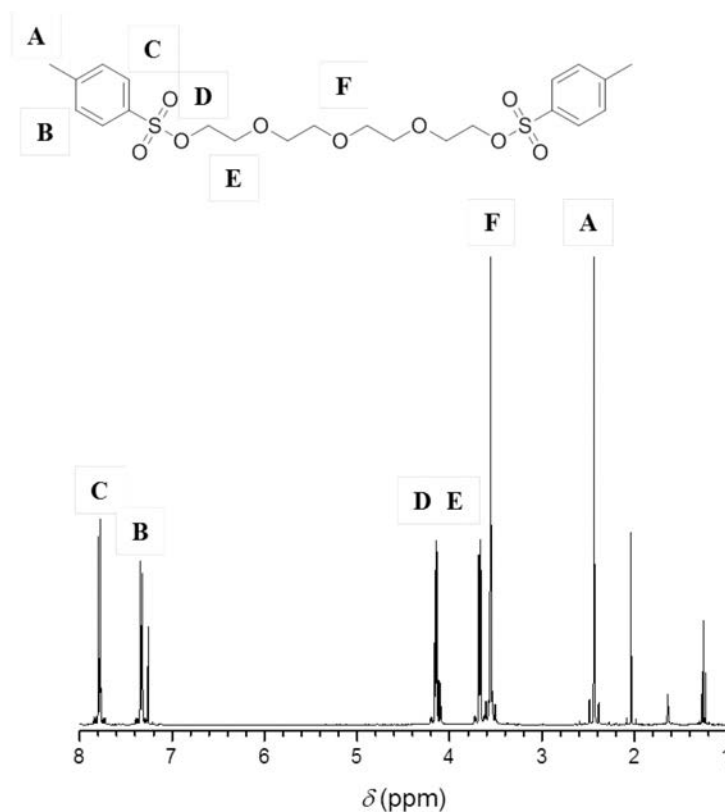


**Figure VII.3**  $^1\text{H-NMR}$  of diethylene glycol bis(2-tosylethyl) ether recorded in  $\text{CDCl}_3$  at 400 MHz at 25 °C.

*Diethylene glycol bis(2-iodoethyl) ether*: In a dry argon purged 250 ml round bottom flask, diethylene glycol bis(2-tosylethyl) ether (8.0 g, 15.9 mmol, 1.0 eq.) was dissolved in acetone (100 ml). Sodium iodide (9.55 g, 63.7 mmol, 4 eq.) was added and the mixture was refluxed for

8 hours. The solvent was removed under reduced pressure. The residue was dissolved in DCM (100 ml) and washed with saturated brine solution (100 ml). The organic phase was dried over anhydrous magnesium sulfate and the solvent was removed under reduced pressure to afford diethylene glycol bis(2-iodoethyl) ether as a yellow oil (5.95 g, 90%, 14.4 mmol).  $^1\text{H}$  NMR (400 MHz,  $\text{CDCl}_3$   $\delta$ :) 3.76 (t,  $^3J = 6.8$  Hz, 4H,  $\text{CH}_2\text{O}$ ), 3.67 (m, 8H), 3.26 (t,  $^3J = 7.1$  Hz, 4H,  $\text{CH}_2\text{I}$ ).  $^{13}\text{C}$ -NMR ( $\text{CDCl}_3$ , 100 MHz, 300 K,  $\delta$ :) 72 (I- $\text{CH}_2\text{CH}_2$ ), 71, 70, 3 ( $\text{CH}_2\text{I}$ ).

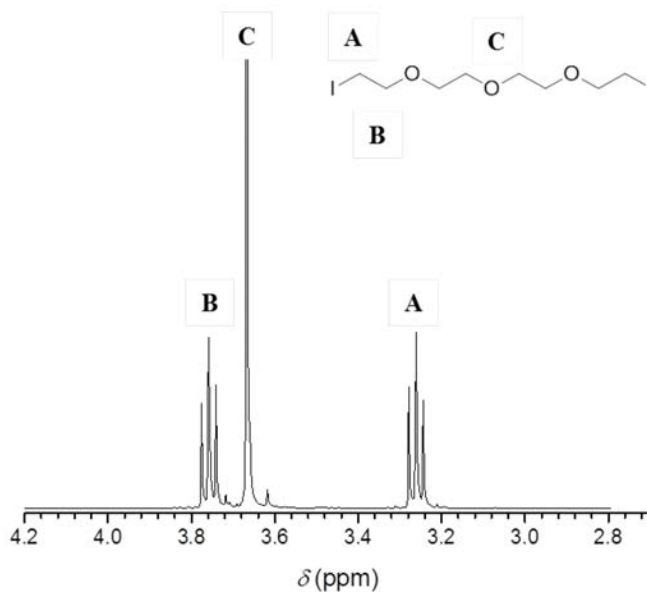


**Figure VII.4**  $^1\text{H}$ -NMR of diethylene glycol bis(2-iodoethyl) recorded in  $\text{CDCl}_3$  at 400 MHz at 25  $^\circ\text{C}$ .

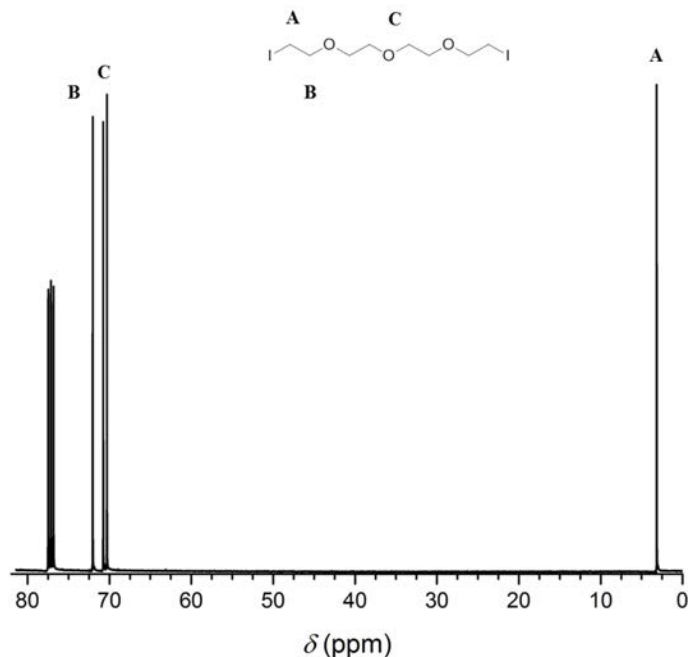


**Figure VII.5**  $^{13}\text{C}$ -NMR of diethylene glycol bis(2-iodoethyl) recorded in  $\text{CDCl}_3$  at 100 MHz at 25 °C.

### Polymerization procedures.

All polymerizations were carried out in dry, argon purged Schlenk tubes or Schlenk flasks heated in an oil bath. The polymerization mixture was degassed with at least three freeze-pump-thaw cycles, followed by purging with argon. A typical polymerization was conducted as follows.

*Polymerization of VP for PEO<sub>500</sub> block copolymer synthesis.* VP (1.16 mL, 10.87 mmol, 870 eq.), *t*-BuOOH solution (0.8 mg of 70 wt.% solution, 6.3  $\mu\text{mol}$ , 0.5 eq.) and PEO-X (0.25 g, 0.013 mmol, 1 eq.) were dissolved in deionized water (2.5 mL). The solution was frozen in liquid nitrogen and sodium sulfite (1.1 mg, 8.8  $\mu\text{mol}$ , 0.7 eq.) was added. The tube was sealed, allowed to thaw and been frozen again. The flask was degassed via three freeze-pump-thaw cycles and immersed in an oil bath at 30 °C. After 8 h, the polymerization was quenched with liquid  $\text{N}_2$  and exposed to air. The polymer solution was intensively dialyzed against deionized water (10 000 MWCO) and lyophilized to afford PEO-*b*-PVP (PEO<sub>500</sub>-*b*-PVP<sub>225</sub>) as a white powder. (Yield: 0.58 g, VP monomer incorporation ( $^1\text{H}$ -NMR) = 52 mol%,  $M_{n,\text{app,SEC}} = 42\,000\text{ g}\cdot\text{mol}^{-1}$  (PEO equivalents in NMP),  $D = 1.3$ ).

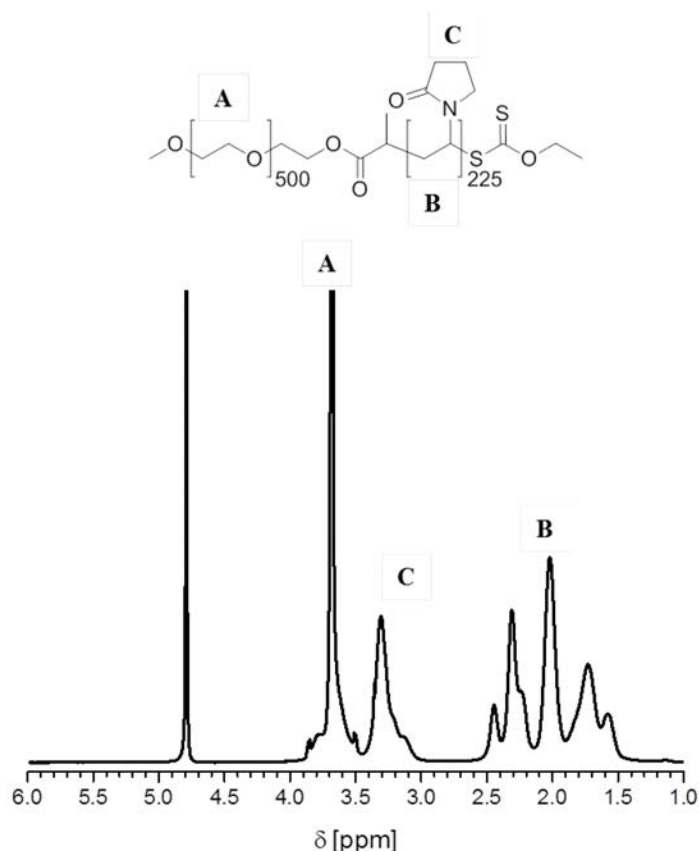


**Figure VII.6** <sup>1</sup>H-NMR of PEO<sub>500</sub>-b-PVP<sub>225</sub> recorded in CDCl<sub>3</sub> at 400 MHz at 25 °C.

*Copolymerization of VP and VIm for PEO<sub>500</sub> block copolymer synthesis.* VP (1.06 mL, 9.79 mmol, 783 eq.), VIm (0.1 mL, 1.09 mmol, 87 eq.), *t*-BuOOH solution (0.8 mg of 70 wt.% solution, 6.3 μmol, 0.5 eq.) and PEO-X (0.25 g, 0.013 mmol, 1 eq.) were dissolved in deionized water (2.5 mL). The solution was frozen in liquid nitrogen and sodium sulfite (1.1 mg, 8.8 μmol, 0.7 eq.) was added. The tube was sealed, allowed to thaw and frozen again. The flask was degassed by three freeze-pump-thaw cycles and immersed in an oil bath at 30 °C. After 9 h, the polymerization was quenched. The polymer solution was intensively dialyzed against deionized water (10,000 MWCO) and lyophilized to afford PEO-*b*-P(VP-*co*-VIm) (PEO<sub>500</sub>-*b*-P(VP<sub>335</sub>-*co*-VIm<sub>55</sub>)) as a white powder. (Yield: 0.85 g, VP/VIm monomer incorporation (<sup>1</sup>H-NMR) = 48 mol%,  $M_{n,app,SEC} = 35\,000\text{ g}\cdot\text{mol}^{-1}$  (PEO equivalents in NMP),  $D = 1.3$ ).

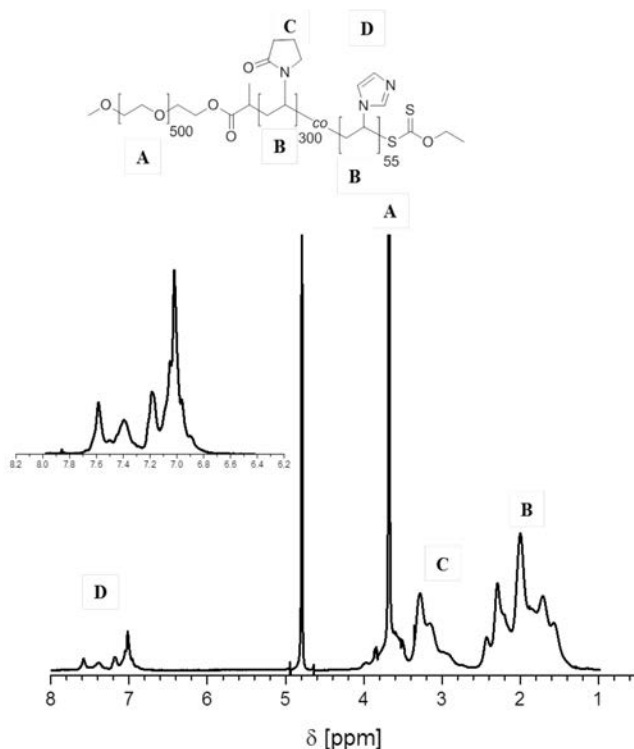


**Figure VII.7**  $^1\text{H-NMR}$  of  $\text{PEO}_{500}\text{-}b\text{-P}(\text{VP}_{335}\text{-}co\text{-VIm}_{55})$  recorded in  $\text{CDCl}_3$  at 400 MHz at 25 °C.

**Preparation of aqueous PEO-*b*-PVP and PEO-*b*-P(VP-*co*-VIm) block copolymer solutions.**

The diblock copolymer solutions of different weight percentages for DLS investigations were prepared as follows. The block copolymers were precisely weighed into vials according to the final weight percentage of the solution. Millipore water was added and the mixture was shaken until the block copolymers were completely dissolved (see Table S1). The solutions were filtered with hydrophilic 0.45  $\mu\text{m}$  syringe filters (Satorius CA filters) prior to DLS examination.

**Crosslinking of aqueous PEO-*b*-P(VP-*co*-VIm) block copolymer solutions.** The filtered aqueous solutions of PEO-*b*-P(VP-*co*-VIm) were treated with a solution of diethylene glycol bis(2-iodoethyl) ether (1.0% solution in MeOH) according to the relative amount of crosslinkable VIm units in the solution. The mixture was shaken for 2 hours and examined via DLS at 25 °C.

**Self-assembly and crosslinking of PEO-*b*-P(VP-*co*-VIm) block copolymer in DMF.** Block copolymer solutions of 0.1, 1.0 and 2.5 wt.% for DLS analysis were prepared as follows. According to the resulting weight percentage in 1.9 g DMF solution, 1.9 mg, 19.0 mg and

47.5 mg of PEO-*b*-P(VP-*co*-VIm) were dissolved in the corresponding amount of DMF. The solution was filtered with hydrophobic 0.45  $\mu\text{m}$  syringe filters and the samples were investigated with DLS at ambient temperature. A 1.0% diethylene glycol bis(2-iodoethyl) ether solution in DMF was prepared and 0.1  $\mu\text{L}$ , 1.0  $\mu\text{L}$  and 2.6  $\mu\text{L}$  were added to the corresponding solutions respectively. The samples were shaken for two hours and investigated again with DLS at 25  $^{\circ}\text{C}$ . In order to prepare crosslinked block copolymer samples for the transformation to aqueous systems, a 5 wt.% solutions of PEO-*b*-P(VP-*co*-VIm) (190 mg in 3.61 g DMF) were prepared. 40  $\mu\text{L}$  of a 5% solution of diethylene glycol bis(2-iodoethyl) ether were added under rapid stirring and the mixture was slightly stirred for 2 hours. The crosslinked solution was then added drop wise to 20 mL Millipore water in order to afford a 1.0 wt.% solution and transferred to a 1,000,000 MWCO dialysis tube and dialyzed against Millipore water for three days. The dialyzed submicron particle solution with an approximate concentration of 0.7 wt.% (assuming that all block copolymers formed particles and maintained in the solution) was then analyzed with DLS at 25  $^{\circ}\text{C}$  and cryo SEM.

**Preparation of dye labelled crosslinked submicron particles.** The Rhodamine B labelled submicron particles were prepared similar to the ones used for the transformation to aqueous systems. Instead of pure DMF, a 0.0026 wt.% solution of Rhodamine B in DMF was used. The incorporated solutions were transferred to Millipore water after crosslinking and dialyzed against Millipore water for 36 h. The dye labelled submicron particle solutions were then investigated with the LSCM/DIC microscope.

### **VII.4.3. Vesicles of double hydrophilic pullulan and poly(acrylamide) block copolymers: A combination of synthetic- and bio-derived blocks**

#### **Synthesis of alkyne terminated pullulan**

*Depolymerization of pullulan:* Pullulan was depolymerized according to a procedure reported in literature.<sup>242</sup> In a dry, argon purged 100 mL round bottom Schlenk flask commercially available pullulan (4.0 g) was dissolved in aqueous hydrochloric acid solution (80 mL, 0.025 mol·L<sup>-1</sup>). The flask was sealed and immersed in a pre-heated oil bath at 85  $^{\circ}\text{C}$ . The solution was stirred for 2.5 h and the depolymerization reaction was stopped by putting the flask into an ice bath. The

cooled reaction mixture was placed in a 10.000 MWCO dialysis tube and extensively dialyzed against deionized water for three days. The solution was lyophilized to afford depolymerized pullulan as colorless solid (3.0 g, 75% recovery,  $M_{n,app,SEC} = 14\ 000\ \text{g mol}^{-1}$ , pullulan standard in acetate with 20% MeOH,  $D = 1.8$ )

*Alkyne functionalization of pullulan:* Alkyne terminated pullulan was synthesized according to a derived procedure reported by Schatz et. al.<sup>153</sup> In a dry, argon purged 100 mL round bottom Schlenk flask pullulan (1.5 g, 0.144 mmol, 1.0 eq.) was dissolved in acetate buffer solution (50 mL, 50 mM). Propargyl amine (0.92 mL, 14.4 mmol, 100.0 eq.) was added and the flask was immersed into a pre-heated oil bath at 50 °C. Sodium cyanoborohydride (0.226 g, 3.6 mmol, 25.0 eq.) was added and the mixture was stirred for 96 hours with a repeated daily addition of sodium cyanoborohydride of 0.226 g (3.6 mmol, 25.0 eq.). The reaction mixture was intensively dialyzed against deionized water (SpectraPor 3.5 kD MWCO tube) for three days and lyophilized to afford alkyne terminated pullulan (1.25 g, 83% recovery,  $M_{n,app,SEC} = 16\ 000\ \text{g mol}^{-1}$ , pullulan standard in acetate with 20% MeOH,  $D = 1.8$ ). The full conversion was confirmed by the disappearance of the anomeric proton signals of the reducing group in the  $^1\text{H-NMR}$  spectrum (400 MHz, DMSO- $d_6$ , 6.67 ppm and 6.32 ppm).

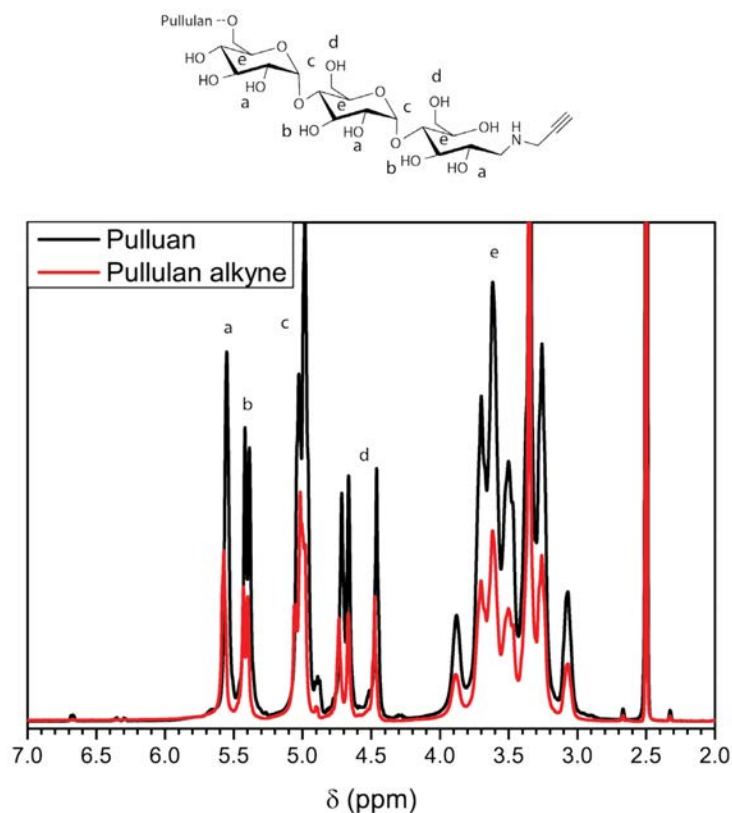


**Figure VII.8**  $^1\text{H}$ -NMR of pullulan before and after alkyne functionalization recorded at 400 MHz in  $\text{DMSO-d}_6$ .

### Synthesis of azide functionalized RAFT chain transfer agent 2 dodecylthiocarbonylthio-2-methylpropanoic acid 3'-azido propyl ester

*3-Azido-1-propanol*:<sup>105</sup> Sodium azide (2.3 g, 35.4 mmol 1.5 eq.) was placed in a 100 mL round bottom flask and dissolved in a mixture of acetone (36 mL) and deionized water (6.0 mL). 3-Bromo-1-propanol (1.96 mL, 22.4 mmol, 1.0 eq.) was added. The mixture was refluxed for 18 h. Acetone was removed under reduced pressure. Deionized water (30 mL) was added. The aqueous phase was extracted with diethyl ether (3 x 30 mL). The combined organic phases were dried over anhydrous magnesium sulfate. The solvent was evaporated under reduced pressure to give 3-azido-1-propanol as yellow oil (2.08 g, 20.6 mmol, 92% yield).  $^1\text{H}$  NMR (400 MHz,  $\text{CDCl}_3$   $\delta$ ): 3.75 (t,  $^3J = 6.0$  Hz, 2H,  $\text{CH}_2\text{OH}$ ), 3.44 (t,  $^3J = 6.6$  Hz, 2H,  $\text{N}_3\text{CH}_2$ ), 1.82 (p,  $^3J =$



6.3 Hz, 2H CH<sub>2</sub>), FT-IR  $\tilde{\nu}$  cm<sup>-1</sup>: 2950, 2875 (CH<sub>2</sub>), 2088 (N<sub>3</sub>), 1455 (CH<sub>2</sub>), 1292, 1259, 1045 (C-OH), 952, 900 (C-H).

*Dodecylthiocarbonylthio-2-methylpropanoic acid*:<sup>105</sup> In a 100 mL round bottom flask, dodecanethiol (5.0 mL, 21 mmol, 1.4 eq.) was dissolved in a suspension of K<sub>3</sub>PO<sub>4</sub> (3.5 g, 16.5 mmol, 1.1 eq.) in acetone (60 mL) at ambient temperature. After stirring for 20 minutes at ambient temperature carbon disulfide (2.72 mL, 45 mmol, 3.0 eq.) was added. The reaction mixture was stirred additional 20 minutes at ambient temperature. 2-Bromo-2-methylpropionic acid (2.505 g, 15 mmol, 1.0 eq.) was added and the reaction was stirred overnight at ambient temperature. 1M HCl (200 mL) was added and the mixture was extracted with DCM (2 x 150 mL). The combined organic phases were washed with deionized water (75 mL), saturated aqueous brine solution (75 mL) and dried over anhydrous magnesium sulfate. The solvent was evaporated under reduced pressure. The crude product was purified by recrystallization from hexane to afford dodecylthiocarbonylthio-2-methylpropanoic acid (5.2 g, 14.3 mmol, 95% recovery) as slightly yellow crystals. <sup>1</sup>H NMR (400 MHz, CDCl<sub>3</sub>,  $\delta$ ): 3.28 (t, <sup>3</sup>J = 7.6 Hz, 2H), 1.72 (s, 6H, CH<sub>3</sub>), 1.67 (t, <sup>3</sup>J = 7.1 Hz, 2H); 1.38 (m, 2H), 1.25 (s, 16H), 0.88 (t, <sup>3</sup>J = 6.7 Hz, 3H, CH<sub>3</sub>).

*Dodecylthiocarbonylthio-2-methylpropanoic acid 3'-azidopropylester*:<sup>105</sup> In a dry, argon purged 100 mL Schlenk flask dodecylthiocarbonylthio-2-methylpropanoic acid (2.5 g, 6.86 mmol, 1.0 eq.) was dissolved in dry DCM (40 mL). 3-Azidopropanol (1.73 g, 17.14 mmol, 2.5 eq.) and DMAP (0.34 g, 2.74 mmol, 0.4 eq.) was added and the stirred reaction mixture was cooled to 0 °C. A solution of DCC (2.82 g, 13.71 mmol, 2.0 eq.) in dry DCM (18 mL) was added drop wise to the cooled solution and stirred for an additional hour at 0 °C. The reaction mixture was allowed to warm to ambient temperature and stirred overnight. A precipitate was filtered off and the solvent was removed under reduced pressure. The crude product was purified by column chromatography on silica gel (EtOAc/ Hexane = 1:20, R<sub>f</sub> = 0.58) to afford dodecylthiocarbonylthio-2-methylpropanoic acid 3'-azido propyl ester (3.19 g, 70% yield, 7.13 mmol) as yellow oil. <sup>1</sup>H NMR (400 MHz, CDCl<sub>3</sub>,  $\delta$ ): 4.17 (t, <sup>3</sup>J = 6.0 Hz, 2H, OCH<sub>2</sub>), 3.35 (t, <sup>3</sup>J = 6.8 Hz, 2H), 3.27 (t, <sup>3</sup>J = 7.5 Hz, 2H), 1.89 (p, <sup>3</sup>J = 6.2 Hz, 2H), 1.69 (s, 6H, CH<sub>3</sub>), 1.65

(p,  $^3J = 7.4$  Hz, 2H,), 1.37 (m, 2H,), 1.25 (m, 16H,), 0.87 (t,  $^3J = 7.0$  Hz, 3H,  $CH_3$ ).  $^{13}C$ -NMR ( $CDCl_3$ , 100 MHz, 300 K,  $\delta$ ): 226 (13-C), 172.9 (17-C), 62.8 (18-C), 55.9 (14-C), 48.2 (20-C), 37.0 (12-C), 31.9 (3-C), 29.6 (5-C, 6-C, 7-C, 8-C), 29.5 (19-C), 29.4 (4-C), 29.1 (9-C), 28.9 (10-C), 28.0 (11-C), 25.4 (C-15, C-16), 22.7 (2-C), 14.1 (1-C). FT-IR ( $\tilde{\nu}$   $cm^{-1}$ ): 2920 ( $CH_2$ ), 2850 (S- $CH_2$ ), 2095 ( $N_3$ ), 1733 (C=O), 1454 (C-H), 1253 (S- $CH_2$ ), 1153 (C-C), 1125, 1063 (trithiocarbonate), 814 (C-C).

### Polymerization procedures

All polymerizations were performed in dry argon purged Schlenk tubes immersed in an oil bath. The polymerization mixture was degassed with at least three freeze-pump-thaw cycles, followed by purging with argon. A typical polymerization was conducted as follows.

*Synthesis of PDMA.*<sup>89</sup> In a dry argon purged 25 mL Schlenk tube, DMA (2.25 g, 22.7 mmol, 227.0 eq.) was dissolved in DMF (5.6 mL). Dodecylthiocarbonylthio-2-methylpropanoic acid 3'-azidopropylester (40.8 mg, 0.1 mmol, 1.0 eq.) and AIBN (3.0 mg, 0.018 mmol, 0.2 eq.) were added and the tube was sealed. The flask was degassed by four freeze-pump-thaw cycles and introduced into an oil bath at 60 °C. The reaction mixture was stirred for six hours. The polymerization was terminated by freezing the flask in liquid nitrogen and exposing the reaction mixture to air. PDMA (2.10 g, 0.125 mmol) was afforded as yellow solid after dialysis (MWCO 1000) against deionized water for 3 days and freeze drying.  $M_{n,app,SEC} = 16\ 800\ g\ mol^{-1}$  (PS equivalents in NMP),  $D = 1.26$ .

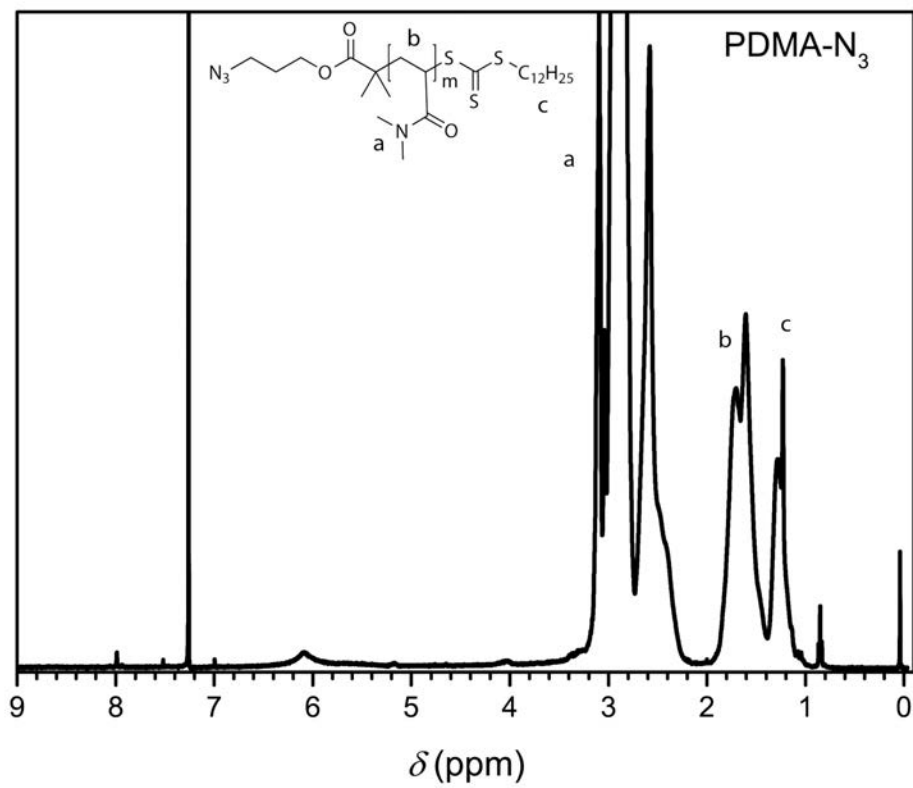


**Figure VII.9**  $^1\text{H}$  NMR of PDMA- $\text{N}_3$  recorded at 400 MHz in  $\text{CDCl}_3$ .

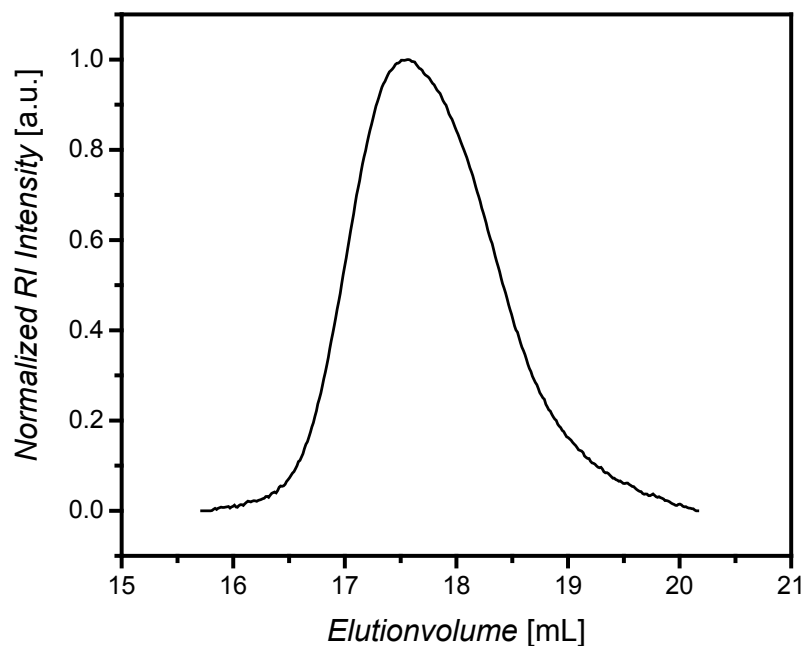


**Figure VII.10** SEC trace of PDMA-N<sub>3</sub> measured in NMP at 70 °C against PS calibration.

*Synthesis of PEA.*<sup>89</sup> In a dry argon purged 25 mL Schlenk tube, EA (1.0 g, 10.09 mmol, 174.0 eq.) was dissolved in DMF (3.2 mL). Dodecylthiocarbonylthio-2-methylpropanoic acid 3'-azidopropylester (23.6 mg, 0.058 mmol, 1.0 eq.) and AIBN (1.7 mg, 0.01 mmol, 0.17 eq.) were added and the tube was sealed. The flask was degassed by four freeze-pump-thaw cycles and immersed into an oil bath at 60 °C. The reaction mixture was stirred for six hours. The polymerization was terminated by freezing the flask in liquid nitrogen and exposing the reaction mixture to air. PEA (0.75 g 0.054 mmol) was afforded as yellow solid after dialysis (MWCO 1000) against deionized water for 3 days and freeze drying.  $M_{n,app,SEC} = 13\,900\text{ g mol}^{-1}$  (PS equivalents in NMP),  $D = 1.37$ .

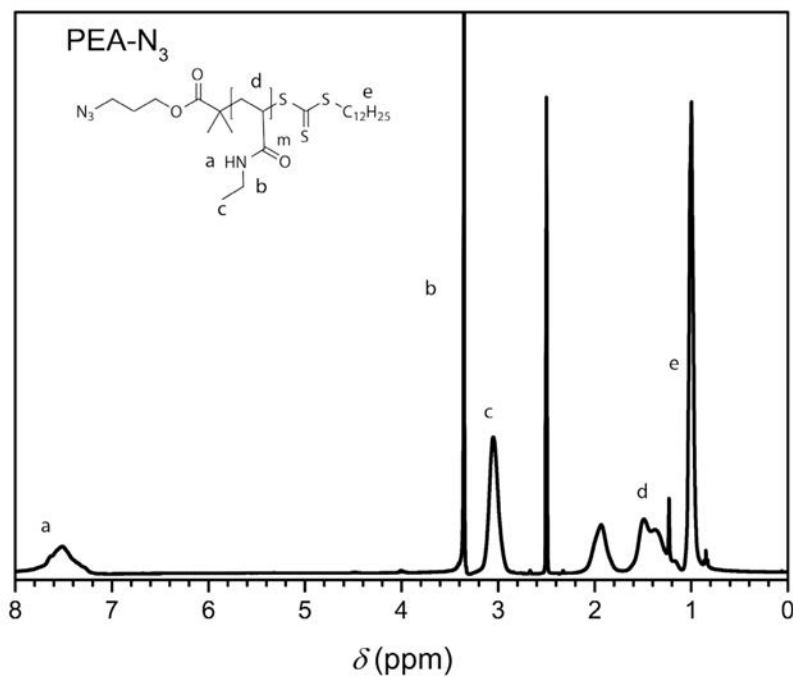


**Figure VII.11** <sup>1</sup>H NMR of PEA-N<sub>3</sub> recorded at 400 MHz in DMSO-d<sub>6</sub>.

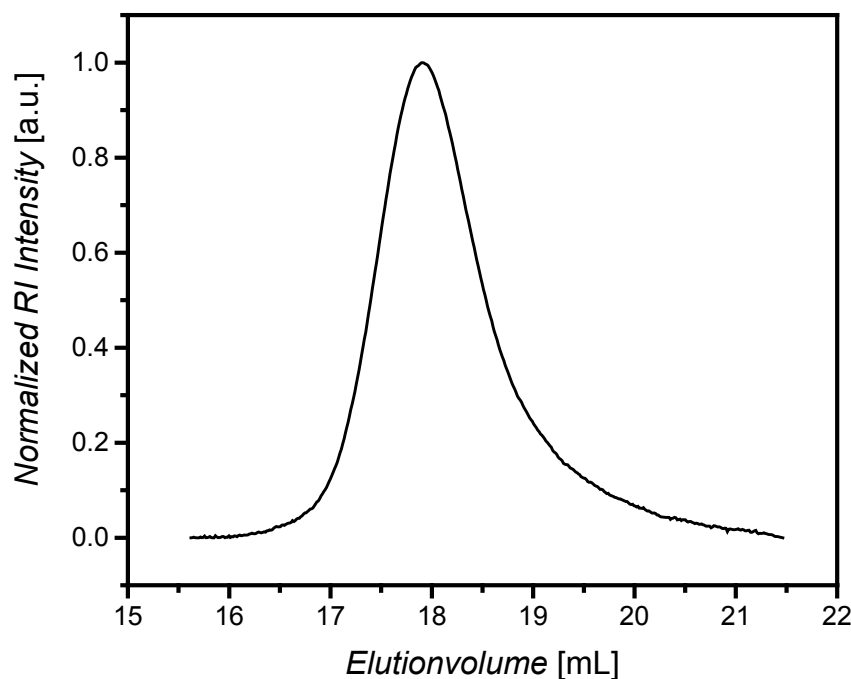


Figure VII.12 SEC trace of PEA- $N_3$  measured in NMP at 70 °C against PS calibration.

### Removal of PDMA- $N_3$ RAFT functionality<sup>262</sup>

AIBN (0.197 g, 1.167 mmol, 38.9 eq.) was dissolved in destabilized THF (60 mL) under vigorous stirring and heated to 60 °C. The mixture was stirred for 30 minutes at 60 °C and THF (3x10 mL) was subsequently added to compensate solvent evaporation. PDMA- $N_3$  (0.5 g, 0.03 mmol, 1.0 eq.) was added to the solution and the reaction mixture was stirred for 90 minutes. Ascorbic acid (0.051 g, 0.291 mmol, 9.7 eq.) was added and the mixture was stirred additional 30 minutes. The reaction mixture was cooled to room temperature and THF was allowed to evaporate overnight. The colorless residue was dissolved in deionized water and dialyzed against water for three days. Remaining AIBN was removed by filtration and the solution was lyophilized to afford hydroxyl terminated PDMA- $N_3$  (0.350 g, 0.021 mmol, 70% recovery) as white powder.

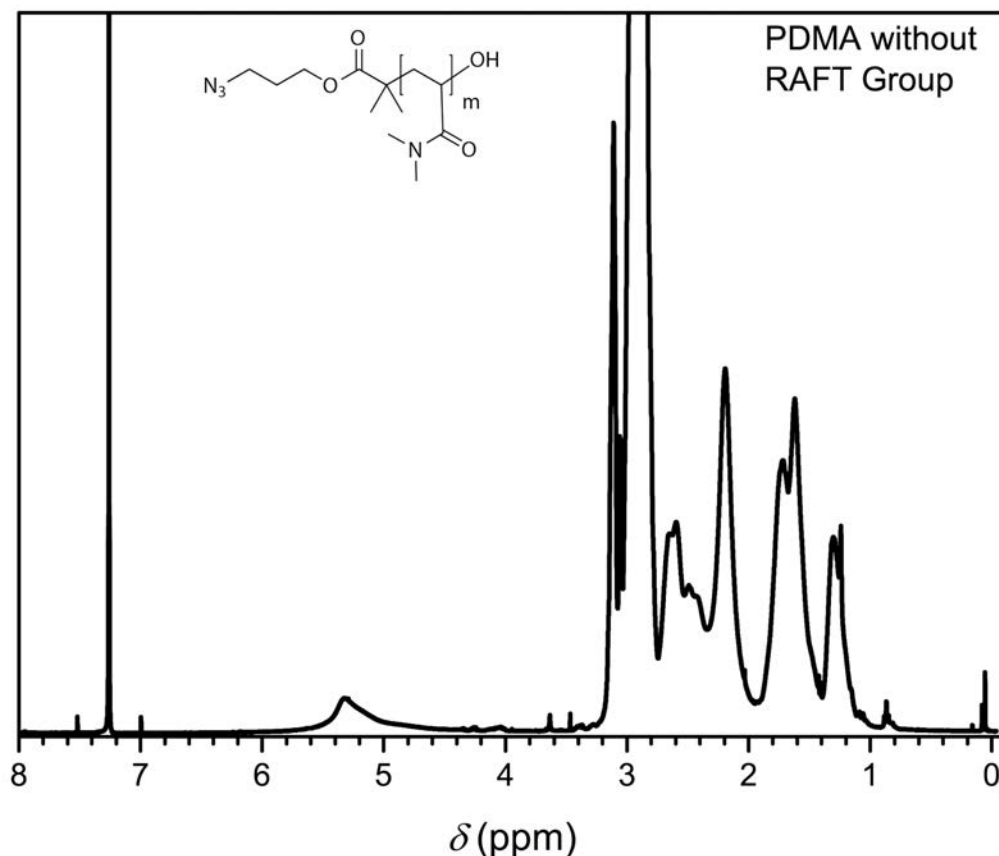
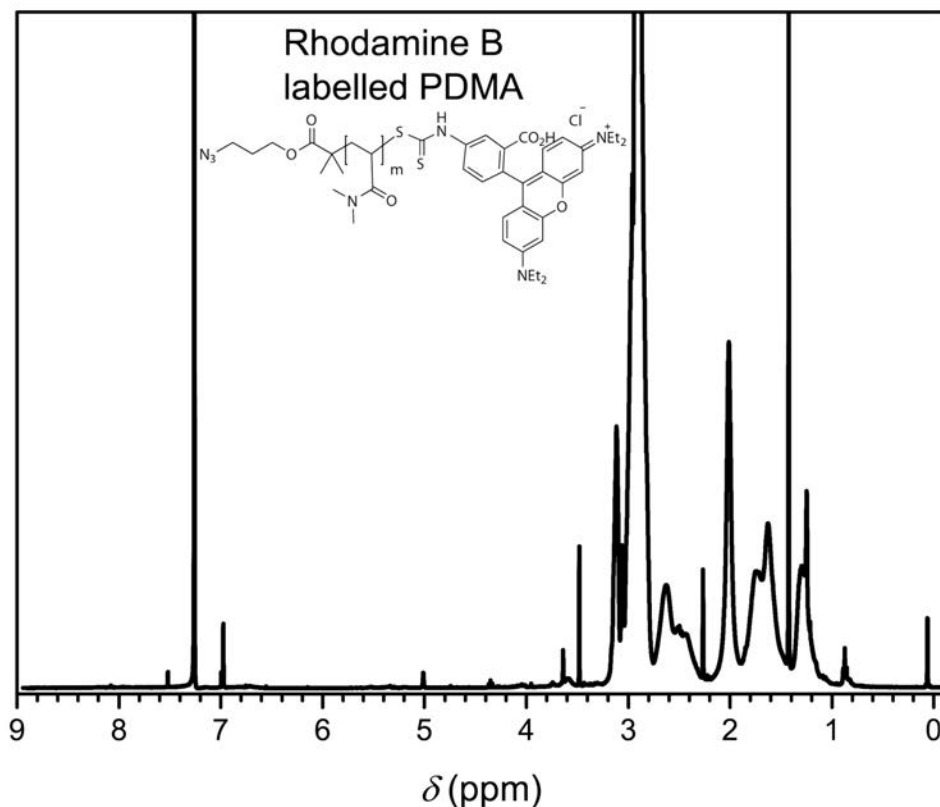


Figure VII.13  $^1\text{H}$  NMR of PDMA- $\text{N}_3$  without RAFT group recorded at 400 MHz in  $\text{CDCl}_3$ .

### Synthesis of Rhodamine B labelled PDMA- $\text{N}_3$

In a dry, argon purged 25 mL Schlenk flask PDMA- $\text{N}_3$  (0.1 mg, 0.006 mmol, 1 eq.) was dissolved in dry DMSO (7 mL). Hexylamine (0.002 mL, 0.015 mmol, 2.5 eq.) was added and the reaction mixture was stirred overnight at 50 °C. The mixture was cooled to room temperature and Rhodamine B ITC (0.013 g, 0.024 mmol, 4 eq.) was added. The reaction mixture was stirred overnight at 50 °C, cooled to room temperature, diluted with deionized water and dialyzed against deionized water for four days. The solution was lyophilized to afford Rhodamine B labelled PDMA- $\text{N}_3$  (63.0 mg, 63% recovery) as purple powder.



**Figure VII.14** <sup>1</sup>H NMR of Rhodamine B labelled PDMA-N<sub>3</sub> recorded at 400 MHz in CDCl<sub>3</sub>.

### Synthesis of azidomethyl polystyrene resin

In a dry, argon purged 100 mL round bottom Schlenk tube chloromethyl polystyrene resin (10.0 g, 24 mmol, 1.0 eq.) was dissolved in dry DMSO (50 mL). Sodium iodide (10.8 g, 72 mmol, 3.0 eq.) and sodium azide (15.6 g, 240 mmol, 10.0 eq.) were added and the reaction mixture was moderately stirred for 48 hours at 80 °C. The afforded resin was filtered over a glass frit (pore size 3) and alternately washed with DCM (6 x 30 mL) and MeOH (6 x 30 mL). The purified resin was finally washed with diethyl ether (30 mL) and dried under vacuum to afford azidomethyl polystyrene resin (9.25 g, 22.2 mmol, 93% recovery) as a white solid. FT-IR ( $\tilde{\nu}$  cm<sup>-1</sup>): 3120, 2855, 2089 (N<sub>3</sub>), 1509, 1450, 750, 697.



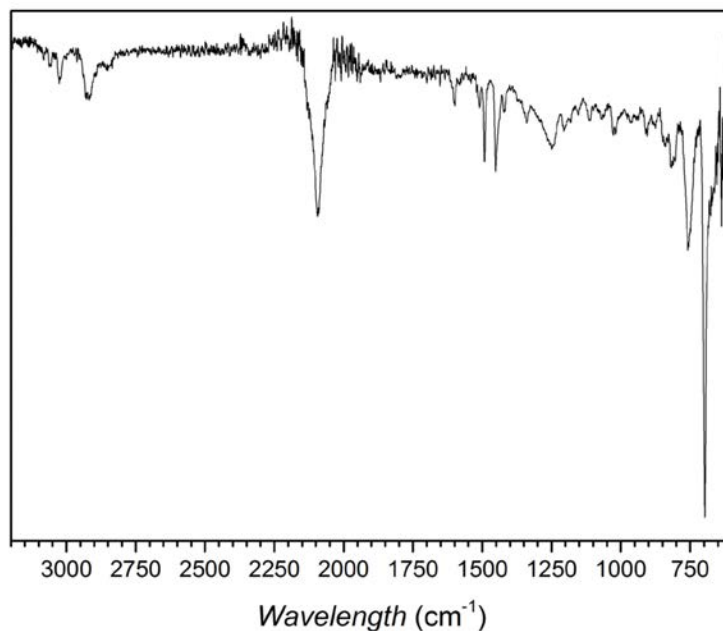


**Figure VII.15** IR spectrum of azidomethyl polystyrene resin recorded at 25 °C.

*CuAAC reactions:* CuAAC coupling reactions were processed by a derived procedure previously described by Bernard et al.<sup>118</sup>

*Pull-b-PDMA.* In a dry, argon purged 25 mL round bottom Schlenk flask, pullulan alkyne (0.28 g, 0.018 mmol, 1.2 eq.) was dissolved in deionized water (2.5 mL). CuSO<sub>4</sub> (1.6 mg, 9.8 μmol, 0.7 eq.) and DMSO (5.0 mL) were added to the solution. A solution of ascorbic acid (5.3 mg, 0.03 mmol, 2.0 eq.) in deionized water (2.5 mL) was added to the reaction mixture. PDMA-N<sub>3</sub> (0.25 g, 0.015 mmol, 1.0 eq.) and PMDETA (4.7 μL, 0.0225 mmol, 1.5 eq.) were dissolved in DMSO (3.0 mL) and added to the reaction mixture. The reaction mixture was stirred at ambient temperature for 48 hours. Azido functionalized PS-Resin (8.0 mg, 0.018 mmol) and ascorbic acid (5.3 mg, 0.03 mmol, 2.0 eq.) were added and the reaction mixture was stirred for additional 48 h. The resin was filtered off and the solution was dialyzed against deionized water for three days followed by lyophilization to afford Pull-b-PDMA (0.481 g, 0.022 mmol, 91% recovery  $M_n = 21\,500\text{ g}\cdot\text{mol}^{-1}$ , pullulan standard in acetate buffer with 20% MeOH,  $D = 1.9$ ) as a white powder.

*Pull-b-PEA.* In a dry, argon purged 25 mL round bottom Schlenk flask, pullulan alkyne (0.140 g, 0.0084 mmol, 1.2 eq.) was dissolved in deionized water (2.0 mL).  $\text{CuSO}_4$  (0.8 mg, 4.9  $\mu\text{mol}$ , 0.7 eq.) and DMSO (2.0 mL) were added to the solution. A solution of ascorbic acid (2.5 mg, 0.014 mmol, 2.0 eq.) in deionized water (1.0 mL) was added to the reaction mixture. PEA- $\text{N}_3$  (0.1 g, 0.007 mmol, 1.0 eq.) and PMDETA (2.2  $\mu\text{L}$ , 0.0105 mmol, 1.5 eq.) were dissolved in DMSO (2.8 mL) and added to the reaction mixture. The reaction mixture was stirred at ambient temperature for 48 hours. Azido functionalized PS-Resin (4.0 mg, 0.009 mmol) and ascorbic acid (2.5 mg, 0.014 mmol, 2.0 eq.) were added and the reaction mixture was stirred additional 48 h. The resin was filtered off and the solution was dialyzed against deionized water for three days followed by lyophilization to afford Pull-*b*-PEA (0.227 g, 8.6  $\mu\text{mol}$ , 95% recovery  $M_n = 26\,500\text{ g}\cdot\text{mol}^{-1}$ , pullulan standard in acetate buffer with 20% MeOH,  $D = 1.6$ ) as a white powder.

*Pull-b-PDMA-RhB.* In a dry, argon purged 10 mL Schlenk tube, pullulan alkyne (28.5 mg, 1.5  $\mu\text{mol}$ , 1.2 eq.) was dissolved in deionized water (1.0 mL).  $\text{CuSO}_4$  (0.1 mg, 0.8  $\mu\text{mol}$ , 0.7 eq.) and DMSO (1.5 mL) were added to the solution. A solution of ascorbic acid (0.5 mg, 0.8  $\mu\text{mol}$ , 2.0 eq.) in deionized water (1.0 mL) was added to the reaction mixture. PDMA- $\text{N}_3$ -RhB (25.0 mg, 1.25  $\mu\text{mol}$ , 1.0 eq.) and PMDETA (0.4  $\mu\text{L}$ , 1.88  $\mu\text{mol}$ , 1.5 eq.) were dissolved in DMSO (1.0 mL) and added to the reaction mixture. The reaction mixture was stirred at ambient temperature for 48 hours. Azido functionalized PS-Resin (1.0 mg, 0.002 mmol) and ascorbic acid (0.5 mg, 0.8  $\mu\text{mol}$ , 2.0 eq.) were added and the reaction mixture was stirred additional 48 h. The resin was filtered off and the solution was dialyzed against deionized water for three days followed by lyophilization to afford pull-*b*-PDMA-RhB (0.053 g, 2.3  $\mu\text{mol}$ , 99% recovery  $M_n = 22\,600\text{ g}\cdot\text{mol}^{-1}$ , pullulan standard in acetate buffer with 20% MeOH,  $D = 2.7$ ) as a purple powder.

*Preparation of aqueous Pull-b-PDMA and Pull-b-PEA block copolymer solutions.* The diblock copolymer solutions of different weight percentages for DLS investigations were prepared as follows. The block copolymers were precisely weighed into vials according to

the final weight percentage of the solution. Millipore water was added and the mixture was shaken until the block copolymers were completely dissolved (see Table S1). The solutions were filtered with hydrophilic 0.45  $\mu\text{m}$  syringe filters (Satorius CA filters) prior to DLS examination.

*Preparation of dye stained block copolymer solutions of Pull-*b*-PDMA and Pull-*b*-PEA.* In order to image the vesicular structures formed by the self-assembly of Pull-*b*-PDMA and Pull-*b*-PEA in water, 2.5 wt.% solutions of the corresponding block copolymers (0.025 g block copolymer in 0.975 g Millipore water) were stained with 10  $\mu\text{L}$  of an aqueous 0.08  $\text{mmol}\cdot\text{L}^{-1}$  Rhodamine B solution. The corresponding solutions were then filtered with hydrophilic 0.45  $\mu\text{m}$  syringe filters (Satorius CA filters) and examined via LSCM.

*Preparation of Pull-*b*-PDMA / Pull-*b*-PDMA-RhB solution.* 11.2 mg Pull-*b*-PDMA were dissolved in 0.4875 g Millipore water. The solution was filtered (0.45  $\mu\text{m}$  CA syringe filters by Satorius) and 10  $\mu\text{L}$  of a 0.04 wt.% solution of Pull-*b*-PDMA-RhB was added. The solution was examined via LSCM.

#### VII.4.4. pH and redox responsive vesicles from double hydrophilic pullulan-*b*-poly(*N*-vinylpyrrolidone) block copolymers

##### Synthesis of *N*-hydroxysuccinimide xanthate 2,5-dioxopyrrolidin-1-yl 2-((ethoxycarbonothioyl)thio)propanoate (NHS-xanthate)

*2,5-dioxopyrrolidin-1-yl 2-bromopropanoate:*<sup>263</sup> In a dry, argon purged 250 mL three neck round bottom flask with condenser and addition funnel *N*-hydroxysuccinimide (4.0 g, 34.75 mmol, 1.2 eq.) was dissolved in dry dichloromethane (70 mL). Dry pyridine (2.57 mL 31.85 mmol, 1.1 eq.) was added and the reaction mixture was cooled to 0 °C. The addition funnel was charged with a mixture of 2-bromopropionylbromide (3.10 mL, 29.58 mmol, 1.0 eq.) and dry DCM (35 mL) under argon flow. The mixture was added dropwise to the reaction within 30 minutes. The reaction was allowed to warm to ambient temperature and stirred for 18 hours. Afterwards, DCM (70 mL) was added. The organic phase was washed with 1M aqueous HCl solution (4 x

70 mL), deionized water (1 x 100 mL), saturated aqueous brine solution (1 x 100 mL) and dried over anhydrous magnesium sulfate. The solvent was removed in vacuum to afford 2,5-dioxopyrrolidin-1-yl 2-bromopropanoate (6.5 g, 29.41 mmol, 99% yield).  $^1\text{H}$  NMR (400 MHz,  $\text{CDCl}_3$ ,  $\delta$ :) 4.61 (q,  $^3J = 7.0$  Hz, 1H, CH), 2.85 (t,  $^3J = 19.2$  Hz, 4H,  $\text{CH}_2$ ), 1.95 (d,  $^3J = 7.0$  Hz, 3H,  $\text{CH}_3$ ).

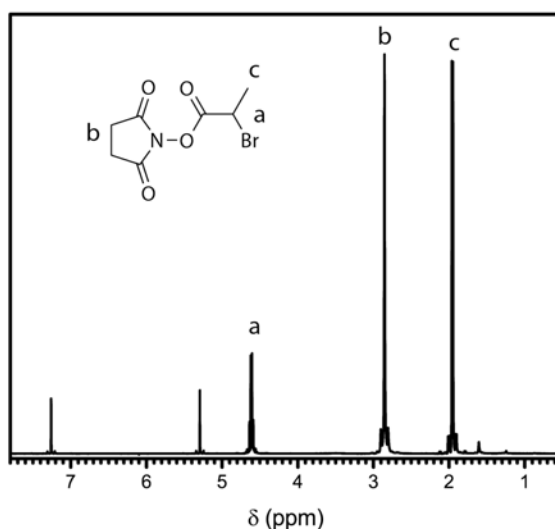


**Figure VII.16**  $^1\text{H}$  NMR of 2,5-dioxopyrrolidin-1-yl 2-bromopropanoate recorded at 400 MHz in  $\text{CDCl}_3$

*2,5-dioxopyrrolidin-1-yl 2-((ethoxycarbonothioyl)thio)propanoate (NHS-xanthate)*: In a dry, argon purged 250 mL round bottom flask 2, 5-dioxopyrrolidin-1-yl 2-bromopropanoate (2.0 g, 9.04 mmol, 1.0 eq.) was dissolved in DCM (100 mL). Dry pyridine (1.09 mL, 13.56 mmol, 1.5 eq.) was added and the reaction mixture was cooled to 0 °C. Potassium *O*-ethyl xanthate (2.21 g, 13.56 mmol, 1.5 eq.) was added portion wise. The reaction mixture was allowed to warm to ambient temperature and stirred overnight. A white salt was filtered off and DCM (200 mL) was added. The organic phase was washed with 1M aqueous HCl solution (4 x 50 mL), deionized water (4 x 75 mL), saturated aqueous brine solution (1 x 25 mL) and dried over anhydrous magnesium sulfate. The solvent was removed under reduced pressure. The crude product was purified by flash column chromatography (EtOAc/ hexane = 1:2,  $R_f = 0.27$ ) on silica gel to afford 2,5-dioxopyrrolidin-1-yl 2-((ethoxycarbonothioyl)thio)propanoate (NHS-xanthate) (1.1 g, 3.87 mmol, 42% yield).  $^1\text{H}$  NMR (400 MHz,  $\text{CDCl}_3$ ,  $\delta$ :) 4.67 (dq,  $^2J_{1,2} = 2.3$  Hz,  $^3J_{2,3} = 7.1$  Hz, 2H, 2-H), 4.61 (q,  $^3J = 7.4$  Hz, 1H, 4-H), 2.83 (s, 4H 8-H, 9-H), 1.70 (d,  $^3J = 7.4$  Hz, 3H,

5-H), 1.42 (t,  $^3J = 7.1$  Hz, 3H, 1-H).  $^{13}\text{C-NMR}$  (100 MHz, 300 K,  $\text{CDCl}_3$ ,  $\delta$ ): 13.5 (1-C), 16.5 (5-C), 25.6 (8-C, 9-C), 44.2 (4-C), 70.9 (2-C), 167.6 (7-C, 10-C), 168.7 (6-C), 209.9 (3-C).

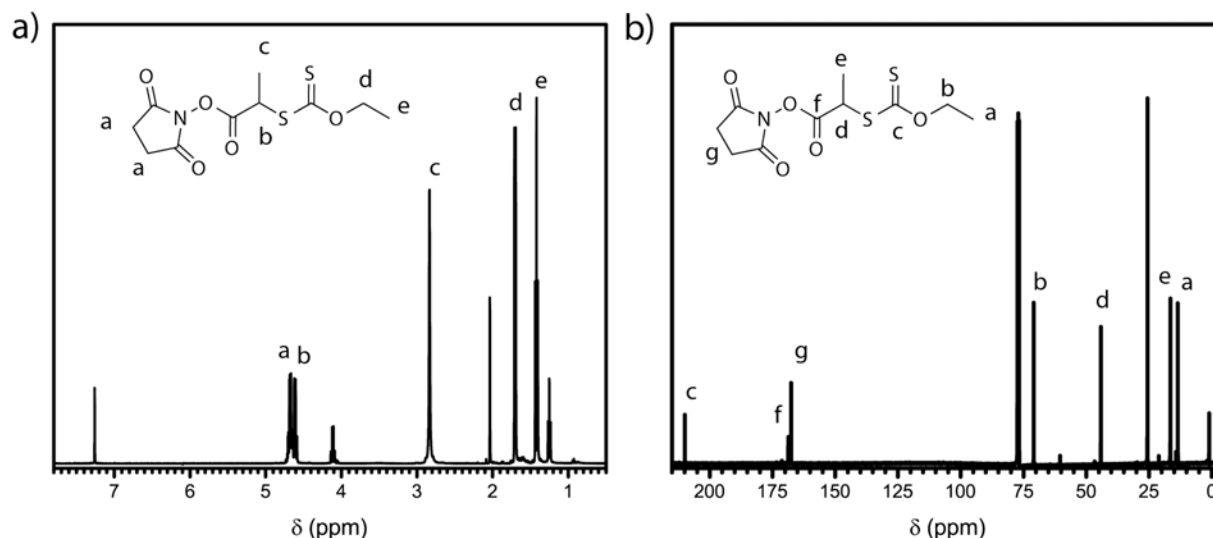


**Figure VII.17** a)  $^1\text{H-NMR}$  of 2,5-dioxopyrrolidin-1-yl 2-((ethoxycarbonothioyl)thio)propanoate in  $\text{CDCl}_3$  at 25 °C; b)  $^{13}\text{C-NMR}$  of 2,5-dioxopyrrolidin-1-yl 2-((ethoxycarbonothioyl)thio)propanoate in  $\text{CDCl}_3$  at 25 °C.

### Synthesis of xanthate terminated pullulan (Pull-X)

*Depolymerization of pullulan:* Pullulan was depolymerized according to a procedure reported in literature.<sup>242</sup> In a dry, argon purged 100 mL round bottom Schlenk flask commercially available pullulan (4.0 g) was dissolved in aqueous hydrochloric acid solution (80 mL,  $0.025 \text{ mol}\cdot\text{L}^{-1}$ ). The flask was sealed and immersed in a pre-heated oil bath at 85 °C. The solution was stirred for 2.5 h and the depolymerization reaction was stopped by putting the flask into an ice bath. The cooled reaction mixture was placed in a 10 000 MWCO dialysis tube and extensively dialyzed against deionized water for three days. The solution was lyophilized to afford depolymerized pullulan as colorless solid (3.0 g, 75% recovery,  $M_{n,\text{SEC}} = 22\,400 \text{ g}\cdot\text{mol}^{-1}$ , pullulan standard in acetate buffer with 20% MeOH,  $D = 1.8$ )

*Amino functionalization of pullulan (Pull-NH<sub>2</sub>):* Amino terminated pullulan was synthesized according to a derived procedure reported by Schatz et. al.<sup>153</sup> In a dry, argon purged 100 mL round bottom Schlenk flask pullulan (2.5 g, 0.112 mmol, 1 eq.) was dissolved in acetate buffer solution (75 mL, 50 mM). Hexamethylene diamine (1.297 g, 11.16 mmol, 100 eq.) was added and the flask was immersed into a pre-heated oil bath at 50 °C. Sodium cyanoborohydride

(0.175 g, 2.79 mmol, 25 eq.) was added and the mixture was stirred for 96 hours with a repeated daily addition of sodium cyanoborohydride. The reaction mixture was intensively dialyzed against deionized water (SpectraPor 3.5 kD MWCO tube) for three days and lyophilized to afford amino terminated pullulan (Pull-NH<sub>2</sub>) (2.45 g, 98% recovery,  $M_{n,SEC} = 16\ 100\ \text{g}\cdot\text{mol}^{-1}$ , pullulan standard in acetate buffer with 20% MeOH,  $D = 1.8$ ). The full conversion was confirmed by the disappearance of the anomeric proton signals of the reducing group in the <sup>1</sup>H-NMR spectrum (400 MHz, DMSO-d<sub>6</sub>, 6.67 ppm and 6.32 ppm).

*Xanthate functionalized pullulan (Pull-X):* In a dry argon purged 50 mL round bottom Schlenk flask Pullulan-NH<sub>2</sub> (2.4 g, 0.150 mmol, 1 eq.) was dissolved in dry DMSO (25 mL). A solution of NHS-xanthate (0.218 g, 0.75 mmol, 5 eq.) in dry DMSO (2.5 mL) was added drop wise to the reaction mixture. The reaction mixture was stirred for two days at ambient temperature. Deionized water (25 mL) was added slowly and the mixture was extensively dialyzed against deionized water (SpectraPor 3.5 kD MWCO tube) for four days. The dialyzed product was lyophilized to afford xanthate terminated Pullulan (Pull-X) (2.3 g, 0.14 mmol, 96% recovery) as a white solid.

### **Polymerization Procedures**

All polymerizations were carried out in dry, argon purged Schlenk flasks heated in an oil bath. The polymerization mixture was degassed with at least three freeze-pump-thaw cycles, followed by purging with argon. A typical polymerization procedure was conducted as follows.

*Polymerization of VP for pullulan block copolymer synthesis after previously reported procedure.*

In a dry argon purged 25 mL round bottom Schlenk flask pullulan xanthate (0.25 g, 0.016 mmol, 1.0 eq.) was dissolved in deionized water (3.2 mL). *N*-vinylpyrrolidone (1.44 mL, 13.52 mmol, 870 eq.) and *t*-BuOOH (0.7 mg, 8 μmol, 0.5 eq.) were added and the reaction mixture was frozen in liquid nitrogen. Na<sub>2</sub>SO<sub>3</sub> (15.0 mg, 12 μmol, 0.75 eq.) was added and the polymerization mixture was degassed by three freeze-pump-thaw cycles. The flask was purged with argon and immersed into an oil bath at 25 °C and stirred for 4 hours. The polymerization mixture was frozen in liquid nitrogen, exposed to air and allowed to thaw. The crude mixture was dialyzed against deionized water (10 000 MWCO Spectra Por) and lyophilized to afford Pull-*b*-PVP

(1.86 g, 0.05 mmol) as white powder.  $M_{n,app,SEC} = 73\,500 \text{ g mol}^{-1}$  (PEO equivalents in NMP),  $D = 2.75$ .

*Polymerization of VP for pullulan block copolymer synthesis with two fold dilution.*

In a dry argon purged 25 mL round bottom Schlenk flask pullulan xanthate (0.25 g, 0.016 mmol, 1.0 eq.) was dissolved in deionized water (5.5 mL). *N*-vinylpyrrolidone (1.44 mL, 13.52 mmol, 870 eq.) and *t*-BuOOH (0.7 mg, 8  $\mu\text{mol}$ , 0.5 eq.) were added and the reaction mixture was frozen in liquid nitrogen.  $\text{Na}_2\text{SO}_3$  (15.0 mg, 12  $\mu\text{mol}$ , 0.75 eq.) was added and the polymerization mixture was degassed by three freeze-pump-thaw cycles. The flask was purged with argon and immersed into an oil bath at 25 °C and stirred for 8 hours. The polymerization mixture was frozen in liquid nitrogen, exposed to air and allowed to thaw. The crude mixture was dialyzed against deionized water (10 000 MWCO Spectra Por) and lyophilized to afford Pull-*b*-PVP (1.69 g, 0.03 mmol) as white powder.  $M_{n,app,SEC} = 59\,700 \text{ g mol}^{-1}$  (PEO equivalents in NMP),  $D = 2.18$ .

*Polymerization of VP for pullulan block copolymer synthesis with co-solvent DMSO.*

In a dry argon purged 25 mL round bottom Schlenk flask pullulan xanthate (0.25 g, 0.016 mmol, 1.0 eq.) was dissolved in a mixture of deionized water (5.5 mL) and DMSO (2.5 mL). *N*-vinylpyrrolidone (1.44 mL, 13.52 mmol, 870 eq.) and *t*-BuOOH (0.7 mg, 8  $\mu\text{mol}$ , 0.5 eq.) were added and the reaction mixture was frozen in liquid nitrogen.  $\text{Na}_2\text{SO}_3$  (15.0 mg, 12  $\mu\text{mol}$ , 0.75 eq.) was added and the polymerization mixture was degassed by three freeze-pump-thaw cycles. The flask was purged with argon and immersed into an oil bath at 25 °C and stirred for 6 hours. The polymerization mixture was frozen in liquid nitrogen, exposed to air and allowed to thaw. The crude mixture was dialyzed against deionized water (10 000 MWCO Spectra Por) and lyophilized to afford Pull-*b*-PVP (1.47 g, 0.025 mmol) as white powder.  $M_{n,app,SEC} = 58\,800 \text{ g mol}^{-1}$  (PEO equivalents in NMP),  $D = 1.77$ .

### Selective oxidation of pullulan

The synthesis was performed according to a procedure reported by Maia et al.<sup>256</sup> The following procedure is exemplified for an oxidation of 5%. The corresponding data for higher oxidations can be obtained from Table VII.2.

In a 50 mL round bottom flask, pullulan (2.0 g, 0.14 mmol) was dissolved in deionized water (32 mL) to afford a 12.5 wt.% solution. The solution was separated into 6 parts containing 5 mL of the pullulan solution. Subsequently, an aqueous solution of NaIO<sub>4</sub> (0.032 g, 0.15 mmol in 1 mL deionized water) was added to the pullulan sample and the reaction mixture was stirred for 20 hours at room temperature. Diethylene glycol (14  $\mu$ L, 0.015 mmol) was added and the reaction mixture was stirred 1 hour, followed by dialysis and lyophilization to afford 5% oxidized pullulan (0.275 g, 0.017 mmol) as a white powder.  $M_{n,SEC} = 14\ 100\ \text{g}\cdot\text{mol}^{-1}$ , pullulan standard in acetate buffer with 20% MeOH,  $D = 2.1$ .

**Table VII.2** Assessment and SEC results of the pullulan oxidation with NaIO<sub>4</sub>.

Oxidation (%)	$m$ (NaIO <sub>4</sub> ) (g)	$V$ (DEG) ( $\mu$ L)	$m$ (Pull) (g)	$n$ (Pull) (mmol)	$M_{n,SEC}$ $\text{g}\cdot\text{mol}^{-1}$
5	0.032	14	0.275	0.017	16 100
10	0.064	28	0.284	0.02	14 400
15	0.128	56	0.289	0.017	16 600
25	0.160	70	0.275	0.021	13 200
35	0.224	98	0.239	0.016	14 800
50	0.320	140	0.252	0.026	9 600

### Selective oxidation of Pull<sub>124</sub>-*b*-PVP<sub>263</sub>

The synthesis was performed according to a procedure reported by Maia et al.<sup>256</sup>

In a 50 mL round bottom flask, Pull<sub>124</sub>-*b*-PVP<sub>263</sub> (1.0 g, 0.17 mmol) was dissolved in deionized water (15.7 mL) to afford a 12.5 wt.% solution. The solution was separated into 2 parts containing 7.7 mL of the Pull<sub>124</sub>-*b*-PVP<sub>263</sub> solution. Subsequently, an aqueous solution of NaIO<sub>4</sub> (0.011 g, 0.05 mmol in 1 mL deionized water for 5% oxidation and 0.021 g, 0.10 mmol in 1 mL deionized water for 10% oxidation) was added to the pullulan sample and the reaction mixture



was stirred for 20 hours at room temperature. Diethylene glycol (5  $\mu\text{L}$ , 0.005 mmol for 5% oxidation and 10  $\mu\text{L}$  for 10% oxidation, respectively) was added and the reaction mixture was stirred 1 hour, followed by dialysis and lyophilization to afford 5% and 10 % oxidized Pull<sub>124</sub>-*b*-PVP<sub>263</sub> (5% oxidation: 0.439 g, 0.017 mmol,  $M_{n,\text{app,SEC}} = 14\ 100\ \text{g}\cdot\text{mol}^{-1}$ , PEO equivalents in NMP,  $D = 2.1$ ; 10% oxidation: 0.433 g, 0.011 mmol,  $M_{n,\text{app,SEC}} = 39\ 200\ \text{g}\cdot\text{mol}^{-1}$ , PEO equivalents in NMP,  $D = 1.8$ ) as a white powder.

### **Crosslinking of oxidized Pull<sub>124</sub>-*b*-PVP<sub>263</sub> self-assemblies**

Oxidized Pull<sub>124</sub>-*b*-PVP<sub>263</sub> (0.050 g) with 5% and 10% oxidation degree was dissolved in Millipore water (0.95 mL) and filtered with a 0.45  $\mu\text{m}$  CA syringe filter. Addition of crosslinker, i.e. a cystamine dihydrochloride stock solution (0.01 g in 0.5 mL Millipore water), proceeded as follows:

1.9  $\mu\text{L}$  (3.8  $\mu\text{L}$  for the 10 % oxidized block copolymer, respectively) of the stock solution was added to the Pull<sub>124</sub>-*b*-PVP<sub>263</sub> solution and the reaction mixture was shaken for 2 days. The reaction mixture was diluted to 0.1 wt.% (100  $\mu\text{L}$  of crosslinked solution was added to 5 mL Millipore water) and dialyzed against Millipore water with a 1 000 000 MWCO dialysis tube for 3 days. The resulting solution was analyzed *via* DLS at 25 °C.

### **Acid induced disassembly of oxidized Pull<sub>124</sub>-*b*-PVP<sub>263</sub> self-assemblies**

Hydrochloric acid (150  $\mu\text{L}$ , 0.1 mol·L<sup>-1</sup>) was added to 2 mL of a 0.1 wt.% solution of crosslinked and dialyzed Pull<sub>124</sub>-*b*-PVP<sub>263</sub> oxidized to 5%. The vial was sealed and immersed in a water bath at 40 °C for 24 h. The pH induced disassembly was monitored *via* DLS at 25 °C.

### **Redox induced disassembly of oxidized Pull<sub>124</sub>-*b*-PVP<sub>263</sub> self-assemblies**

A 0.1 wt.% solution of crosslinked and dialyzed Pull<sub>124</sub>-*b*-PVP<sub>263</sub> oxidized to 5% was degassed with argon for 10 minutes. TCEP (20.0 mg, 0.08 mmol) was added and the sealed vial was immersed in a water bath at 40 °C for 24 h. The redox induced disassembly was monitored *via* DLS at 25 °C.

## VIII. References

1. A. L. Demain and S. Sanchez, *J. Antibiot.*, 2009, **62**, 5-16.
2. N. C. Lloyd, H. W. Morgan, B. K. Nicholson and R. S. Ronimus, *Angew. Chem., Int. Ed.*, 2005, **44**, 941-944.
3. P. Ehrlich and A. Bertheim, *Ber. Dtsch. Chem. Ges.*, 1912, **45**, 756-766.
4. H. Sakurai, Y. Yoshikawa and H. Yasui, *Chem. Soc. Rev.*, 2008, **37**, 2383-2392.
5. T. Owa and T. Nagasu, *Expert Opin. Ther. Pat.*, 2000, **10**, 1725-1740.
6. J. P. Paul and L. D. Heather, *Curr. Drug. Targets Infect. Disord.*, 2001, **1**, 241-247.
7. G. Ozcengiz and A. L. Demain, *Biotechnol. Adv.*, 2013, **31**, 287-311.
8. A. J. Huh and Y. J. Kwon, *J. Control. Release*, 2011, **156**, 128-145.
9. M. S. Butler, M. A. Blaskovich and M. A. Cooper, *J. Antibiot.*, 2017, **70**, 3-24.
10. D. M. Livermore, M. Blaser, O. Carrs, G. Cassell, N. Fishman, R. Guidos, S. Levy, J. Powers, R. Norrby, G. Tillotson, R. Davies, S. Projan, M. Dawson, D. Monnet, M. Keogh-Brown, K. Hand, S. Garner, D. Findlay, C. Morel, R. Wise, R. Bax, F. Burke, I. Chopra, L. Czaplewski, R. Finch, D. Livermore, L. J. V. Piddock and T. White, *J. Antimicrob. Chemother.*, 2011, **66**, 1941-1944.
11. S. Mitragotri, P. A. Burke and R. Langer, *Nat. Rev. Drug Discov.*, 2014, **13**, 655-672.
12. A. H. Delcour, *Biochim. Biophys. Acta*, 2009, **1794**, 808-816.
13. V. J. Stella, *J. Pharm. Sci.*, 2010, **99**, 4755-4765.
14. Y. N. Vaishnav and F. Wong-Staal, *Annu. Rev. Biochem.*, 1991, **60**, 577-630.
15. T. M. Allen and P. R. Cullis, *Science*, 2004, **303**, 1818-1822.
16. V. P. Torchilin, *J. Control. Release*, 2001, **73**, 137-172.
17. N. Chavain and C. Biot, *Curr. Med. Chem.*, 2010, **17**, 2729-2745.
18. R. Duncan and M. J. Vicent, *Adv. Drug Deliv. Rev.*, 2013, **65**, 60-70.
19. R. Haag and F. Kratz, *Angew. Chem., Int. Ed.*, 2006, **45**, 1198-1215.
20. G. Pasut and F. M. Veronese, *Adv. Drug Deliv. Rev.*, 2009, **61**, 1177-1188.
21. A. Abuchowski, J. R. McCoy, N. C. Palczuk, T. van Es and F. F. Davis, *J. Biol. Chem.*, 1977, **252**, 3582-3586.
22. A. Abuchowski, T. van Es, N. C. Palczuk and F. F. Davis, *J. Biol. Chem.*, 1977, **252**, 3578-3581.
23. R. P. Brinkhuis, F. P. J. T. Rutjes and J. C. M. van Hest, *Polym. Chem.*, 2011, **2**, 1449-1462.
24. D. E. Discher and A. Eisenberg, *Science*, 2002, **297**, 967-973.
25. J. C. M. Lee, H. Bermudez, B. M. Discher, M. A. Sheehan, Y.-Y. Won, F. S. Bates and D. E. Discher, *Biotechnol. Bioeng.*, 2001, **73**, 135-145.
26. B. Obermeier, F. Wurm, C. Mangold and H. Frey, *Angew. Chem., Int. Ed.*, 2011, **50**, 7988-7997.
27. F. K. Bedu-Addo, P. Tang, Y. Xu and L. Huang, *Pharm. Res.*, 1996, **13**, 710-717.
28. M. L. Graham, *Adv. Drug Deliv. Rev.*, 2003, **55**, 1293-1302.
29. A. L. Klibanov, K. Maruyama, V. P. Torchilin and L. Huang, *FEBS Lett.*, 1990, **268**, 235-237.
30. K. Knop, R. Hoogenboom, D. Fischer and U. S. Schubert, *Angew. Chem.*, 2010, **122**, 6430-6452.
31. C. E. Mora-Huertas, H. Fessi and A. Elaissari, *Int. J. Pharm.*, 2010, **385**, 113-142.
32. A. Sunder, M. Krämer, R. Hanselmann, R. Mülhaupt and H. Frey, *Angew. Chem., Int. Ed.*, 1999, **38**, 3552-3555.

33. Y. Liu, S. Ding, R. Dietrich, E. Märtlbauer and K. Zhu, *Angew. Chem., Int. Ed.*, 2017, **56**, 1486-1490.
34. D. J. Siegwart, J. K. Oh and K. Matyjaszewski, *Prog. Polym. Sci.*, 2012, **37**, 18-37.
35. H.-G. Elias, in *Makromoleküle*, WILEY-VCH Verlag GmbH & Co. KGaA, 2009, DOI: 10.1002/9783527626472.ch12, pp. 376-416.
36. K. Plochocka, *J. Macromol. Sci., Rev. Macromol. Chem. Phys.*, 1981, **C20**, 67-148.
37. S. M. Samoilov, *J. Macromol. Sci., Rev. Macromol. Chem. Phys.*, 1981, **C20**, 333-399.
38. R. Van Der Meer, H. N. Linssen and A. L. German, *J. Polym. Sci., A, Polym. Chem.*, 1978, **16**, 2915-2930.
39. P. Wittmer, *Macromol. Chem. Phys.*, 1979, **3**, 129-156.
40. H.-G. Elias, in *Makromoleküle*, WILEY-VCH Verlag GmbH & Co. KGaA, 2009, DOI: 10.1002/9783527626533.ch11, pp. 458-478.
41. H.-G. Elias, in *Makromoleküle*, WILEY-VCH Verlag GmbH & Co. KGaA, 2009, DOI: 10.1002/9783527626533.ch7, pp. 244-290.
42. H.-G. Elias, in *Makromoleküle*, WILEY-VCH Verlag GmbH & Co. KGaA, 2009, DOI: 10.1002/9783527626533.ch6, pp. 154-243.
43. C. Heuck, *J. Prakt. Chem. /Chem-Ztg*, 1970, **94**, 147-&.
44. H. H. Brintzinger, D. Fischer, R. Mülhaupt, B. Rieger and R. M. Waymouth, *Angew. Chem., Int. Ed.*, 1995, **34**, 1143-1170.
45. R. Godoy Lopez, F. D'Agosto and C. Boisson, *Prog. Polym. Sci.*, 2007, **32**, 419-454.
46. H. Jatzkewitz, *Biol. Chem.*, 1954, **297**, 149-156.
47. X. Liu, Y. Xu, Z. Wu and H. Chen, *Macromol. Biosci.*, 2013, **13**, 147-154.
48. K. Matyjaszewski, in *Advances in Controlled/Living Radical Polymerization*, American Chemical Society, 2003, vol. 854, ch. 1, pp. 2-9.
49. O. W. WEBSTER, *Science*, 1991, **251**, 887-893.
50. M. Szwarc, *Nature*, 1956, **178**, 1168-1169.
51. M. Szwarc, M. Levy and R. Milkovich, *J. Am. Chem. Soc.*, 1956, **78**, 2656-2657.
52. D. Baskaran, *Prog. Polym. Sci.*, 2003, **28**, 521-581.
53. V. H. Schreiber, *Macromol. Chem. Phys.*, 1960, **36**, 86-88.
54. M. Szwarc, in *Fortschritte Der Hochpolymeren-Forschung*, Springer Berlin Heidelberg, Berlin, Heidelberg, 1960, DOI: 10.1007/BFb0050501, pp. 275-306.
55. T. P. Davis, D. M. Haddleton and S. N. Richards, *J. Macromol. Sci. Polymer Rev.*, 1994, **34**, 243-324.
56. K. Hatada, T. Kitayama and K. Ute, *Prog. Polym. Sci.*, 1988, **13**, 189-276.
57. B. Obermeier, F. Wurm, C. Mangold and H. Frey, *Angew. Chem., Int. Ed.*, 2011, **50**, 7988-7997.
58. P. J. Flory, *J. Am. Chem. Soc.*, 1940, **62**, 1561-1565.
59. H. Staudinger and H. Lohmann, *Liebigs Ann.*, 1933, **505**, 41-51.
60. C. Mangold, F. Wurm and H. Frey, *Polym. Chem.*, 2012, **3**, 1714-1721.
61. M. C. Woodle, *Chem. Phys. Lipids*, 1993, **64**, 249-262.
62. P. J. Photos, L. Bacakova, B. Discher, F. S. Bates and D. E. Discher, *J. Control. Release*, 2003, **90**, 323-334.
63. I. Bjurhager, J. Ljungdahl, L. Wallstrom, E. K. Gamstedt and L. A. Berglund, *Holzforschung*, 2010, **64**, 243-250.
64. T. Aida, *Prog. Polym. Sci.*, 1994, **19**, 469-528.
65. J. E. Puskas and G. Kaszas, *Prog. Polym. Sci.*, 2000, **25**, 403-452.
66. J. P. Kennedy, *J. Polym. Sci., A, Polym. Chem.*, 1999, **37**, 2285-2293.
67. R. Faust, A. Fehervari and J. P. Kennedy, *J. Macromol. Sci., Pure Appl. Chem.*, 1983, **A18**, 1209-1228.
68. J. P. Kennedy, S. C. Feinberg and S. Y. Huang, *J. Polym. Sci. A Polym. Chem.*, 1978, **16**, 243-259.

69. J. P. Kennedy, S. Y. Huang and S. C. Feinberg, *J. Polym. Sci. A Polym. Chem.*, 1977, **15**, 2869-2892.
70. J. Puskas, G. Kaszas, J. P. Kennedy, T. Kelen and F. Tudos, *J. Macromol. Sci., Pure Appl. Chem.*, 1983, **A18**, 1229-1244.
71. N. Adams and U. S. Schubert, *Adv. Drug Deliv. Rev.*, 2007, **59**, 1504-1520.
72. R. Hoogenboom, *Angew. Chem., Int. Ed.*, 2009, **48**, 7978-7994.
73. R. Konradi, C. Acikgoz and M. Textor, *Macromol. Rapid Commun.*, 2012, **33**, 1663-1676.
74. H. Schlaad, C. Diehl, A. Gress, M. Meyer, A. L. Demirel, Y. Nur and A. Bertin, *Macromol. Rapid Commun.*, 2010, **31**, 511-525.
75. D. M. Haddleton, A. V. Muir and S. N. Richards, *Plast. Eng.*, 1997, **40**, 123-138.
76. H. Höcker, *Macromol. Symp.*, 1996, **101**, 1-9.
77. G. Moad, E. Rizzardo and D. H. Solomon, *Macromolecules*, 1982, **15**, 909-914.
78. C. J. Hawker, *Acc. Chem. Res.*, 1997, **30**, 373-382.
79. A. D. Jenkins, R. G. Jones and G. Moad, *Pure Appl. Chem.*, 2010, **82**, 483-491.
80. J.-S. Wang and K. Matyjaszewski, *J. Am. Chem. Soc.*, 1995, **117**, 5614-5615.
81. M. Kato, M. Kamigaito, M. Sawamoto and T. Higashimura, *Macromolecules*, 1995, **28**, 1721-1723.
82. K. Matyjaszewski and J. H. Xia, *Chem. Rev.*, 2001, **101**, 2921-2990.
83. K. Matyjaszewski, *Macromolecules*, 2012, **45**, 4015-4039.
84. W. Jakubowski, K. Min and K. Matyjaszewski, *Macromolecules*, 2006, **39**, 39-45.
85. I. Bremner, *Am. J. Clin. Nutr.*, 1998, **67**, 1069S-1073S.
86. J. Y. Uriu-Adams and C. L. Keen, *Mol. Aspects Med.*, 2005, **26**, 268-298.
87. J. Chiefari, Y. K. Chong, F. Ercole, J. Krstina, J. Jeffery, T. P. T. Le, R. T. A. Mayadunne, G. F. Meijs, C. L. Moad, G. Moad, E. Rizzardo and S. H. Thang, *Macromolecules*, 1998, **31**, 5559-5562.
88. A. F. Hirschbiel, W. Konrad, D. Schulze-Sünninghausen, S. Wiedmann, B. Luy, B. V. K. J. Schmidt and C. Barner-Kowollik, *ACS Macro Lett.*, 2015, **4**, 1062-1066.
89. B. V. K. J. Schmidt, M. Hetzer, H. Ritter and C. Barner-Kowollik, *Polym. Chem.*, 2012, **3**, 3064-3067.
90. B. V. K. J. Schmidt, M. Hetzer, H. Ritter and C. Barner-Kowollik, *Macromolecules*, 2013, **46**, 1054-1065.
91. Y. K. Chong, T. P. T. Le, G. Moad, E. Rizzardo and S. H. Thang, *Macromolecules*, 1999, **32**, 2071-2074.
92. M. Mertoglu, S. Garnier, A. Laschewsky, K. Skrabania and J. Storsberg, *Polymer*, 2005, **46**, 7726-7740.
93. G. Moad, J. Chiefari, Y. K. Chong, J. Krstina, R. T. A. Mayadunne, A. Postma, E. Rizzardo and S. H. Thang, *Polym. Int.*, 2000, **49**, 993-1001.
94. J. J. Vosloo, M. P. Tonge, C. M. Fellows, F. D'Agosto, R. D. Sanderson and R. G. Gilbert, *Macromolecules*, 2004, **37**, 2371-2382.
95. J. Rzayev and M. A. Hillmyer, *Macromolecules*, 2005, **38**, 3-5.
96. G. Moad, Y. K. Chong, A. Postma, E. Rizzardo and S. H. Thang, *Polymer*, 2005, **46**, 8458-8468.
97. A. Guinaudeau, S. Mazieres, D. J. Wilson and M. Destarac, *Polym. Chem.*, 2012, **3**, 81-84.
98. M. J. Monteiro and J. de Barbeyrac, *Macromolecules*, 2001, **34**, 4416-4423.
99. G. Pound, F. Aguesse, J. B. McLeary, R. F. M. Lange and B. Klumperman, *Macromolecules*, 2007, **40**, 8861-8871.
100. R. T. A. Mayadunne, E. Rizzardo, J. Chiefari, Y. K. Chong, G. Moad and S. H. Thang, *Macromolecules*, 1999, **32**, 6977-6980.

101. C. Schilli, M. G. Lanzendörfer and A. H. E. Müller, *Macromolecules*, 2002, **35**, 6819-6827.
102. J. Chiefari, R. T. A. Mayadunne, C. L. Moad, G. Moad, E. Rizzardo, A. Postma and S. H. Thang, *Macromolecules*, 2003, **36**, 2273-2283.
103. M. Destarac, C. Brochon, J.-M. Catala, A. Wilczewska and S. Z. Zard, *Macromol. Chem. Phys.*, 2002, **203**, 2281-2289.
104. C. L. McCormack and A. B. Lowe, *Acc. Chem. Res.*, 2004, **37**, 312-325.
105. S. R. Gondi, A. P. Vogt and B. S. Sumerlin, *Macromolecules*, 2007, **40**, 474-481.
106. B. Gacal, H. Durmaz, M. A. Tasdelen, G. Hizal, U. Tunca, Y. Yagci and A. L. Demirel, *Macromolecules*, 2006, **39**, 5330-5336.
107. T.-D. Kim, J. Luo, Y. Tian, J.-W. Ka, N. M. Tucker, M. Haller, J.-W. Kang and A. K. Y. Jen, *Macromolecules*, 2006, **39**, 1676-1680.
108. G. Franc and A. K. Kakkar, *Chem. Soc. Rev.*, 2010, **39**, 1536-1544.
109. L. M. Campos, K. L. Killops, R. Sakai, J. M. J. Paulusse, D. Dameron, E. Drockenmüller, B. W. Messmore and C. J. Hawker, *Macromolecules*, 2008, **41**, 7063-7070.
110. A. Gress, A. Völkel and H. Schlaad, *Macromolecules*, 2007, **40**, 7928-7933.
111. A. Dondoni, *Angew. Chem., Int. Ed.*, 2008, **47**, 8995-8997.
112. R. Huisgen, G. Szeimies and L. Möbius, *Chem. Ber.*, 1967, **100**, 2494-2507.
113. V. V. Rostovtsev, L. G. Green, V. V. Fokin and K. B. Sharpless, *Angew. Chem., Int. Ed.*, 2002, **41**, 2596-2599.
114. C. Barner-Kowollik, F. E. Du Prez, P. Espeel, C. J. Hawker, T. Junkers, H. Schlaad and W. Van Camp, *Angew. Chem., Int. Ed.*, 2011, **50**, 60-62.
115. S. R. S. Ting, A. M. Granville, D. Quémener, T. P. Davis, M. H. Stenzel and C. Barner-Kowollik, *Austr. J. Chem.*, 2007, **60**, 405-409.
116. K. Kempe, A. Krieg, C. R. Becer and U. S. Schubert, *Chem. Soc. Rev.*, 2012, **41**, 176-191.
117. K. Kempe, S. L. Ng, K. F. Noi, M. Müllner, S. T. Gunawan and F. Caruso, *ACS Macro Lett.*, 2013, **2**, 1069-1072.
118. J. Bernard, M. Save, B. Arathoon and B. Charleux, *J. Polym. Sci. A Polym. Chem.*, 2008, **46**, 2845-2857.
119. J. M. Baskin, J. A. Prescher, S. T. Laughlin, N. J. Agard, P. V. Chang, I. A. Miller, A. Lo, J. A. Codelli and C. R. Bertozzi, *Proc. Natl. Acad. Sci. U.S.A.*, 2007, **104**, 16793-16797.
120. R. K. V. Lim and Q. Lin, *Chem. Commun.*, 2010, **46**, 1589-1600.
121. P. J. Flory, *J. Chem. Phys.*, 1942, **10**, 51-61.
122. M. L. Huggins, *J. Am. Chem. Soc.*, 1942, **64**, 1712-1719.
123. L. Leibler, *Macromolecules*, 1980, **13**, 1602-1617.
124. F. S. Bates and G. H. Fredrickson, *Macromolecules*, 1994, **27**, 1065-1067.
125. M. W. Matsen and M. Schick, *Macromolecules*, 1994, **27**, 6761-6767.
126. J. M. G. Swann and P. D. Topham, *Polymers*, 2010, **2**, 454-469.
127. M. W. Matsen and F. S. Bates, *Macromolecules*, 1996, **29**, 1091-1098.
128. H.-C. Kim, S.-M. Park and W. D. Hinsberg, *Chem. Rev.*, 2010, **110**, 146-177.
129. G. J. d. A. A. Soler-Illia, E. L. Crepaldi, D. Grosso and C. Sanchez, *Curr. Opin. Colloid Interface Sci.*, 2003, **8**, 109-126.
130. M. Antonietti and S. Forster, *Adv. Mater.*, 2003, **15**, 1323-1333.
131. A. D. Bangham, *Chem. Phys. Lipids*, 1993, **64**, 275-285.
132. B. M. Discher, Y.-Y. Won, D. S. Ege, J. C.-M. Lee, F. S. Bates, D. E. Discher and D. A. Hammer, *Science*, 1999, **284**, 1143-1146.
133. S. HYDE, T., *J. Phys. Colloques*, 1990, **51**, C7-209-C207-228.
134. L. Chuenchom, R. Kraehnert and B. M. Smarsly, *Soft Matter*, 2012, **8**, 10801-10812.
135. C. Liang, K. Hong, G. A. Guiochon, J. W. Mays and S. Dai, *Angew. Chem., Int. Ed.*, 2004, **43**, 5785-5789.

136. D. C. Drummond, O. Meyer, K. Hong, D. B. Kirpotin and D. Papahadjopoulos, *Pharmacol. Rev.*, 1999, **51**, 691-744.
137. N. V. Rooijen and A. Sanders, *J. Immunol. Methods*, 1994, **174**, 83-93.
138. V. P. Torchilin, *Nat Rev Drug Discov*, 2005, **4**, 145-160.
139. M. J. Janiak, D. M. Small and G. G. Shipley, *J. Biol. Chem.*, 1979, **254**, 6068-6078.
140. J. N. Israelachvili, D. J. Mitchell and B. W. Ninham, *J. Chem. Soc., Faraday Trans.*, 1976, **72**, 1525-1568.
141. H. Shen and A. Eisenberg, *J. Phys. Chem. B.*, 1999, **103**, 9473-9487.
142. R. Dimova, U. Seifert, B. Pouligny, S. Förster and H.-G. Döbereiner, *Eur. Phys. J. E*, 2002, **7**, 241-250.
143. J. Du and Y. Chen, *Macromolecules*, 2004, **37**, 5710-5716.
144. M. Monduzzi, *Curr. Opin. Colloid Interface Sci.*, 1998, **3**, 467-477.
145. M. Regenbrecht, S. Akari, S. Förster and H. Möhwald, *Surf. Interface Anal.*, 1999, **27**, 418-421.
146. M. I. Angelova, S. Soléau, P. Méléard, F. Faucon and P. Bothorel, in *Trends in Colloid and Interface Science VI*, eds. C. Helm, M. Lösche and H. Möhwald, Steinkopff, Darmstadt, 1992, DOI: 10.1007/BFb0116295, pp. 127-131.
147. R. Dimova, U. Seifert, B. Pouligny, S. Förster and H.-G. Döbereiner, *Eur. Phys. J. E*, 2002, **7**, 241-250.
148. Y. Okumura, H. Zhang, T. Sugiyama and Y. Iwata, *J. Am. Chem. Soc.*, 2007, **129**, 1490-+.
149. R. Bleul, R. Thiermann and M. Maskos, *Macromolecules*, 2015, **48**, 7396-7409.
150. F. Chécot, S. Lecommandoux, Y. Gnanou and H.-A. Klok, *Angew. Chem., Int. Ed.*, 2002, **41**, 1339-1343.
151. K. E. Gebhardt, S. Ahn, G. Venkatachalam and D. A. Savin, *J. Colloid Interface Sci.*, 2008, **317**, 70-76.
152. H. Kukula, H. Schlaad, M. Antonietti and S. Förster, *J. Am. Chem. Soc.*, 2002, **124**, 1658-1663.
153. C. Schatz, S. Louguet, J. F. Le Meins and S. Lecommandoux, *Angew. Chem., Int. Ed.*, 2009, **48**, 2572-2575.
154. P. H. Seeberger and D. B. Werz, *Nature*, 2007, **446**, 1046-1051.
155. K. K. Upadhyay, A. N. Bhatt, A. K. Mishra, B. S. Dwarakanath, S. Jain, C. Schatz, J.-F. Le Meins, A. Farooque, G. Chandraiah, A. K. Jain, A. Misra and S. Lecommandoux, *Biomaterials*, 2010, **31**, 2882-2892.
156. K. K. Upadhyay, J. F. L. Meins, A. Misra, P. Voisin, V. Bouchaud, E. Ibarboure, C. Schatz and S. Lecommandoux, *Biomacromolecules*, 2009, **10**, 2802-2808.
157. F. Ahmed, A. Hategan, D. E. Discher and B. M. Discher, *Langmuir*, 2003, **19**, 6505-6511.
158. S. Haas, N. Hain, M. Raoufi, S. Handschuh-Wang, T. Wang, X. Jiang and H. Schönherr, *Biomacromolecules*, 2015, **16**, 832-841.
159. A. Kumar, S. V. Lale, S. Mahajan, V. Choudhary and V. Koul, *ACS Appl. Mater. Interfaces*, 2015, **7**, 9211-9227.
160. E. Mabrouk, D. Cuvelier, F. Brochard-Wyart, P. Nassoy and M.-H. Li, *Proc. Natl. Acad. Sci. U.S.A.*, 2009, **106**, 7294-7298.
161. G. P. Robbins, M. Jimbo, J. Swift, M. J. Therien, D. A. Hammer and I. J. Dmochowski, *J. Am. Chem. Soc.*, 2009, **131**, 3872-3874.
162. A. Ranquin, W. Versées, W. Meier, J. Steyaert and P. Van Gelder, *Nano Lett.*, 2005, **5**, 2220-2224.
163. F. Liu, V. Kozlovskaya, S. Medipelli, B. Xue, F. Ahmad, M. Saeed, D. Cropek and E. Kharlampieva, *Chem. Mater.*, 2015, **27**, 7945-7956.
164. J. Du and S. P. Armes, *J. Am. Chem. Soc.*, 2005, **127**, 12800-12801.

165. M. Kumar, M. Grzelakowski, J. Zilles, M. Clark and W. Meier, *Proc. Natl. Acad. Sci. U.S.A.*, 2007, **104**, 20719-20724.
166. R. Stoenescu, A. Graff and W. Meier, *Macromol. Biosci.*, 2004, **4**, 930-935.
167. M. Marguet, C. Bonduelle and S. Lecommandoux, *Chem. Soc. Rev.*, 2013, **42**, 512-529.
168. R. Peters, M. Marguet, S. Marais, M. W. Fraaije, J. C. M. van Hest and S. Lecommandoux, *Angew. Chem., Int. Ed.*, 2014, **53**, 146-150.
169. H. Wei, S.-X. Cheng, X.-Z. Zhang and R.-X. Zhuo, *Prog. Polym. Sci.*, 2009, **34**, 893-910.
170. C. Weber, R. Hoogenboom and U. S. Schubert, *Prog. Polym. Sci.*, 2012, **37**, 686-714.
171. D. C. Drummond, M. Zignani and J.-C. Leroux, *Prog. Lipid Res.*, 2000, **39**, 409-460.
172. K. M. Huh, H. C. Kang, Y. J. Lee and Y. H. Bae, *Macromol. Res.*, 2012, **20**, 224-233.
173. N. Nath and A. Chilkoti, *Adv. Mater.*, 2002, **14**, 1243-1247.
174. X. Liang, V. Kozlovskaya, C. P. Cox, Y. Wang, M. Saeed and E. Kharlampieva, *J. Polym. Sci. A Polym. Chem.*, 2014, **52**, 2725-2737.
175. M. Chanana, S. Jahn, R. Georgieva, J.-F. Lutz, H. Bäumler and D. Wang, *Chem. Mater.*, 2009, **21**, 1906-1914.
176. I. Tan, Z. Zarafshani, J.-F. Lutz and M.-M. Titirici, *ACS Appl. Mater. Interfaces*, 2009, **1**, 1869-1872.
177. A. S. Hoffman, *J. Control. Release*, 1987, **6**, 297-305.
178. M. Bathfield, J. Warnant, C. Gerardin and P. Lacroix-Desmazes, *Polym. Chem.*, 2015, **6**, 1339-1349.
179. N. Chan, S. Y. An, N. Yee and J. K. Oh, *Macromol. Rapid Commun.*, 2014, **35**, 752-757.
180. A. E. Smith, X. W. Xu, S. E. Kirkland-York, D. A. Savin and C. L. McCormick, *Macromolecules*, 2010, **43**, 1210-1217.
181. V. A. Vasantha, S. Jana, S. S. C. Lee, C. S. Lim, S. L. M. Teo, A. Parthiban and J. G. Vancso, *Polym. Chem.*, 2015, **6**, 599-606.
182. C. He, S. W. Kim and D. S. Lee, *J. Control. Release*, 2008, **127**, 189-207.
183. H. Otsuka, Y. Nagasaki and K. Kataoka, *Adv. Drug Deliv. Rev.*, 2003, **55**, 403-419.
184. O. Onaca, R. Enea, D. W. Hughes and W. Meier, *Macromol. Biosci.*, 2009, **9**, 129-139.
185. H.-O. Johansson, G. Karlström, F. Tjerneld and C. A. Haynes, *J. Chromatogr. B*, 1998, **711**, 3-17.
186. N. L. Abbott, D. Blankschtein and T. A. Hatton, *Macromolecules*, 1992, **25**, 5192-5200.
187. B. T. Nguyen, W. Wang, B. R. Saunders, L. Benyahia and T. Nicolai, *Langmuir*, 2015, **31**, 3605-3611.
188. W. J. Frith, *Adv. Colloid Interface Sci.*, 2010, **161**, 48-60.
189. R. H. Tromp, M. Vis, B. H. Erne and E. M. Blokhuis, *J. Phys.: Condens. Matter*, 2014, **26**, 464101.
190. M. Vis, V. F. D. Peters, R. H. Tromp and B. H. Ern , *Langmuir*, 2014, **30**, 5755-5762.
191. A. Taubert, E. Furrer and W. Meier, *Chem. Commun.*, 2004, DOI: 10.1039/b405610h, 2170-2171.
192. A. Taubert, G. Glasser and D. Palms, *Langmuir*, 2002, **18**, 4488-4494.
193. A. Taubert, C. K bel and D. C. Martin, *J. Phys. Chem. B.*, 2003, **107**, 2660-2666.
194. A. Taubert, D. Palms,  . Weiss, M.-T. Piccini and D. N. Batchelder, *Chem. Mater.*, 2002, **14**, 2594-2601.
195. F. Y. Ke, X. L. Mo, R. M. Yang, Y. M. Wang and D. H. Liang, *Macromolecules*, 2009, **42**, 5339-5344.
196. O. Casse, A. Shkilnyy, J. Linders, C. Mayer, D. Haussinger, A. Volkel, A. F. Thunemann, R. Dimova, H. Colfen, W. Meier, H. Schlaad and A. Taubert, *Macromolecules*, 2012, **45**, 4772-4777.
197. J. Wu, Z. Wang, Y. Yin, R. Jiang, B. Li and A.-C. Shi, *Macromolecules*, 2015, **48**, 8897-8906.

198. A. Blanz, N. J. Warren, A. L. Lewis, S. P. Armes and A. J. Ryan, *Soft Matter*, 2011, **7**, 6399-6403.
199. S. M. Brosnan, H. Schlaad and M. Antonietti, *Angew. Chem., Int. Ed.*, 2015, **54**, 9715-9718.
200. T. Rudolph, S. Crotty, M. von der Luehe, D. Pretzel, U. S. Schubert and F. H. Schacher, *Polymers*, 2013, **5**, 1081-1101.
201. R. Duncan, *Nat. Rev. Drug Discov.*, 2003, **2**, 347-360.
202. Y. Levy, M. S. Hershfield, C. Fernandez-Mejia, S. H. Polmar, D. Scudieri, M. Berger and R. U. Sorensen, *J. Pediatr.*, 1988, **113**, 312-317.
203. J. Rieger, F. Stoffelbach, C. Bui, D. Alaimo, C. Jerome and B. Charleux, *Macromolecules*, 2008, **41**, 4065-4068.
204. H. F. Gao and K. Matyjaszewski, *J. Am. Chem. Soc.*, 2007, **129**, 6633-6639.
205. C. Hua, S. M. Peng and C. M. Dong, *Macromolecules*, 2008, **41**, 6686-6695.
206. B. Y. Zhang, H. Zhang, R. Elupula, A. M. Alb and S. M. Grayson, *Abstr. Pap. Am. Chem. Soc.*, 2014, **247**.
207. D. Fournier, R. Hoogenboom and U. S. Schubert, *Chem. Soc. Rev.*, 2007, **36**, 1369-1380.
208. S. Saeki, N. Kuwahara, M. Nakata and M. Kaneko, *Polymer*, 1976, **17**, 685-689.
209. A. Guinaudeau, O. Coutelier, A. Sandeau, S. Mazieres, H. D. N. Thi, V. Le Drogo, D. J. Wilson and M. Destarac, *Macromolecules*, 2014, **47**, 41-50.
210. Y. Mu, H. Kamada, H. Kodaira, K. Sato, Y. Tsutsumi, M. Maeda, K. Kawasaki, M. Nomizu, Y. Yamada and T. Mayumi, *Biochem. Biophys. Res. Commun.*, 1999, **264**, 763-767.
211. W. R. Thrower and H. Campbell, *The Lancet*, 1951, **257**, 1096-1099.
212. N. Bailly, M. Thomas and B. Klumperman, *Biomacromolecules*, 2012, **13**, 4109-4117.
213. K. Knop, R. Hoogenboom, D. Fischer and U. S. Schubert, *Angew. Chem., Int. Ed.*, 2010, **49**, 6288-6308.
214. C. R. Kinnane, G. K. Such, G. Antequera-García, Y. Yan, S. J. Dodds, L. M. Liz-Marzan and F. Caruso, *Biomacromolecules*, 2009, **10**, 2839-2846.
215. S. L. Ng, G. K. Such, A. P. R. Johnston, G. Antequera-García and F. Caruso, *Biomaterials*, 2011, **32**, 6277-6284.
216. C. F. Huang, R. Nicolay, Y. Kwak, F. C. Chang and K. Matyjaszewski, *Macromolecules*, 2009, **42**, 8198-8210.
217. X. J. Lu, S. L. Gong, L. Z. Meng, C. Li, S. Yang and L. F. Zhang, *Polymer*, 2007, **48**, 2835-2842.
218. G. Pound, Z. Eksteen, R. Pfukwa, J. M. McKenzie, R. F. M. Lange and B. Klumperman, *J. Polym. Sci., A, Polym. Chem.*, 2008, **46**, 6575-6593.
219. H. Wiese and D. Horn, *J. Chem. Phys.*, 1991, **94**, 6429-6443.
220. T. Alfrey and C. C. Price, *J. Polym. Sci.*, 1947, **2**, 101-106.
221. K. L. Petrak, *J. Polym. Sci. C Polym. Lett.*, 1978, **16**, 393-399.
222. A. A. Toropov, V. O. Kudyskin, N. L. Voropaeva, I. N. Ruban and S. S. Rashidova, *J. Struct. Chem.*, 2004, **45**, 945-950.
223. B. Wicklein, A. Kocjan, G. Salazar-Alvarez, F. Carosio, G. Camino, M. Antonietti and L. Bergstrom, *Nat. Nanotechnol.*, 2015, **10**, 277-283.
224. J. Yuan and M. Antonietti, *Polymer*, 2011, **52**, 1469-1482.
225. J. Yuan, D. Mecerreyes and M. Antonietti, *Prog. Polym. Sci.*, 2013, **38**, 1009-1036.
226. J. Yuan, S. Soll, M. Drechsler, A. H. E. Müller and M. Antonietti, *J. Am. Chem. Soc.*, 2011, **133**, 17556-17559.
227. J. Willersinn, M. Drechsler, M. Antonietti and B. V. K. J. Schmidt, *Macromolecules*, 2016, **49**, 5331-5341.



228. T. Heinze, T. Liebert, B. Heublein and S. Hornig, in *Polysaccharides II*, ed. D. Klemm, 2006, vol. 205, pp. 199-291.
229. R. K. Shukla and A. Tiwari, *Carbohydr. Polym.*, 2012, **88**, 399-416.
230. M. Naessens, A. Cerdobbel, W. Soetaert and E. J. Vandamme, *J. Chem. Technol. Biotechnol.*, 2005, **80**, 845-860.
231. S. G. Lévesque, R. M. Lim and M. S. Shoichet, *Biomaterials*, 2005, **26**, 7436-7446.
232. E. M. Bachelder, E. N. Pino and K. M. Ainslie, *Chem. Rev.*, 2017, **117**, 1915-1926.
233. M. Nishikawa, A. Kamijo, T. Fujita, Y. Takakura, H. Sezaki and M. Hashida, *Pharm. Res.*, 1993, **10**, 1253-1261.
234. K. Jeremic, L. Ilic and S. Jovanovic, *Eur. Polym. J.*, 1985, **21**, 537-540.
235. I. W. Sutherland, *Trends Biotechnol.*, 1998, **16**, 41-46.
236. W. M. Kulicke and T. Heinze, *Macromol. Symp.*, 2005, **231**, 47-59.
237. M. E. Gounga, S. Y. Xu, Z. Wang and W. G. Yang, *J. Food. Sci.*, 2008, **73**, E155-E161.
238. K.-C. Cheng, A. Demirci and J. M. Catchmark, *Appl. Microbiol. Biotechnol.*, 2011, **92**, 29-44.
239. R. S. Singh, N. Kaur and J. F. Kennedy, *Carbohydr. Polym.*, 2015, **123**, 190-207.
240. S. B. Chen, M. H. Alves, M. Save and L. Billon, *Polym. Chem.*, 2014, **5**, 5310-5319.
241. Y. Perez, A. Valdivia, L. Gomez, B. K. Simpson and R. Villalonga, *Macromol. Biosci.*, 2005, **5**, 1220-1225.
242. L. Ilic, K. Jeremic and S. Jovanovic, *Eur. Polym. J.*, 1991, **27**, 1227-1229.
243. H.-G. Elias, in *Makromoleküle*, WILEY-VCH Verlag GmbH & Co. KGaA, 2009, DOI: 10.1002/9783527626496.ch2, pp. 4-39.
244. B. H. Zimm, *J. Chem. Phys.*, 1946, **14**, 164-179.
245. W. Schärtl, in *Light Scattering from Polymer Solutions and Nanoparticle Dispersions*, Springer Berlin Heidelberg, Berlin, Heidelberg, 2007, DOI: 10.1007/978-3-540-71951-9\_1, ch. 1, pp. 1-24.
246. T. Kato, T. Okamoto, T. Tokuya and A. Takahashi, *Biopolymers*, 1982, **21**, 1623-1633.
247. R. H. Lambeth, S. Ramakrishnan, R. Mueller, J. P. Poziemski, G. S. Miguel, L. J. Markoski, C. F. Zukoski and J. S. Moore, *Langmuir*, 2006, **22**, 6352-6360.
248. M. Sedlák, *J. Phys. Chem. B.*, 2012, **116**, 2356-2364.
249. Y. Zhu, L. Liu and J. Du, *Macromolecules*, 2013, **46**, 194-203.
250. J. S. Lowe, B. Z. Chowdhry, J. R. Parsonage and M. J. Snowden, *Polymer*, 1998, **39**, 1207-1212.
251. J. Willersinn, A. Bogomolova, M. B. Cabré and B. V. K. J. Schmidt, *Polym. Chem.*, 2017, **8**, 1244-1254.
252. F. Lecolley, L. Tao, G. Mantovani, I. Durkin, S. Lautru and D. M. Haddleton, *Chem. Commun.*, 2004, DOI: 10.1039/B407712A, 2026-2027.
253. U. Hasegawa, A. J. van der Vlies, E. Simeoni, C. Wandrey and J. A. Hubbell, *J. Am. Chem. Soc.*, 2010, **132**, 18273-18280.
254. K. H. Bouhadir, D. S. Hausman and D. J. Mooney, *Polymer*, 1999, **40**, 3575-3584.
255. J. P. Draye, B. Delaey, A. Van de Voorde, A. Van Den Bulcke, B. Bogdanov and E. Schacht, *Biomaterials*, 1998, **19**, 99-107.
256. J. Maia, L. Ferreira, R. Carvalho, M. A. Ramos and M. H. Gil, *Polymer*, 2005, **46**, 9604-9614.
257. J. McCann, J. M. Behrendt, J. F. Yan, S. Halacheva and B. R. Saunders, *J. Colloid Interface Sci.*, 2015, **449**, 21-30.
258. S. K. Tripathi, R. Goyal and K. C. Gupta, *Soft Matter*, 2011, **7**, 11360-11371.
259. D. B. Williams and C. B. Carter, in *Transmission Electron Microscopy: A Textbook for Materials Science*, Springer US, Boston, MA, 2009, DOI: 10.1007/978-0-387-76501-3\_2, pp. 23-38.

260. JEOL, Scanning Electron Microscope A To Z, <http://www.jeolusa.com/RESOURCES/Electron-Optics/Documents-Downloads/EntryId/598>, (accessed 04.08.2017, 2017).
261. M. Shao, P. Dongare, L. N. Dawe, D. W. Thompson and Y. M. Zhao, *Org. Lett.*, 2010, **12**, 3050-3053.
262. B. V. K. J. Schmidt and C. Barner-Kowollik, *Polym. Chem.*, 2014, **5**, 2461-2472.
263. M. Conradi and T. Junkers, *Macromolecules*, 2014, **47**, 5578-5585.

## IX. List of Publications

**Willersinn, J.**; Bogomolova, A.; Brunet Cabre, M.; Schmidt, B. V. K. J. Vesicles of double hydrophilic pullulan and poly(acrylamide) block copolymers: A combination of synthetic- and bio-derived blocks *Polym. Chem.* **2017**, *8*, 1244.

**Willersinn, J.**; Drechsler, M.; Antonietti, M.; Schmidt, B. V. K. J. Organized Polymeric Submicron Particles via Self-Assembly and Cross-Linking of Double Hydrophilic Poly(ethylene oxide)-*b*-poly(*N*-vinylpyrrolidone) in Aqueous Solution *Macromolecules* **2016**, *49*, 5331.

Jiang, T.; Bartholomeyzik, T.; Mazuela, J.; **Willersinn, J.**; Bäckvall, J.-E. Palladium(II)/Brønsted Acid-Catalyzed Enantioselective Oxidative Carbocyclization–Borylation of Enallenes *Angew. Chem., Int. Ed.* **2015**, *54*, 6024.

Staff, R. H.; **Willersinn, J.**; Musyanovych, A.; Landfester, K.; Crespy, D. Janus nanoparticles with both faces selectively functionalized for click chemistry *Polym. Chem.* **2014**, *5*, 4097.

## **X. Declaration**

Die vorliegende Dissertation entstand im Zeitraum zwischen Januar 2015 und April 2017 am Max-Planck-Institut für Kolloid- und Grenzflächenforschung unter Betreuung von Prof. Dr. Dr. h.c. Markus Antonietti.

Hiermit erkläre ich, dass die vorliegende Arbeit selbstständig angefertigt wurde und keine anderen als die angegebenen Hilfsmittel und Quellen verwendet wurden.

The present work was carried out during the period from January, 2015 to April, 2017 at the Max Planck Institute of Colloids and Interfaces under supervision of Prof. Dr. Dr. h.c. Markus Antonietti.

I declare that I have written this work on my own and used no other than the named aids and references.

Jochen Willersinn

Potsdam, 14.04.2017